

OPTIMIZATION OF FULLERENES' SYNTHESIS USING A MODIFIED REACTOR : THE CHEMISTRY OF BUCKMINSTERFULLERENE WITH INORGANIC RADICALS AND METAL - HEXACARBONYLS

By
SUBRATA ROY

HM

195

)

ROY

PT



DEPARTMENT OF CHEMISTRY
INDIAN INSTITUTE OF TECHNOLOGY KANPUR

NOVEMBER 1995

**'OPTIMIZATION OF FULLERENES' SYNTHESIS USING
A MODIFIED REACTOR: THE CHEMISTRY OF
BUCKMINSTERFULLERENE WITH INORGANIC
RADICALS AND METAL-HEXACARBONYLS**

*A Thesis Submitted
in Partial Fulfillment of the Requirements
for the Degree of*

DOCTOR OF PHILOSOPHY

by

SUBRATA ROY

to the

**DEPARTMENT OF CHEMISTRY
INDIAN INSTITUTE OF TECHNOLOGY
KANPUR**

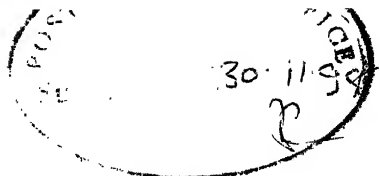
NOVEMBER, 1995

- 6 AUG 1997
CENTRAL LIBRARY
I. I. T., KANPUR

Vol. No. A 123647

M-1995-D-ROY-OPT

To
My Uncle
Bijoy Chandra Roy



STATEMENT

I hereby declare that the matter embodied in this thesis is the result of investigations carried out by me in the Department of Chemistry, Indian Institute of Technology, Kanpur, India under the supervision of Professor S. Sarkar.

In keeping with the general practice of reporting scientific observations, due acknowledgement has been made wherever the work described is based on the findings of other investigators.

Kanpur

Subrata Roy
SUBRATA ROY

DEPARTMENT OF CHEMISTRY
INDIAN INSTITUTE OF TECHNOLOGY KANPUR INDIA

CERTIFICATE I

This is to certify that Mr. SUBRATA ROY has satisfactorily completed all the courses required for the Ph. D. degree programme. These courses include:

CHM 505 Principles of Organic Chemistry
CHM 524 Modern Physical Methods in Chemistry
CHM 525 Principles of Physical Chemistry
CHM 545 Principles of Inorganic Chemistry
CHM 626 Solid State Chemistry
CHM 670 Scientific Instrumentation
CHM 800 General Seminar
CHM 801 Special Seminar
CHM 900 Ph. D. Thesis

Mr. Subrata Roy was admitted to the candidacy of the Ph. D. degree in August 1989, after he successfully completed the written and oral qualifying examinations.



(P. K. Ghosh)

Head,

Department of Chemistry
IIT Kanpur



(P. Guptabhaya)

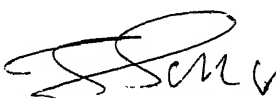
Convenor,

Departmental Post Graduate Committee
Department of Chemistry

IIT Kanpur

CERTIFICATE II

Certified that the work contained in this thesis entitled: *Optimization of Fullerenes' Synthesis using a Modified Reactor: The Chemistry of Buckminsterfullerene with Inorganic Radicals and Metal-hexacarbonyls*, has been carried out by Mr. Subrata Roy under my supervision and that the same has not been submitted elsewhere for a degree.



(Professor S. Sarkar)

Thesis Supervisor

Department of Chemistry

IIT Kanpur

Acknowledgements

It is with great pleasure that I place on record my heartfelt thanks to my thesis supervisor Professor S. Sarkar for his guidance and encouragement throughout the course of this work. Working under his guidance was a worth experience which will always be remembered and cherished.

I also pay my sincere gratitude to Mr. R. K. Jha for fabrication of the reactor. I also give my special thanks to the staff, work shop-department of chemistry and central work shop I. I. T Kanpur.

I acknowledge Mr. A. K. Tewary, Hi-tech Engenering Kanpur, for fabricating the power supply.

Thanks to my friend, Dr. Amalendu Chandra for providing the graphite rods in time.

Thanks to Dr. U. S. Mehrotra, DMSEERDE Kanpur, for recording the XPS spectra, helpful discussion and keen interest of my work. Dr. D. S. Dewvadi, DMSRDE Kanpur, for the necessary arrangements in recording the XPS spectra and encouragement.

Thanks to RSIC-Lucknow and ACMS-IIT Kanpur, for recording the various measurements. Thanks to Computer Center and Cetral Library IIT Kanpur for necessary help.

Thanks to Prof. T. K. Chandrasekhar, Prof. V. Chandrasekhar, Prof. P. K. Bharadwaj and Dr. P. Gupta-bahya to use all their laboratory facilities and keen interest of my work.

Thanks to Dr. N. S. Gajbhiye for the association of first 3 years in his laboratory.

I wish to make special mention of Subhasish Basu Mazumder, Tapan Khan, Atanu

Saha, Dr. Samar Kr. Das, Rabin Maity and Dr. Rangan kr. Guha for their help in various aspects of my research work and moral support.

Thanks to Mr. Nayab Ahamed and D. K. Kanujia for kind cooperation in recording the spectra.

Thanks to Rajen Gurjer and Alope Saran for helping the laser measurements.

It was an experience worth remembering to worked with khukudi (Mrs. Bharadwaj), P. K. Chaudhuri and Dr. V. K. Shankarnarayan. I thanks them for their pleasant association.

Thanks to the staff, the department of chemistry, glass blowing and central purchase section of I. I. T. Kanpur.

Thanks to Manoj Mukhopadya and B. K. Jain for neat drawing of the figures.

Thanks to Mrs S. Sarkar for hospitality and affection.

Thanks Dr. Promod Kumar, Behera, Dharampal, Mim, Frenchi, Shome da, Dr. Indrajit Basak, Dr. Gautom Roy (boga da), G. K. Singh, Swapan, Dr. A. K. Jana (maogambo), Dr. Manab Das, Dr. Samiran Mandal, Dr. R. K. Shukla, Deba, Sushanto, Nilu, Subit, Dr. Sanjay Kumar, Dr. Tarakaswer (kapuchino), Dr. Balakrishnan, Sriram, Chotalal, Mohesh, Lala and others for their association and staying at III-Kanpur is enjoyable.

Sincere thanks to my wife for her patience, moral support and encouragement. I also thank her for typing and proof reading of the thesis.

Last but by no means the least I take the opportunity to acknowledge my parents, my father-in-law and mother-in-law and my sisters for their love, affection, encouragement and patience.

Synopsis

The thesis entitled, Optimization of Fullerenes' Synthesis using a Modified Reactor: The Chemistry of Buckminsterfullerene with Inorganic Radicals and Metal-hexacarbonyls, consists of eight chapters.

A general survey of the chemistry and physico-chemical aspects of C_{60} is given in chapter 1.

The scope of the present work is described in chapter 2. Yield of the fullerene depends on the various parameters of the reactor like, (i) He- gas pressure, (ii) power required in burning the graphite rods, (iii) others. But systematic studies are lacking in this area. Optimization of yield of the fullerenes' is possible by the systematic investigation with the variation of these key parameters.

The chemistry of C_{60} in relevance to alkenes or arenes character has not yet extensively investigated. Our aim in these aspects is to study the reactivity of C_{60} with different kinds of molecules which are very reactive with the alkenes and arenes in normal conditions.

C_{60} and other fullerenes are unstable in the day light at room temperature. However they are synthesized under the most exotic conditions. The difference in the stability between these two environments are possibly related to the presence of oxygen, humidity and solvent interactions at ambient conditions compared to the inert atmosphere of the reactor. A systematic approach in this area is helpful to investigate the chemistry related to the instability of C_{60} and other fullerenes under laboratory conditions.

The fabrication of a modified arc reactor and yield optimization have been described in chapter 3. Section 3.1.3-3.1.6 deals with the fabrication, optimization of the fullerenes' yield and separation of C_{60} from fullerenes. In section 3.1.7, soot generated from other sources than graphite vapourization are analyzed. Mass spectra indicates, the motif

'corannulene' is absent in these soots. The experimental observation made in section 3.1.4 to 3.1.7 are discussed and the kinetics of fullerenes' formation is qualitatively discussed in section 3.2.

The chapter 4 deals with the reactivity of NO, NOCl, NO₂, SO₂⁻, HOCl and ¹O₂ with C₆₀. Reaction methodology and experimental details are given in section 4.1-4.2. A stable compound is formed in the reaction between C₆₀ and NO₂ which is characterized as polyhydroxy-polynitro buckminsterfullerene. In the first stage of this reaction a multiple nitro addition occurs on C₆₀ which isomerizes partly to nitrito form. This nitrito group on subsequent hydrolysis by atmospheric moisture yields nitrofullerenols consisting of 6-8 nitro and 7-12 hydroxy groups per C₆₀. Intramolecular hydrogen bonding between hydroxy and nitro group is responsible for extra stability of the partially hydrolyzed compound. C₆₀ radicals are formed in the intermediate of the reaction which has been confirmed by EPR spectroscopy. Based on the IR, XPS, EPR, and chemical test (Griess's test) a reaction mechanism has been proposed for the nitration products of the C₆₀. The details of the above mentioned facts are discussed in section 4.3. The geometry and delocalization of the odd electron in the molecule is one of the determining factors to overlap with π -orbital of C₆₀. In other words σ type radicals are more reactive with C₆₀ than π type of radicals and these are discussed in the section 4.4.

Chapter 5 of the thesis deals with the thermal and photochemical interaction between metal hexacarbonyls and C₆₀. In section 5.2.1-5.2.4 experimental details of these reactions are described. A solid product is isolated on the sunlight irradiation of C₆₀ and W(CO)₆ in benzene. FAB mass, X-ray photoelectron spectral data and elemental analysis of this product are given in section 5.3.1 and mass peak at 988 is assigned for the red brown solid with the composition [W(CO)₃(C₆₀)₃]. Probable path of this reaction, i.e associative or dissociative, are also described in this section. Irradiation with different selective wave-length indicates that primary event is the formation of a 16-electron species W(CO)₅. In section 5.3.2-5.3.4, cyclic voltammetry and XPS results of the red brown solid are described. These results provide ample proof that electron is donated from the C₆₀ to the metal center in spite of it's high electronegativity and metal is not bonded

with C_{60} in η^2 coordination. Local symmetry of the carbonyl moiety is determined from IR analysis, is presented in section 5.3.5. Section 5.3.6 deals with why $Mo(CO)_6$ and $Cr(CO)_6$ are not reacting with C_{60} in the similar photolytic conditions. The importance of the large 5d-orbital and large spin-orbit coupling of tungsten has been discussed in this reaction.

Chapter 6 deals with the role of oxygen towards C_{60} and effect of solvent. Synthesis of 1, 2, 3, 4, 4a, 6a, 7, 8, 9, 10, dehydro dibenzo-O-dioxan (epidioxide) and attempted synthesis of norascaridol are given in section 6.2.1-6.2.7. These are prepared from the reaction between bi-1-cyclohexen-1-yl, cyclohexadiene, respectively with singlet oxygen. The singlet oxygen is generated by using C_{60} as photosensitizer.

X-ray photoelectron spectra and peak deconvolution analysis of C 1s of pure C_{60} is presented in section 6.3.1 and 6.3.2. In section 6.3.3, the time dependent IR spectra and sunlight irradiation on C_{60} indicated that 1530 cm^{-1} band is oxygen concentration independent. Carbonyl or etheral absorption are not seen in sunlight irradiated samples. IR absorption are taken also with the repeated washing of C_{60} with benzene, carbon disulfide and carbon tetrachloride. These IR studies highlight that solvents are responsible for C_{60} cage destruction.

In section 6.3.4, X-ray powder patterns of (i) freshly prepared C_{60} , (ii) sunlight irradiated C_{60} , (iii) aged C_{60} under aerobic conditions and (iv) freshly prepared C_{60} repeatedly crystallized out from benzene and carbon disulfide as solvents are recorded. Lattice parameters, crystal-lattice size are calculated and probable crystal structures with their Miller indices are assigned.

EPR studies are given in section 6.3.5, EPR measurements of the fullerene soot have been carried out in the absence of light and in the presence of oxygen. Time dependent EPR spectra of the freshly prepared soot and C_{60} are recorded and analyzed. EPR spectra highlight that the paramagnetic species is carbon centered and oxygen is reactive only in the presence of light which suggested that with oxygen it forms a cluster like,



Electrochemistry of the C_{60} thin films prepared at ambient conditions are carried out. The film has two reversible reduction peak and one irreversible oxidation peak. In continuous cycling of the voltammogram, the film activity is gradually ceases with continuous dropping of the current heights. On photoirradiation the 1st reduction wave of C_{60} film is absent. However on repeated cycling voltammograms show both the 1st and 2nd reduction waves similar to unexposed C_{60} films. Based on these observations a possible mechanism for electro chemical response of C_{60} oxygenated thin films and photo exposed oxygenated films have been proposed. This part of work is presented in section 6.3.6.

UV-visible spectra of the ageing C_{60} has been presented in section 6.3.7. Di-ethyl ether is not a good solvent for soot washing. The existence of C_{60}^+ at room temperature has been confirmed and suggested this cationic species is primarily responsible for fullerene degradation.

Based on XPS, IR, XRD, EPR, electrochemistry and electronic spectral studies, it has been proposed that oxygen is not responsible for destruction of the C_{60} cage. Instead oxygen encapsulated C_{60} molecule which prevent it to isomerize in the presence of light. Solvents are incorporated in the crystal lattice during fullerene extraction from the soot which play the crucial role for cage destruction. The conversion of face centered cubic (fcc) to hexagonal close packing (hcp) under the influence of solvent, light and oxygen have been discussed. These are presented in the discussion section 6.3.9.

Highlights and future scope of the present work are discussed in chapter 7 and references are given in chapter 8.

Contents

1	Introduction	1
1.1	Shape	2
1.2	Availability of fullerene from various source	4
1.2.1	Artificial Soot	4
1.2.2	Natural soot	5
1.2.3	Geological Samples	5
1.2.4	Astronomical Samples	6
1.3	Fullerene Separation	6
1.4	The mechanism of Fullerene Formation	7
1.5	Electronic Structure of C ₆₀	9
1.6	Thermodynamic and Kinetic Stability	13
1.6.1	Valence Bond Approach	14
1.7	Vibrational and Raman Spectra	16
1.8	Solubility	17

1.9	Photochemical and Photophysical Properties of C ₆₀	19
1.9.1	Electronic Absorption Spectra	19
1.9.2	Excited State Properties	20
1.10	Electrochemical Properties of C ₆₀	21
1.11	Aromaticity	23
1.12	Chemistry of Buckminsterfullerene	24
1.12.1	Gas Phase Reactivity	25
1.12.2	Organometallic Complexes	26
1.12.3	Charge-Transfer Complexes	26
1.12.4	Hydrogenation	29
1.12.5	Halogenation	30
1.12.6	Cycloaddition	30
1.12.7	Oxygenation	31
1.12.8	Free Radical Addition	31
1.12.9	Hydroxylation	32
1.12.10	Biologically Relevance Compounds	34
2	Scope of the Work	35
3	Design and Fabrication of a Fullerene reactor: Optimization of the Key Parameters in Fullerenes' Synthesis.	42

3.1	Experimental Sections	43
3.1.1	Material Used	43
3.1.2	Physical Measurements	43
3.1.3	Fullerene Reactor Design	44
3.1.4	Soot Production from the Reactor	50
3.1.5	Parameter Adjustment for Optimum Fullerene Yield	51
3.1.6	Separation and Characterization of C ₆₀	54
3.1.7	Attempted Fullerene Separation from Natural Soot	58
3.2	Results and Discussion	58
3.3	Conclusions	65
4	Reactivity with NO, NO ₂ /N ₂ O ₄ , SO ₂ , HOCl and ¹ O ₂	66
4.1	Experimental Section- Part I.	66
4.1.1	General Conditions	66
4.1.2	Materials	67
4.1.3	Physical Measurements	67
4.1.4	Chemical Analysis	68
4.2	Experimental Part-II. Reaction Methodology.	68
4.2.1	Reaction between C ₆₀ and Nitric oxide.	68
4.2.2	Synthesis of Polynitro-Polyhydroxy Buckminsterfullerenes	69

4.2.3	Reaction Between C_{60} and SO_2^-	71
4.2.4	Reaction Between HOCl and C_{60}	71
4.2.5	Photochemical Reaction Between C_{60} And O_2	71
4.2.6	Reaction Between C_{60} and 1O_2	71
4.3	Results and Discussion	72
4.3.1	XPS PeakFit Numerical Summary	87
4.4	Conclusions	90
5	Reactivity with Metal Hexa-Carbonyls (Cr, Mo and W)	92
5.1	Experimental Section : Part-I	93
5.1.1	General Conditions	93
5.1.2	Materials	93
5.1.3	Physical Measurements	93
5.2	Part-II; Reaction Methodology	94
5.2.1	Synthesis of $W(CO)_{6-x}(C_{60})_x$	94
5.2.2	Photochemical Reaction of $Cr(CO)_6$ and $Mo(CO)_6$ with C_{60} . . .	95
5.2.3	Thermal Reaction of $Cr(CO)_6$, $Mo(CO)_6$ and $W(CO)_6$ with C_{60} .	96
5.2.4	Thermal Reaction of $Cr(CO)_6$, $Mo(CO)_6$ and $W(CO)_6$ with C_{60} , in prescence of Me_3NO	96
5.3	Results and Discussion	96

5.3.1	Characterization of the Isolated Compound	102
5.3.2	Electrochemistry	106
5.3.3	X-ray Photoelectron Spectroscopy	110
5.3.4	XPS Numerical Summary	113
5.3.5	IR Spectroscopy	115
5.3.6	Discussion: Photochemical Reactivity of Metalhexacarbonyls with C ₆₀ and Importance of the W(CO) ₅ Fragment.	116
5.4	Conclusions	122
6	Reactivity with Oxygen and Solvent	123
6.1	Experimental Sections: Part I	127
6.1.1	General Conditions	127
6.1.2	Materials	128
6.1.3	Physical Measurements	128
6.2	Experimental Part II : Synthetic Methodology	131
6.2.1	Preparation of 1:1'-dihydroxy-1:1' dycyclohexyl	131
6.2.2	Synthesis of Bi-1-cyclohexene-1-yl	132
6.2.3	Preparation of Peroxide, 1, 2, 3, 4, 4a, 6a, 7, 8, 9, 10-decahydrodibenzo- o-dioxin	132
6.2.4	Preparation of Cyclohexene	133
6.2.5	Preparation of 3, Bromo-Cyclohexene	133

consist of C_{60} clusters like $[C_{60}^+, e^-]$, and the EPR spectrum of it is governed by the delocalized electrons over C_{60} [241]. The disappearance of the EPR signal at liquid nitrogen temperature, as shown in figure 6.12(d) suggested that at low temperature most likely a polymeric aggregate like $[...C_{60}^+...O_2^-...C_{60}^+...O_2^-...]$ has formed.

6.3.6 Electrochemistry

Electrochemical behaviour of C_{60} film is shown in Fig 6.15 (a). The films were prepared by evaporation of the 50 μ l of 0.1 mM C_{60} benzene solution on the Pt-electrode (1mm diameter) surface. The benzene was evaporated very rapidly with the help of a dry air blower from the electrode surface for uniform film growth. Figure 6.18(a) shows the cyclic voltammogram contained two reduction waves at cathodic peaks potentials at -0.64 V and -0.96 V and three anodic peaks at +0.08 V, -0.46 V and -0.76 V. It shows the 1st reduction wave, the smaller anodic peak, splits by 180 mV from the cathodic peak and the large intensity peak appeared at more positive potential which separated by 720 mV from the cathodic peak. The peak potentials are presented in table 6.6 The reported [105] voltammogram of C_{60} (prepared in inert atmosphere) has two reduction waves with two cathodic and two anodic peaks where cathodic and anodic peak are separated by 560 mV for 1st reduction wave and 2nd reduction wave peaks are separated by 220 mV in presence of same cation.

The change in the voltammogram upon continuous cycling over the second, third and upto fourteen are given in figure 6.18(b). In the second scan, small anodic peak of the 1st reduction wave is (figure 6.18(a)) almost vanish. The other anodic peak shifts to 0.1 V more negative potential, however cathodic peak potential remains in the same position. In case of second reduction wave, the cathodic and anodic peaks potential does not perturb much, a minor shift (4 mV) of the cathodic peak to more negative potential is observed. 1st anodic peak potentials of the 1st reduction wave further shifted to 100 mV more negative potential in the 2nd scan whereas cathodic potential remains in the same positions. Moreover this cathodic peak occurred in the same potentials at 2nd, 3rd,

6.2.6	Preparation of Cyclohexa-1,3 diene	134
6.2.7	Preparation of Norascaridol	134
6.3	Results and Discussion	134
6.3.1	X-ray Photo-electron Spectroscopy (XPS)	137
6.3.2	Peak Fit Numerical Summary	139
6.3.3	IR-spectroscopy	140
6.3.4	X-ray Powder Diffraction	145
6.3.5	Electron Paramagnetic Resonance	154
6.3.6	Electrochemistry	163
6.3.7	Electronic Spectra	170
6.3.8	Mass Spectra	174
6.3.9	Discussion: The Probable Path of C ₆₀ degradation	174
6.4	Conclusions	181
7	Highlights and Future Scope of the Present Work.	182

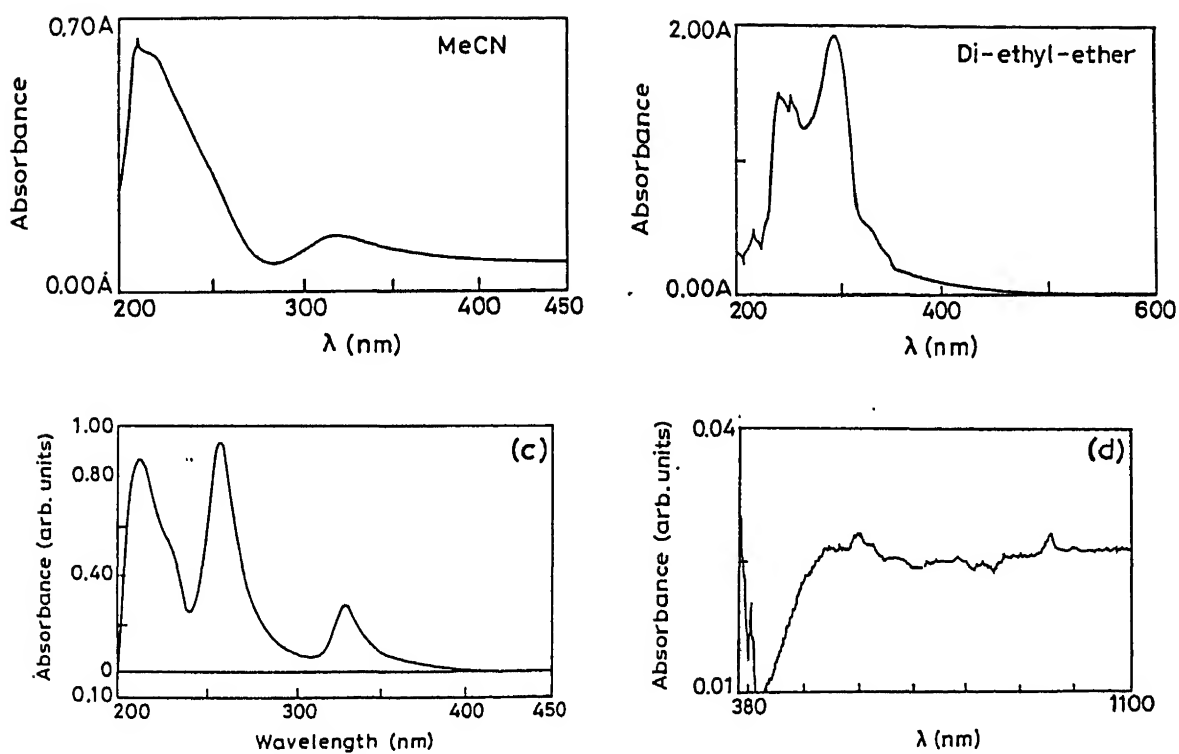


Figure 6.21: UV-Vis spectra of aging C_{60} : (a) acetonitrile (b) Di-ethyl ether (c) Iso-propanol (200-450 nm) and (d) Iso-propanol (380-1100 nm).

List of Figures

1.1	The structure of C_{60} , buckminsterfullerene, the archetype of the fullerene family. It has truncated-icosahedron symmetry, (I_h), as does the European football.	2
1.2	Compound (3), substructure of C_{60}	8
1.3	Scheme of the fullerene formation, during graphite vaporisation.	9
1.4	Relationship between the $\sigma - \sigma$ and $\sigma - \pi$ interorbital angles and the hybridization at a carbon atom between the extremes of planar and tetrahedral geometry in C_{3v}	11
1.5	Hückel molecular orbital, energy levels in units of β . Occupation of an orbital is denoted by solid arrows, levels refer to irreducible representation of the icosahedral point group	12
1.6	Corannulene (4), the motif of C_{60} molecule.	15
1.7	Pentagonal family, with the increase in number of fused pentagonal rings, systems are become highly strained (strain increases according to the order (5-8).	15
1.8	Ideal aromatic system (9) for fused system. 10 for meta, 11 for para and 12 for ortho fused system.	16

1.9	Scheme, photochemical reaction of C_{60}	21
1.10	Paracyclene unit of C_{60} , the driving force for attaining aromaticity	22
1.11	Planar substructure of C_{60} i.e. Poly-alkene (16), [5] radialene (17), and paracyclene (18).	24
1.12	X-ray crystal structure of $[C_{60}(OSO_4)(4\text{-tert-butyl pyridine})_2]$	27
1.13	X-ray crystal structure of $[Et_3P_2Pt]_6C_{60}$	28
1.14	Cyclopentadienyl (20) and allylic radical (19) are the two type of radical easily formed in the C_{60} surface.	32
1.15	X-ray crystal structure of $C_{60}Br_6$. Br atom is attached with the C_{60} surface, by 1, 4 addition.	33
3.1	Schematic diagram of the fullerene reactor	45
3.2	Section diagram of the water cooled electrode	47
3.3	Section diagram of the vacuum seal for movable electrode	48
3.4	Graphite holder design	49
3.5	FAB mass spectrum of the soxhlet mixture	52
3.6	UV-Visible spectrum of the soxhlet mixture, in benzene.	52
3.7	Yield of the fullerenes' vs He pressure, where current is fixed at 15 V and 80 A.	53
3.8	Yield of the fullerene vs current	54
3.9	FAB mass spectrum of the chromatography separated C_{60}	55

The band at 2850 and 2950 cm^{-1} arises possibly the hydrogen atom shown in inset, 3 and 4, of figure 6.26. C_{60} and its derivative produced singlet oxygen at ambient conditions which easily oxidized the 5 of figure 6.26. Geometry optimization of the oxygenated C_{60} derivatives, by Raghavachari et. al., [277] suggested that oxygen addition in the 6-5 bonds are energetically more favourable than 6-6 bonds. Therefore it may be cyclopentadiene type of intermediate, as shown in figure 6.27 4, is responsible for this cage destruction. This slow process for cycloaddition and oxidation of the double bond of C_{60} probably stem from kinetic rather than thermodynamic effects.

Conversion of hexagonal lattice from the cubic lattice is shown in figure 6.27. It shows when benzene approach for cycloaddition a strain is build up in the crystal and this indicates from the crystallite size of sunlight exposed sample, which is small (25 nm) compared to freshly prepared sample (40 nm). It is known smaller the crystallite size greater is the stress on the lattice [260, 261]. To relief this strain the crystal distorted to the hexagonal system which is shown in figure 6.27 C. Here two opposite face centered atom of (B) take the center positions. The position of the other face centered we are unable to detect, but they produce the stacking fault in the Hexagonal system (C).

6.4 Conclusions

Singlet oxygen generated using photosensitizer C_{60} is more reactive towards diene, not molecule itself. XPS studies suggested at ambient conditions some of the upper layer of C_{60} are affected and is not oxidized strongly. The aliphatic band appear in the C_{60} spectrum not due to solvent impurity, instead lattice occupied solvents are interacting with the π bond of C_{60} by 1,4 cycloaddition fashion. At ambient conditions, a $[\text{C}_{60}\dots(\text{O})_2]^-$ type adsorbed complex is formed. Electronic spectra, electrochemical and EPR studies strongly suggested that C_{60}^+ is formed. This electron deficient C_{60} form a bond with the solvent benzene which is easily oxidised by oxygen or singlet oxygen. Oxygen molecule with partial negative charge protect the C_{60} molecule from photochemical transformation.

3.10	FTIR spectrum of chromatographically pure C_{60} on KBr pellets, (above) from 4000-400 cm^{-1} and (below) 1500-400 cm^{-1}	56
3.11	Electronic absorption spectra of C_{60} ; (a) n-hexane (b) benzene	57
3.12	FAB mass spectrum of the benzene soot	59
3.13	FAB mass spectrum of the mustered oil soot	60
3.14	FAB mass spectrum of the LPG soot	61
4.1	Scheme; reaction between C_{60} and the molecules/or radicals.	73
4.2	IR spectra of the compound 1	74
4.3	Part of the FAB mass spectrum of the solid 1	75
4.4	Nitrogen percentage analysis of the orange-red compound at different time in laboratory conditions.	76
4.5	IR spectra of the compound 1, after washing with water 5 times	78
4.6	Plot optical density vs washing fraction. Optical density is measured by Griess' test.	79
4.7	EPR spectra of the compound 2. $g=2.0002$, $\delta H=200$ G. Operating Parameter $\nu=9.437$ GHz, Power=100 mW, Mod.Amplitude= 4×10 G, Gain= 2×10^4	81
4.8	X-ray photoelectron (XPS) spectra of compound 1. (a) C 1s (b) N 1s and (c) N 1s after water treatment of 1	83
4.9	Peak analysis, from spectral deconvolution of the C 1s X-ray photoelectron spectrum of 1.	84

- [90] Wasielewski , M. R. ; O'Neil , M. P. ; Lykke , K. R. ; Pellin , M. J. ; Ceruen , D. *M. J. Am. Chem. Soc.* , **1991** , *113* , 2774.
- [91] Ebbesen, T. W.; Tanigaki, K.; Kuroshima, S. *Chem. Phys. Lett.*, **1991**, *181*, 501.
- [92] Kim , D. ; Lee , M. ; Suh , Y. D. ; Kim , S. K. *J. Am. Chem. Soc.* , **1992** , *114* , 4429.
- [93] Sun , Y. P. ; Wang , P. ; Hamilton , N. B. *J. Am. Chem. Soc.* , **1993** , *115* , 6378.
- [94] Palit , D. K. ; Sapre , A. V. ; Mittal , J. P. ; Rao , C. N. R. *Chem. Phys. Lett.* , **1992** , *195* , 1.
- [95] O'Brien, M. C. M.; Chancey, C. C. *Am. J. Phys.*, **1993**, *61*, 688.
- [96] Tutt. L. W. ; Kost , A. *Nature* , **1992** , *356* , 225.
- [97] Wang , Y.; *Nature*, **1992**, *356*, 585.
- [98] Hwang , K. C. ; Manzerall. D. *Nature* , **1993** , *361* , 138.
- [99] Wudl . F. *Acc. Chem. Res.* , **1992** , *25* , 157.
- [100] Allemand , P. M. ; Koch , A. ; Wudl , F. ; Rubin , Y. ; Diederich , F. ; Alvarez , M. M. ; Anz , S. J. ; Whetten , R. L. *J. Am. Chem. Soc.* , **1991** , *113* , 1050.
- [101] Dubois , D. ; Kadish , K. M. ; Flanagan , S. ; Wilson , L. J. *J. Am. Chem. Soc.* , **1991** , *113* , 7773.
- [102] Dubosis, D., Moninot, G., Kutner, W., Jones, M. T., Kadish, K. M. *J. Phy. Chem* **1992**, *96*, 6126.
- [103] Xie, Q., Cordero, E. P., Echegoyen, L., *J. Am. Chem. Soc.*, **1992**, *114* 3978.
- [104] Diedrich, F; Whetten, R. L. *Angew. Chem. Int. Ed. Engl.*, **1991**, *30*, 678
- [105] Jehoulet , C. ; Bard , A. J. ; Wudl , F. *J. Am. Chem. Soc.* , **1991** , *113* , 5456.

- [224] O'Brien, S. C.; Heath, J. R.; Curl, R. F.; Smalley, R. E. *J. Chem. Phys.* , 1988 , 88 , 220.
- [225] Juha. L.; Krasa, J.; Iaska, L.; Hamplova, V.; Kubat, P. *Appl. Phys. B*, 1993, 57, 83.
- [226] Orfanopoulos, M.; Kambourakis, S. *Tet. lett.*, 1994, 35, 1945.
- [227] Tokuyama, H.; Nakamura, E. *J. Org. Chem.*, 1994, 59, 1135.
- [228] Arai, T.; Murakami, Y.; Suematsu, H.; Kikuchi, K.; Achiba, Y.; Ikemoto, I.; *Solid State Commun.*, 1992, 84, 827.
- [229] Duclos. S. J.; Haddon, R. C.; Glarum, S. H.; Hebard, A. F.; Layons, K. B.; *Solid State Commun.*, 1991, 80, 481.
- [230] Nissen, M. K.; Wilson, S. M.; Thewalt, M. L. W. *Phys. Rev. Lett.*, 1992, 69, 2423.
- [231] Vassalo, A. M.; Pang, L. S. K.; Cole-Clarke, P. A.; Wilson, M. A. *J. Am. Chem. Soc.*, 1991, 113, 7820.
- [232] Zhou, P.; Rao, A.M.; Wang, K. A.; Robertson, J. D.; Eloi, C.; Meier, M. S.; Ren, S. L.; Bi, X.- X.; Eklund, P. C.; *Appl. Phys. Lett.*, 1992, 60, 2871.
- [233] Frimer, A. A. *Chem. Rev.*, 1979, 79, 359.
- [234] Tong, W. M.; Ohlberg, A. A.; You, H. K.; Williams, R.s.; Anz, S. J.; Alvarez, M. M.; Whetten, R. L.; Rubin, Y.; Diederich, F. N. *J. Phy. Chem.*, 1991, 95, 4709.
- [235] K. Kamaräs, Akselord, L.; Roth, S.; Mittelbach, A.; Hönle, W. ; VoSchnering, H. G. ; *Chem. Phys. lett.*, 1993, 214, 338.
- [236] Atake, T.; Tanaka, T; Kawaji, H.; Kikuchi, K.; Saito, K.; Suzuki, S.; Aciba, Y.; Ikemoto, I.; *Chem. Phy. Lett.*, 1992, 196, 321.
- [237] Gorun, S. M.; Greegan, K. M.; Sherwood, R. D.; Cox, D. M.; Day, V. W.; Day, C. S.; Upton, R. M.; Briant, C. E. *J. Chem. Soc.; Chem. Commun.*, 1991, 1556.

4.10	Peak analysis from spectral deconvolution of the O 1s X-ray photoelectron spectrum of compound 1 . (a) Without water treatment. (b) Washed with water.	86
4.11	Reaction mechanism of NO ₂ addition in C ₆₀ . V is the isolated product. Here only one nitro group is shown, but other nitro and hydroxy functionality also present in this moiety.	88
5.1	Scheme; reaction between the metal hexacarbonyl and C ₆₀	97
5.2	Electronic absorption spectra; (a) Progress of the reaction between C ₆₀ and W(CO) ₆ in benzene on sunlight irradiation. Spectra are recorded in 5 minutes interval. (b) Spectrum of the above solution, which is continued for 1 hours and kept in, recorded after 24 hrs.	98
5.3	UV-visible spectra of M(CO) ₆ , where M=Cr, Mo and W and C ₆₀ in benzene. (a) At ambient conditions (b) Exposing the solutions for 45 minutes in sunlight. W(CO) ₆ shows the reactivity.	100
5.4	Electronic absorption spectra; W(CO) ₆ and C ₆₀ in benzene are irradiated with 514, 488 and 454 nm laser pulses.	101
5.5	Part of the FAB Mass spectrum of the compound.	103
5.6	FTIR spectrum of the compound 1	104
5.7	UV-visible spectrum of the compound in benzene	105
5.8	CV of the (a) C ₆₀ and (b) complex. Glassy carbon working electrode, scan rate 50 mV/s and 0.1 M TBAP supporting electrolyte. Asterisk indicates unidentified peak.	107

5.9	CV of the blank $W(CO)_6$. Glassy carbon working electrode, (a) scan rate 50 mV/s and (b) scan rate 100 mV/s using 0.1 M TBAP supporting electrolyte.	108
5.10	XPS Peak analyses of the compound, (a) C 1s (b) O 1s.	111
5.11	XPS binding energy, W 4f _{7/2} , W 4f _{5/2} of the complex.	112
5.12	FTIR spectrum of the aging compound	114
5.13	FTIR spectra of the compound. (a) Expanded spectrum in the carbonyl region. (b) Spectrum in the 800-400 cm ⁻¹ region.	117
5.14	(a) Orbital correlation diagram of metal carbonyl (ref.[205]). (b) Movement of the d-orbital towards the vacant side (ref.[205])	119
5.15	(a) Possible Excited state in the metal center (ref.[208]). (b) Reaction path for metal hexacarbonyl in photochemical reaction (ref. [222].	120
6.1	Gas chromatograph: (a) C ₆₀ in CCl ₄ (b) diene and (c) reaction mixture.	135
6.2	IR spectra: (a) diene 2 and (b) reaction mixture 3	136
6.3	(a) Deconvolution analyses; (a) C 1s and (b) O 1s, of the XPS signal of C ₆₀ 138	
6.4	IR spectra: Record after (a) after separation (b) 7 days (c) 25 days days. Intensity of the band at 1530 cm ⁻¹ remains constant.	141
6.5	IR spectra record in presence of sunlight; (a) without exposed (b) exposed for 2 hours and (c) irradiation for 5 hours.	142
6.6	IR spectra; (a) C ₆₀ washed in benzene (b) washed in benzene (c) 5 times dissolved in benzene (d) 5 times in CCl ₄ (e) twice with CS ₂	143
6.7	X-ray powder pattern of freshly prepared C ₆₀	146

6.8	X-ray powder pattern of the C_{60} in presence of sunlight	148
6.9	X-ray powder pattern of C_{60} taken after 25 days	151
6.10	X-ray Powder pattern of C_{60} after dissolved in CS_2	152
6.11	X-ray powder diffraction of the (a) washed in ether (b) 5 times washed in benzene (c) immersed in ether for 24 hours (d) record (c) after 45 minutes.	153
6.12	EPR spectra of the solid C_{60} . $\nu=9.4$ GHz, mod; 1.6×1 G; Power=20 mW. (a) Freshly prepared $g=2.003$, $\delta=1.8$ G and gain 5×10^3 (b) after 7 days $g=2.0029$, $\delta=1.5$ G and gain 8×10^3 and Spin concentration decreases by a factor 6 from (a). (c) Spectra recorded after 30 days where spin concentration decreases by 78% from (a), other parameters are same of the above. (d) At liquid Nitrogen temperature.	155
6.13	(a) Simulation of the figure 6.12 (a) in Lorentzian function. (b) EPR spectrum of the soxhlet mixture at $\nu=9.4$ GHz, mod.=1.6 G, power=20mW. ca $g=2.0033$ and $\delta H=1.7$ G.	156
6.14	EPR spectra of the soot, mod=1.6 G, power 20 mw, (a) collected in dark at ambient conditions (b) mod= 1.6×10 G, gain= 5×10^4 (c) after 24 hours, sample cover with a black paper (d) kept 24 hours in presence of light. .	157
6.15	EPR spectra of the soot (a) collected same as previous figure (b) record in the same scale of the previous figure (c) kept 24 hours in presence of light.	159
6.16	EPR spectra, soot collected in dark cover with a black paper. (a), (b) measured in the identical condition of figure 6.14 (a),(b) and figure 6.15 (a),(b). (c) Record after 24 hours. (d) Record after 72 hours from (a) . (d) Record after 96 hours from (a). (e) Signal, (d), in liquid nitrogen temperature.	161

6.17 (a) Lorentzian line shape analysis of figure 6. 16 (b) and 6. 16 (d). (b) Gaussian line shape analysis of figure 6. 16 (b) and 6. 16 (d)	162
6.18 Cyclic voltammogram of the C ₆₀ film. (a) Film prepared at ambient conditions (b) Voltammogram recorded in the continuous cycling. Pt working electrode, scan rate 200 mV/s and TBAP, supporting electrolyte.	164
6.19 Cyclic voltammogram of the sunlight irradiated (a) Pt-electrode (1 mm dia.) (b) Pt-wire. Supporting electrolyte 0.1 M TBAClO ₄ and scan rate 200 mV/s.	165
6.20 Mechanism of the C ₆₀ film in electrochemical process. (a) At ambient conditions and (b) on sunlight exposure.	167
6.21 UV-Vis spectra of aging C ₆₀ : (a) acetonitrile (b) Di-ethyl ether (c) Iso-propanol (200-450 nm) and (d) Iso-propanol (380-1100 nm).	171
6.22 C ₆₀ cationic spectra (a) benzene (750-1100 nm) (b) Benzene (400-750 nm) (a) after flash chromatography of the (a). (d) In acetone	172
6.23 Part of the FAB mass spectrum of the ether washed C ₆₀	175
6.24 Isomeric structure from S-T transformation.	175
6.25 Oxygen and solvent interaction with C ₆₀	177
6.26 Mechanism of cycloaddition with benzene and C ₆₀ . 2 oxygenated C ₆₀ , 3 benzene interaction with cyclohexadine unit of C ₆₀ , 4 benzene interaction with cyclopentadiene and 5 Oxygenated products (shown in the inset). Hydrogen positions are shown in the inset.	179
6.27 Transformation of fcc to hcp. A is fcc, B is fcc where solvent interacted with the C ₆₀ atom and produce strain in the lattice. C is hexagonal system with solvated molecules.	180

7.1	Delocalization energy vs ring size	183
-----	--	-----

List of Tables

1.1	Calculated and experimental bond length (\AA) of C_{60}	13
1.2	C_{60} infrared line position (cm^{-1}) and Raman line position (cm^{-1}).	17
1.3	Solubility of C_{60} in various solvents	18
1.4	Wave-lengths and molar extinction coefficients of C_{60} , in electronic absorption spectrum.	20
1.5	Photophysical properties of C_{60}	20
3.1	Dimensions of the reactor accessories of figure 3.1	44
4.1	C 1s peak analysis of the compound 1	89
4.2	O 1s peak analysis.	89
4.3	O 1s peak analysis after washing the compound 1 with water.	90
5.1	Peak potential of the C_{60} and complex.	109
5.2	C 1s peak summary of the compound.	113
5.3	O 1s peak summary of the compound.	115

6.1	C 1s peak analysis of the ageing C_{60}	140
6.2	O 1s peak analysis of the ageing C_{60}	140
6.3	IR absorption band of C_{60} , after washing five times with C_6H_6 (figure 6.6 (c).	145
6.4	X-ray diffraction results of pure C_{60} (figure 6.7).	147
6.5	X-ray diffraction results of sunlight irradiated C_{60} (figure 6.8).	149
6.6	Peak potential and peak separation for the first and second reduction wave in figure. 6.a.	166
6.7	Peak potential and peak separation of figure 6.18 (b)	168
6.8	Peak potential and peak shifts in figure 6.19(a)	168
6.9	Peak potential and peak shifts in figure 6.19 (b)	168
6.10	Wave-length of C_{60} in n-hexane at different conc.	174

Chapter 1

Introduction

In late 1990, Krätschmer, Huffman and co-workers reported the isolation of macroscopic quantities of C_{60} and other fullerenes [1]. The availability of significant quantities of fullerenes has sparked a variety of research programmes throughout the world, ranging from studies of the fundamental properties of the molecule to application based work in several industries. Probably no chemical research has attracted as much as positive publicity in the popular press as well as in scientific journals related to Buckminster fullerenes and its rapidly growing family of related molecules [2]. C_{60} have been awarded ‘Molecule of the year’ for the year 1991 from Science magazine [3].

The molecule gained its fame in the year 1990, due to the development of bulk synthesis method, however buckminsterfullerene was of great interest to the research community from the year 1985. Kroto, Smalley and their co-workers at Rice University observed some strange properties of the carbon clusters that the mass spectrum contained only even number of carbon atoms ranging from 30 to 100 and in addition, condition were found for the cluster having 60 carbon atoms that it’s intensity become 40 times as high as nearby even clusters [4]. They produced these clusters by vaporizing the graphite with the irradiation of pulse laser followed by instantaneous cooling with the jet of a He gas and finally scanned through mass spectrometer. It was proposed that the special cluster C_{60} has the structure of a truncated icosahedron, as shown in figure

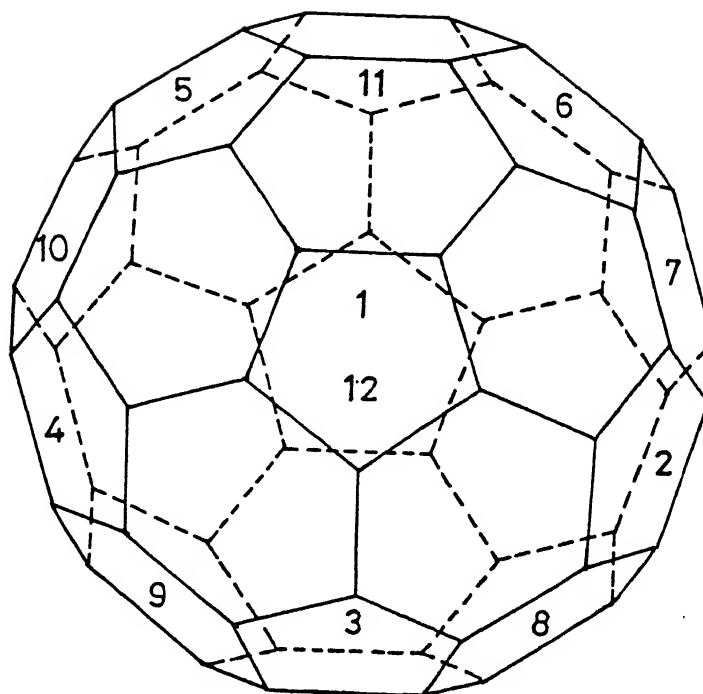


Figure 1.1: The structure of C_{60} , buckminsterfullerene, the archetype of the fullerene family. It has truncated-icosahedron symmetry, (I_h), as does the European football.

1.1, a closed sphere of twenty hexagons and twelve pentagons where the pentagons does not have any adjacent pentagons and all the carbon atoms are equivalent. It was named Buckminsterfullerene after the architect R. Buckminster Fuller, who invented structurally similar geodesic domes [5].

1.1 Shape

The carbon cluster was generated by laser ablation of graphite only even numbered clusters in the C_{60} - C_{600} ion range were present and these even-numbered species containing

a central cavity called 'fullerenes' [6]. Specifically, it was proposed that these molecules with the composition C_{20+2x} can take the stable form of hollow closed nets composed of 12 pentagons (five members rings, 5MRS) and x hexagones (six membered rings, 6MRS). Geometrically, the buckminsterfullerene (buckyball) is a truncated regular icosahedron (I_h). The truncated icosahedron is familiar to sport fans. A soccer ball is made by sewing together pentagonal and hexagonal patches of leather in a configuration that yields a truncated icosahedron. In the C_{60} molecule, each vertex of the truncated icosahedron is occupied by (figure 1.1) a carbon atom and each atom is bonded to three other carbon atom along the edges of the solid. The C_{60} molecule itself, with its 60 carbon atoms, has 12 pentagonal faces and 20 hexagonal faces. C_{70} , (D_{5h}) which has oblong shapes of a rugby football, consists of 12 pentagons and 25 hexagons. There are smaller fullerene molecules such as C_{44} , with 12 pentagons and 12 hexagons and also much larger molecules, such as giant fullerene C_{540} , with 12 pentagons and 260 hexagons. These number are not an accidental incident, it is a consequence of a theorem of the great 18th century mathematician L. Euler. According to it a fullerene polyhedron with n vertices, have 12 pentagonal and $(n/2 - 10)$ hexagonal faces and $3n/2$ edges [6].

A large number of molecular and electronic properties of buckminsterfullerene and its isomer, as well as other fullerenes were reported in the following years [7]. Initially this proposal was hard to accept because whole initial proposition was based on mass spectroscopic evidence. Though experimental studies such as photoelectron spectroscopy of C_{60}^- [8], gas phase ultraviolet spectra [9], gas phase chemical reactivity [10] and production and dissociation of endohedral metal complexes of carbon cluster [11] give indication about the hollow cage structure of the carbon cluster. All these reports unequivocally support the stability, rigidity as well as geometry of the C_{60} molecule. Unfortunately, these studies did not suggest an elegant test to confirm the structure of C_{60} . However, calculation of the vibrational frequencies [12-15] and electronic absorption [9] of buckminsterfullerene became important for identifying it after it had been synthesized in quantity.

1.2 Availability of fullerene from various source

1.2.1 Artificial Soot

The buckminsterfullerene story began in interstellar space. In 1983, D. Huffman and Krätschmer, shared an interest in the properties of soot formed by heating graphite [18]. They were keen to find out if such soot could form in interstellar space [17], they heated graphite rods electrically in a low-pressure atmosphere of helium or argon inside a bell jar. From the resulting clouds of black smoke they collected thin layers of soot on the surfaces of quartz discs. They transferred these discs to a UV-visible spectrophotometer and noticed that their artificially produced soot showed some extra 'humps' in its absorption spectrum. Krätschmer had thought that the extra humps might be due to some contamination of their apparatus with oil vapour from the vacuum pump, and when they lowered the pressure inside the bell jar, the humps did indeed become less visible. Everything seemed to point to an experimental artifact and they soon turned their attention elsewhere.

In the mean time in 1985, buckminsterfullerene proposal was published and in the subsequent years the UV-Visible [9], IR [12, 14, 15] and photoelectron spectra [8] were recorded from different laboratories. At a conference in the year 1988 on interstellar dust, Huffman proposed that the extra humps in the ultraviolet spectrum of carbon soot, which he and Krätschmer had got before six years were due to buckminsterfullerene [16]. Afterwards they measured the mass spectrum and the ultraviolet and infrared absorption spectra of the soot formed in the bell-jar, which fairly closed to the prediction for buckminsterfullerene. They confirmed their results from the IR spectra of the soot from the rods of carbon-13 [19].

A large number of research group were also successful to prepare the fullerene soot by other methods which are :

(i) Laser ablation of graphite [20] : Graphite are vaporized by a high frequency laser

pulses and the resulting carbon vapours are annealed by a furnace. This experimental assembly is the considerable modification of the 1985's experimental set up. In this technique yield of the fullerenes became considerably high but the experimental set up was quite expensive for which this method has not gained much popularity.

(ii) Sunlight evaporation of Graphite [21, 22] : Graphite is evaporated by sunlight radiation where flux density of sunlight is increased by a hemispherical radar. This reactor is expensive but near future large scale synthesis may be possible by this method.

(iii) Radio-frequency (r.f) method [23] : Evaporation of the graphite is done by a radio-frequency source.

1.2.2 Natural soot

Chemists are now speculating that buckminsterfullerene might be found from a lighting candle but still now fullerenes are not obtained from the soot produced at ambient conditions. Some research group have been able to produce fullerene soot from (i) combustion of benzene and acetylene in a fixed ratio of oxygen/argon [24, 25] (ii) naphthalene pyrolysis [26] (iii) chemical vapour decomposition of the toluene extract of ether insoluble camphor soot [27].

1.2.3 Geological Samples

On the earth, natural fullerenes C_{60} and C_{70} have been identified in fulgurite [28] (a glassy rock that form where lightning strikes certain soils) and shungite [29] (a highly metamorphosed carbon rich rock within precambrian sediments found in Karelia in Russia). C_{60} and C_{70} were also detected in a 1.85 billion year old Sudbury impact structure in Ontario, Canada [30]. The oxidation of the fullerenes during the 1.85 billion years of exposure was apparently prevented by the presence of sulfur in the form of sulfide-silicate complexes associated with the fullerenes. Fullerenes are also found from the Cretaceous-Tertiary (K-T) boundary layer [31], this K-T boundary layer may have originated in the

extensive worldwide wildfires that were associated with the cataclysmic impact event that terminated the Mezozou era about 65 million year ago.

1.2.4 Astronomical Samples

The molecule C_{60} , was discovered during laboratory experiments motivated by problems associated with what kind of carbon particles present in the interstellar dust [32]. Scientist speculated that C_{60} might be abundant in clouds of red stars and therefore it belongs among the older molecules [33]. Recently another report came in regarding the presence of C_{60}^+ ion in the meteorite [34].

1.3 Fullerene Separation

The soluble portion of the soot is extracted in common non-polar organic solvents by soxhlet technique or ultracentrifugation and the separation of C_{60} and C_{70} are done by column chromatography [35-39]. Commonly, separation is achieved with hexane-toluene (95-5, v:v)^{25a} mobile phase on neutral alumina but it is tedious and time consuming. Due to the low solubility of C_{60} in hexane, several liters of eluent is required. State-of-the art of individual fullerene separation from soxhlet mixture is an active area of research through out the world [40]. The use of activated charcoal/silica gel columns allows the relatively facile separation of the gram quantities of pure C_{60} and give better crystallinity than alumina column [41].

Another area for fullerene separation is the host-guest chemistry which offers the promise of cheap and convenient methods for the rapid isolation of highly pure fullerenes. The fundamental behind it is that certain cyclic host molecule posses cavities having the correct dimension for the inclusion of a fullerene guest. The first successful purification of fullerene by host-guest chemistry is published from two independent groups in the same year [42, 43]. Both relied on the specificity exhibited by calix[8] arene for C_{60} to develop

preparatively useful methods for the purification of fullerenes. The nature of bonding between the host and the guest fullerene is not clear but primary interaction comes from one π -bonding of one aromatic surface of one guest. The size selectivity is so important that in a soxhlet mixture γ -cyclodextrins (γ -CD, cavity diameter 850 pm) form complex with C_{60} . Neither the inclusion of C_{70} is observed, nor complex formation with α cavity (500 pm) or β -CD cavity (650 pm) is detected [44]. This kind of size selective purification is very much useful for the specific purification of the higher fullerene. Preparation of tangible quantities (~ 1 g) of C_{70} from a silica gel/charcoal stationary phase in the column chromatography makes C_{70} more accessible to every chemist [45].

1.4 The mechanism of Fullerene Formation

Experiments using mixture of $^{12}\text{C}/^{13}\text{C}$ labeled graphites demonstrate that the rate of carbon isotope incorporation in the C_{60} molecule follow the Poission distribution [46, 47]. This implies that in any phase of the growth process, carbon atom must be involved in the construction of fullerenes. After a certain number of C atom ($n \geq 30$) the C_n linear chain formation is unfavorable than the C_n clusters formation due to entropy factor.

Why only the even number carbon atom formed these cage structures from graphite sheet is a central mystery. Smalley proposed a mechanism for the formation of fullerene from the carbon atoms, which is known as 'pentagonal road model', and is widely acceptable mechanism till date [48]. Carbon atoms in graphite are arranged in a honeycomb pattern of hexagons, and the plane was tilted in a flat sheet during vaporization. Any atom in the interior of such a sheet at the edge have dangling bonds that are highly reactive. One way to accommodate the dangling bonds is the sheet to curl, so that nearby hexagons are brought together. According to 'pentagonal road model' energetically most favourable form of an arbitrary graphite sheet is characterized by (1) only five and six-membered ring as structural elements (2) as many five membered rings as possible and (3) an avoidance of unstable pentalene units [48].

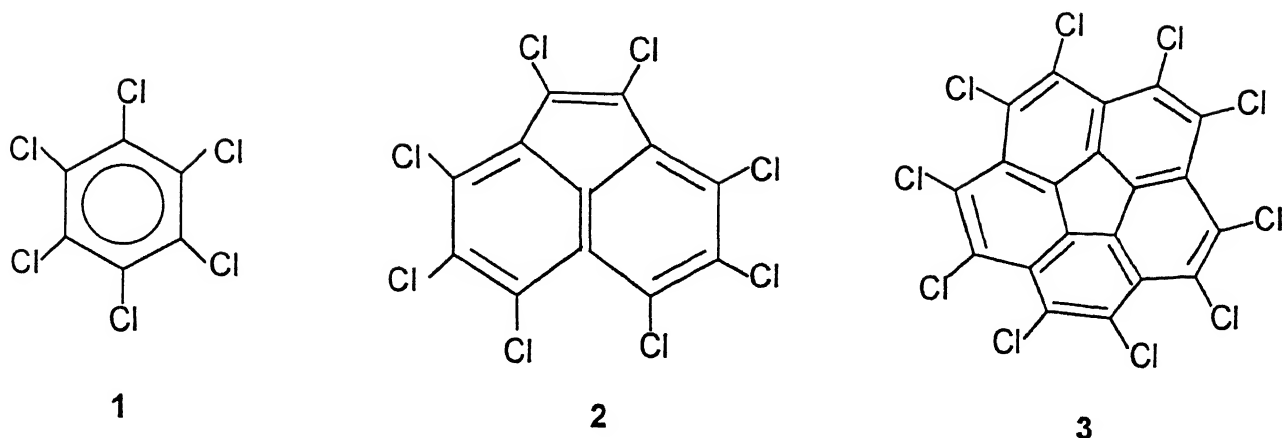


Figure 1.2: Compound (3), substructure of C_{60} .

Reactive components are mixed with the buffer gas helium, the compounds produced in this process give indication about the possible intermediates of the fullerenes formation. When graphite vaporization is performed in the presence of Cl_2 , besides small amount of fullerene ($\leq 5\%$), the perchlorinated cyclic compounds **1-3** are isolated in good yields [49] which is shown in figure 1.2. The decachloroanthracene (**3**), is the essential part of the fullerene structure. This five membered ring in the above structure supports the pentagonal-road mechanism.

Bowers et. al. from their 'gas phase ion chromatography' experiments proposed another mechanism for the formation of fullerene which is known as 'fullerene road model' [50]. This ion chromatograph can separate ions that have the same mass but differ in isomeric structure of electronic configuration. In figure 1.3 these results are shown schematically. This scheme highlights carbon initially from linear chains followed by planar rings system and collisions between the size selective rings produce the fullerenes [51, 52].

Fullerenes are synthesized during graphite vaporization only under a narrow set of

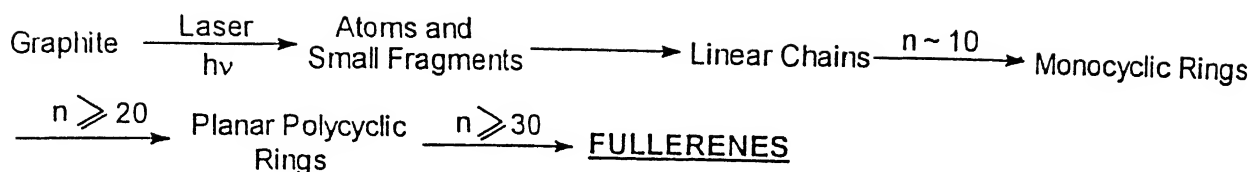


Figure 1.3: Scheme of the fullerene formation, during graphite vaporisation.

experimental conditions. Both temperature of the plasma and pressure of the helium gas are critical for fullerene formation [53]. The readiness with which buckminsterfullerene formed in high temperature plasma is a big question to the scientist. Though a number of possible mechanism have been reported but no complete answer is still emerged about how fullerenes actually grow and form. Most astonishing fact is that under which condition fullerene is created, at plasma temperature of over 3000°C where the $T\Delta S$ term should favour the creation of highly symmetric molecules over the structurally little organized carbon vapour [54].

1.5 Electronic Structure of C_{60}

If the fullerenes are composed solely of conjugated six-membered rings (6MR) such as occurs in benzene and graphite, they would be like an alternate hydrocarbons. In that case the energy levels of the occupied and unoccupied molecular orbitals (HOMO and LUMO) are symmetrically disposed about the energy zero. The homologation of benzene rings are ultimately produced a surface like graphite.

In the graphite vaporization (fullerene preparation) a large number of dangling bonds are produced and in order to remove the dangling bonds entirely, the edges of the surface must be eliminated, and this requires the surface to close on itself to produce a spheroid. The curvature imposed on the surface modified the electronic structure of the sheet in two ways [55-60], (i) electronic structure of the carbon atoms and (2)

bonding in the cluster. The curvature of the surface at a carbon atom is expressed by the pyramidalization angle $[(\theta_M - 90)^\circ]$ [57, 58], which is shown figure 1.4. As the σ bonds at a conjugated carbon atom deviate from planarity, the primary effect is a change in hybridization, a rehybridization of the carbon atom takes place so that a π orbital is no longer of purely p-orbital character and the σ -orbital no longer contain all of the s - orbital character. Figure 1.4 shows, the extent of hybridization depends on the pyramidalization angle. It shows the fullerenes are of intermediate hybridization ($s^m p$) [56, 58] where,

$$m = \frac{2 \sin^2(\theta_{\sigma\pi} - \pi/2)}{1 - 3 \sin^2(\theta_{\sigma\pi} - \pi/2)}$$

This equation shows that a constant amount of s character mixed into the π - molecular orbitals formed from the carbon atomic orbitals of C_{60} .

In figure 1.5 the non alternate character of C_{60} is reflected in the asymmetric distribution of the (HOMO) and (LUMO) about the zero of energy [55]. In C_{60} there are three MOs at -0.139β (t_{1u}) and three at -0.382β (t_{1g}), and thus it is suggesting that it will add up to twelve electrons under suitable conditions. However, calculated reactivity index is low, this suggest that the molecule has sufficient resistance from the chemical attack. C_{60} in its ground state has a lot of degenerate orbitals however on electron addition the LUMO will not undergo a distortion to a point group of lower symmetry as a result of the second-order Jahn-Teller effect [55].

Since its discovery in 1985, C_{60} has been the subject of many quantum mechanical calculations [55-66]. In fact, the free electron model highlight's the essential feature of the electronic structure of the molecule e.g the symmetry and the associated degeneracy of all the molecular orbitals. The bond lengths are calculated by several molecular orbital (MO) calculations which is given in table 1.1. These calculation also provided reliable structural and spectral parameters, in particular those associated with vibrational, electronic and photoelectron spectra. All the calculation have predicted the two distinct bond lengths, close-shell ground state and appreciable HOMO-LUMO gap.

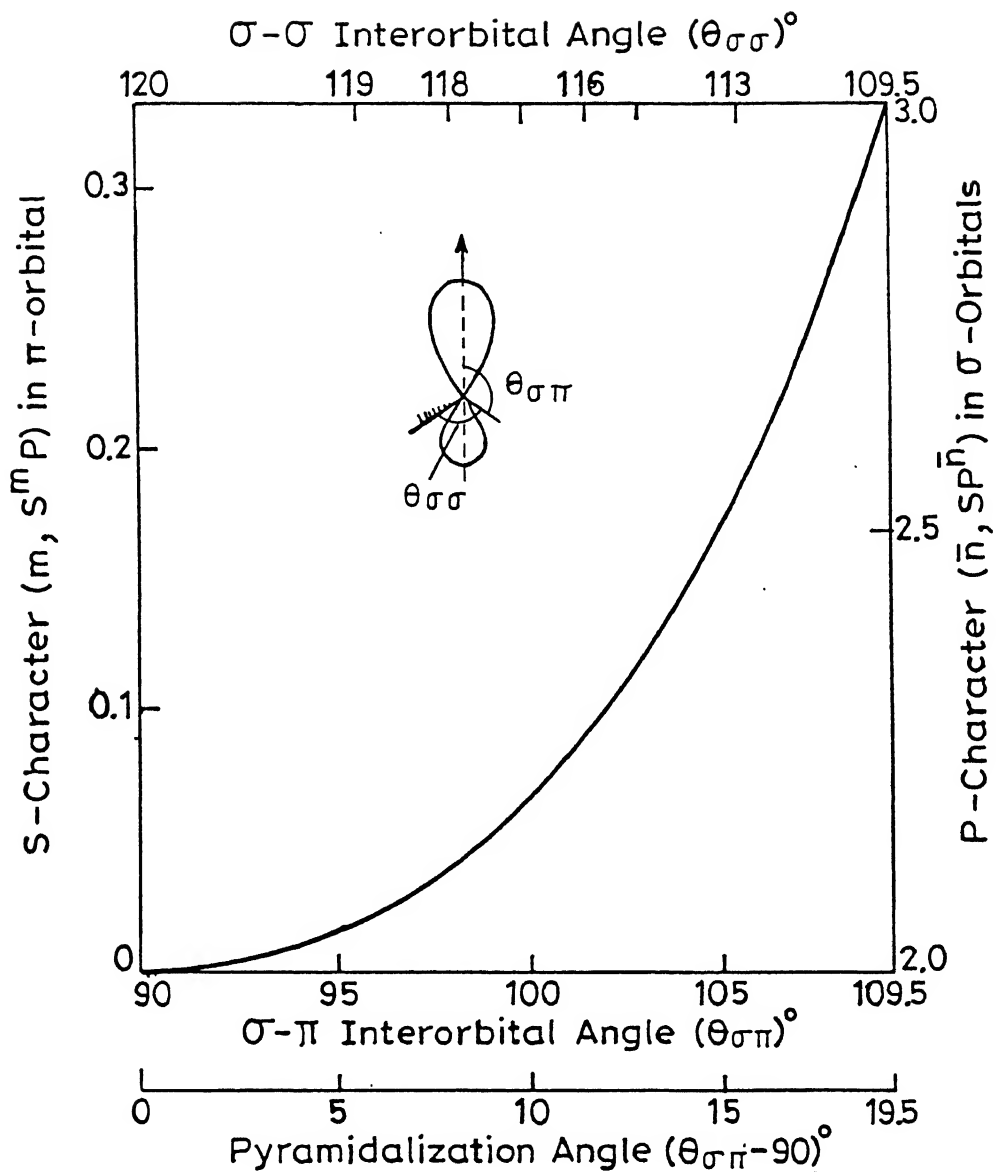


Figure 1.4: Relationship between the $\sigma - \sigma$ and $\sigma - \pi$ interorbital angles and the hybridization at a carbon atom between the extremes of planar and tetrahedral geometry in C_{3v} .

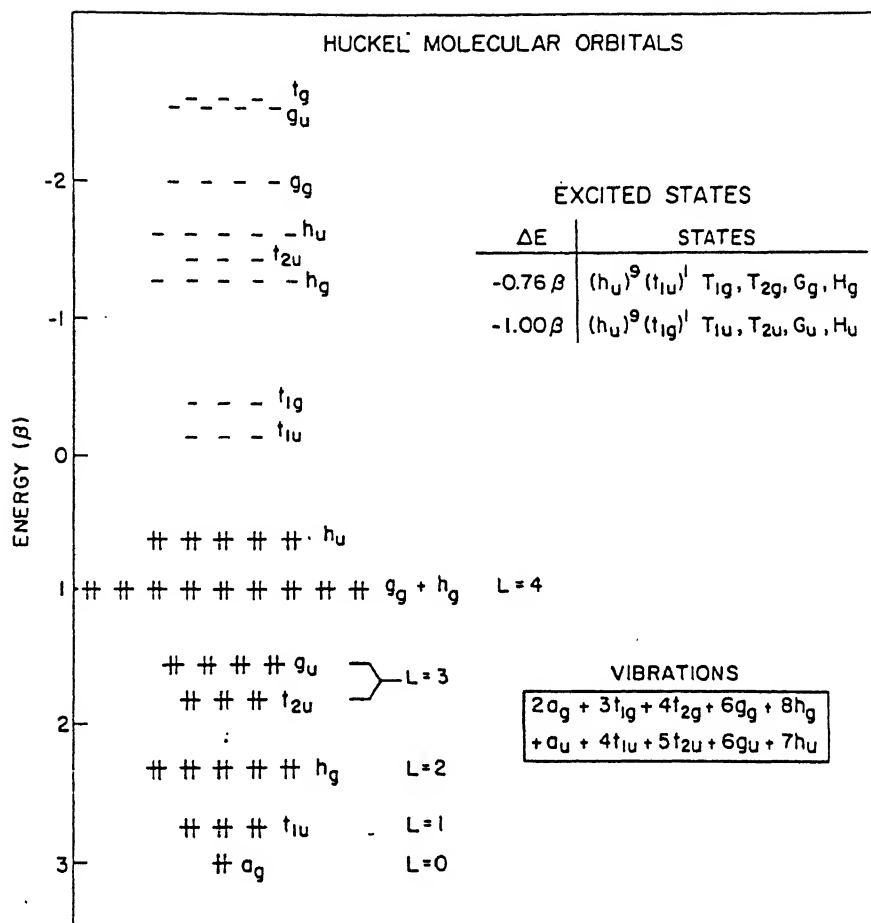


Figure 1.5: Hückel molecular orbital, energy levels in units of β . Occupation of an orbital is denoted by solid arrows. levels refer to irreducible representation of the icosahedral point group

Table 1.1: Calculated and experimental bond length (\AA) of C_{60} .

Calculated			
Method	$r_1/6-6$	$r_2/6-5$	References
MNDO	1.400	1.474	[61]
AMI	1.385	1.464	[62]
PRDDO	1.360	1.436	[63]
HF/STO-36	1.376	1.463	[64]
HF/DZP	1.372	1.453	[65]
HF/TZP	1.370	1.445	[66]
MPZ	1.405	1.445	[66]
Experimental			
Solid state	1.40	1.45	[67]
NMR			
Single crystal	1.340		[68]
X-ray diffrac.			
Electron diffrac.	1.401	1.458	[69]
Neutron powder	1.366-1.412	1.420-1.487	[70]
diffraction	or 1.391	or 1.455	

1.6 Thermodynamic and Kinetic Stability

Solid C_{60} has remarkable stability and can be sublimed without decomposition at 400°C under reduced pressure[71]. The thermodynamic stability of C_{60} by a variety of quantum mechanical and molecular mechanics methods produced greatly diverging results; the calculated heat of formation ΔH_f° at 298 K vary between $973 \text{ kcal mol}^{-1}$ ($16.2 \text{ kcal mol}^{-1}$ per carbon atom) to $263 \text{ kcal mol}^{-1}$ [71-74]. But most reasonable value seems to be resolved by Beckhans et.al by their combustion studies of highly pure crystalline C_{60} which provide $\Delta H_f^\circ = 544.99 \text{ kcal mol}^{-1}$. This experimental result is in good agreement with the ΔH_f° calculated from MM3 force field [73]. Despite this large thermodynamic instability, crystalline C_{60} is kinetically a perfect stable molecule under ambient conditions.

Ion-beam collision experiments, in which C_{60}^+ or C_{60}^- collides with silicon or graphite surface at speeds up to 50000 km/hr show high inelasticity of the ions, but

no evidence for impact induced fragmentation [75] This behavior differs from the other molecules or similar sized cluster ions that have been tested, including benzene and naphthalene, which show fragmentation under these drastic conditions suggested that the C_{60} structural framework is highly stable. The face centered cubic (fcc) structure of C_{60} are stable upon hydrostatic compression to at least 20 GPa indicating bulk C_{60} is a solid composed of extremely hard pseudospherical molecules bonded by weak Vander Waals interaction [76].

1.6.1 Valence Bond Approach

The extra stability of the fullerene molecule is best described by the valence bond theory. The validity of the application of the Hückel rule to three dimensional structure is still not clear. According to $(4n+2)\pi$ electrons, C_{50} and C_{70} are predicted to be aromatic and presumably more stable than other fullerenes. Ironically C_{60} is the most stable among the fullerene family. Therefore application of the Hückel rule alone as a guide to stability will be unsatisfactory. Polyaromatic hydrocarbons with five and six membered rings are abundant but three and four-membered rings are very unstable and higher membered rings are likely to occur readily where cages must contain 12 five membered rings with variable hexagons according to Euler rule. The bonding or connectivity in a big molecule is difficult to understand for that Randic suggested the nature of the smallest circuit within a molecule reflects the overall classification and behavior [77].

Closed-cell electronic structures are likely to be preferred and cages with $60 + 6k$ atoms (where k is 0 or 2) can have close-cell electronic structure [60]. The networks should conform to the usual valence requirements of carbon, in that each atom should be three connected to other atoms by one double and two single bonds therefore many resonance structure are possible [78].

The corannulene (4) is one of the motif of the C_{60} molecule, is shown in figure 1.6, indicates that the structure in which pentagon is completely surrounded by hexagon is

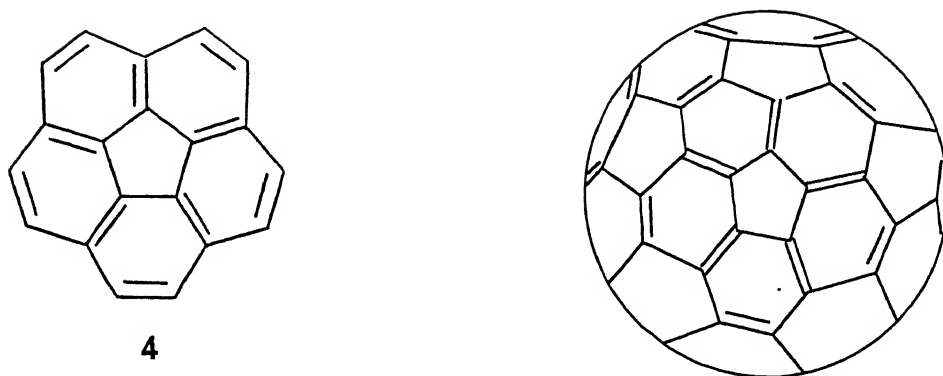


Figure 1.6: Corannulene (4), the motif of C₆₀ molecule.

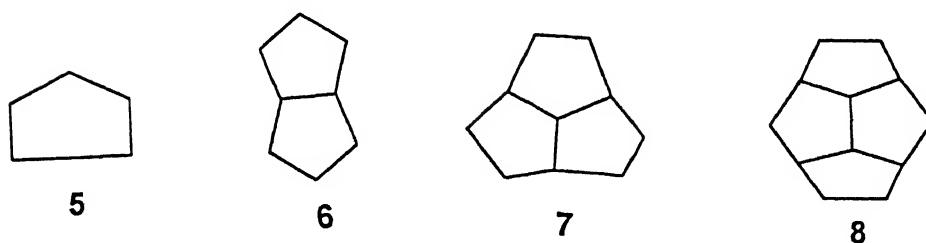


Figure 1.7: Pentagonal family, with the increase in number of fused pentagonal rings, systems are become highly strained (strain increases according to the order (5-8)).

stable [79]. This observation suggests that a cage in which all 12 pentagons are completely surrounded by hexagons has optimum stability and one in which pentagons are fused, likely to be less stable. When fused pentagons are considered the local strain increases according to the order (5-8), as shown in the figure 1.7. This is known as isolation pentagonal rule (IPR) and is very rational for the stability of fullerene, its isomers and fullerene derivatives.

C₆₀ and higher fullerene can have large number of isomers and according to Taylor, the most stable isomer is that containing the highest number of benzenoid rings i.e. those with alternating double and single bonds with all exo-cyclic bonds single, are ideally

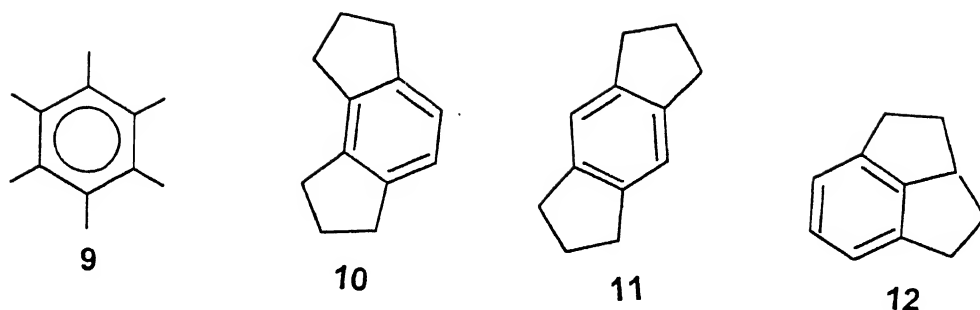


Figure 1.8: Ideal aromatic system (9) for fused system. 10 for meta, 11 for para and 12 for ortho fused system.

aromatic [80, 81]. From the above criteria it was considered in a 'meta' relationship (10, figure 1.8) this allows for the ideal bond distribution in the adjacent hexagonal rings. In contrast if they are in a 'para' or 'ortho' relationship (11, 12, figure 1.8) the ideal bond distribution cannot be achieved. So, it is possible to account for the stability of the fullerene by applying the method hitherto applied to planar aromatics i.e, the highest proportion of benzenoid ring are the most stable. Only C_{60} has this perfect bond alternation in each of its twenty hexagonal rings and is thus the most stable fullerene.

1.7 Vibrational and Raman Spectra

The high symmetry of C_{60} makes IR and Raman spectra to be unusually simple. There are 174 normal modes in C_{60} , many have identical energies, and so they cannot be distinguished from one another in the spectrum. There are 46 potentially distinguishable vibrational energy levels, but group theoretical arguments show only four three-fold degenerate t_{1u} vibrations give rise to observable lines in the infrared spectrum [15, 82, 83]. After C_{60} was available in quantity Krätschmer and co-workers¹ measured its infrared spectrum, which agreed with the theoretical calculations of the C_{60} vibrational frequencies.

The molecule has only two degrees of freedom that conserve I_h symmetry and is

Table 1.2: C₆₀ infrared line position (cm⁻¹) and Raman line position (cm⁻¹).

ν_{IR}	ν_{Raman}	Assignment
	273	H _g squashing
	437	H _g
	496	A _g breathing
527		T _{1u} IR active
577		T _{1u} IR active
	710	H _g
	774	H _g
	1099	H _g
1183		T _{1u} IR active
	1250	H _g
	1428	H _g
1428		T _{1u} IR active
	1470	A _g Pent pinch
	1575	H _g

responsible for the Raman spectrum. These motions are symmetric bond stretching and antisymmetric bond stretching between 5 and 6 MRS. These a_g motions, especially the antisymmetric mode, give prominent spontaneous Raman spectrum. There are several h_g modes, which also have allowed Raman spectral band. The observed IR and Raman absorption bands are given in table 1.2 [83].

1.8 Solubility

The solubility of C₆₀ and other fullerene is of both practical and fundamental interest and the solubility of C₆₀ in organic solvent plays a crucial role in the extraction, chromatographic separation and reaction in solvent media. C₆₀ is essentially not soluble in polar and H-bonding solvents like acetone, THF, MeCN, nitromethane, methanol and ethanol [84, 85]. It is sparingly soluble in alkane like pentane, hexane and decane with the solubility increasing with the number of carbons, Solubility of C₆₀ in different solvent is shown in Table 1.3.(ref. 35b) Fullerene with their unique cage structures, are interact with solvents in interesting ways that would provide new information on the mechanism of

Table 1.3: Solubility of C_{60} in various solvents

Solvent		$[C_{60}]$ mg/ml	ϵ
Alkanes			
	n-pentane	0.005	1.84
	n-Hexane	0.043	1.89
	Cyclohexane	0.036	2.02
	Decalins	4.6	2.20
Haloalkanes			
	Dichloromethane	0.26	9.08
	Chloroform	0.16	4.81
	Carbon-tetrachloride	0.32	2.24
	Trichloroethylene	1.4	3.40
	1,1,2,2-Tetrachloroethane	5.3	8.20
Polar			
	Methanol	0.00	33.62
	Ethanol	0.001	24.30
	Acetone	0.001	20.70
	Acetonitrile	0.000	37.50
Benzene			
	Benzene	1.7	2.28
	Toluene	2.8	2.44
	Xylenes	5.2	2.40
	Tetralin	16	2.76
	Benzonitrile	0.41	25.60
	Bromobenzene	3.3	5.40
	1,2-dichlorobenzene	27	9.93
	Chlorobenzene	7	5.71
Napthalene			
	1-Methyl napthalene	33	2.92
	Dimethyl napthalene	36	2.90
	1-Phenyl napthalene	50	2.50
	1-Chloro napthalene	51	5.00
Miscellaneous			
	Carbon disulfide	7.9	2.64
	THF	0.000	7.60
	Pyridine	0.89	12.30

solute-solvent interactions. The fullerenes have rigid, well defined geometries, in contrast to other solutes whose shapes undergo conformational changes and whose intramolecular vibrational partition functions may undergo large and solvent dependent changes.

1.9 Photochemical and Photophysical Properties of C_{60}

Buckminsterfullerene possesses interesting photophysical and photochemical properties due to its I_h symmetry where carbon atoms are connected to each other by sp^2 and π bonds.

1.9.1 Electronic Absorption Spectra

Hare et. al. [86] and Ajie et.al. [35] reported the UV-Visible spectrum of chromatographically separated C_{60} in n-hexane and toluene. The wave length maxima for C_{60} and their molar extinction coefficients are given in Table 1.4. Spectral regions of C_{60} in n-hexane in the range (200-700 nm) have been categorized as follows [87]

(i) The strong band region between 190 and 350 nm which has 3 intense peaks at 211, 256 and 328 nm arises due to the dipole allowed transitions $^1A_g \rightarrow ^1T_{1u}$ of C_{60} . In addition, there are shoulders or inflexions arise at 195, 227 and 295 nm due to $^1A_g \rightarrow ^3T_{1u}$ transitions.

(ii) A region of much weaker bands between 350 and 430 nm some of which are sharp structured and appears to be due to electronic transitions exhibiting some vibrational structure due to dipole forbidden $^1A_g \rightarrow ^1T_{2u}$ transitions.

(iii) A broad weak continuum between 430 and 640 nm, whose maximum is at about 540 nm, which is superposed by several peaks and some weak shoulders. These bands are appeared due to dipole forbidden vibronic $^1A_g \rightarrow ^1T_{1g}$ transitions. Three extremely weak bands also reported in between 640 and 690 nm.

Overall the visible absorption spectrum contains vibrational structure from one or two

Table 1.4: Wave-lengths and molar extinction coefficients of C_{60} , in electronic absorption spectrum.

UV-visible spectrum in the ground state		
λ_{max} (nm)	213, 257, 327	ref.[86]
ϵ (dm ³ mol ⁻¹ cm ⁻¹)	135000, 175000, 51000	
Singlet Singlet absorption spectrum		
λ_{max} (nm)	513, 759, 885	ref.[88, 91]
ϵ (dm ³ mol ⁻¹ cm ⁻¹)	5400, 3700, 6300	
Triplet Triplet absorption spectrum		
λ_{max} (nm)	457, 509, 747	ref. [88, 89]
ϵ (dm ³ mol ⁻¹ cm ⁻¹)	3400, 3000, 1500	

Table 1.5: Photophysical properties of C_{60} .

		References
Singlet energy	46.1 Kcal mol ⁻¹	[88]
Triplet energy	37.5 Kcal mol ⁻¹	[88]
Singlet decay rate constants	7.2×10^8 S ⁻¹	[92, 94]
Triplet decay rate constants	$(2.1 \times 10^4$ S ⁻¹	[91, 94]
Fluorescence quantum yield	2×10^{-4} ; 2.2×10^{-4}	[93]
	n-hexane; toluene	

forbidden electronic transitions. The combination of transparency (420-440) nm and in the red (≥ 635 nm) regions give dilute solution a distinct purple colour to the eye.

1.9.2 Excited State Properties

The excited electronic structure of fullerene is still now unclear. C_{60} give a weak fluorescence which is observed in the room temperature in n-hexane and toluene solution [88]. However weak phosphorescence has been seen in the liquid helium temperature for C_{60} , suggesting a triplet is formed in high yield [90]. The triplet state of C_{60} is efficiently quenched by 3O_2 in air saturated benzene. The singlet-triplet splitting in C_{60} is small due to large diameter, and large spin-orbital interaction governs the intersystem crossing (ISC) near quantitatively.

C_{60} dissolved as monomers in solution (liquid or glassy) exhibits properties reminiscent

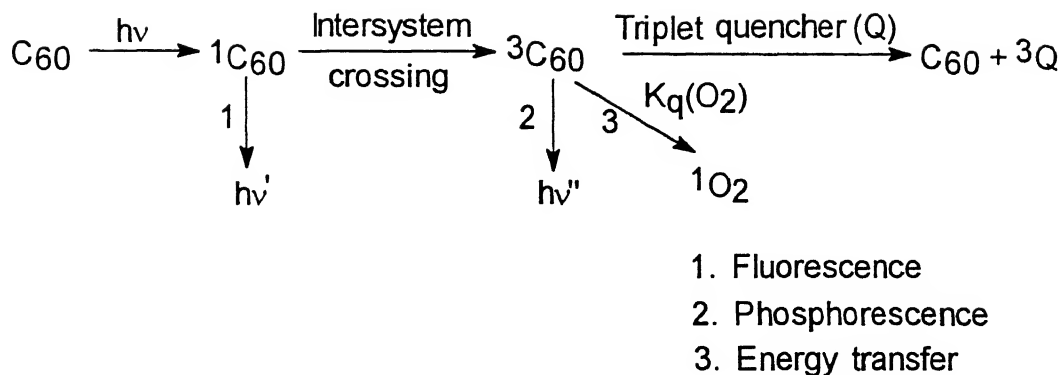


Figure 1.9: Scheme, photochemical reaction of C_{60}

of aromatic molecules. Degenerate states (figure 1.5) are subjected to Jahn-Teller (JT) distortion when electron are excited from the ground state. As molecular orbitals are delocalized over a relatively large surface area (C_{60} is roughly 10 \AA° in diameter), then any Jahn-Teller distortion which occur will be weak. C_{60} does distort along Jahn-Teller active co-ordinates on excitation into one of its low-lying triplet orbitals which is either the LUMO or to the next lowest, which is also threefold degenerate. However quantum mechanical calculation by Negri et. al [82] and Raman-Spectrum of the photo excited species [95] suggest h_g mode is the most strongly involved in the Jahn-Teller active distortion.

Extensive conjugation makes C_{60} a highly optically important material for practical application, initial result from different workers suggest that C_{60} and higher fullerenes can be used as optical limiters [96], i.e. after the threshold light energy it becomes opaque. It can be used as photo conductor [97] in a polymer host, and also in solar-energy conversion [98].

1.10 Electrochemical Properties of C_{60}

A property which governs the chemical reactions of C_{60} and C_{70} is that upto six electrons can be added, reversibly. Because delocalization of electrons is poor in the fullerenes,

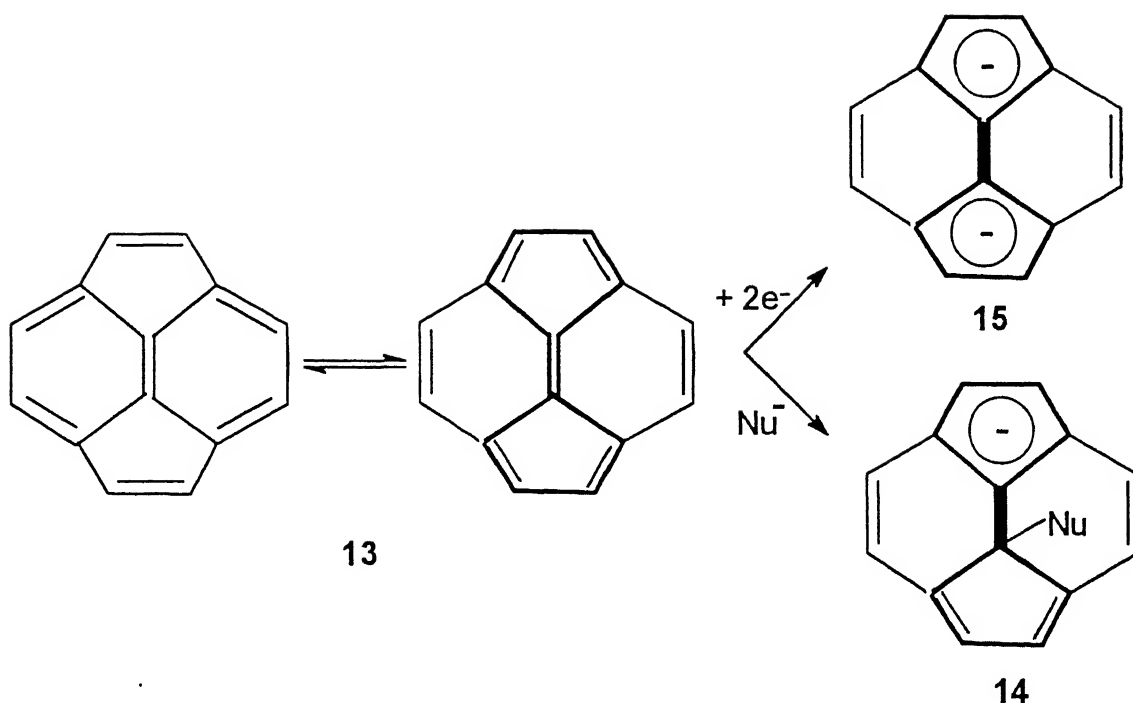


Figure 1.10: Paracyclene unit of C_{60} , the driving force for attaining aromaticity

the addition pattern (figure 1.10) suggest a localized structure. There are six paracyclene unit in C_{60} (a $4n\pi$ system) so it is accounted that each unit would provide a driving force for the capture of up to two electrons either by direct electron transfer to give a $(4n+2)\pi$ electrons containing dianion or in the form of a lone pair to give 'cyclopentadienide' monoadduct [99] which is given in figure 1.10. These paracyclene units arranged octahedrally and the driving force for octahedral addition is in the creation of eight isolated benzenoid rings in C_{60} .

C_{60} and C_{70} are oxidising agents due to their low-lying LUMO orbitals. Several voltammetric studies of C_{60} and C_{70} dissolved in nonpolar solvents such as C_6H_6 , CH_2Cl_2 , THF, etc. containing quaternary ammonium salts as supporting electrolytes are reported [100-102]. Generally the reduction is characterized by a series of reversible

cyclic voltammetric (CV) waves representing stepwise one-electron reduction. Six such waves have been reported for C_{60} in C_6H_6/CH_3CN mixed solvent at temp $-10^\circ C$ [103]. Reduced form of C_{60} in these solvents and electrolytes are stable and remained soluble on the CV time scale. A complex oxidation reaction occurs in benzonitrile solvent at quite positive potential in a multielectron irreversible CV wave and highlighting the instability of radical cation [102].

Electrochemical studies showed that C_{60} is a very strong oxidizing agent, comparable to methyl viologen and flavin chromophores, and its 1st reduction ($E_0 = -180$ mV in THF against Ag/AgCl) is at least 1V more positive potential than those of most polycyclic aromatic hydrocarbons [104]. The electrochemical behaviour of thin film of C_{60} is very different than that of dissolved species [105, 106]. The cyclic voltammogram of it was carried out in acetonitrile solution containing quaternary ammonium (R_4N^+) salts in which C_{60} is not soluble and a stepwise reduction is seen in these films. The film behavior is considerably more complex than the dissolved species.

1.11 Aromaticity

Smalley and co-workers have suggested in their first paper that C_{60} be the first example of a 'spheroidal aromatic molecule' [4]. Aromaticity is a chemical concept and lot of debates in the literature regarding the definition of aromaticity exists. Most widely acceptable definition of the aromaticity is if a compound 'sustains an induced π -electron ring current and the magnitude of this ring current is taken to be the quantitative measurement of aromaticity' [107, 108]. Magnetic susceptibility value [109, 110] of C_{60} is lower than typical aromatic molecule like benzene and the value is well matched the theoretical calculation [107]. Sensitivity of the magnetic susceptibility of C_{60} depends on the relative strength of the two inequivalent bonds in the molecule.

Anisotropic nature of the carbon chemical shift in ^{13}C NMR give the quantitative picture of the aromaticity and in that respect ^{13}C NMR at low temperature shows peaks

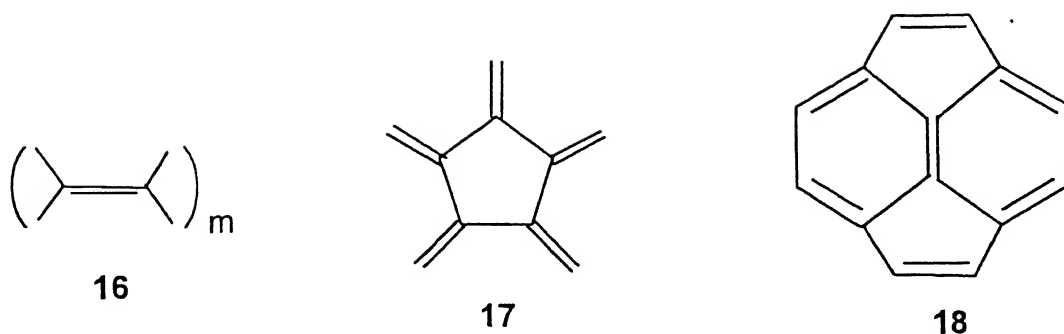


Figure 1.11: Planar substructure of C_{60} i.e. Poly-alkene (16), [5] radialene (17), and paracyclene (18).

at 220, 180, and 40 ppm, justify its aromatic nature [111]. However due to orientational disorder a sharp signal at 143 ppm at room temperature, proves the more alkene character [67, 112]. Haddon and co-workers concluded that it may be difficult to fit the fullerene into traditional aromatic or nonaromatic categories. Overall, the C_{60} 5MR ring is paramagnetic and 6MR ring is diamagnetic which indicate that it constitutes a class of compounds of 'ambiguous aromatic character' [107, 113].

1.12 Chemistry of Buckminsterfullerene

Initially it was assumed that C_{60} would be an extremely stable aromatic molecule and this was supported by the calculation that there are 12,500 resonating structures possible for C_{60} [78]. But initially everyone overlooks the most important aspects of strained five membered rings adjacent to benzenoid rings which have tendency to avoid double bonds in the pentagonal rings. Therefore overall delocalization is poor and C_{60} 's chemistry is mainly governed by local and global strain which is inherent in the molecule.

The chemistry of C_{60} has been characterized as that of an electron deficient polyalkene without significant delocalization. The figure 1.11 shows the sub-structure [5]radialene, Pyracyclene, and polyalkenes are the model compounds for chemical reactivity of C_{60} studies [114]. The fullerene without boundary conditions are, use as an ideal graphite sheet, there are no peripheral atoms to serve as sites of preferred reactivity. After the macro-

scopic isolation of C_{60} its chemistry is extensively studied. So far numerous chemical derivatization of fullerene is reported [115-117] in the literature which fall in the category of (a) gas phase reactions (b) organometallic complexes (c) charge-transfer complexes (d) organic compounds (e) biologically active compounds.

1.12.1 Gas Phase Reactivity

Oxygen and methylene adducts of C_{60} and C_{70} have been synthesized [118]. Photochemical processes are introduced and the amount of adducts could be increased by the use of UV-irradiation during the various stages of preparation and extraction. Under certain conditions a series of $C_{60}^+(\text{CH}_2)_n$, where $n=1-6$, are produced. Irradiation of the ether washed C_{60} or C_{70} gave a new photochemical reaction, leading to a series of $(C_{60})O_n$ with $n=2-5$ [118].

C_{60}^+ and C_{70}^+ have shown enhanced reactivity when generated in situ with $\text{Fe}(\text{CO})_5$ in the gas phase. $\text{Fe}(\text{CO})_4C_{60}^+$ and $\text{Fe}(\text{CO})_3C_{60}^+$ are produced in about equal amounts when isolated C_{60}^+ is allowed to react, however in the case of $\text{Cr}(\text{CO})_6$ no reaction was observed. Collision induced decay (CID) of the $\text{Fe}(\text{CO})_4C_{60}^+$ product shows consecutive loss of carbon monoxide molecule to give finally FeC_{60}^+ [120].

The synthesis of bis- $(C_{60})_2\text{Ni}^+$ in the gas phase and its observation at longer trapping time in the fourier transform mass spectrometer suggest that this species is quite stable [121]. Doubly charged gas-phase anions are fairly rare but C_{60} formed quite easily C_{60}^{2-} in the gas phase [122]. Very little is known on the reactivity of C_{60} with small molecules. Gas phase reactivity studies suggest that C_{60} and C_{70} are unreactive with NO , CO , SO_2 and NH_3 . But C_{60} reacts very slowly with H_2 and O_2 at partial pressure up to 120 Torr in a laser vaporization plasma [123].

1.12.2 Organometallic Complexes

C_{60} is a versatile ligand for the generation of unusual organometallic complexes. The first characterization mono adduct $[C_{60}(OSO_4)(4\text{-tert-butyl pyridine})_2]$ was reported by Hawkins et.al [124]. It's X-ray crystal structure, shown in figure 1.12, confirmed the soccerball shape of C_{60} . The O-Os-O unit is added regioselectively exclusively at a double bond common to two annelated six-membered rings (6-6 bond) in the fullerene framework. This structural analysis also provide the important finding that the 6-6 bonds (double bonds) are shorter than the bonds common to both a five and a six-membered rings (5-6 bonds), which have single bond character. According to this, C_{60} can be described topologically by annelated cyclohexatriene and [5] radialene units. The complex with electron rich Pt [125] and Ir [126] fragments and the structural analysis of the resulting C_{60} adducts indicate that C_{60} function as an electron poor olefin. The electron distribution in these complexes is similar to that in $[O_2Ir(CO)Cl(PPh_3)_2]$. Sixfold platinum substituted derivative $[Et_3P_2Pt]_6C_{60}$ (figure 1.13) is remarkable in a number of respects as [125]:

- (a) This is the first example of multiple substituted fullerene with metal fragments.
- (b) Its X-ray crystal structure analysis proves that the six platinum complex fragments are added to C_{60} in an octahedral fashion with the point group symmetry T_h .
- (c) Complex occurs exclusively on the 6MR - 6MR double bonds and a maximum of six such fragments attached to the framework due to $(Et_3P)_2Pt$ moiety blocks the four adjacent C=C bonds.

1.12.3 Charge-Transfer Complexes

One important feature of the fullerenes (C_{60} and C_{70}) is their ready and reversible uptake of upto six electrons. This high electron affinity is exploited in the first chemical modification of C_{60} in the preparation of superconductors like K_3C_{60} , Rb_3C_{60} etc. [127, 58] and ferromagnets $[TDAE]C_{60}$ [TDAE = tetrakis (dimethylamino) ethylene] [128] and these were prepared by charge transfer with electropositive metals and organic donor molecules respectively.

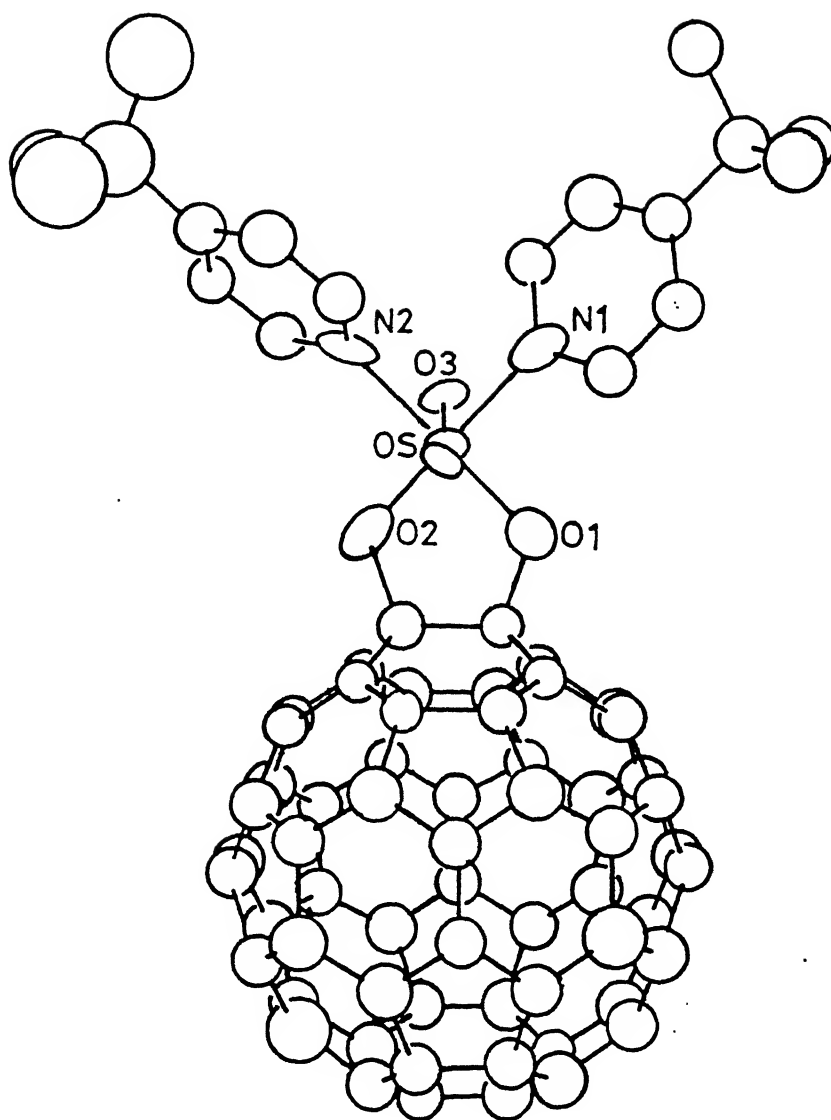


Figure 1.12: X-ray crystal structure of $[C_{60}(OSO_4)(4\text{-tert-butyl pyridine})_2]$

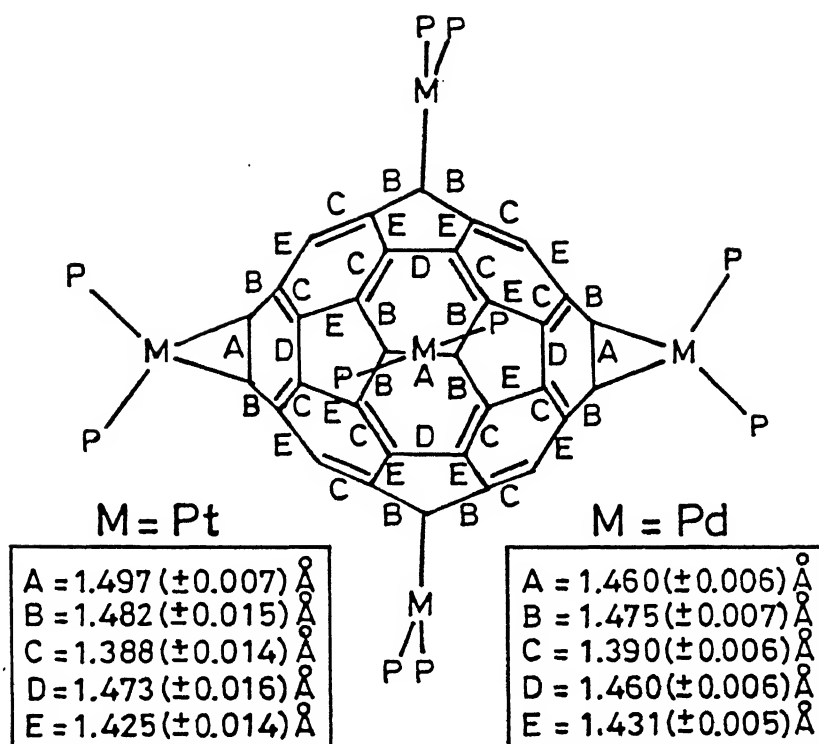


Figure 1.13: X-ray crystal structure of $[\text{Et}_3\text{P}_2\text{Pt}]_6\text{C}_{60}$

An abinitio calculations predicted that both C_{60}^- and C_{60}^{2-} are in bonding states. A crystalline (tpp)Chromium(III) complex [tpp = tetraphenyl porphyrinato) with C_{60}^- as counter ion was reported and position of the equilibrium in this system was dramatically influenced by the solvent. Spectroscopic data indicate that $Al^{III}(tpp)$ also react with C_{60} by electron transfer, producing C_{60}^- . The synthesis of C_{60}^{n-} salts from C_{60} requires very precise stoichiometric control of a strong reducing agent and moreover the selection of a strong reducing agent at $\sim 0.45V$ window for the appropriate stability of each C_{60}^{n-} ion [129-131]. Cobaltocene and sodium are used as reducing agent to produce C_{60}^{1-} , C_{60}^{2-} and C_{60}^{3-} and a judicious choice of cation produces a series of charge transfer salt, like $[Na(crown)(THF)_2][C_{60}]$; $[Na(crown)(THF)^3]^3[C_{60}^{3-}]$. The magnetic properties of the above mentioned salts are very much puzzling. The Jahn-Teller distortion of C_{60}^- has been studied both theoretically and experimentally. The electronic ground state ($^2T_{1u}$) as well as the first excited state ($^2T_{1g}$) of I_h symmetry are subject to the symmetry lowering resulting to distortion to D_{5d} symmetry [130].

1.12.4 Hydrogenaton

The first derivatization of C_{60} was achieved with the Birch reduction which gave colourless $C_{60}H_{36}$ [132]. However the simplest hydrocarbon derivative of C_{60} , $C_{60}H_2$ was obtained by the addition of BH_3 and acid hydrolysis of the initial hydrocarbon product, $C_{60}H(BH_3)$, with acetic acid [133]. More controlled anion formation also obtained from the reaction of C_{60} with t-butyl-lithium [134]. The product was t-bu C_{60} (where Bu = C_4H_9) with small amounts of $(t-Bu)_n C_{60}^{n-}$ ($n = 2-6$) and in the presence of acid gave hydrogenated C_{60} . t-buHC $_{60}$ exit in two isomers but one of the isomers is less stable. t-BuHC $_{60}$ is a very strong organic acid ($pK_a = 5.7$) with a weak (71 Kcal mol^{-1}) C-H bond dissociation energy [135]. The MNDO/PM-3 calculation for $C_{60}H_2$ predicted that the most stable structure corresponds to 1,2 addition than 1,4 addition isomer [136].

1.12.5 Halogenation

The chlorination and bromination of fullerenes were first shown by Olah et.al [137]. Fluorination and chlorination of C_{60} gave a mixture of products which was still uncharacterized. Fluorination of C_{60} occurred in most uncontrolled manner resulting in the formation of mixtures of $C_{60}F_{36}$, $C_{60}F_{34}$, $C_{60}F_{40}$ [138] and even some groups reported the formation of $C_{60}F_{60}$ [139]. The bromine addition products $C_{60}Br_6$ [140], $C_{60}Br_8$ [140], $C_{60}Br_{24}$ [141] were crystallized and their crystal structures have also been reported. Here the crystal structure of $C_{60}Br_8$ is shown in figure 1.15. Bromination occurred preferentially in a 1,4 addition for steric reasons. The 1,4 addition mode is attributed due to the large spatial requirements of bromine atoms [142]. Halogen derivatives are key intermediates in organic synthesis. At present fullerene bromination is the most controlled halogenation, but gives the most insoluble derivatives. Fluoro derivatives are very soluble and reactive also. Local density functional calculation suggests that the 1,2 addition is favoured for F, Cl where as the 1,4 addition is favoured in the case of Br and I. The geometry optimization in $C_{60}X_2$, where $X = F, Cl, Br, \text{ and } I$, from MNDO calculations suggests that eclipsing interaction in 1, 2 $C_{60}X_2$ and the electronic effect due to placing a double bond in a five membered ring in 1, 4 $C_{60}X_2$ determines the preference for 1, 2 or 1, 4 addition [142].

1.12.6 Cycloaddition

The electron withdrawing nature of fullerenes makes them distinctly electrophilic and dieno/dipolarophilic for Diels - Alder cycloaddition which takes place readily [143]. Stoichiometric controlled reaction of diazoalkane and diazoacetates with C_{60} give methano-bridged [60]fullerene and the primary intermediate of these reaction is [3+2] cycloaddition product i.e dihydropyrazole [99]. In these processes various types of 'fulleroids' are formed [99, 117, 144] like

- (a) opened π - homoaromatic bridged at 5-6 ring juncture
- (b) open π - homoaromatic at a 6-6 ring juncture

- (c) σ - homoaromatic at the 6-6 ring juncture and
- (d) open azo-fulleroids.

Notable cycloaddition product was obtained by the UV - irradiation of solid C_{60} in the absence of oxygen yielding a polymeric product $(C_{60})_n$ ($n \leq 20$). This was a case of photochemically allowed (2+2) cycloaddition [145].

1.12.7 Oxygenation

Wood et.al. [118] have suggested from their collision activated dissociation (CAD) experiments that C_{60} and C_{70} are very much reacting with oxygen and finally concluded that these adducts are covalently bonded. C_{60} epoxide was isolated and characterized by two groups independently the following methods.

- (a) UV-irradiation in a oxygen saturated C_{60} solution, in benzene, predominantly give $C_{60}O$ epoxide [146].
- (b) Epoxide and 1,3 - dioxolane are formed when C_{60} are reacted with dimethyldioxirane [147].

In the presence of ppm level O_2 during graphite vapourization fullerene has been oxidized to oxido-fullerene [148]. Still now the nature of O_2 addition is unclear. It was also proposed that the fullerene cage can be opened by the combined effect of oxygen and low energy light [149].

1.12.8 Free Radical Addition

Extensive investigation of the reaction of radicals with C_{60} and C_{70} were performed by ESR spectroscopy. The radicals, $Me\cdot$, $Ph\cdot$, $PhS\cdot$, $PhCH_2\cdot$, $CBr_3\cdot$, $CCl_3\cdot$, $CF_3\cdot$ and $Me_3CO\cdot$ react readily with C_{60} [150]. The molecule C_{60} has 30 carbon-carbon double bonds to which free radical can be added. Multiple additions product from the above radicals have been reported. But most pioneering work on radical derivatives is photochemically generated benzyl radicals which produce radical and non radical adducts like R_nC_{60} (R

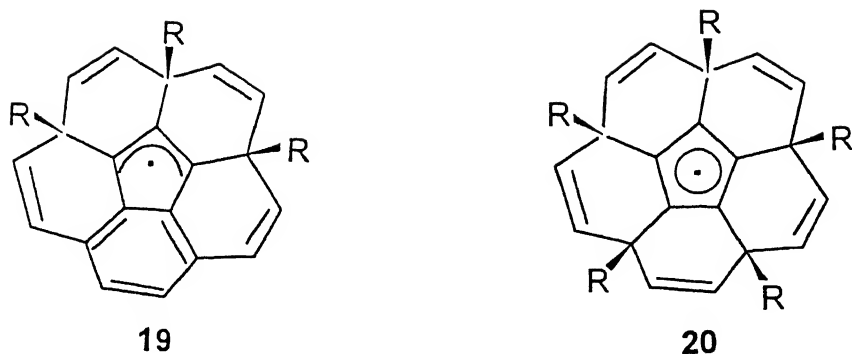


Figure 1.14: Cyclopentadienyl (20) and allylic radical (19) are the two type of radical easily formed in the C₆₀ surface.

= C₆H₅CH₂) with $n = 1$ to 15. Radical adducts with $n = 3$ and 5 are stable above 50°C [151] and it was inferred from EPR spectroscopy that the allylic R₃C₆₀ and cyclopentadienyl R₅C₆₀ radicals formed (figure 1.14). These radicals are highly localized as the extensive delocalization would mean putting double bonds in pentagonal rings. Another factor that also governs the extraordinary stability of these radicals can be attributed due to the steric protection of the surface radicals site by surrounding benzyl substituents. Remarkably the structure of the pentabenzyl radical and C₆₀Br₆ are similar which are shown in figure 1.15. Therefore bromination occurred via C₆₀Br₅ but it cannot be effectively stabilized by hyperconjugation and so acquires a further bromine atom. The facile reactivity of C₆₀ with alkyl radicals suggests that caution should be used in interpreting mass spectra of fullerenes because mass peak may arise from the radical or matrix fragmented radical ion source.

1.12.9 Hydroxylation

Chiang and coworkers first demonstrated that acid chemistry is an efficient method for introducing multiple hydroxy groups into fullerene molecules [152]. They in the subsequent paper reported the formation of polyhydroxy organocarboxylated fullerene derivatives through the electrophilic addition of nitronium tetrafluoroborate into fullerenes in the presence of a carboxylic acid in a nonaqueous medium. Hydrolysis of the ester moi-

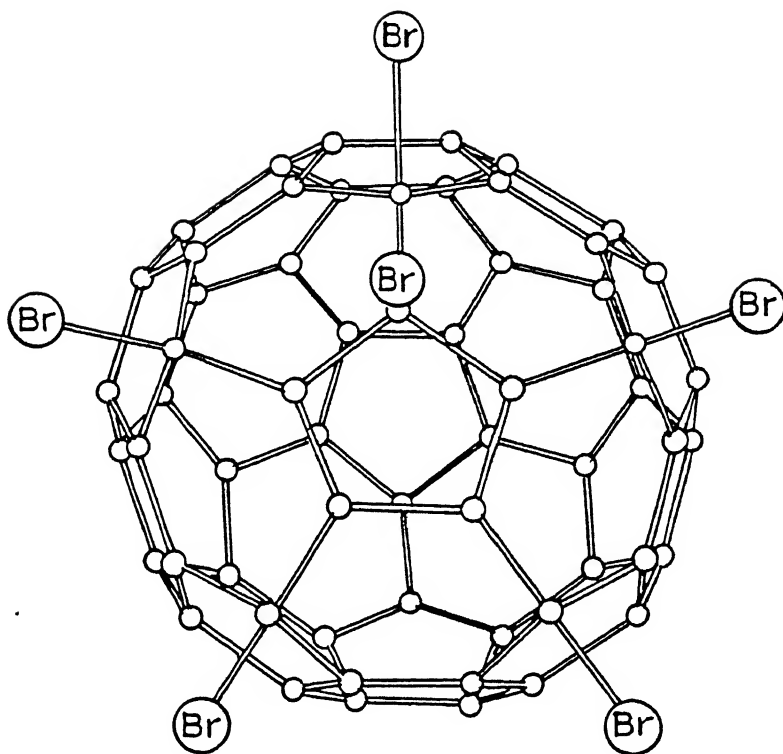


Figure 1.15: X-ray crystal structure of $C_{60}Br_6$. Br atom is attached with the C_{60} surface, by 1, 4 addition.

ety in these derivatives provides an efficient route for the preparation of water-soluble fullerenols produced by the formation of a nitro intermediate. Absence of the nitro group in the derivative is interpreted as electrophilic addition of nitronium ion in the initial state followed by nucleophilic substitution of hydroxyl group [153]. But fullerenols are produced in low yield, even if H_2SO_4 alone is used, suggesting $\text{NO}_2\text{-OH}$ and H-OH adducts are intermediates, as are $\text{NO}_2\text{-OCOR}$ adducts in the similar reaction with nitronium tetrafluoroborate/carboxylic acids. Number of hydroxyl groups present in the fullerenols depends on the method of preparation.

1.12.10 Biologically Relavence Compounds

Large spherical hydrocarbon derivatives bearing polar functional groups have gained increasing attention for their biological activity. Amentadine, rimabntadine, the derivative of adamantane (radius 7.4 \AA) are potential antiviral agents. Lot of hopes in future, derivatives of C_{60} (dia. $\sim 10 \text{ \AA}$) with it's spherical surface will be a good substrate in biologically active molecule. C_{60} derivative has been able to interact with the active site of H1V-1 protease [154]. This has been examined by computer modelling as well as by other physico chemical analysis. Water soluble diamide diacid diphenyl fullerene derivatives have been able to inhibit the HIV enzyme activity [154]. At present the scarcity of water soluble C_{60} derivatives hampered the progress of this study. Water miscible fullerene carboxylic acid has biological activity like cytotoxicity and G-selective DNA cleaving ability (in presence of low energy light) [155]. This is truly remarkable in that the biological activity is observed only under irradiation with visible light and not in the dark, suggesting that fullerene may serve as useful photosensitive biochemical probe. A recent study highlights that the DNA cleavage is occurred due to the action of singlet oxygen generated by photoactivation of fullerene molecule [156]. Synthesis of α -amino acid derivative of C_{60} [157] and fullerene peptide [158] have given new direction in the C_{60} -biological chemistry.

Chapter 2

Scope of the Work

Except the Krätschmer-Huffman (K-H) technique [1], most of the methods [21-27] mentioned in the introduction chapter for the production of fullerenes have not gain much popularity due to (i) the yield of the fullerenes are very poor compared to K-H method and (ii) the experiments are difficult to perform in normal laboratory conditions.

20 to 30% of the vaporized carbon is transformed to fullerenes in the K-H technique [159]. Unfortunately this approach (dc plasma discharge method) is limited to graphite rods with diameter of 1/8 inch or less making it impractical for large scale synthesis of fullerenes. Another drawback of this method is that it requires a fairly complex apparatus with special feed mechanism to align the two electrodes for maintaining a constant arc gap. However, the apparatus is deassembled for scraping the fullerene soot as well as for the insertion of new graphite rods. Hence for every operation extra cares have to be taken for the proper alignment of two graphite electrodes.

In 'contact arc' method the yield of fullerenes from 6-mm diameter rods is about 15% [132]. The yield drops off linearly with increasing rod diameter [160] and this observation has not been adequately explained. In the subsequent years a lot of research activity started all over the world for the technological development of the fullerene reactor [86], [161-167]. To date, the most easily accessible apparatus for the 'contact arc'

method is the gravity feed apparatus [161] which is relatively inexpensive and simple device. Henceforth this method rapidly became the method of choice for commercial fullerene production.

Production of fullerene by K-H method is still a highly expensive process. Based on these observation our aim is design a fullerene reactor that should satisfy the following criterion:

- (i) design should be simple enough, therefore fabrication of the reactor can be possible in any workshop by simple machining.
- (ii) excessive heat that is produced due to graphite resistivity heating is a major technological problem in the contact arc apparatus. Excessive heat can easily damage the O'rings, joints, and other sealing materials which are essential components for the fullerene reactor. Hence cooling is the integral part of a reactor and emphasis are given for required cooling of the reactor.
- (iii) He-pressure and current (power?) are the two most important parameters for fullerene production. Optimization of this two parameters are not only useful for high yield fullerene synthesis, but it can also highlights some hidden facts of the fullerene formation kinetics. Till date, to our knowledge no such optimization has been reported on contact arc technique. Only one report (based on our knowledge) relation to this has been published by Scrivens et.al [164] in dc plasma technique. But execute this type of experiment it required modification in the design of the reported [132, 161, 166] contact arc reactor.

The state-of-art separation of C_{60} from fullerene mixture is a challenge to every synthetic chemist. In the pre-fullerene era (the year before the method of macroscopic isolation procedure of fullerene was established) experimental observation from the gas phase reaction, by Zhang et.al [10], suggest that fullerenes especially C_{60} is quite inert to chemical attack towards reactive small molecules such as NO, SO_2 , CO, H_2 , O_2 and NH_3 . In support of Zhang's observation and by resonance energy calculation, it was suggested that C_{60} is a 'super aromatic' molecule [78]. However calculated value of heat of formation [114], strain energy [57], magnetic susceptibility [109] etc. reported from

different groups were quite anomalous. Because of the description of bonding in such large molecules, particularly with those which potentially show extensive conjugations have traditionally been controversial [168, 169]. Moreover, *ab initio* calculations for such molecules with a reasonably good basis set have computer limitation [169]. Thus the theoretical calculation i.e bond length determination, geometry optimization, chemical reactivity index etc., are published in the literature primarily based on semi-empirical quantum mechanical calculations and they probably not a very authentic guide for synthetic fullerene chemistry. So, some intuitive chemistry can be developed based on purely experimental conditions.

Buckminsterfullerene cages consist of entirely sp^2 hybridized carbons which have electron-withdrawing (-I) effects [170]. This behaviour makes C_{60} a good substrate for nucleophilic addition. Position of the nucleophile, in nucleophilic addition mechanism of the alkenes, directed by the anisotropic atoms presents in the alkenes [171] like H, O, N, etc. As C_{60} is a perfectly isotropic molecule, the reactive index or addition of the nucleophile in fullerene carbon carbon double bond can not be simply judged from the analogy based on planar alkenes. Another important difference in reactivity of fullerenes compared to the normal alkenes is that the addition in fullerene moiety always occurred in the bridged carbon atoms. However, addition and substitution have been observed in the alicyclic (norbornyl) and aromatic (naphthalene, anthracene etc.) bridged systems other than bridged carbon atoms [171].

One of the most exciting observation in the fullerene research is 'fullerene is soluble in most of the common organic solvents' [1]. Thus investigate the chemical reactivity of the fullerene in liquid state is possible and in the following years a large number of new derivatives of technological and biochemical importance is prepared. In the gas phase experiments with large quantities of C_{60} , the reactive neutral molecules [118, 119, 122] e.g NH_3 , O_2 , etc, have given quite contradictory results compared to the experimental observations by Zhang et.al [10]. Photochemically generated reactive neutral radicals efficiently add to the C_{60} 's double bond and the successive radical adducts and photolysis of C_{60} in the presence of donor molecule produce the radical anion of C_{60} [150]. These

observations suggest that C_{60} is a good radical sponge, however NO , CO^\cdot , the two most reacting molecules are reluctant to react with C_{60} in the gas phase contrast justify the statement that C_{60} is a good radical sponge suggesting that it is rather choosy with the radical partner. The addition of NO_2 with C_{60} in the gas phase, producing a stable $C_{60}NO_2^-$, is not adequately explained [123] and this species $C_{60}NO_2^-$ has been characterized from mass spectra only. Chiang et.al [152, 153] has been used nitrating reagent could derivatize C_{60} but did not succeed to isolate any nitro adduct of C_{60} . They have observed that C_{60} attached NO_2^+ ion is easily substituted by the nucleophile OH^- ion, and isolated product leading to the formation of fulleranol. But most puzzling question is 'how an electron deficient NO_2^+ ion is attached to the highly electron deficient C_{60} molecule?' Thus it would be highly interesting to see if NO and NO_2 have same reactivity with C_{60} .

The organometallic chemistry of C_{60} is becoming a flourishing subdiscipline of the fast expanding fullerene research [116]. Pt, Ir, and Os derivatives of C_{60} are prepared in most pure form and single-crystal X-ray structure of these are also solved [125, 126, 124] and in these derivatives, C_{60} behaves as an alkene giving η^2 coordination. In the gas phase experiments, M^+ induced to react with C_{60} and the resulting complex MC_{60}^+ was characterized by mass spectroscopy [119, 120]. The complex, analogous to the metallocenes $[Ni(C_{60})_2]^+$ has been prepared in the similar way [121]. Thus the chemical behaviour of C_{60} like an electron deficient olefin similar to tetracyanoethylene does not justify. Magnetic susceptibility measurements [109, 110] and theoretical calculations by Haddon et.al [107] suggest that C_{60} has vanishingly small diamagnetic ring current. This small diamagnetic contribution comes from the mobile π electrons of the molecule. At low temperature ^{13}C NMR chemical shifts is in the typical aromatic region [111]. The magnetism of C_{60} highlights that it has ambiguous aromatic character [113].

$Fe(CO)_5$ reacts with C_{60} in the gas phase forming a $C_{60}Fe$ adduct, though details bonding are not discussed in that report [120]. Decomposition of the metal-metal bond from $Re_2(CO)_9$ both thermally and photochemically generating highly reactive $.Re(CO)_5$ which adds to the C_{60} moiety by η^2 fashion [172]. Douthwaite et. al.[173] reported

that Mo, Cr, and other metal-carbonyls also bind to the C_{60} moiety by η^2 fashion. As six member ring of the C_{60} ring is electron rich compared to five member ring, and calculations from Haddon [114] and Merynick et. al. [174] suggest that metal having large spatial d-orbital can participate in the η^6 fashion. This suggestion from the two research groups is interesting to study the reactivity of d^6 -metal hexacarbonyls with C_{60} where size of the d-orbitals are gradually increased from 3d - 4d - 5d. Product analysis in this substitution reaction can give a better insight into the chemical behaviour (i.e alkene, arene) of C_{60} .

Fragmentation studies of C_{60} in the presence of high energy ion beam [75] univocally suggested that the carbon carbon bonds of C_{60} are very stable. However, Taylor et. al.[175, 176] suggested that fullerene reacts with oxygen in the presence of UV-light and oxidized the carbon-carbon double of C_{60} at ambient conditions and its structure is broken. Oxygen atom is attached to the C_{60} surface in a controlled fashion by the use of appropriate technique, such as reaction of it with dimethyldioxirane [147] and UV irradiation of a oxygen saturated C_{60} solution [146]. Product analysis from the above process has suggested the formation of C_{60} epoxide.

Werner et. al.[177, 178] extensively studied the oxygenation chemistry of C_{60} in the atmospheric conditions and interpreted that oxygen is covered the C_{60} molecule in a clathrate or icosaspirals fashion via an epoxide linkage. At ambient conditions IR spectra of C_{60} give peaks at 2300 and 1537 cm^{-1} but this two IR absorption bands do not justify the epoxide linkage which normally appears in the 1100-1000 cm^{-1} region [179].

Nature of the oxygen addition in C_{60} and other fullerenes is least understood due to the unavailability of the C_{60} oxygenation product at ambient conditions. DTA, TG and DSC studies from different groups indicate that the oxidation of the C_{60} takes place at above 400°C and the initial carbon oxygen bond formation takes place at 200°C [180-182]. Therefore from the thermodynamically it is quite unlikely that the carbon-oxygen bond formation in C_{60} takes place at ambient conditions.

C_{60} is an optically active molecule due to extended conjugated π -electrons and the $\pi - \pi^*$ transitions is easily occurred in the visible region. In the excited state a large number of isomeric structures of lower symmetry i.e D_{5d} , D_{3h} , C_{2v} etc are formed due to sigmatropic rearrangements [183]. Except I_h symmetry the other symmetry structure of the C_{60} molecule do not follow the 'isolation pentagonal rule', thus causing the instability of the fullerene molecule in normal day light. Foot et.al [89] observed the absorption spectra of C_{60} in benzene remained unchanged for 9 days in the presence of sunlight. The HPLC separation on this sunlight irradiated C_{60} solution do not show any extra peak for C_{60} derivatives but shows an unidentified peak for C_{70} . Arbogast et. al. [88] observed that C_{60} is not destructed during fluorescence suggesting the photochemical fragmentation reactions of C_{60} quite unlikely.

Kroll et.al [149] from photoelectron spectroscopic studies indicated the presence of reactive species such as O_2^- and excited O_2 produced through the decay from O_2^- which oxidizes the C_{60} molecule. This reactive oxygen is produced in the photoinduced way but the exact nature of this reaction sequence is still not clear. Taliani et. al. [184] suggested that the photochemical degradation of solid C_{60} produces to $C_{60}O_2$ and $C_{60}O_4$. In this process, one $C=C$ of the C_{60} framework reacts with electronically excited molecular oxygen, 1O_2 ($^1\Delta_g$) which is produced by energy transfer from photogenerated triplet C_{60} to ground state oxygen triplet 3O_2 . The endoperoxide produce in these processes eventually decomposes to the cage open dicarbonyl species. But singlet oxygen does not react with solid C_{60} which has given a new dimensions to the fullerene oxygenation chemistry [185]. Origin of the paramagnetic center of C_{60} in the presence of oxygen [186] and the nature of the generated radical species are not explained. The details EPR study of C_{60} molecule at ambient conditions can highlight some of the hidden fact of oxygenation addition.

Kroll et. al. [149] interpreted their photo-electron experimental results based on the observation in low temperature (20°K). But C_{60} undergoes a phase transition to simple cubic structure as a consequence of orientational ordering at 260 K [187, 188]. Therefore, C_{60} oxygen interaction at low-temperature measurement is not quite similar to that at

ambient condition because at ambient conditions C_{60} belongs to a fcc structure with orientational disorder. C_{60} film showed semiconductor behaviour. Exposing the films to pure O_2 or air at $21^\circ C$ leads to the decrease of conductivity as well as photoconductivity due to oxygen contamination [189].

Since the discovery of C_{60} its vibrational spectral properties have been extensively studied both experimentally and theoretically. However the observed IR bands are greater in number than what theoretically predicted (four bands) for I_h symmetry. Heat of formation, Lattice constants determination from X-ray diffraction, magnetic measurement or other physical measurements need always highly pure sample. Painsstaking efforts are needed to eliminate solvent molecule either by sublimation or by extended vacuum annealing from chromatographically pure C_{60} . C_{60} with its cage structure interacts with these solvent molecules but how this solvent molecules are attached to the neutral C_{60} molecules is another mystery. Till date no proper explanation has been given in this aspect. The explanation given in this aspect is that 'the fullerene with their cage structure interact with the solvent molecule in an interesting way' [85].

There has been much interest in the mechanism of oxidative damage to DNA and its biological consequences in living cells. Oxidation of DNA decreases its transformation efficiency, inhibits DNA replication, and causes G to T tranversions. These effects are generally believed to be related to human problems such as cancer and ageing. Photosensitized oxidation plays an important role in oxidative damage due to the environmental chemicals and natural cell constituents. Singlet oxygen is one of the major species that can cause these effects. Irradiation of a mixture of DNA and detergent like C_{60} carboxylic acid with low-energy light results in guanine (G) selective strand cleavage [156]. This base-selective cleavage was ascribed to the action of singlet oxygen generated by photoactivation of fullerene molecule and recent experiments demonstrated that C_{60} carboxylic acid does generated singlet oxygen in water [155]. It is of interesting to examine whether or not the chemical reactivity of singlet oxygen is affected by the fullerene sensitizer.

Chapter 3

Design and Fabrication of a Fullerene reactor: Optimization of the Key Parameters in Fullerenes' Synthesis.

The most common method for the preparation of fullerene is the Krätschmer-Huffman (K-H) method [1]. The technique behind the K-H method is high purity graphite rods which are vapourized in a low helium pressure. There are two major variants of the graphite vapourization, namely, carbon contact arc [132] and carbon plasma discharge [159]. In contact arc method, the graphite electrodes are kept in constant contact through either a gravity feed mechanism or through the use of a feed spring. Fundamental principle behind the contact arc method is that the power is dissipated in an arc rather in resistive heating of the graphite rods. Number of reports based on the design of the apparatus were published in the literature [161, 162, 163, 164, 165, 166]. Here we describe the fabrication of a fullerene reactor with some modifications.

3.1 Experimental Sections

3.1.1 Material Used

Stainless steel, brass, copper and teflon were purchased from the local market. These were used after proper machining. The materials which have maintained the vacuum were used after polishing. O-rings used were of two categories like neoprime, maximum thermal resistance was 110°C, and other is silicone which was sustained upto 280°C. The ball-bearing (sk&f, India) were purchased from local shop and used as such. Cable wire of ordinary quality were used. He-gas (IOL, India) of 99.9% purity and graphite electrodes (Johnson-Matthey, Canada, 99.99%) were used. Toluene, benzene, n-hexane, hexane (petroleum fraction) were distilled over sodium wire and CaH_2 , but not degassed. For chromatography, Al_2O_3 -Brokemann 1 grade (Acme India) was used.

3.1.2 Physical Measurements

Mass Spectra:

FAB mass spectra of the fullerene and chromatographically separated C_{60} samples were recorded on Jeol SX 102/DA-6000 Mass spectrometer/data system using Xenon (6 KV, 10 mA) as the FAB gas. m-Nitrobenzyl alcohol has been used as the matrix. Concentrated C_{60} solution in benzene was subjected to mass spectra as such.

IR Spectra :

Solvent was evaporated from the chromatographically separated C_{60} and the solid obtained was dried in vacuum (10^{-3} torr) at 150°C for 2 hours before IR measurements. Powdered C_{60} and spectroscopic grade KBr(E-Merck) were mixed in a 1:9 ratio and the pellets were made with a hydraulic pressure of 400 pounds. The spectra was recorded in a Perkin-Elmer 1600 FTIR in 4 and 2 cm^{-1} resolution in the range 4000-400 cm^{-1} and 1600-400 cm^{-1} respectively.

UV-visible spectra :

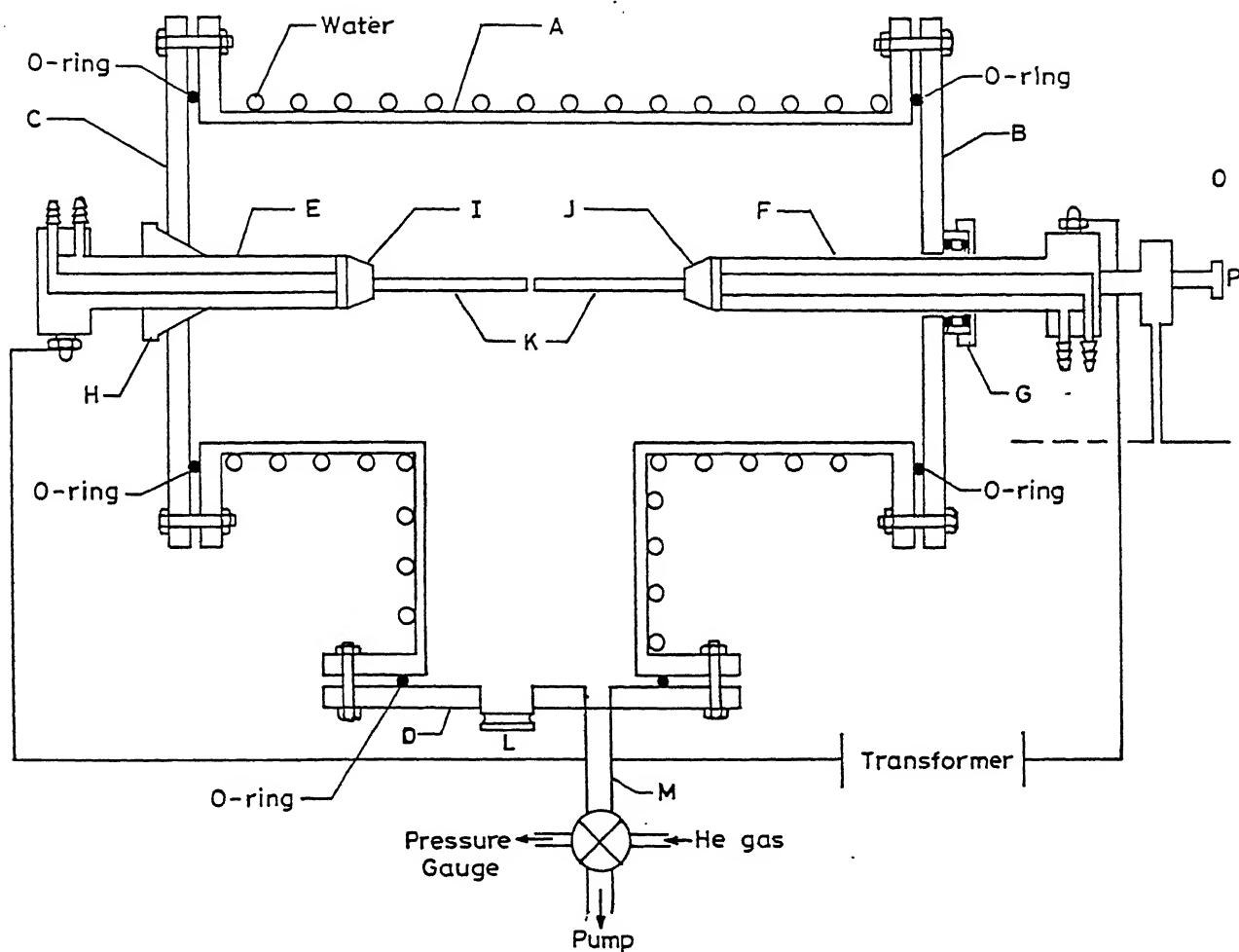


Figure 3.1: Schematic diagram of the fullerene reactor

graphite rods (K). Electrodes alignments during evaporation were monitored through the view port L with the help of arcing light. This view port was placed at the center of the flange D. He-gas flow and vacuum were done into the reactor using the port M. All the flanges and accessories were demountable in this reactor and vacuum sealing of it were done by O'-rings and bolts. The position of the O'-rings and bolts is shown in figure 3.1.

Figure 3.2 is the section diagram of the water cooled electrodes. Notation of C, I and E were same as shown in figure 3.1. The teflon gasket (1) was working as an insulator of the reactor and at the same time it also worked for vacuum sealing of the electrode E in the port G. Groove 2 (trapezium type) was made in G to hold the teflon gasket. The gasket were tightened by a self design screw 3. A copper tube (4) was inserted into the electrode E for efficient cooling of the holder (I). The electrical and water inlet connections were done on the electrode from the outer portion of the electrode and the diameter of this portion (figure 3.2) was greater than the other part (the portion which was moved inside the reactor) of the electrode. O-rings were used in the union of electrodes for additional safety. The water inlets 6 are connected to a tap-water for the continuous circulation of cooled water. The electrical connections were given through the bolt 7.

The vacuum sealing used for the movable electrode (F) of the reactor is shown in figure 3.3. A well polished brass spacer was placed in between the two O-rings in the port G. Among this two O-rings, which directly was contacted with the screwing nut compressed more as a result developed pressure on the metal (spacer) and in this process it compressed the other O-rings (figure 3.3). This ensure better centering of the electrode when movable electrode was moved under vacuum [190].

Figure 3.4 represents the graphite holder assembly. These graphite holders were detachable from the water cooled electrode. These detachable electrodes were used because during the experiments if graphite rod by accident touched to the other electrode directly (without via graphite-graphite contact) the arcing caused melting of the electrode holders which required redrilling of the holder. Figure 3.4 (a) is the side view of the graphite holder. The main holder (I) was conical shape. The holder (I) cut into three pieces with

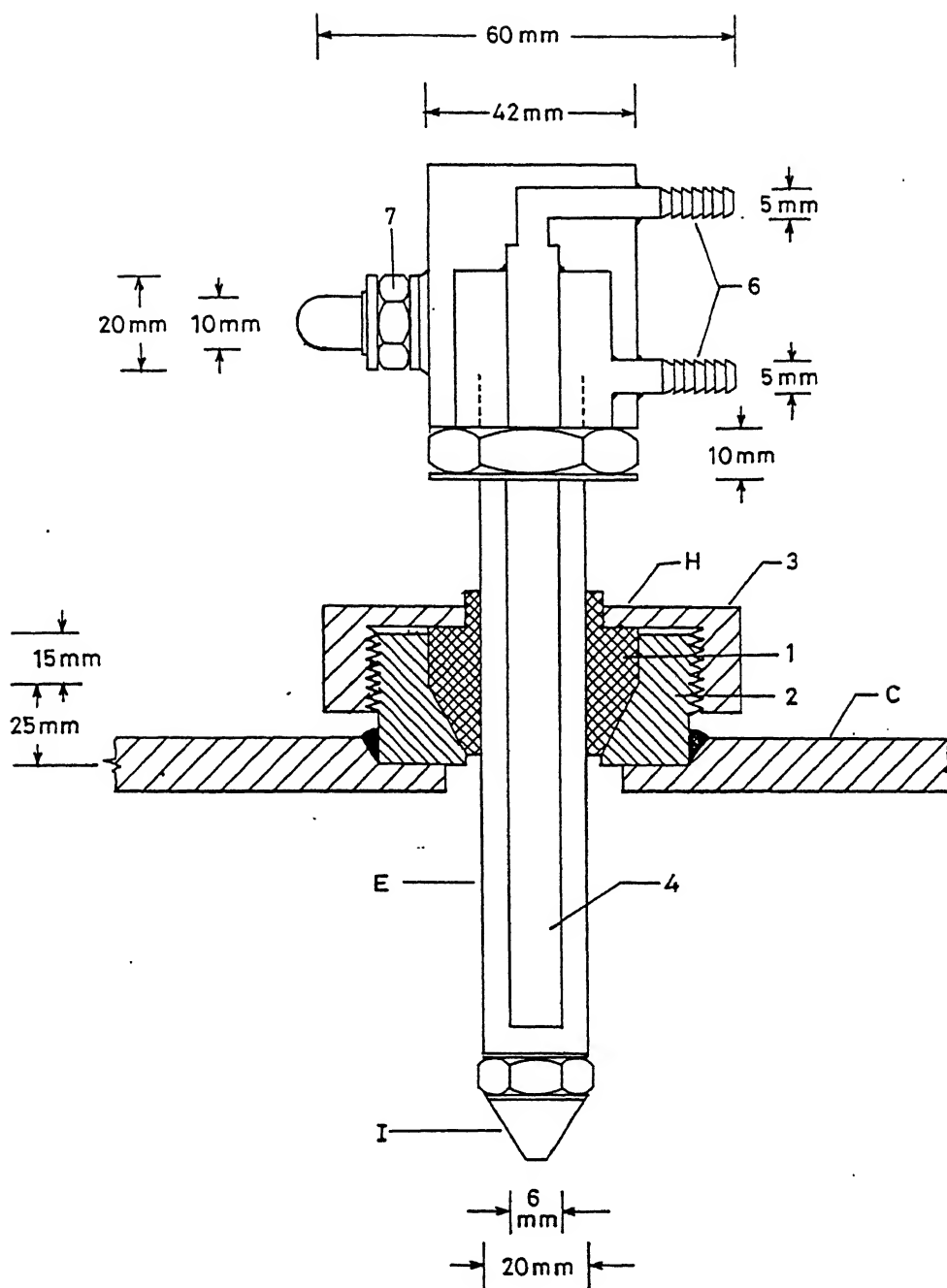


Figure 3.2: Section diagram of the water cooled electrode

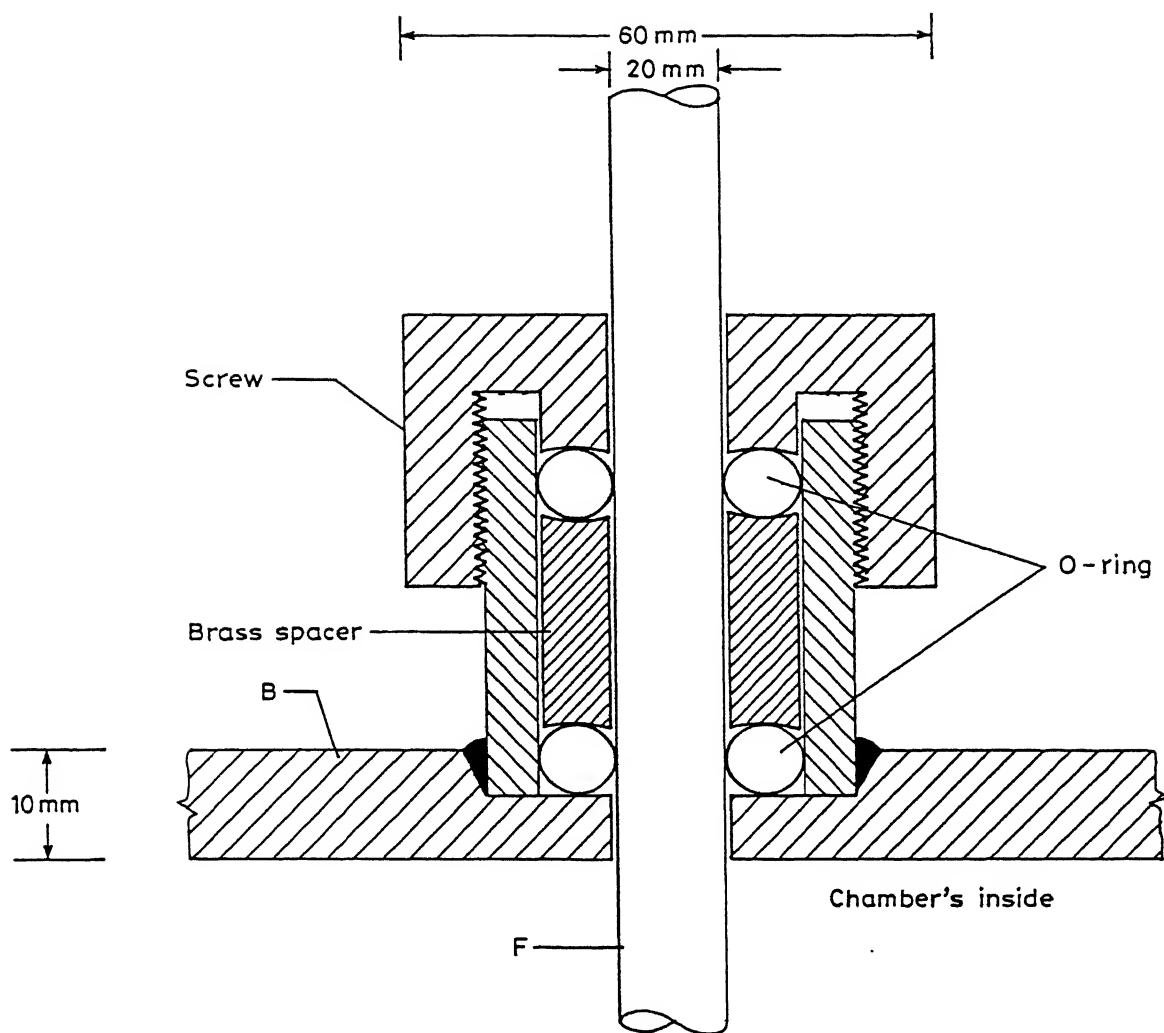


Figure 3.3: Section diagram of the vacuum seal for movable electrode

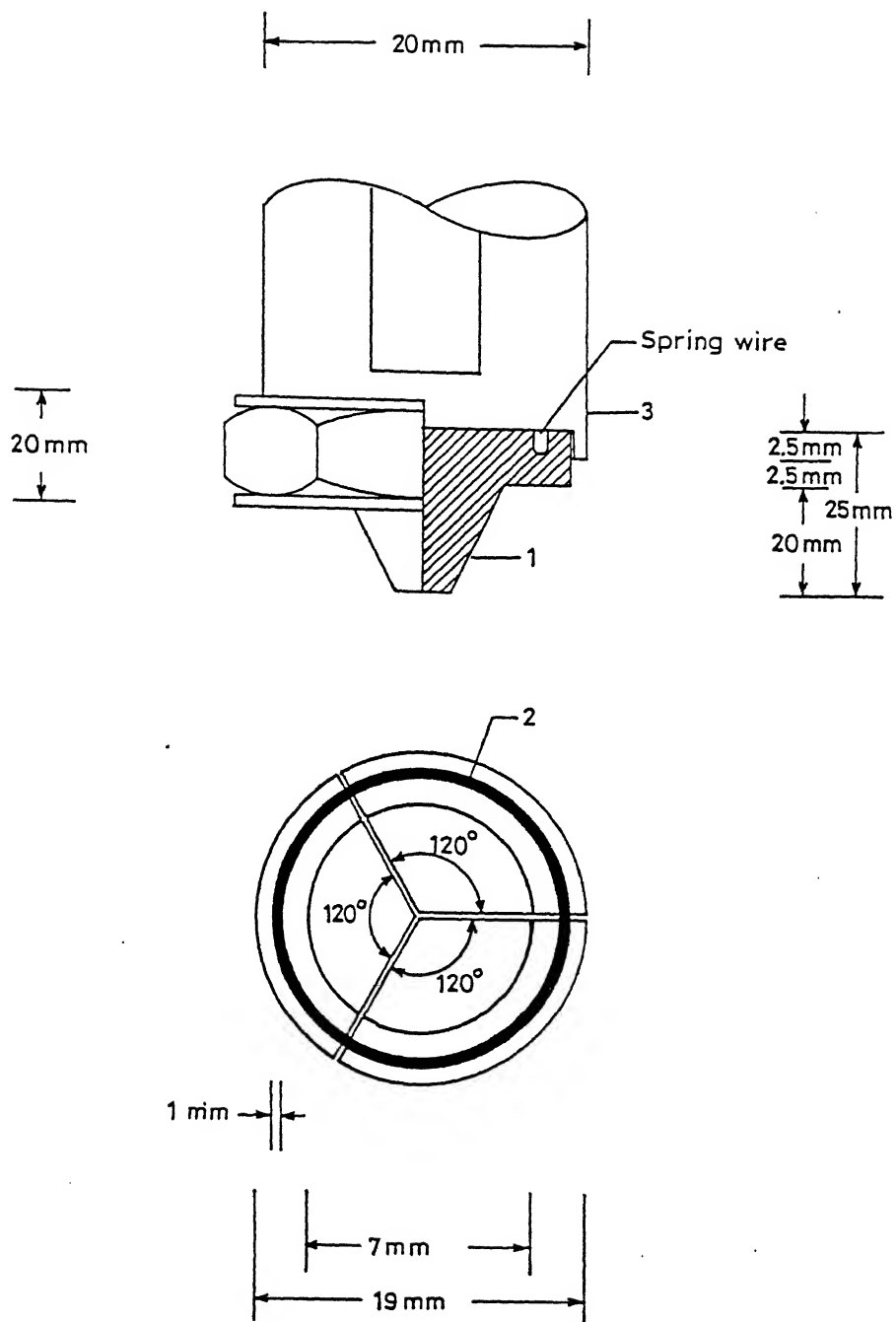


Figure 3.4: Graphite holder design

an angle of 120° to each other as shown in figure 3.4 (b). These pieces were hold using a spring wire II. The main holder (I) was placed into the grove (III) of the water cooled electrodes, D and F. The graphite rods were tighten with a steel nut (IV).

3.1.4 Soot Production from the Reactor

The reaction chamber (A) of figure 3.1 was evacuated to 10^{-3} Torr base pressure by a mechanical pump. The apparatus was purged twice by He-pump filling cycles and evacuated. Finally He-gas pressure was adjusted to 400 mbar by a gas needle valve. The evaporation of the graphite rods was done in static He-gas pressure. The reaction vessel was isolated from the pump by a high vacuum valve whose position in the assembly is shown in figure 3.1. Before starting the arc two things we have been checked, (i) The alignment of the graphite rods and (ii) the water circulation in the reactor, routinely. After switch on the power supply (250A, 25V), gap between the two graphite rods were slowly reduced until arcing started. Once arcing was established it was continued for 30 sec. Arcing and the movements of the electrodes were monitored through the glass view port (L). A white smoke was evolved when two electrodes touches. The light produced was so intense, welding goggles were necessary to monitor the arcing. After few arcing a thick layer of soot were deposited on the glass window which prevented the smooth viewing of the arcing.

After each 30 sec of arcing the power was turned off. This arcing and cooling were repeated to consume 5 cm length of the electrode in about 45 minutes. For precaution, the graphite rod were not burnt down below 1 cm because failure to do this would have caused the arc to jump to the copper holder. Additional graphite electrodes were burned in the same run by turning off the power supply, the apparatus was filled to atmospheric pressure with He and allowed to cool, replacing the consumed graphite stub with a new rod. The slag forms on the other electrode was removed before the next run, otherwise rod did not burn uniformly. Repumping the system down to 10^{-3} torr, bringing the desired He gas atmosphere, turning the power supply back on and initiating a new arcing. The

carbon deposited inside reactor were scraped and in a typical run 3.58 gm of soot was collected by burning 6 rods (length of the each rod was 5 cm).

3.1.5 Parameter Adjustment for Optimum Fullerene Yield

Soot from the arcing procedure was kept in a thimble and the soluble products from it were extracted by soxhlet method, using hot toluene. Extraction was judged to be complete (after 6 hours) when red material ceased to leach out from the soxhlet thimble. Subsequent removal of the solvent in vacuum yields ~ 0.45 gm of the solid material. The black powder was suspended in diethyl ether for 10 minutes. The yellow di-ethyl ether solution decanted off from the black powder and powder was dried in vacuum resulting ~ 0.35 gm of solid. This was redissolved in benzene and subjected to FAB mass spectra, which is shown in Fig 3.5. Strong peaks at $m/z = 720$ and 840 were appeared due to C_{60} and C_{70} respectively. Besides these two peaks the other peaks appear at $m/z = 600, 624, 648, 672, 696, 744, 768, 792, 816, 864, 888, 912, 936, 984$ in the spectrum. For pure carbon containing materials, the presence of these m/z peaks may be accounted for the presence of C_n where $n = 50, 52, 54, 56, 58, 62, 64, 66, 68, 72, 74, 76, 78$, and 82 . This kind of mass spectrum has been reported by other workers [1, 36], but product distribution are not same in all the cases and it depends on large number of factors [191].

The fullerene yield at 15 V and 80 A in different He-pressure are given in figure 3.7. The yield is calculated by following procedure: 400 ml dry toluene was taken in the soxhlet extraction and the solubility of the soot with the variation of parameters are compared with the optical density at λ (max) at 470 and 540 nm. UV/Visible spectrum of the crude soluble portion (one case) is reproduced in figure 3.6. Figure 3.7 shows that there is a local yield (6%) maxima at about 200 mbar. The highest yield obtained (12%) at 400 mbar after going through a yield minimum at (250-300) mbar. The pressure was monitored by a standard Büchi-vacuum meter (switzerland).

The next adjustable parameter was the necessary current for burning the graphite

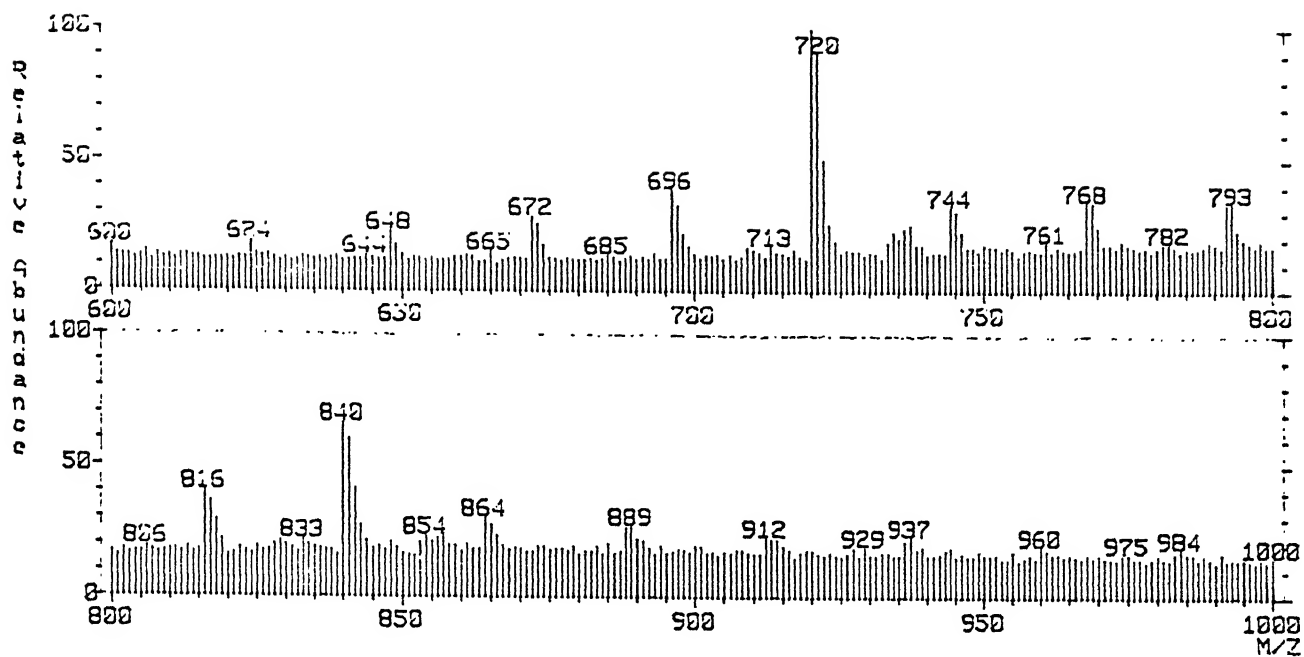


Figure 3.5: FAB mass spectrum of the soxhlet mixture

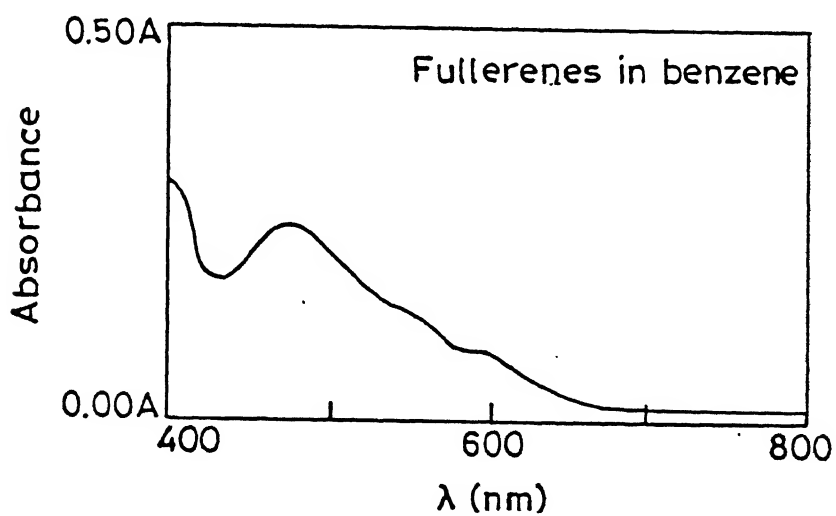


Figure 3.6: UV-Visible spectrum of the soxhlet mixture, in benzene.

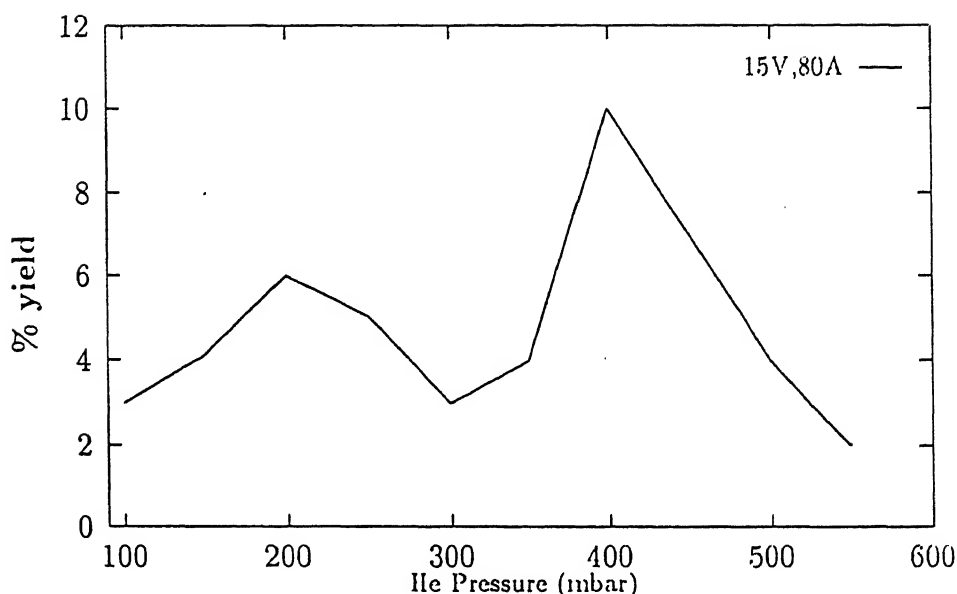


Figure 3.7: Yield of the fullerenes' vs He pressure, where current is fixed at 15 V and 80 A.

rod. A regulated A/C power supply, 0-25 V and 0-250 A, was locally fabricated. It is a common phenomenon in arcing that the set voltage is dropped from its initial set voltage [192]. We observed in our power supply the voltage drops (1-2) V from the initial set voltage. In the contact arc technique the current level depends on the contact pressure developed between the graphite rods during arcing [167]. Graphite rod was feed into the the reactor at the 4 mm/min and this adjustment was done from the ball bearing P (figure 3.1). It was also observed that when the pressure between the graphite rods was high the current reached to ≥ 200 A. In this case the electrode was moved back side slightly (manually), until the current level dropped bellow 100 A. Finally the current was adjusted to the desired level. The variation in each experiment was maintained within ± 10 A. A commercial circuit breaker was used in the power supply for additional safety. Yield of the fullerene was measured at different currents at a fixed voltage. Current vs yield at 400 mbar He-atmosphere is shown in figure 3.8.

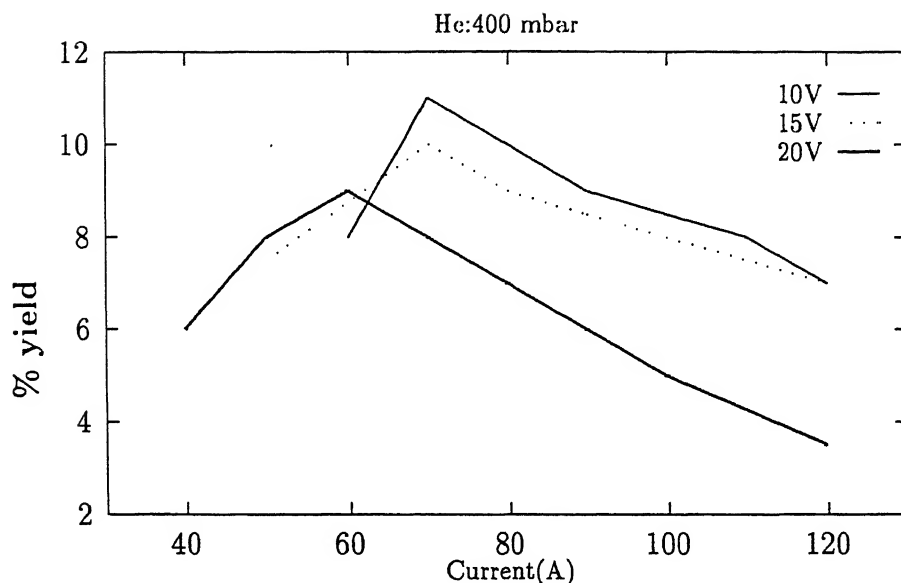


Figure 3.8: Yield of the fullerene vs current

3.1.6 Separation and Characterization of C_{60}

The crude product obtained after soxhlet extraction was dissolved in 500 ml of dry toluene. Some of the solid material remain insoluble and it was reluctant to dissolved on further addition of fresh solvent. The amount of insoluble material were not consistent in every batch. How this insoluble materials was formed in this process was not clear. This solution was concentrated further and subjected to column chromatography (inner diameter 3 cm and length 30 cm) using neutral alumina as the solid adsorbant. Separation of C_{60} and C_{70} was done by using hexane(petroleum fraction)/n-hexane as eluent. As fullerene solubility in this solvent was very low (section 1.8) so movement of the material in solid adsorbant was extremely slow.

C_{60} , C_{70} and others were not separated from the soxhlet extraction in this chromatography method using solvents like benzene, toluene, carbon-disulfide etc. in which they are more soluble. To overcome this problem according to the procedure described by Diederich and co-workers [148], 100 gm of neutral alumina was added to the concentrated fullerenes solution and was made a slurry. Finally toluene was evaporated in vacuum from the slurry and the resulting mixture was applied at the top of the column.

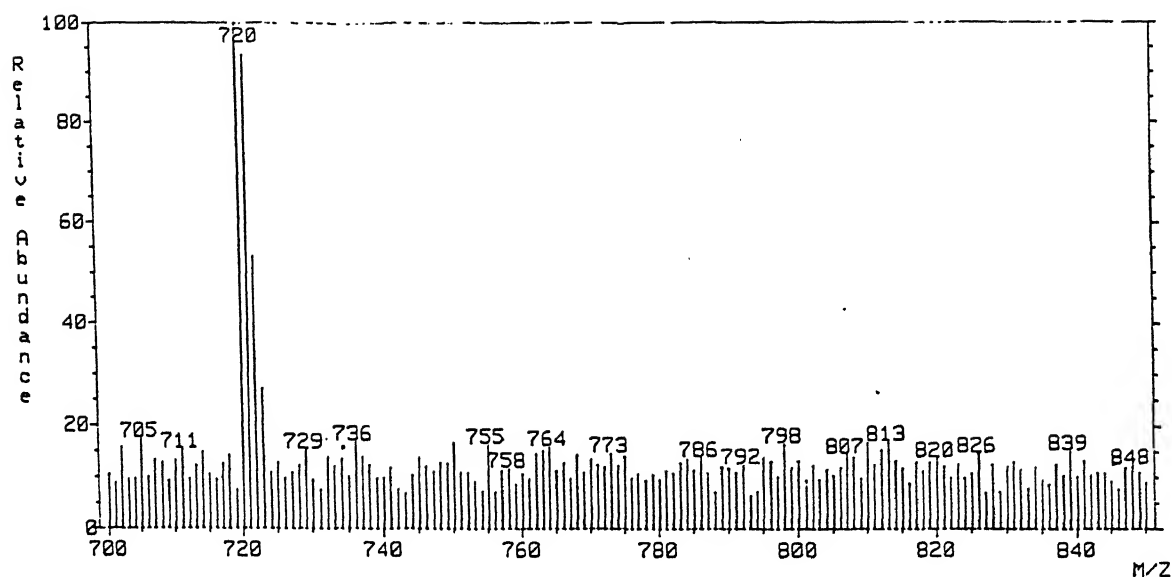


Figure 3.9: FAB mass spectrum of the chromatography separated C_{60}

Elution was done with (95:5) hexane-toluene mixture where a purple solution separated first and followed by a pink colour eluent. The solvent was evaporated from the first fraction and to get the crystalline product which was dissolved in benzene and its FAB mass spectrum was recorded. The figure 3.9, mass spectrum shows that chromatographically separated sample contained only C_{60} and free from other fullerenes. Some unidentified compounds were adsorbed at the top of the column which could not be eluted using conventional solvent mixtures. Yields of C_{60} in this method was not consistent, in every batch of separation. In some cases only 2% of C_{60} was obtained from the crude product.

The infrared spectrum (figure 3.10) of the chromatographically pure samples shows four strong absorption bands at 527, 577, 1183, 1428 cm^{-1} . This IR spectrum is in agreement with reported IR spectra [1, 83]. The UV-visible absorption spectrum of this chromatographically purified C_{60} give bands (figure 3.11) at λ_{max} =213, 257, 327 and 405 in n-hexane and broad bands at 480-625 nm region in benzene. These UV-visible spectra are in good agreement with the reported λ_{max} by Ajie et.al. [35], Hare and their

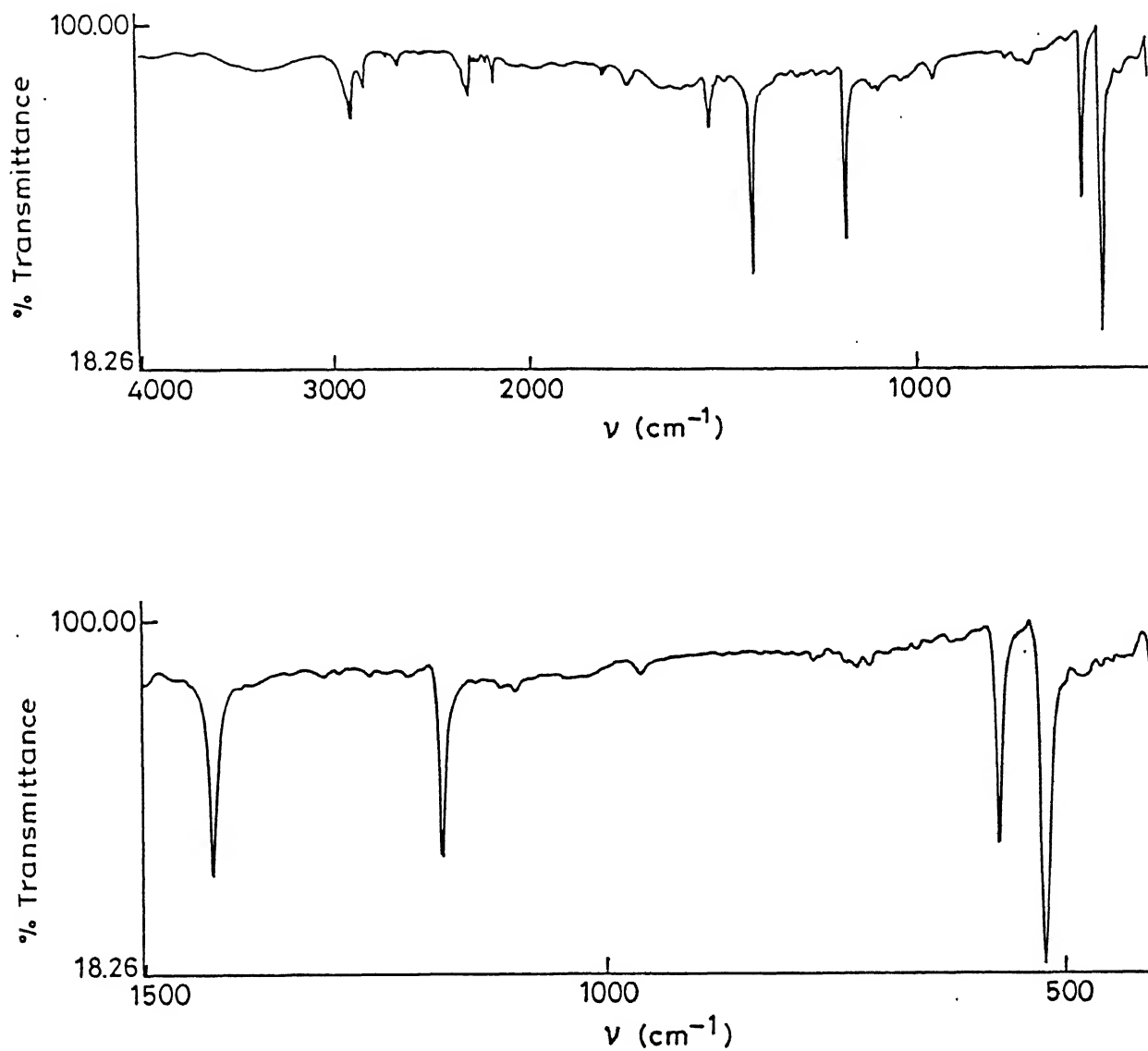


Figure 3.10: FTIR spectrum of chromatographically pure C_{60} on KBr pellets, (above) from 4000-400 cm^{-1} and (below) 1500-400 cm^{-1} .

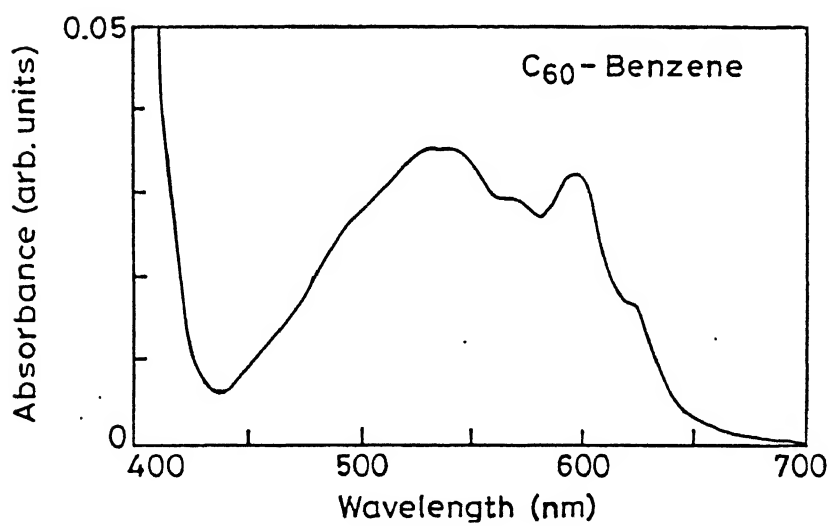
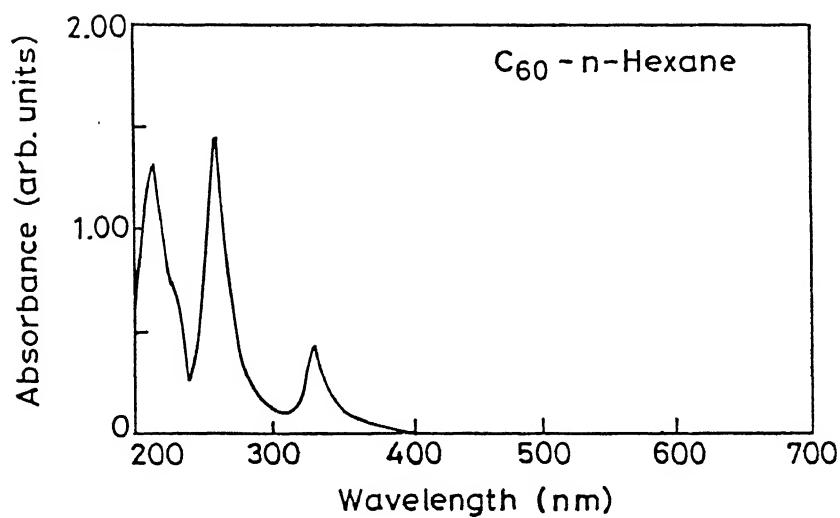


Figure 3.11: Electronic absorption spectra of C_{60} ; (a) n-hexane (b) benzene

coworkers [86].

3.1.7 Attempted Fullerene Separation from Natural Soot

Soots were collected from the various source such as: (1) benzene and acetylene flame (2) LPG flame and (3) combustion of mustard oil.

(1) A sooty flame was produced from the laboratory spirit lamp using benzene as fuel. ~ 1 gm of soot after 4 hours of operation was collected, expending 200 ml of benzene. The soot was scraped from the backside of a water cooled aluminium container. The material was washed in diethyl-ether and soxhlet extracted for 5 hour in toluene. The solution was concentrated and flash chromatographed in 50:50 toluene/n-hexane. FAB mass spectrum (figure 3.12) of this chromatography separated solution did not show the presence of mass peak at $(m/z) = 720$ or 840 , which are the most abundant fullerenes among the fullerenes family.

(2) Similar to the above described experiment (1), the soot was prepared from mustard oil. Figure 3.13, mass spectrum shows that this soot does not contain C_{60} and C_{70} . A gas burner was used for the preparation of Liquid Petroleum Gas (LPG) soot and soot was collected in the back side of water cooled container. Mass spectrum showed (figure 3.14) the absence of the desirable fullerenes.

3.2 Results and Discussion

Figure 3.7 and figure 3.8 shows the yield of fullerenes was dependent on the helium gas pressure and the effective power during burning. It has also been suggested that fullerene yields are depend other factors also, (a) rod diameter [160] and (b) He-gas flow in the reactor if the arc is operated in a dynamic He gas pressure [164]. In the present case, we have done the experiments using a fixed rod diameter (1/4 inch) and in a static He-gas pressure. Thus we are unable to predict the role of the above two factors on the overall

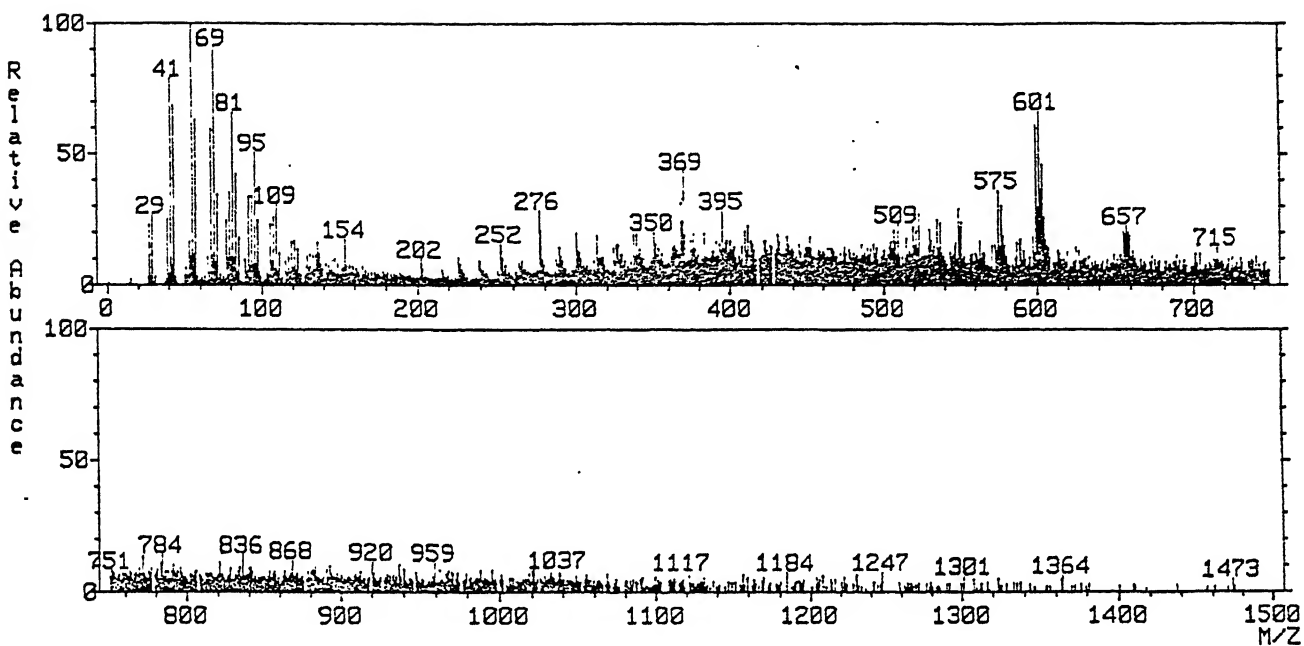


Figure 3.12: FAB mass spectrum of the benzene soot

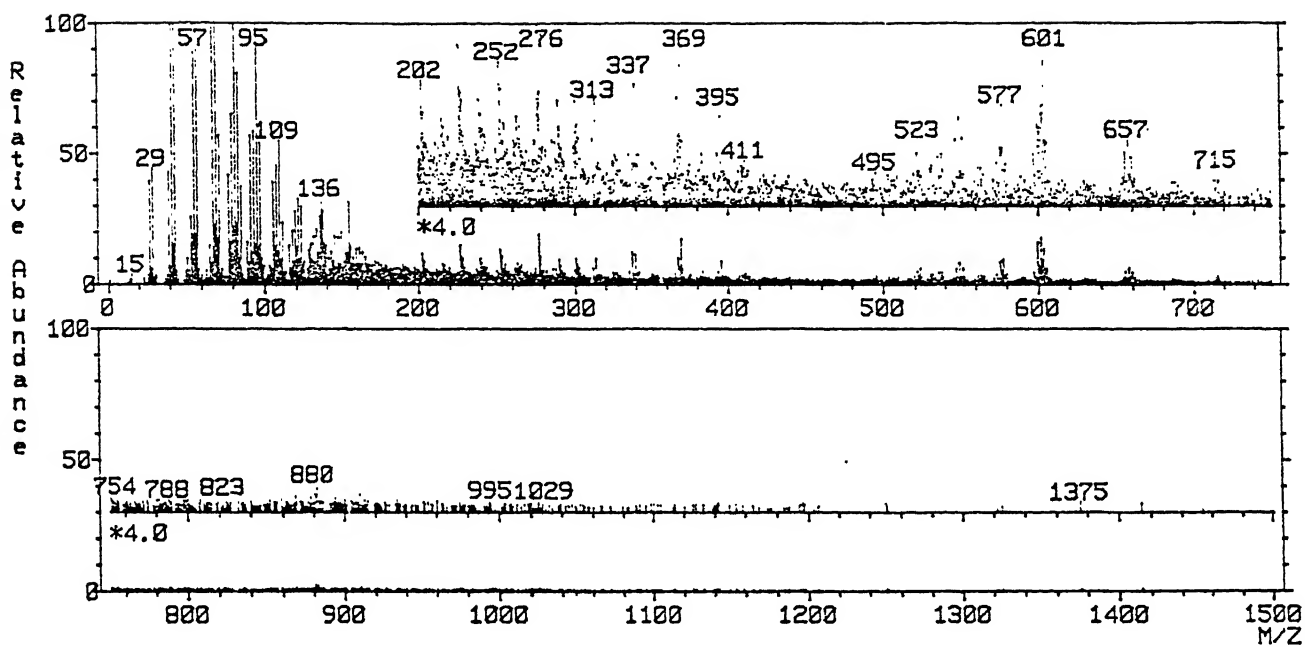


Figure 3.13: FAB mass spectrum of the mustered oil soot

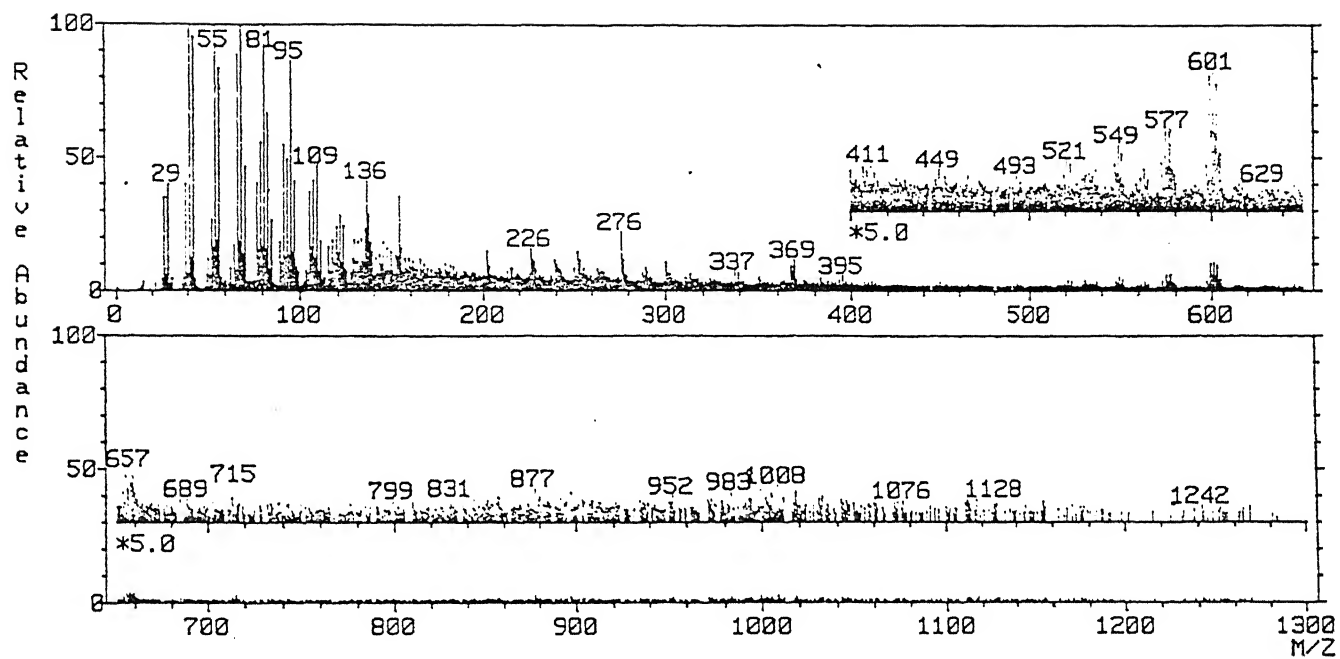


Figure 3.14: FAB mass spectrum of the LPG soot

fullerene yield.

Helium pressure is the operating parameter that is commonly reported for the synthesis of fullerenes. Figure 3.7 shows that maximum fullerene yield ($\sim 12\%$) is observed when the He gas pressure is 400 mbar at power 15 V, 80 A. A local yield maxima at 200 mbar He pressure is also observed. Surprisingly the yield is very poor in between (250-350) mbar He pressure. This observation is similar to the observation of Scrivens et. al. [164] and these authors prepared the soot using the d.c plasma reactor in a dynamic He-gas pressure.

Fullerene yields are measured at different power and 400 mbar He gas pressure. These results are given in figure 3.8. The maximum yield obtained at various power levels are $15\% (\pm 5\%)$ at 10 V, 100 A, $13\% (\pm 3\%)$ at 15V, 80 A and $10\%(\pm 5\%)$ at 20 V, 60 A. The reported fullerene yields (max.) from the contact arc reactor are $10\pm 2\%$ at 100-200 A and 10-20 V by Haufler et.al. [132], Koch et. al. $\sim 11\%$ at 70 A but voltage is not mentioned by Koch et. al. [161] and $\sim 12\pm$ at 32 V and 90 A by Olha and co-workers in a multiadaptor vapourization system [163]. However, Rao et. al. observed 10-30% yield at 100-180 A and 5-8 V [25]. The fullerene yields we produced are comparable to the the above mentioned reported yields however the yield observed at 100-180 A and 5-8 V is considerably higher than our as others [132, 161, 163]. Figure 3.8, is also indicates that in every case the maximum yields are achieved when the power are keeping between 0.9-1.2 KW. Parker et. al.[159] and Scrivens and co-workers [164] reported, at ~ 1 KW obtained the maximum fullerene yield from the dc-plasma reactor. We observed when the power level was ≤ 700 W, a difficult problem that was to maintain an uniform arc with sufficient time (30 sec.). Time required to burn the 5 cm rods at 10 V and 80-100 A was 2 hours, however the same length of rods were burn within ≤ 30 minute at 20 V, 120-140 A.

Nothing is known about the kinetics of the fullerene formation. Most of the mechanisms published so far are based on speculation [53]. Pentagonal road model by Smalley et. al. [48] and size selective collision by Bower's et. al. [50, 51] are seems very attractive

to explain the formation of C_{60} but it does not adequately explain the variable yields of the fullerene in the different set of conditions. It is not clear at this moment that dimension of the reactor has any influence on the fullerene yield. Figure 3.7 and figure 3.8 suggested that efficient synthesis of fullerene occurred at the narrow range of experimental parameters. Thus it seems kinetics of the fullerene formation must be fairly specific.

In a different type of experiment Smalley et. al. [20, 48] vapourized the graphite with the help of a pulse laser and the resulting carbon vapour is passed into a tube furnace with the help of He-gas. They observe that when the furnace is kept at room temperature, the soot produced does not contain any fullerene, however at 500°C furnace temperature soot formed does contain fullerene. They optimize the furnace temperature in the range $1300\text{-}1500^{\circ}\text{C}$, when the soot produced maximum amount of fullerene. From these observations they suggested an 'annealing temperature' which is very crucial for high yield production of the fullerene. However it is observed (figure 3.8), at high power 20 V, 120 A, the yield of fullerene is 3-4%, Koch et. al. [161] is reported at 130 A the yield is 3%, Scrivens et. al. [164] and Parker et. al. [159] have noted similar type observation that at high power graphite rods are burnt fast but the yield is very poor. Based on the above observation it indicates that the temperature is not the principle guiding factor for the fullerene formation. As in the high power ($\sim 2.5\text{ KW}$), temperature of the surrounding space which cover the carbon arc is more/larger compared to 1 KW power.

In the carbon arc the hot gas containing carbon atoms that react to give small reactive fragments like C_2 , C_3 , C_4 and C_5 etc. bonds on and eventually form fullerene [46, 47]. The heat of formation value of C_{60} , C_{70} and higher fullerene and nanotubes are quite different [53, 54]. So, entropy factor, $T\Delta S$, is the determining factor for the specific shape of the fullerene when the carbon vapour are condensed. Migration of the carbon vapour from the hot arcing point to the less hot environment most likely depends on the thermal mass diffusion co-efficient of the carbon atoms (vapour). Figure 1.3 suggests carbon grows first in linear chains, transfer to monocyclic planar rings and form new families of planar bi, tri and tetracyclic rings. These large planar rings on selective

collisions by size are induced to isomerize into the fullerenes. Bower's et. al [50] further suggested that in arc reactor the atomic carbon 'soup' diffused out of the arc, and initially formed chains and then rings. We believe that at high power, specially with the increase of voltage (to our knowledge where voltage are kept beyond 40 V in K-H or contact arc type reactor) velocity and momentum of the ejecting carbon particles from the graphite rods are increased. Hence the collisions between the carbon particles are random, so size selective collisions are less in number. Another reason of the poor yield at high power is, as temperature is proportional to the power, that the thermal agitations of the carbon vapour (atoms) are increased which may also reduce the size selective collisions between the planar rings. This may be one of the reason for getting high yield (15%) at 10 V and 100 A, figure 3.8. From the above results it is suggested that slow evaporation of the graphite rods is an essential criterion for getting good yield.

Figure 3.12 to figure 3.14 are the FAB mass spectra of the different kinds of soot which are collected from several sources. These spectra showed the absence of both C_{60} or C_{70} . Corannulene (figure 1.6) with its five-membered rings, provides the puckering necessary for building of fullerene structures and is considered to be the precursor molecule [79]. However the absence of peak at $m/z=250$ from the spectra (figure 3.12-figure 3.11) indicates fullerene produced from the combustion of benzene soot has different kind of mechanism [24]. Possibly fullerene intermediates are more reactive in the presence of H_2 and O_2 . This may be the one of the reason for natural soot not containing any identifiable quantity of fullerene. Howard et. al. [24] prepared fullerene from specially designed burner from a premixed laminar flame where carbon to oxygen ratio is 0.729. However in this process they got maximum yield 1.26 %. This type specific conditions are not achieved at the natural conditions of burning, in the present study.

3.3 Conclusions

We have described an inexpensive and easily fabricated fullerene reactor for the arc discharge type. The described reactor allows one to control the gas pressure and required power level for optimization of the fullerene yield. The metallic spacer in the vacuum seal of the movable electrode maintained the alignment of the graphite rod. Advantage of this type of vacuum seal is that the electrode of larger dimensions can pass through easily. As fullerene is formed under very specific conditions in the arc or plasma discharge, so systematic study of the yield with different power and He-gas would provide the details about the fullerene formation kinetics. At present we do not have any idea about the local yield maxima in figure 3.7. Intuitively we suggest that fullerene formation zone in the vicinity of arc is not a spherical zone rather it forms a hyperboloid surface where water cooled electrode may influence this yield.

Chapter 4

Reactivity with NO, NO₂/N₂O₄, SO₂, HOCl and ¹O₂

Carbon-carbon double bonds react easily with different kinds of radicals and have produced billions of new organic and organo-metallic compounds. Reaction mechanism between carbon-carbon double bond with a variety of radicals have extensively been studied [171]. In this chapter, our aim is to study the behaviour of some reactive molecules like NO, NO₂/N₂O₄, SO₂, HOCl, O₂ and ¹O₂ with C₆₀ whose reactivity with planar olefinic carbon carbon double bonds is well established.

4.1 Experimental Section- Part I.

4.1.1 General Conditions

All the reactions were performed in oven dried apparatus and reactions were carried out in air, unless specified otherwise.

4.1.2 Materials

Commercial grade solvents, benzene, toluene, hexane, n-hexane, acetonitrile, DMF and DMSO, were distilled prior to use but not degassed. Analytical grade reagents were used as such.

4.1.3 Physical Measurements

Elemental analyses:

C, H, N analyses were performed with a EA 1108 elemental analyzer in RSIC Lucknow.

Infrared spectra:

Spectra were recorded in KBr pellets on Perkin-Elmer 1320 and FT 1600 Perkin Elmer series instruments, as discussed in section 3.2.

UV-Visible :

Spectra were recorded as described same as section 3.2.

Mass spectra :

FAB mass spectra were recorded similarly as discussed as section 3.2.

EPR spectra :

EPR measurements were done with a Varian E-109 spectrometer. Liquid samples were recorded using flat cell and 6 mm diameter quartz tube. DPPH were used for internal standard of the spectrometer.

X-ray photo-electron spectra :

The spectra were recorded on a PE/ESCA/SAM model-550 using MgK_{α} radiation source. X-ray was generated at power 15 KV, 20 mA. The operating voltage was 1900 V. Survey scan was done in full scale (X-axis, 0-1000 eV; Y-axis, 0-300 K). The important peaks were further resolved with the variation of scan speed, chart speed and intensity scale. Powdered sample were pressed on the one side of a indium metal which were used as the substrate material of the sample. Sample was kept for 4 hours at 10^{-4} torr for removing the solvents before inserting it into the main analyzing chamber, at 10^{-9} torr. The X-ray line was not monochromatized and resolution limit was 0.7 eV. The instrument was

calibrated with respect to gold (Au 4f binding energy at 84.00 eV). The peak position was further resolved (simulated) by commercial curve fitting package (Jandel Scientific PeakFit, version 3.18, Copyright (C) 1992 AISN software).

NMR :

^1H NMR (400 MHz) spectra were recorded on a Bruker WM-400 FT-NMR spectrometer using DMSO-d_6 . Tetramethylsilane (TMS) was used as an internal standard for NMR studies.

4.1.4 Chemical Analysis

Griess-Ilosray test for detection of NO_2^- : [193]

Small portion of the solid was dissolved in 5 ml of distilled water. 1 ml of the test solution was mixed with a 50 μl sulphanilic acid, followed by 50 μl of α -naphthyl amine reagent. A red azodye ($\lambda_{\text{max}}=520\text{-}525\text{ nm}$) is formed. 01 μg of HNO_2 is sufficient for the diazotization of sulphanilic acid [193].

The sulphanilic acid, in 100 ml warm 30% acetic acid, and the α -naphthyl amine reagent was prepared according to the standard procedure [193]. 100 μl test solution was added into 2.5 ml of water in a UV-Visible cell followed by 50 μl of naphthylamine, the time was noted when β -naphthylamine was added. After 30 sec. a pink colour was fully developed and the optical density of this solution was recorded.

4.2 Experimental Part-II. Reaction Methodology.

4.2.1 Reaction between C_{60} and Nitric oxide.

Method 1 :

2 gm ammonium ferrous sulphate, dissolved in 0.1 M sulfuric acid (20 ml) was taken in a 500 ml two necked flask. A dropping funnel containing a aqueous solution of 2 gm

NaNO_2 was placed in one neck. 15 mg C_{60} , dissolved in 50 ml benzene, was taken in an another two necked 100 ml flask. Two gas bubblers attached with polyethylene tube were fitted in series, one end of it was connected to the flask which containing C_{60} solution, and the other end was connected to the gas generating flask. The gas bubblers contained a 10% aqueous solution of Na_2CO_3 (first from the gas generating flask) and concentrated sulfuric acid was taken in the second one to it, for remove any NO_2 formed in and dry NO respectively. Water suction was employed to create low vacuum in the C_{60} flask for easy flowing of the gas from the generating flask to the reaction flask. The NO gas was passed through the C_{60} solution for 2 hours and then it was kept overnight. But the colour of the C_{60} solution remained unchanged and on evacuation pure C_{60} was separated out.

Method 2 :

6 ml concentrated HNO_3 and 18 ml concentrated HCl were taken in a 250 ml flask previously purged with nitrogen and a benzene solution of C_{60} (25 ml) was added into it. The flask was tightly closed and the reaction mixture was occasionally shaken and kept for 2 days. The colour of the C_{60} solution remained unchanged during this period. The benzene layer was taken into another flask and the solution was evaporated under vacuum which yielded unreacted C_{60} .

Method 3 :

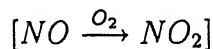
Glass wires arrangements were the same as described in method 1. In a 500 ml flask 1:3 volume ratio of conc. HNO_3 and conc. HCl was taken and the evolved NOCl gas was passed into the C_{60} solution for 2 hours. There was no colour change of the C_{60} solution during this period and C_{60} was recovered back from the benzene solution after evacuation under vacuum.

4.2.2 Synthesis of Polynitro-Polyhydroxy Buckminsterfullerenes

Method 1 :

Experimental set up used here was identical to that described in the section 4.2.1 (method

1). The only difference in this case was that a three necked flask was used for gas generation. This third neck was kept open with a glass tube connection to get fresh air into the solution to oxidize nitric oxide to nitrogen dioxide. i.e.



The NO_2/N_2O_4 gas was allow to pass through the C_{60} solution only through a concentrated sulfuric acid bubbler to make this gas moisture free. Within 5 minutes of the passage of this gas purple colour of the C_{60} solution changed to orange-red. Further passage of NO_2 gas did not change the colour, suggesting the completion of the reaction. The flask was detached from suction and gas generating systems, and 75 ml of hexane/pet-ether (60-80)⁰ C was added to the orange-red solution which was kept for 5 hours. Deep orange-red solid was separated out. The mother liquor was decanted off, the solid (1) was washed with hexane, vacuum dried and analyzed.

Elemental analysis : C, 55.45%; H, 0.60%; N, 9.20%.

IR, ν_{max} (KBr): 3250 (br), 1624(w), 1560 (br), 1336 (br), 1050 (br), 809 (br) cm^{-1} .

XPS: C 1s=285.5, N 1s=407 and 399, O 1s=534 eV.

Mass Spectra: m/z= 720 (100%), 737, 754, 768, 805.

Method 2 :

Into a 20 ml benzene solution of C_{60} , 10 ml of concentrated HNO_3 acid was added in a 50 ml round bottom flask. The reaction mixture was stirred with the help of a magnetic stirrer for 10 hours and was kept for the 6 hours. The purple colour of the benzene solution slowly changed to orange yellow. The benzene layer was carefully separated out and 50 ml n-hexane/pet-ether was added into it. A yellow-orange solid was precipitated out. The precipitated was washed repeatedly with hexane and vacuum dried. IR spectrum of the solid (2) in KBr showed absorption bands at :

IR ν_{max} (KBr): 3300, 1635, 1565, 1330, 1010, 800 cm^{-1}

4.2.3 Reaction Between C_{60} and SO_2^-

In a 150 ml flask, 20 mg of C_{60} in 50 ml dry benzene was taken and this was purged with argon gas for 30 minutes. 1 gm of solid sodium dithionite and 20 ml water (argon purged) were added into it and the mixture was stirred for 6 hours. The predissociation, ($S_2O_4^{2-} \rightleftharpoons 2SO_2^-$) of the dithionite ion generates the active SO_2^- [194]. On keeping this mixture for several hours, there was no change in the colour of the benzene solution and unreacted C_{60} was recovered back from the benzene layer.

4.2.4 Reaction Between HOCl and C_{60}

C_{60} (10 mg) in toluene (50 ml) and aqueous 10^{-3} (M) NaOH solution (25 ml) were taken in a 250 ml flask. Freshly prepared Cl_2 gas was passed through the aqueous layer of the mixture in slow rate for 30 minutes. This reaction flask was kept in an ice bath to maintain $0^\circ C$ temperature. After 24 hours the electronic spectrum of the toluene solution was recorded, but optical density of C_{60} at λ_{max} 405, 540 and 623 nm remained unchanged from the starting solution suggesting no reaction occurred under these conditions.

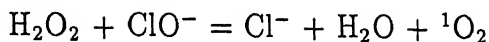
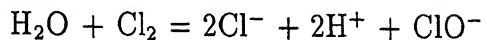
4.2.5 Photochemical Reaction Between C_{60} And O_2

Air saturated 20 ml of benzene solution of C_{60} was taken in a 50 ml round bottom flask which was kept for 2 days in sunlight. The progress of the reaction was monitored by UV-visible spectroscopy. There was no noticeable change in the absorption spectra from the starting solution even after two days.

4.2.6 Reaction Between C_{60} and 1O_2

0.5 ml (20%) H_2O_2 was added in the reaction medium identical to that described in section 4.2.4 and progress of this reaction was monitored for 6 hours. It is known [194, 195]

that singlet oxygen can be produced from the reaction between hydrogen peroxide and hypochlorite ion in the presence of alkali as:



The toluene layer was separated and subjected to UV-visible spectroscopy. There was no change in the absorption spectrum observed from the starting solution suggesting no reaction between C_{60} and ${}^1\text{O}_2$ in toluene/aqueous medium under the experimental conditions.

4.3 Results and Discussion

All the molecules and radicals tried herein to react with C_{60} are well known [171] to react with normal olefinic carbon-carbon double bonds. The observed reactivity of these molecules or radicals with C_{60} is schematically shown in figure 4.1. It shows that only concentrated HNO_3 acid and NO_2 (N_2O_4) reacts with C_{60} .

The orange-red product which was obtained with the reaction of NO_2 slowly changed to yellow colour on exposure to laboratory atmosphere. It was observed that it was the moisture or the humidity that caused the colour change apparently due to hydrolysis. The air brought this change in colour from orange-red to yellow was contained appreciable quantity of HNO_2 (N_2O_3) which was tested by Griess's reagents. The product obtained from the nitric acid treatment of the benzene solution of C_{60} apparently has similar composition to that of air exposed residue of the orange-red products.

The IR spectrum of the orange-red solid (1) is reproduced in figure 4.2. In this spectrum the vibrations at 1560, 1336, 809 cm^{-1} are typical to nitro group [196]. In addition, the broad band around 3400-3250 cm^{-1} is assigned to $\nu(\text{OH})$ and a band centered at 1050 cm^{-1} may be due to coupled $\nu(\text{C}_n\text{-O})$ [197]. The compound 1 is soluble

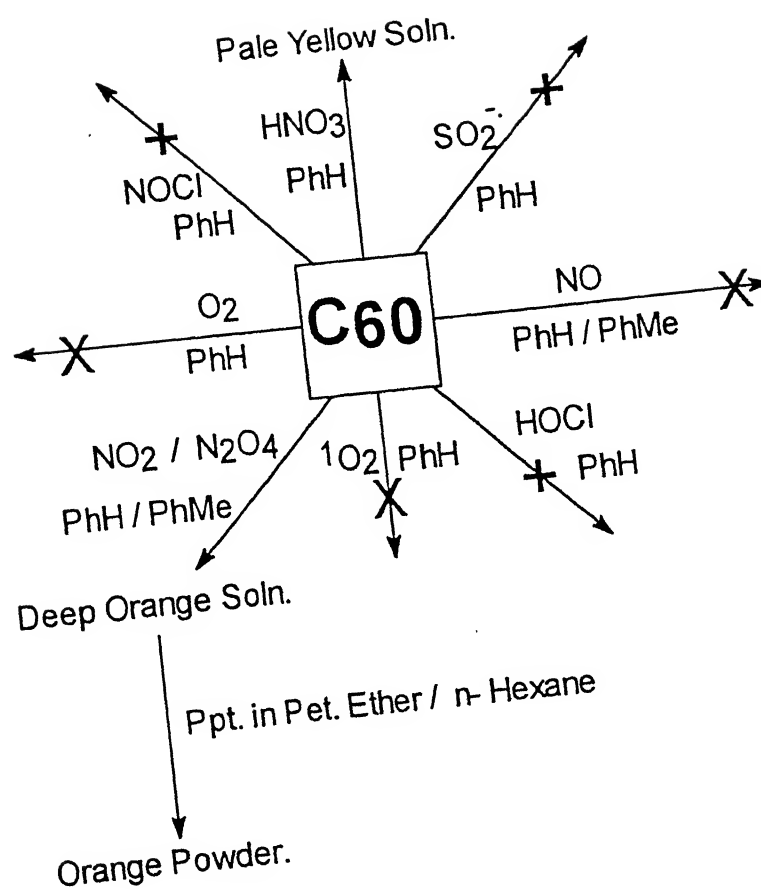


Figure 4.1: Scheme; reaction between C_{60} and the molecules/or radicals.

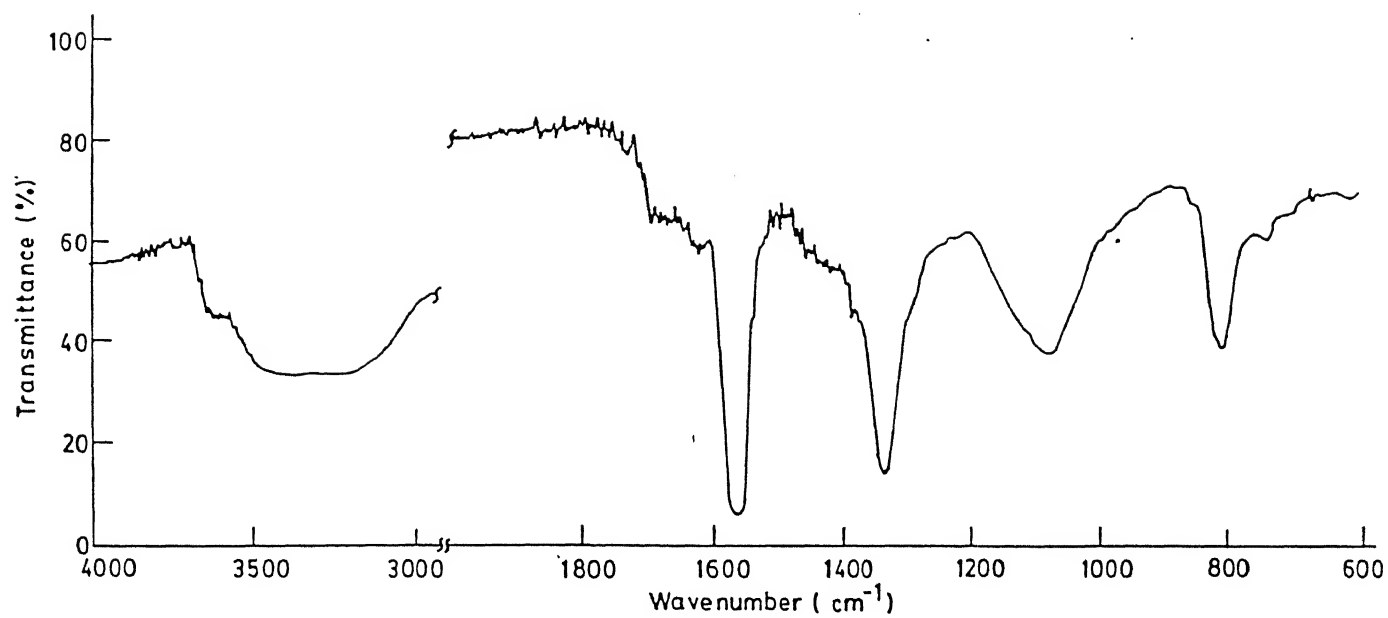


Figure 4.2: IR spectra of the compound1

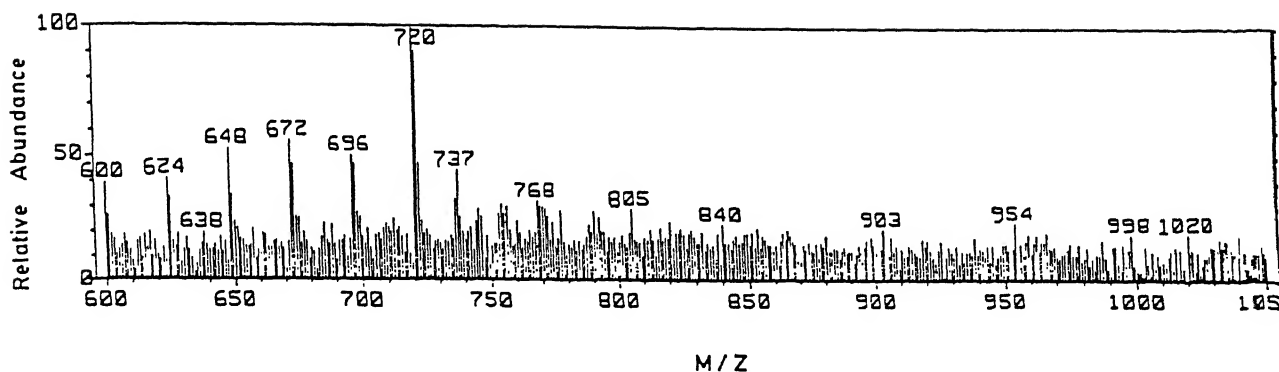


Figure 4.3: Part of the FAB mass spectrum of the solid 1

in MeCN, DMF, DMSO. This suggest that 1 is more polar than pure C_{60} . It is also sparingly soluble in water and produce a pale yellow solution.

The FAB mass spectrum of the compound 1 is shown in figure 4.3. It shows several peaks at $m/z = 768, 754, 737, 720, 696, 672, 648, 638, 624$ and 600 . The appearance of peaks at $720, 696, 672, 648, 624$ and 600 are interesting. These peaks correspond to C_{60} and it's fragments with the loss of C_2 units (multiple in number) and in the range from C_{60} to C_{50} respectively. We have started the reaction with pure C_{60} but it's FAB mass spectrum did not show fragments with the consecutive loss of C_2 units in the identical conditions. The fragmentation of the compound 1 under FAB mass conditions can be rationalized due to oxidative degradation. The other identifiable m/z peaks at $737, 754, 768$ and 805 correspond to $C_{60}OH$, $C_{60}(OH)_2$, $C_{60}O_3$ and $C_{60}(OH)_5$ respectively. The appearance of oxygenated species, with the absence of any nitro species, suggests that the nitro group in the C_{60} derivative degrades oxidatively with the stepwise loss of C_2 units. So in this oxidative degradation process it was observed that the lower even number fullerenes i.e C_{58} to C_{50} were extra stable. The absence of odd number fullerenes in this mass range by oxidative degradation suggests that it is less stable compared to even numbered fullerenes which was earlier established by other experimental [4, 198] and theoretical works [5, 79].

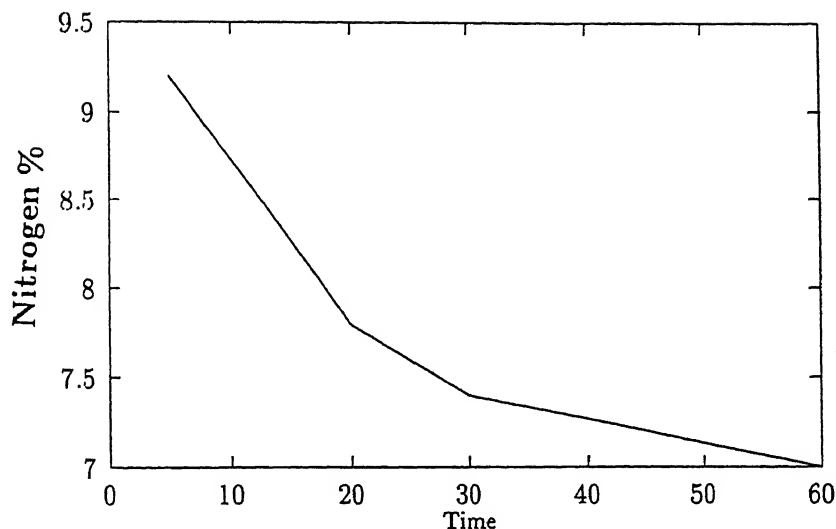


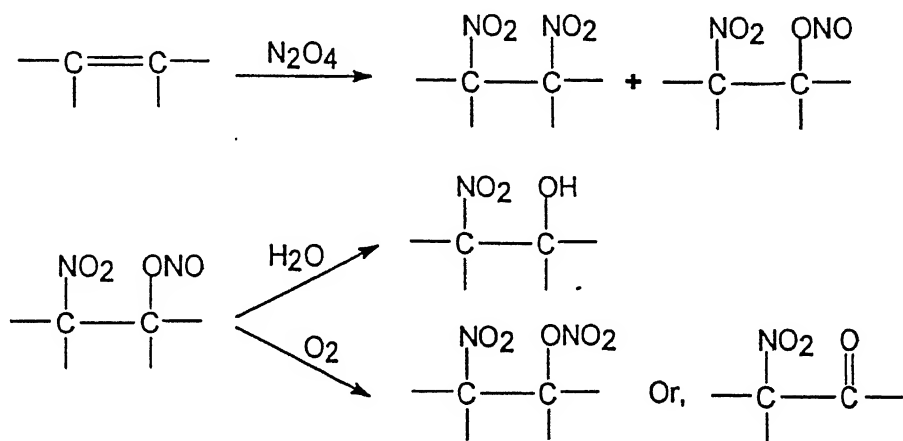
Figure 4.4: Nitrogen percentage analysis of the orange-red compound at different time in laboratory conditions.

It was found to be difficult to get a fixed composition of the compound **1**. This is caused by its rapid hydrolysis even under brief exposure to laboratory atmosphere with concomitant loss of nitrogen. Elemental analyses carried out on different batches of the compound **1** and an average composition is determined as $[C_{60}(NO_2)_x(OH)_y]$ Where, $x = 6-8$ and $y = 7-12$. For compound **2**, prepared according to the procedure as described in the section 4.2.2 (method 2), the average composition is determined as $[C_{60}(NO_2)_x(OH)_y]$ Where, $x = 2-4$ and $y = 11-16$. Compound **1** on exposure to air changed to (compound **2**) which is also sparingly soluble in water and its aqueous solution responded positively with the Griess's dye test (method of analysis described in section in 4.1.4), confirming the presence of NO_2^- ion in this solution.

To understand the nature of the loss of nitro group attached to compound **1**, the time dependent nitrogen analysis was performed under air exposure at various time intervals. In figure 4.4 the plot of nitrogen percentage against time clearly indicates that from the initial time of exposure to an interval of time the loss of nitrogen was rapid. However on longer exposure time the loss of nitrogen content did not ceases but progress at a slower rate. This suggests that an intermediate composition is formed very rapidly and from

this composition onwards the rate of denitration is sluggish. The infrared spectrum of compound 1 (figure 4.2) showed a weak vibration at 1624 cm^{-1} which may be due to the presence of $\nu(\text{NO})$ of the nitrito group. The reaction of olefin with $\text{N}_2\text{O}_4/\text{NO}_2$ is known [171] to produce nitro as well as nitrito derivatives. Thus it may be presumed that the addition of $\text{N}_2\text{O}_4/\text{NO}_2$ across carbon carbon double bond of C_{60} may proceed similarly as schematically shown below:

Scheme 1



Compound 1 when repeatedly washed with water and quickly vacuum dried showed the absence of the vibration at 1624 cm^{-1} as shown in figure 4.5. Interestingly this band did, however, reappears on ageing suggesting the slow conversion of nitro group into nitrito moiety. The aliphatic nitrito group on hydrolysis transform to hydroxyl group is well known in organic chemistry (scheme 1). However isomerization of the nitro group to nitrito group is known [197] in transition metal complexes. Interestingly the mixed nitro and nitrito derivatives of olefin respond to the conversion of $-\text{ONO}$ group to either $-\text{ONO}_2$ or to carbonyl moiety at ambient conditions (scheme 1). In the present case absence of any IR absorption band in the region of $\nu(\text{C}=\text{O})$ ruled out the possibility of similar chemistry for the compound 1.

When compound 1 was treated with a fixed volume of water and kept for 5 hours and centrifuged, the centrifugate responded the test of nitrite by Griess's reagent. The residue left was treated with another quantum of fresh water and kept for 5 hours, centrifuged and the centrifugate was tested for nitrite. This process was repeated for

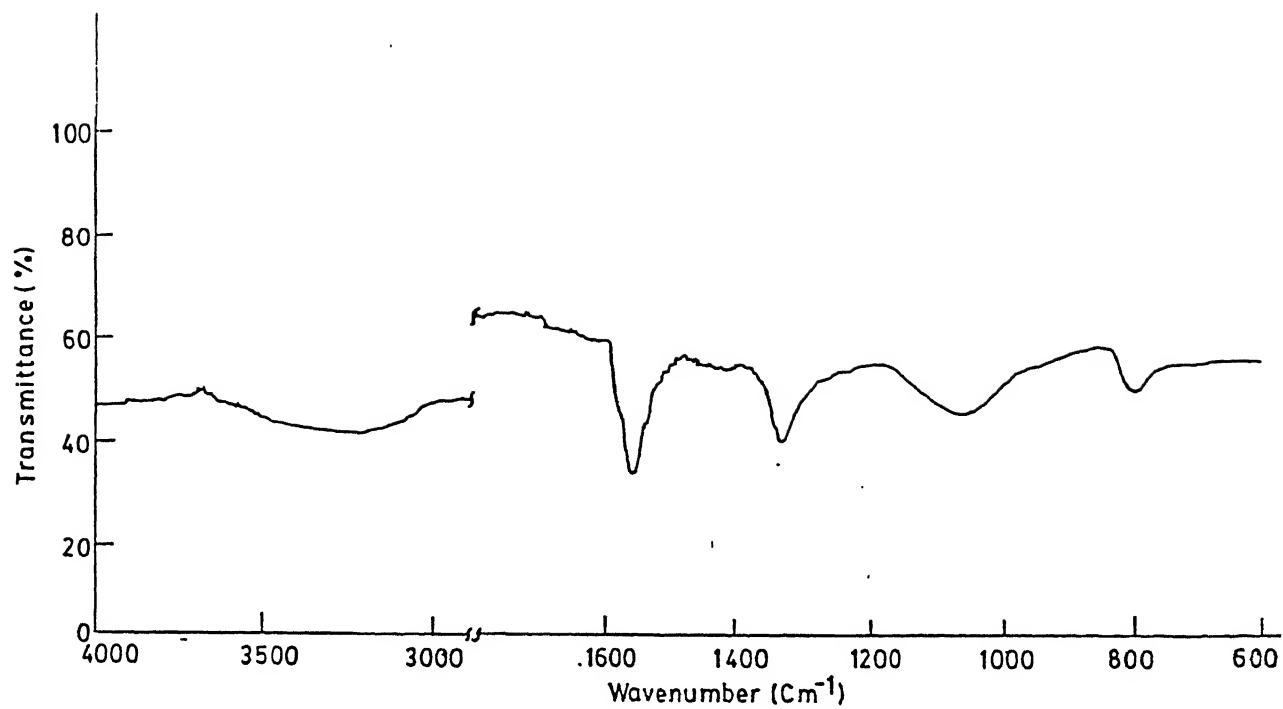


Figure 4.5: IR spectra of the compound **1**, after washing with water 5 times

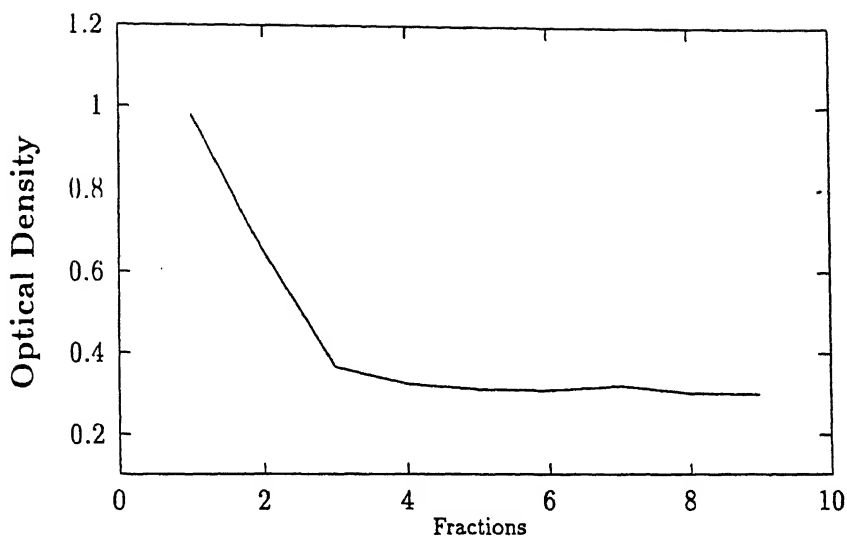
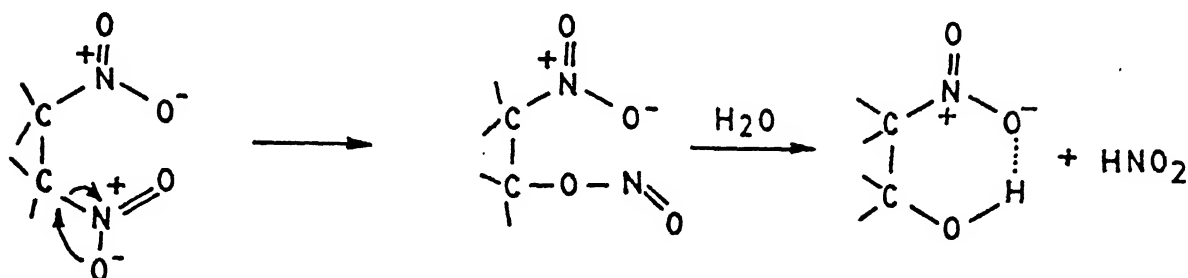


Figure 4.6: Plot optical density vs washing fraction. Optical density is measured by Griess' test.

several times. A plot of the optical density observed for the diazo test (Griess's reagent) vs time showed that initially the formation of HNO_2 was more but after the 3rd washing and onwards the optical density virtually remained constants, as shown in figure 4.6. This observation suggests that after some time the rate of release of HNO_2 from the compound was constant. The hydrolysis of nitrito group at the 1st washing is expected to be instantaneous and after the lapse of 5 hours no initially formed nitrito group would be expected to remain attached to C_{60} moiety. The higher rate of the formation of HNO_2 at the second stage of washing may suggest a mechanism wherein the bonded nitro group may isomerize to nitro group which subsequently responded to hydrolysis. However, the release of HNO_2 became slower in subsequent washings suggesting some stabilization of the left out attached nitro group. And explanation for this observation may be viewed in the following way. Product 1 which initially comprised of nitro as well as nitrito functionality quickly responds to hydrolyze the attached nitrito group formed by the initial reactions with $\text{N}_2\text{O}_4/\text{NO}_2$ similar to olefin. Once the nitrito group are hydrolyzed then the nitro groups isomerizes to nitrito groups which hydrolyzes in a slower rate depending on the rate of isomerization. Finally the reaction of the release of HNO_2 slowed down sufficiently by the stabilization of the left out nitro group by hydrogen

bond from the adjacent hydroxyl group. These hydroxyl bonded species is very similar to ortho nitro phenol. Formation of this type of hydrogen bonded species restricted further spontaneous isomerization of nitro group. This process is schematically shown bellow.

Scheme 2



In the spectrum the appearance of $\nu(\text{OH})$ around 3250 cm^{-1} , may be due to hydrogen bonding (figure 4.2). The slow conversion of attached C_nNO_2 to C_nONO is similar as observed in the phase reaction [123].

When a mixture of C_{60} in benzene with concentrated HNO_3 acid was subjected to EPR study (in a flat quartz cell) an EPR signal was observed within a few seconds with the addition of HNO_3 acid. A similar spectrum may be observed when NO_2 gas was sufficiently diluted to argon was treated with a benzene solution of C_{60} . The room temperature EPR signal of this experiments is shown in figure 4.7. Under identical conditions blank experiments did not show any EPR signal for the presence of NO_2 . The microwave power of the instrument was increased to its limit (200 mW) and no saturation of the EPR signal was observed. Krusic et. al. [151] have shown that free radical addition of C_{60} does generates finally cyclopentadienyl radical which is EPR active at the high microwave power (200 mW). Therefore the formation of the compound 1 using $\text{N}_2\text{O}_4/\text{NO}_2$ or HNO_3 may be via an intermediate like $\text{C}_{60}(\text{X})_5$ where $\text{X}=\text{NO}_2$ or $\text{ON}=\text{O}$. The observed EPR signal was very broad ($\Delta H \sim 200\text{ G}$) which may obscure the hyperfine interaction.

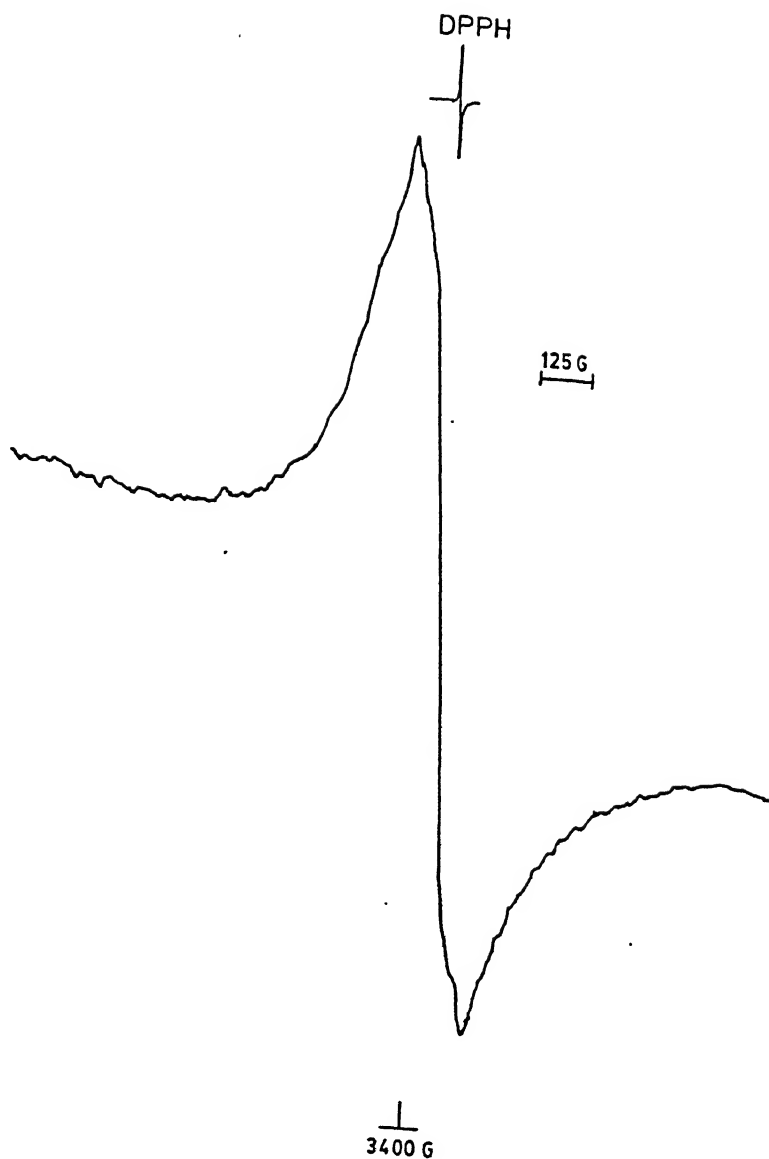


Figure 4.7: EPR spectra of the compound **2**. $g=2.0002$, $\delta H=200$ G. Operating Parameter $\nu=9.437$ GHz, Power=100 mW, Mod.Amplitude= 4×10 G, Gain= 2×10^4 .

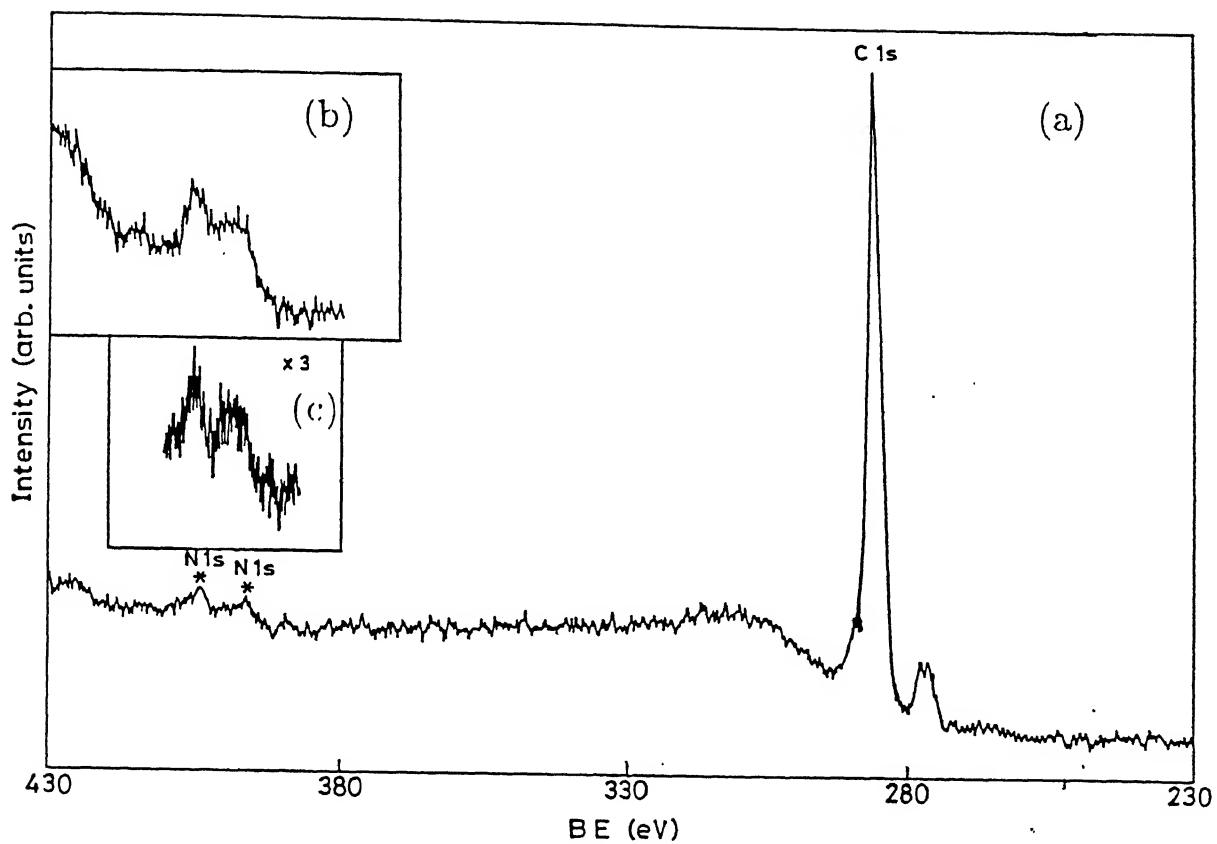


Figure 4.8: X-ray photoelectron (XPS) spectra of compound 1. (a) C 1s (b) N 1s and (c) N 1s after water treatment of 1

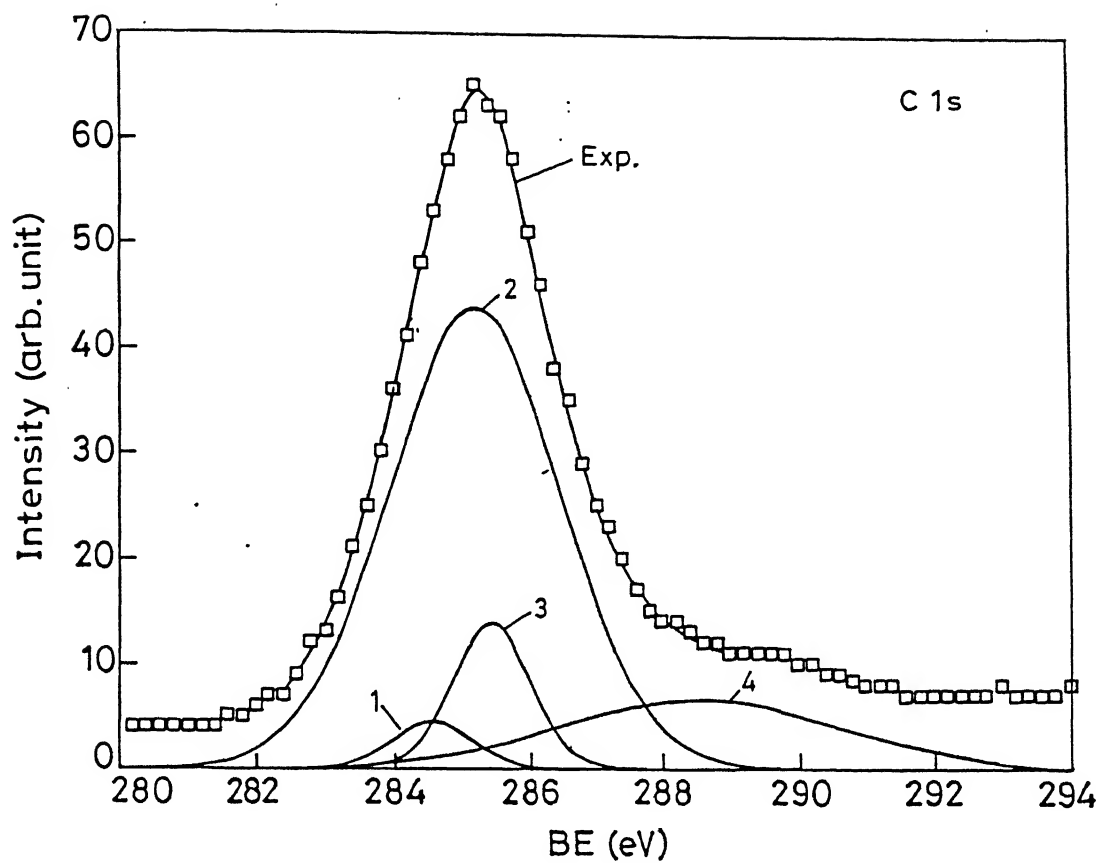


Figure 4.9: Peak analysis, from spectral deconvolution of the C 1s X-ray photoelectron spectrum of **1**.

with hydrogens the C 1s core level energy is observed near 285 eV for pure C₆₀ and for polyethylenes [203]. In table 4.1 the details of the C 1s peak analyses is given. At 284.5 eV, 3% C 1s binding energy has arises from the lower oxidation state of carbon, this indicates electron density is more in this carbon atom compared to free carbon. The major contribution of the C 1s binding energy is appeared due to the peak 2, at 285.20 eV (70%). This may be assigned as the bare carbons which is attached to other carbon centers with nitrogen and oxygen groups. The C 1s peak at 285.42 eV comprise of 10% area may presumably be originated from the attachment of bare carbon which are attached to carbon that containing relatively more electron withdrawing functionality compared to the previous situation. It is extremely difficult to quantitative assignment of this two peaks in a meaningful way. C 1s (~17%) binding energy at 288.54 eV has FWHM ~5.0 eV. This broad nature of the peak can not be account for monooxygenated or mononitrated species. The 3.54 eV shift, compared to C 1s at 285.0 eV, can be attributed to the primary carbon directly attached with oxygen and nitrogen.

Oxygen deconvolution analyses of the compound 1 is shown in figure 4.10. It shows the total O 1s binding energy comes from the the peaks at 522.2 (10%) and 531 (90%) eV. However when the compound was washed in water for 5 times the O 1s peak analysis shows three peaks at 522.5, 531.6 and 539.9 eV, as shown in figure 4.10.b. The details of O 1s peak analysis are presented in table 4.2 and 4.3. Peaks of the water washed compound (peak 2 of figure 4.10b) is shifted 0.6 eV in higher energy compared to the untreated water (peak 2 of figure 4.10.a) and one peak comprised of 3% area (peak 3 figure 4.10b) is appeared in the higher energy side which is absent in other case (figure 4.10a)i This suggested that oxygen in the water washed compound is in higher oxidation states compared to the untreated water. IR absorption bands (figure 4.2) at ~3250 cm⁻¹ indicates that hydrogen bonding most likely responsible for reduced the electron density over the oxygen atom. The appearance of O 1s at ~522 eV in both the spectra suggest that oxygen atom is negatively charged compared to free oxygen [149].

The nitro groups are bonded initially with C₆₀ in several positions (more than twelve as determined from compositional analyses), thus the neighbouring oxygen atom of the

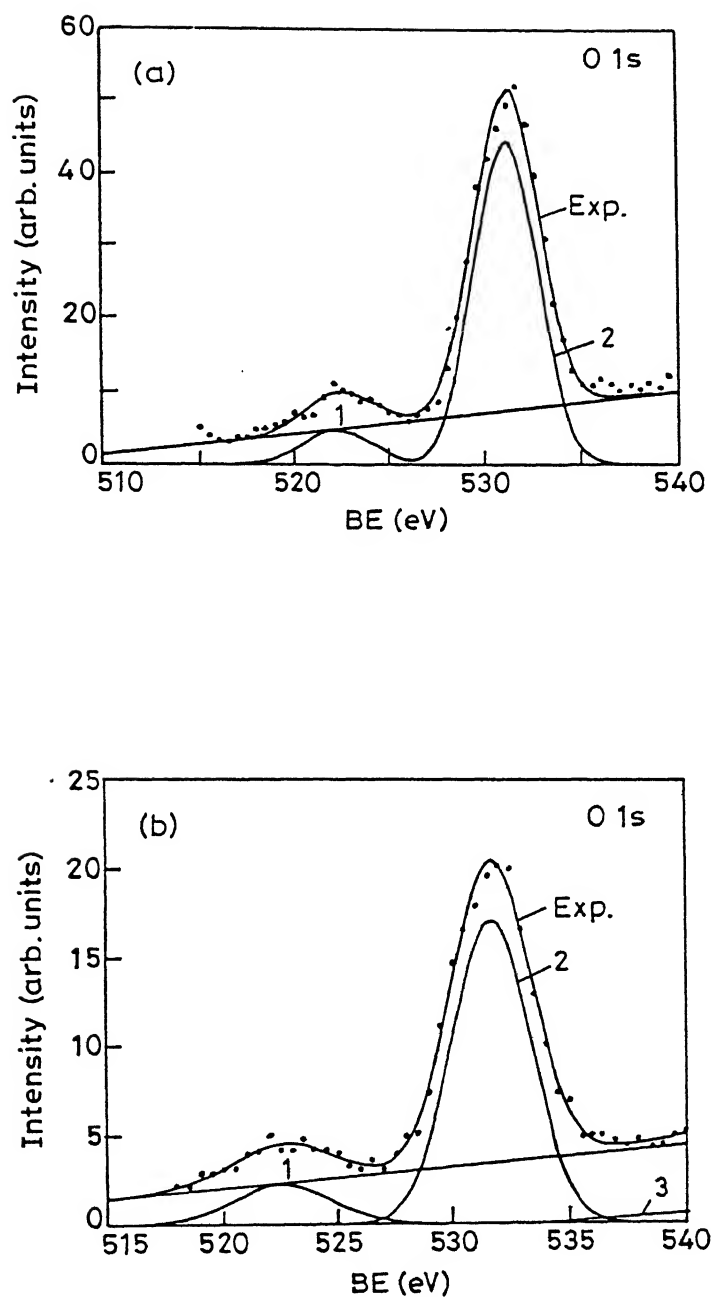


Figure 4.10: Peak analysis from spectral deconvolution of the O 1s X-ray photoelectron spectrum of compound 1. (a) Without water treatment. (b) Washed with water.

nitro group (carring the negative charge) has experienced repulsion. This repulsion can be minimized if one -C-NO₂ group is rearrange to one -C-ONO group, as shown in scheme 2. But reason behind this slow transformation is not clear to us in this moment.

The geometry optimization of the from MNDO method, hydrogen and halogenated derivatives of fullerene, by MNDO method, shows that 1,4 addition is favoured in case of bromo and chloro derivatives however hydrogen and fluorine derivatives of C₆₀ prefers 1, 2 addition products [136, 142]. X-ray crystal structure of bromo derivatives of C₆₀, as shown in figure 1.15, also highlights the 1,4 addition of the bromine atom [140]. For bromine and chlorine atom, a strong eclipsing interaction is prevailed compared to smaller size hydrogen and fluorine atom and this eclipsing interaction is responsible for the stable 1, 4 addition product. As nitro group is occupied more space compared to hydrogen and fluorine hence compound 1 should be a 1,4 addition product.

Based on the above studies the probable mechanism of the nitration addition reaction with C₆₀ is proposed which is shown in figure 4.11. The mechanism (figure 4.11) shows that N₂O₄/NO₂ addition with C₆₀ in benzene or toluene gives four kind of isomers. Isomer (I) and (II) are formed according to the normal 1,2 addition like scheme 1. Isomer (III) and (IV) are produced by 1,4 addition of the N₂O₄/NO₂ groups in C₆₀. II, III and IV are rapidly hydrolyzed due to the presence of nitrito groups. (I) with an allylic rearrangements (according to step 2) formed a 1,4 addition products and this on further rearranges produce the compound 1 which is shown in step 3 in figure 4.11.

4.3.1 XPS PeakFit Numerical Summary

The background coefficients has been calculated for the peak analysis by the following polynomials :

$$Y = a + bx + cx^2 + dx^3$$

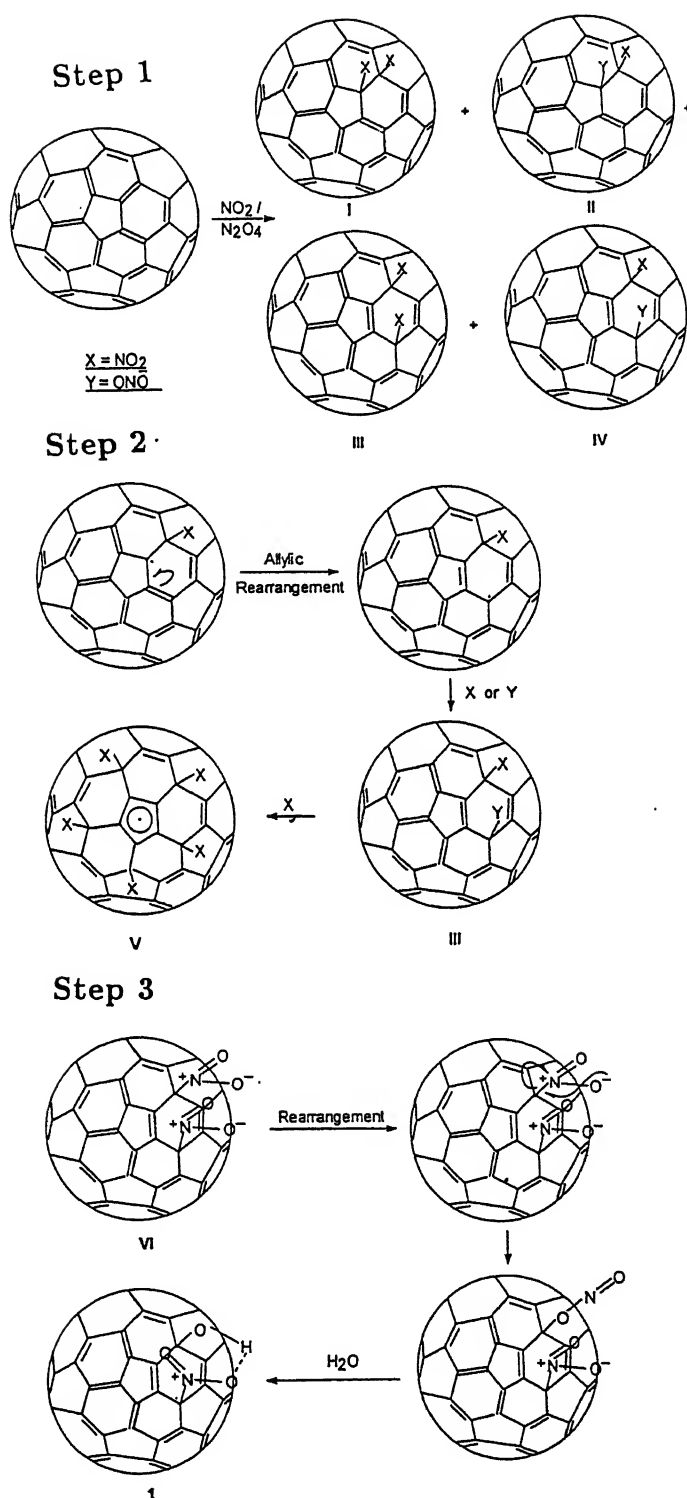


Figure 4.11: Reaction mechanism of NO_2 addition in C_{60} . **1** is the isolated product. Here only one nitro group is shown, but other nitro and hydroxy functionality also present in

Table 4.1: C 1s peak analysis of the compound 1.

Peak	Type	Amplitude	Center (eV)	FWHM (eV)	% Area
1	Gaussian	4.3202752	284.511	1.343	3.1146309
2	Gaussian	43.746474	285.2072	2.978	69.908279
	Gaussian	13.748384	285.4265	1.377	10.161675
4	Gaussian	6.5474463	288.5422	4.804	16.8154415

Table 4.2: O 1s peak analysis.

Peak	Type	Amplitude	Center (eV)	FWHM (eV)	% Area
1	Gaussian	4.9025525	522.24356	4.20	10.672125
2	Gaussian	44.350543	531.08859	3.8	89.327875

(a) Other details of the table 4.1

Total Points: 70 Active Points : 70

Background Order: a=3.8730159, b=-0.013832, c=0.0003952, d=5.646x10⁻⁶

Curve-Fit std. Error=0.545823555.

Confidence Limit= 99%.

(b) Other details of the table 4.2

Total points: 50 Active points: 50

Background coefficients: a=-54.2155, b=0.0264434, c=0, d=3.18x10⁻⁷

Curve-Fit std. Error=1.2952396.

Confidence Limit= 99%.

(a) Other details of the table 4.3

Total points: 51 Active points: 45

Background coefficients: a=-11.04675, b=-0.017463, c=0, d=1.574x10⁻⁷

Curve-Fit std. Error=0.526276832

Confidence Limit= 99%.

Table 4.3: O 1s peak analysis after washing the compound **1** with water.

Peak	Type	Amplitude	Center (eV)	FWHM (eV)	% Area
1	Gaussian	2.1816016	522.50969	5.09	13.634268
2	Gaussian	17.015044	531.69165	3.948016	84.033278
3	gaussian	0.5035842	539.99999	7.4051361	2.33224539

4.4 Conclusions

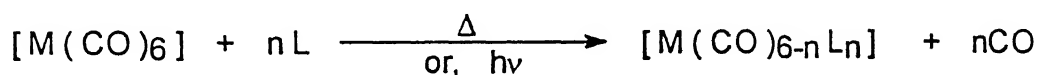
The molecules or radicals which we had taken in this study, as shown schematically in figure 4.1, are very reactive towards olefinic double bond [171]. Thus the presence of an unpaired electron is not sufficient to induce reactivity with the C_{60} molecule and also indicates that carbon-carbon double bond of C_{60} has low reactivity compared to the planar olefinic carbon-carbon double bond. Hückel molecular orbital calculation on C_{60} molecule provide similar kind of suggestion [55]. For strong bond formation the directional approach between two overlapping atom or molecule is most important. though the radicals formed on the C_{60} surface is very much localized [151]. From gas phase structural analyses of NO and NO_2 it is known that odd electron in NO_2 molecule is more delocalized compared to the the odd electron of NO_2 [205]. Possibly greater odd electron delocalization of the reacting partner does not form a strong bond with C_{60} due to the the p-orbital does not form an angle 90° with the σ -orbitals and this deviation of the angle is necessary for the curvature conservation of the C_{60} molecule [114]. In the reaction between the above mentioned molecules or radicals, as shown schematically in figure 4.1, with the normal bridged systems like acyclic and aromatic the EPR spectra of these bridged radicals suggested that they are consistent with pyramidal geometry at the bridged carbon atoms [206]. It is known that diazo-methane, azide type of radicals are very much reacting with C_{60} and large number of derivatives of C_{60} are also reported [99, 117]. One possible explanation for the low reactivity of sulfur di oxide radicals may be it is a soft Lewis acid, but in can acts also as a soft base in favorable cases [205], and gas phase experiment of C_{60} shows it has very poor reactivity with the strong Lewis acid BF_3 [123]. In a very recent report Smalley et. al observed SO_2 gas change the C_{60} colour

[31] but product is not isolated and characterized. From the above facts we proposed that the radical which has more σ character may reacts faster than the radical of π character. Low reactivity of singlet oxygen is not clear to us.

Chapter 5

Reactivity with Metal Hexa-Carbonyls (Cr, Mo and W)

Metal-olefin complexes and a large number of metal-arene complexes have been prepared by the substitution of CO groups from the metal carbonyl by olefin and arene ligands [194, 207]. So far, most important properties of metal hexacarbonyls (metal= Chromium, Molybdenum, Tungsten) are their use as the starting material for a wide range of substitution reactions, where the metal does not change its oxidation state. Heat or UV radiation is often used to assist the evolution of CO in these substitution reactions and in some cases complete substitution of CO groups occur [208, 210]. These known reactions are shown schematically below.



Where, M = Cr, Mo, & W

L = Mono-, bi-, tri- dentate Ligands.

In substitution reactions d-electron configuration of the metal carbonyl fragments retained the essential geometric feature of the parent 18-electron carbonyl complex.

5.1 Experimental Section : Part-I

5.1.1 General Conditions

All reactions were carried out under nitrogen or argon atmosphere. Solvents were purged with argon or nitrogen prior to use. Moderate vacuum was employed whenever necessary.

5.1.2 Materials

The preparation and isolation procedure of C_{60} was described in chapter 3. Benzene, n-hexane, cyclohexane were distilled from sodium wire. MeCN was distilled over CaH_2 . Solvents were purchased from S. D. Fine Chemicals, India. $Cr(CO)_6$, $Mo(CO)_6$ and $W(CO)_6$ (E-Merck, Germany, Aldrich, USA) were purchased and used as received.

5.1.3 Physical Measurements

Elemental Analysis

C, H, N analyses were done as described earlier in section 4.1.3.

IR Spectroscopy

The IR spectra, in KBr pellets, were recorded in the Perkin-Elmer 1600 Series FTIR spectrometer. Liquid IR (solvent CCl_4) spectra were taken in Perkin-Elmer 1800 series spectrometer.

UV-visible spectroscopy

UV-visible spectra were measured in dry and degassed solvents similarly as described in section 3.1.2.

X-ray Photoelectron Spectroscopy

Instrument and operating parameters were same as mentioned in section 4.1.3. Solid sample was pressed on indium metal substrate at ambient conditions for recording the spectra. Peak analysis (simulation) of the C 1s and O 1s were done as described in section

4.1.3.

Electrochemistry

Electrochemistry was carried out using a conventional three electrode cell. A platinum (1 mm diameter) and glassy carbon electrode were served as working electrode and a platinum wire was used as the counter electrode. The reference electrode was a Ag/AgCl which was separated from the working solution by a fritted glass bridge (vycertip). Cyclic Voltammetry (CV) were performed with a BAS CV-27 analyzer. All experiments were carried out at $25^{\circ} \pm 1^{\circ}$ C. The supporting electrolyte, TBAClO₄ (TBA= Tetrabutyl ammonium) was used at concentration of 0.1 M. All the redox potential data are reference to ferrocenium/ferrocene couple.

Laser

Coherent-Innova 70 cw Laser source of variable wave lengths were used. In the present work 514, 488 and 454 nm wave-lengths of power 800 mW/0.5 cm², 900 mW/0.05 cm², 700 mW/0.5 cm² respectively were used.

Colour Filter

Corning glass filters, Kodack LTd. USA, of variable thickness were used.

5.2 Part-II; Reaction Methodology**5.2.1 Synthesis of $W(CO)_{6-x}(C_{60})_x$**

50 mg (0.06 mmol) of C₆₀ was taken in a 500 ml round bottom flask and dissolved it in 150 ml dry benzene. In another 250 ml flask 106 mg (~ 0.3 mmol) of W(CO)₆ dissolved in 100 ml of dry benzene. Both the solution were purged with argon for an hour and kept in an ice bath to maintain the temperature well below 10 °. W(CO)₆ solution was mixed with the C₆₀ solution under argon and the mixed solution was irradiated for three hours by sunlight (maintaining the temperature of the reaction vessel at a temperature 5 to 10 ° C). A moderate vacuum was employed in the reaction vessel

by water suction. The initial purple colour of the solution changed to greenish brown within a few minutes, which slowly changed to reddish brown after 30 minutes and this brown colour remained unchanged on further irradiation (~ 3 hrs). This solution was concentrated to 10 ml, under vacuum, and this concentrated solution was flash chromatographed (column diameter 2 cm x length 5 cm) in argon atmosphere. The eluent was treated with n-hexane (~ 50 ml) till the clear solution became hazy and kept it in the refrigerator. On standing a reddish solid separated out in the reaction flask and it was filtered, repeatedly washed with n-hexane to free from the unreacted $\text{W}(\text{CO})_6$ and dried in vacuum. The compound was kept under inert atmosphere in refrigerator for further characterization.

Elemental analysis, C; $\sim 74.2\%$.

Mass (m/z) = 988, 950, 904, 750, 748, 696.

IR (KBr); $[\nu (\text{cm}^{-1})] = 2083, 1957, 1460, 1425.6, 1182.3, 1167.5, 1095.5, 1075, 1021, 952, 935, 875, 804, 736, 700, 667.5, 616, 581, 564, 526, 484, 465, 444.6, 422, 404.$

UV-Vis; λ (Benzene) = 431, 552 (br) and 655 (br) nm. Dichloromethane = 345, 435, 560 nm.

XPS (Binding Energy, eV); C 1s = 285.7; O 1s = 535 and W $4f_{7/2}$, W $4f_{5/2}$ = 34.6, 36.85, 38.35 and 40.6 eV.

5.2.2 Photochemical Reaction of $\text{Cr}(\text{CO})_6$ and $\text{Mo}(\text{CO})_6$ with C_{60}

On sunlight irradiation, benzene solution of $[\text{Cr}(\text{CO})_6 + \text{C}_{60}]$ and $[\text{Mo}(\text{CO})_6 + \text{C}_{60}]$ changed initially to a light yellow colour solution, procedure adopted in this reaction same as described in section 5.2.1. However on long exposure precipitation appeared in both cases and the purple colour of C_{60} in solution persisted. After centrifugation the residue were analyzed and found to be chromium oxide and molybdenum oxide respectively. The yield of these oxides vary in every batch of preparation. Blank experiments of $\text{M}(\text{CO})_6$ in benzene, where $\text{M} = \text{Cr}, \text{Mo}$, under identical conditions produced the similar colour change in the initial stage. These solution on further exposure it gave a pale

green (Cr) precipitate and pale brown (Mo) precipitate from the respective solution and characterized as chromium oxide and molybdenum oxide. This suggest that Cr(CO)_6 and Mo(CO)_6 did not react with C_{60} under the condition employed herein.

5.2.3 Thermal Reaction of Cr(CO)_6 , Mo(CO)_6 and W(CO)_6 with C_{60}

100 mg of M(CO)_6 ($\text{M} = \text{Cr, Mo and W}$) and 30 mg of C_{60} in 250 ml toluene were refluxed for 24 hours but the purple colour of C_{60} remained unchanged during this period. UV-visible spectra (optical density of C_{60} is considered) of these solutions indicate that C_{60} remained unchanged without the formation of any other species.

5.2.4 Thermal Reaction of Cr(CO)_6 , Mo(CO)_6 and W(CO)_6 with C_{60} , in presence of Me_3NO .

C_{60} (30 mg) and M(CO)_6 (100 mg), where $\text{M} = \text{Cr, Mo and W}$, were refluxed for 24 hours in presence of 2 mg of N-N tri methyl N-oxide. A light green colour solution was observed, however UV-visible spectra of these solution suggest that C_{60} was not participating in this reaction.

5.3 Results and Discussion

The methodology adopted to prepare metal hexacarbonyl derivatives of C_{60} are shown in figure 5.1. It shows only W(CO)_6 reacts with C_{60} under photolytic conditions and produce a red brown solid. The red brown solid, prepared as described in section 5.2.1, is not soluble in common organic solvents like benzene, toluene, methylene chloride, chloroform and carbon tetra chloride, acetonitrile etc.

The benzene solution of W(CO)_6 and C_{60} were irradiated using sunlight for 5, 10,

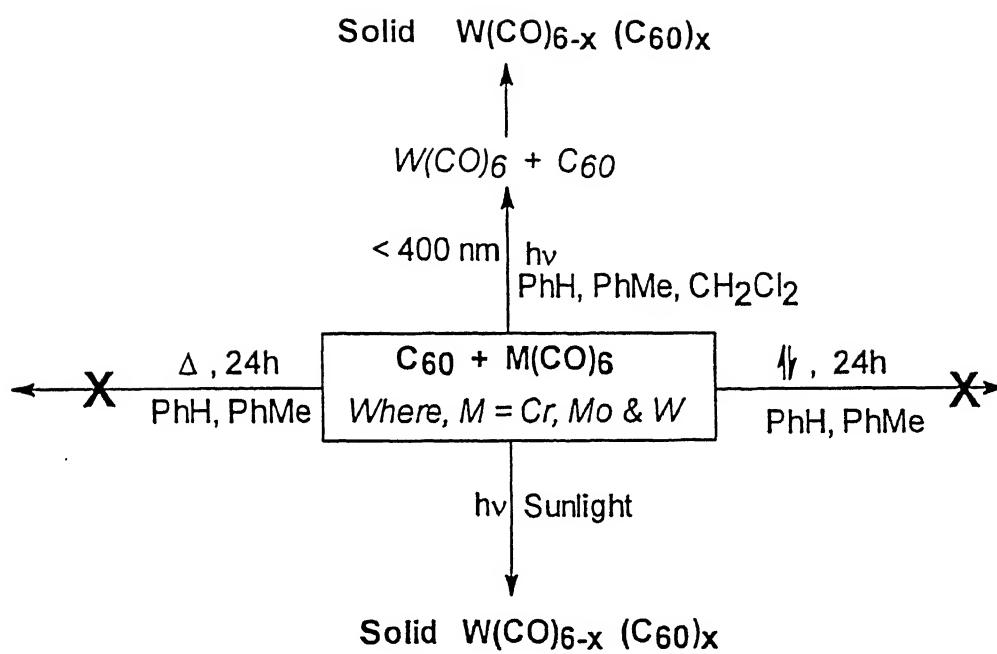


Figure 5.1: Scheme; reaction between the metal hexacarbonyl and C_{60}

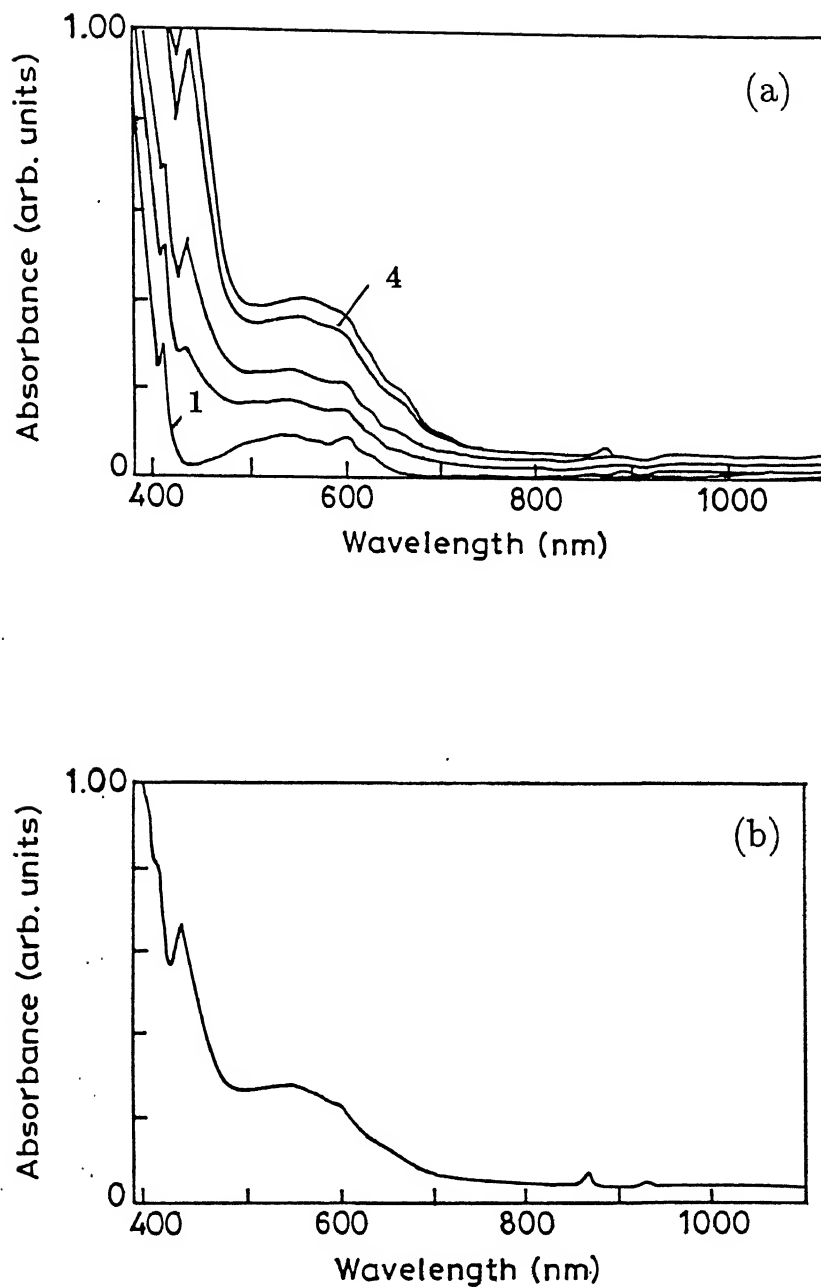


Figure 5.2: Electronic absorption spectra; (a) Progress of the reaction between C_{60} and $W(CO)_6$ in benzene on sunlight irradiation. Spectra are recorded in 5 minutes interval. (b) Spectrum of the above solution, which is continued for 1 hours and kept in, recorded after 24 hrs.

15, and 20 minutes and its UV-visible spectra in the respective time intervals is shown in figure 5.2 (a). A hyperchromic shifts of the absorption bands at 405, 540 and 620 nm is observed in peak 4 (figure 5.1 (a)) as compared to peak 1, without sunlight excitation. However, this irradiated solution on keeping for 24 hours showed a hypochromic shift of the band at 405 nm which is shown in figure 5.2 (b). This suggests that the complex is formed under present conditions, react with solvent on storage.

The failure of the synthesis of $W(CO)_{6-x}(C_{60})_x$ in thermal conditions, as described in section 5.2.3 and 5.2.4, suggested that the photochemistry of $W(CO)_6$ and/or C_{60} are the guiding factors for the syntheses of this compounds. We were also unable to syntheses any derivative of $Cr(CO)_{6-x}(C_{60})_x$ and $Mo(CO)_{6-x}(C_{60})_x$ under thermal conditions, as described in section 5.2.3 and 5.2.4. Equimoleculer mixtures of $M(CO)_6$, where $M=Cr$, Mo and W and C_{60} were taken anerobically in benzene showed no reactivity under ambient conditions as shown in figure 5.3 (a). However, when these solutions were irradiated by sunlight, the $W(CO)_6$ containing C_{60} solution changed its colour, Mo and Cr -hexacarbonyls do not react with C_{60} under the identical conditions, as shown in figure 5.3 (b). This suggests that $W(CO)_6$ has some special properties which may be responsible for this reactivity with C_{60} under photochemical process.

Substitution reactions of $W(CO)_6$ with different kinds ligands are extensively studied and it has been suggested that the reaction can proceed either dissociative or associative pathway [211]. In the present case, the reaction is carried out in presence of sunlight thus excited state of either $W(CO)_6$ or C_{60} or both are responsible for this reaction. Sunlight constitutes UV ($\sim 18\%$), visible($\sim 33\%$) and IR ($\sim 50\%$) radiation of the total sunlight which falls on the earth, though it varies with latitude and longitude of the earth [212].

A benzene solution containing equivalent amount of $W(CO)_6$ and C_{60} were irradiated using 514, 488 and 454 nm laser pulses separately for 1 hour. The UV-visible spectra of these irradiating solutions remained unchanged from the starting ones, which is shown in figure 5.4. The narrow range of radiation, which cause the reaction between $W(CO)_6$ and C_{60} in benzene solution, was identified in the following way. An assorted narrow

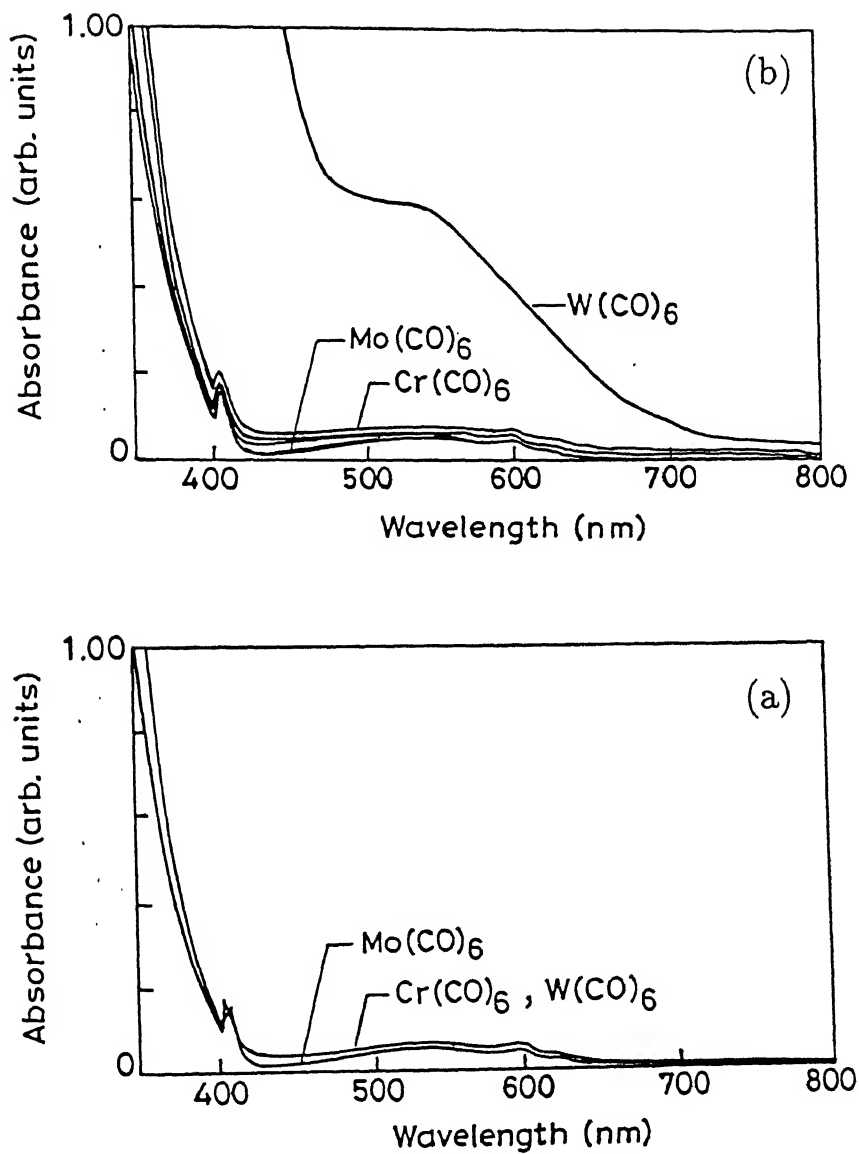


Figure 5.3: UV-visible spectra of M(CO)_6 , where $\text{M}=\text{Cr}$, Mo and W and C_{60} in benzene. (a) At ambient conditions (b) Exposing the solutions for 45 minutes in sunlight. W(CO)_6 shows the reactivity.

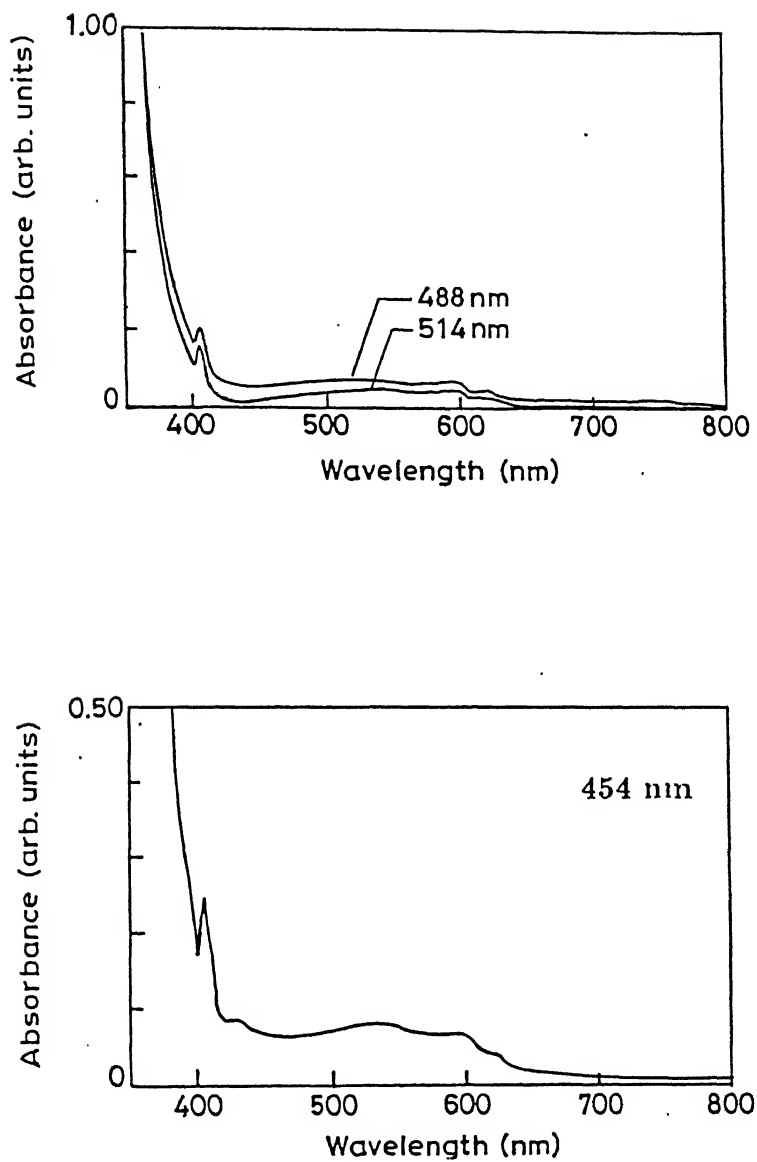


Figure 5.4: Electronic absorption spectra; W(CO)_6 and C_{60} in benzene are irradiated with 514, 488 and 454 nm laser pulses.

band pass colour filters of corning glass and different standardized solution filters, like Khasa filters etc., were used in these experiments. To prevent IR irradiation from the sunlight the quartz cell containing the solution, where $W(CO)_6$ and C_{60} were taken in 1:1 ratio, was immersed in cold water in each experiments. It was observed that the filter allowing radiation in the range 300-400 nm (filter No. 5850, Kodack LTD., USA,) only found to be effective for this reaction. These set of experiments were also repeated using a slide projector lamp. It is known, C_{60} in benzene is excited to triplet state in near quantitative yield irrespective of 354 or 515 nm radiation and the fluorescence quantum yield of C_{60} has been shown to be wave-length independent [88, 92, 93, 94]. The failure to bring the desired reaction using visible part of the radiation strongly suggests that the excited state of C_{60} is not primarily responsible for such reactions.

Interestingly $W(CO)_6$ dissociated to $W(CO)_5$ plus CO on irradiation with light at ~ 358 nm. Thus, it may be stated that the dissociation of $W(CO)_6$ is the crucial step for the reaction. The generation of highly reactive $M(CO)_5$ moiety containing 16 electron from the 18 electron $M(CO)_6$, where $M=Cr, Mo$ and W , generally reacts with any ligand or group including rare-gases [194]. Under favourable conditions, the species $M(CO)_5L$ thus form may subsequently lose -CO group to produce tetra or even tri-carbonyls species provided L contributes the essential coordination sites [205, 211]. If L is a six electron donors, like benzene or other arenes, in the complex $M(CO)_3L$ where L can bonded with the metal center in η^6 fashion [208].

5.3.1 Characterization of the Isolated Compound

Mass spectra

Incomplete combustion of pure C_{60} and C_{60} derivatives is a general phenomenon due to the large heat of formation value of pure C_{60} [71, 72]. Prediction of the composition for the C_{60} derivatives from elemental analysis, specially C percentage, is concluded with erroneous results. The carbon and XPS analyses of the compound suggest that the ratio

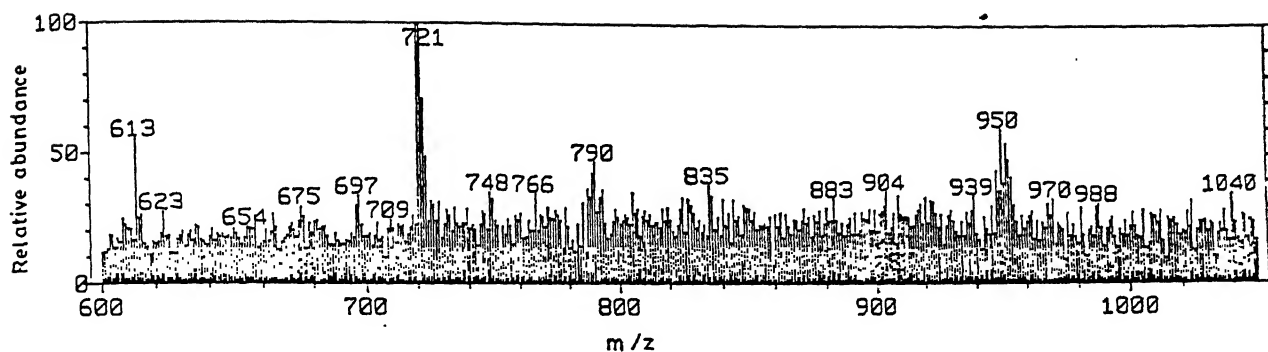


Figure 5.5: Part of the FAB Mass spectrum of the compound.

between C_{60} and W atom is 1:1.

Part of the FAB mass spectrum of the compound is shown in figure 5.5. It comprised of peaks at $m/z=988, 950, 904, 750, 748, 696$. The most intense peak (100%) appeared at $m/z=720$ which is due to C_{60} and it appeared from the fragmentation of the parent compound. The peak at $m/z=988, 950$ and 904 showed the presence of tungsten, due to its isotopic distribution, and are responsible for $C_{60}W(CO)_3$ ($m/z=988$), $C_{60}W(CO)OH_2$ ($m/z=950$) and $C_{60}W$ ($m/z=904$). Mass at $m/z=950$ and 904 are possibly arises due to the loss of carbonyl group from the fragmentation of 988 mass peak. Hydroxy groups in $C_{60}W(CO)(OH)_2$ ($m/z=950$) may come from the fragmentation of *m*-nitrobenzyl alcohol. It is known that matrix *m*-nitrobenzyl alcohol fragmented in the FAB conditions and hydroxy groups are attached to C_{60} [213, 214]. Peaks at 750 and 748 are assigned to $C_{60}(CO)(OH)_2$ and $C_{60}(CO)$ respectively.

IR spectra

The IR spectrum of the red-brown solid is shown in figure 5.6. It shows several vibrations at $2083, 1957, 1460, 1425.6, 1182.3, 1167.5, 1095.5, 1075, 1021, 952, 935, 875, 804, 736, 700, 667.5, 616, 581, 564, 526, 484, 465, 444.6, 422$ and 404 cm^{-1} respectively. The two strong absorption bands centered at 2083 and 1975 cm^{-1} which are typically

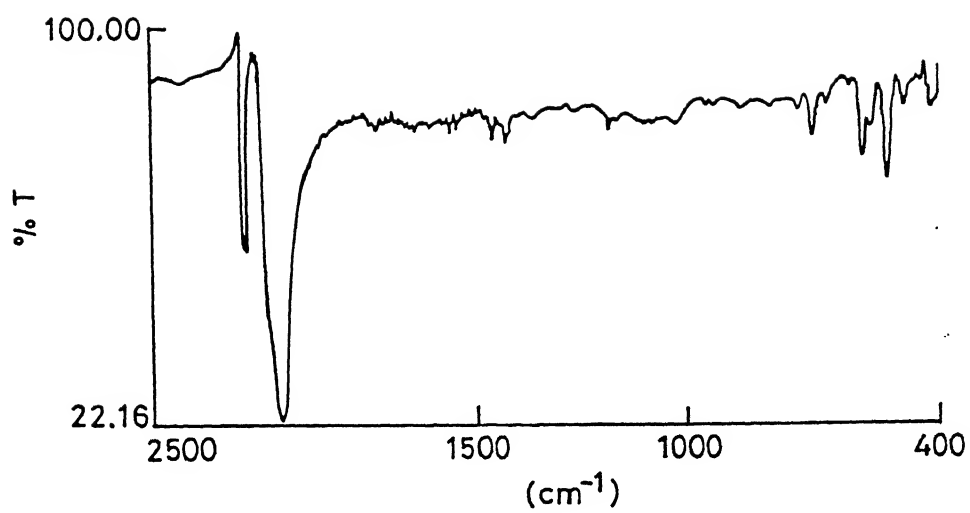


Figure 5.6: FTIR spectrum of the compound 1.

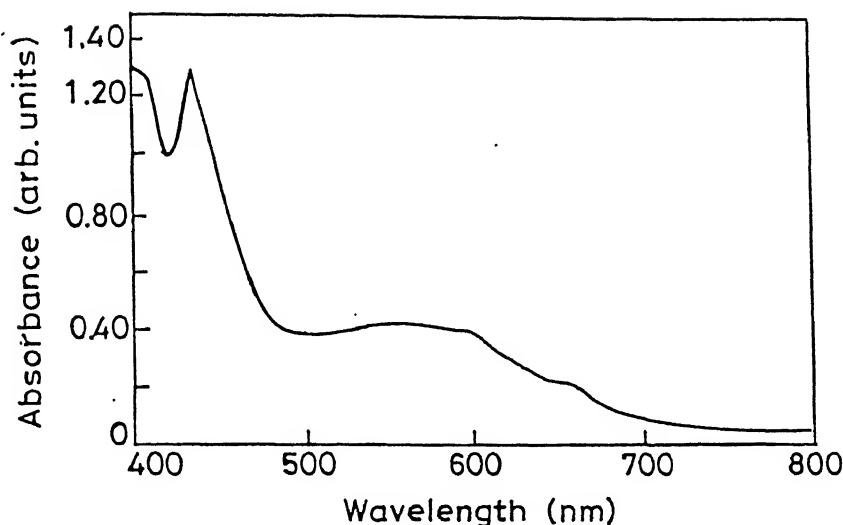


Figure 5.7: UV-visible spectrum of the compound in benzene

due to the carbonyl stretching vibrations. For pure C_{60} four IR active bands appeared at 1428, 1181, 577 and 526 cm^{-1} (*vide figure 3.10.*) and is well matched with the reported spectrum [1, 83]. The appearance of new IR band at 1460, 1425.6, 1167.5, 581 and 564 cm^{-1} for the compound suggested, the IR spectrum of the compound is very little perturbed from pure C_{60} spectrum. Absence of the strong aromatic $\nu(\text{C-H})$ vibration at (850-750) cm^{-1} suggested compound contain only C_{60} attached metal-hexacarbonyl. The shift of $\nu(\text{CO})$ in figure 5.6 compared to free CO (2143 cm^{-1} in gas phase [197] are 60 and 186 cm^{-1} , however in case reported $C_{60}(\text{CO})$ adsorbed species it is 8 and 15 cm^{-1} [215]. Therefore this compound is a strongly bonded species.

Electronic Spectra

The electronic spectrum of the compound in benzene is shown in figure 5.7 and shows peaks at 431, 552 (br) and 655 (br) nm. The spectral feature of these derivatives are differ slightly from that of the pure C_{60} , in the 450-750 nm region. C_{60} has six low lying molecular orbitals and its electronic transitions from HOMO to LUMO $h_u \rightarrow t_{1g}$ is symmetry forbidden [55]. This indicates that the coordination of C_{60} with metals involve small perturbations of the electronic structure of C_{60} . In the visible range, the spectrum of the compound (figure 5.7) does not differ much to that of free C_{60} , possibly

this complex has ligand located excited states which do not differ very much from the free C_{60} . Thus the new band around 431 nm may be due to intra ligand (C_{60}) transitions. The intra-ligand transition of the complex, $(\eta^5\text{-indenyl})(CO)Ir(\eta^2\text{-}C_{60})$, observed at 435 nm [216]. The restricted solubility of these complex in large number of solvents presented difficulty to identify the location of absorption features in the ultra-violet region.

5.3.2 Electrochemistry

A mixed solvents comprising benzene and acetonitrile, in a volume ratio of 1:4.5, is used in this cyclic voltammetric study. In this process the stability of the complex is managed for the cyclic voltammetric time scale of study but on continuous cycling for thrice the solution become purple colour. Cyclic voltammogram of pure C_{60} is shown in figure 5.8(a) and produce three reduction peaks in the potential scale of -2.00 V, and value of this potential is given in table 1.

The cyclic voltammogram of the electronegative C_{60} has characteristic six reversible reduction potentials [103]. But the observed voltammogram of the C_{60} are dependent on nature of the solvent, supporting electrolyte, and scan rate [101, 102, 217].

CV of the complex (solvent composition, scan rate and supporting electrolyte are identical to that of C_{60}) is shown in figure 5.8b. It shows five reduction waves and one oxidation wave and values are presented in table 5.1. The first and second reduction potential of the complex are reversible in nature but its $E_{1/2}$ are shifted to ~ 50 mV more positive potential than pure C_{60} . C_{60} has a well defined third reduction potential at $E_{1/2} = -1.39$ V. However the complex in the same potential window shows another three reduction potentials at (E_{pc}) at -1.28, -1.45 and -1.60 V.

The $W(CO)_6$ (30 mg) dissolved in benzene (50 ml) and the mixture was irradiated by sunlight for 45 minutes anerobically and CV of the blank $W(CO)_6$ solution was recorded in the identical experimental set up of C_{60} and complex, which is shown in figure 5.9. It has no reduction peak as well as oxidation peak in the first cycle. However on continuous

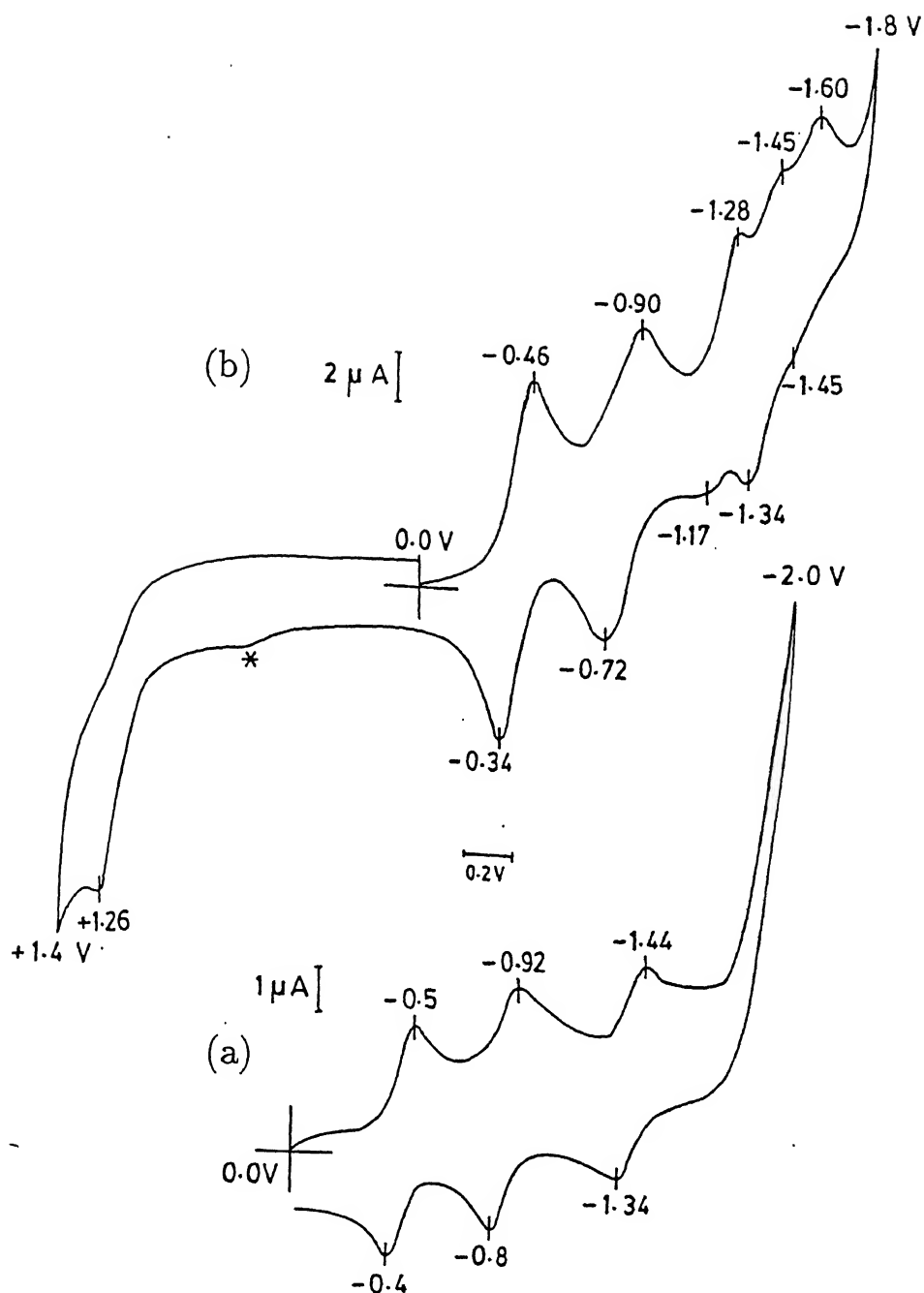


Figure 5.8: CV of the (a) C_{60} and (b) complex. Glassy carbon working electrode, scan rate 50 mV/s and 0.1 M TBAP supporting electrolyte. Asterisk indicates unidentified peak.

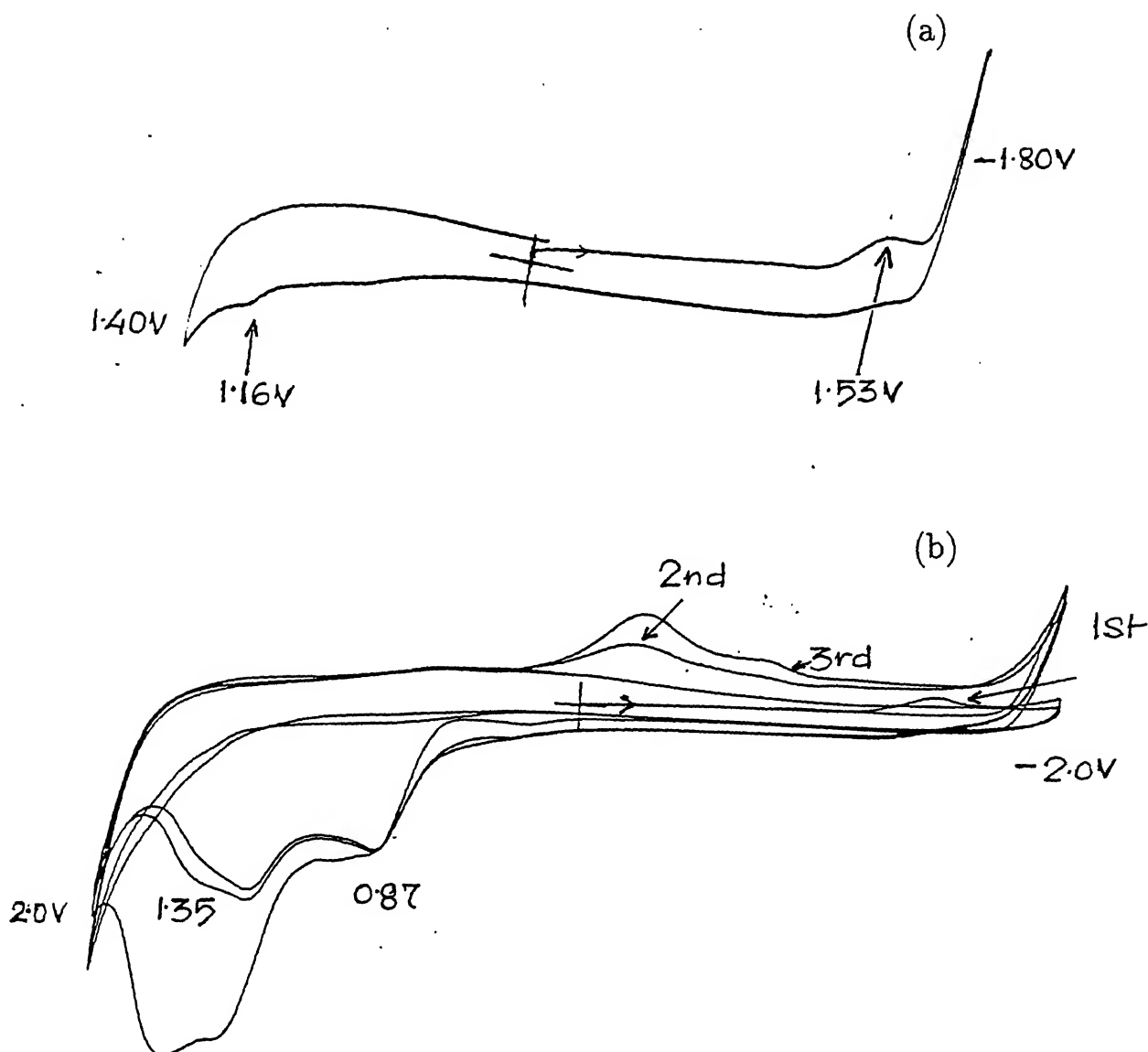


Figure 5.9: CV of the blank $W(CO)_6$. Glassy carbon working electrode, (a) scan rate 50 mV/s and (b) scan rate 100 mV/s using 0.1 M TBAP supporting electrolyte.

Table 5.1: Peak potential of the C₆₀ and complex.

C ₆₀ , figure 5.8 (a)					
	E _{1/2} 1st (V)	E _{1/2} 2nd (V)	E _{1/2} 3rd (V)		
	-0.45	-0.86	-1.39		
Complex, figure 5.8(b)					
E _{pa} (V)	E _{1/2} 1st (V)	E _{1/2} 2nd (V)	E 3rd (V)	E 4th (V)	E 5th (V)
+1.24	-0.4	-0.81	-1.225	-1.345	-1.525

cycling (in the 3rd cycle) shows two irreversible oxidation peaks at 0.85 V and 1.35 V. This suggests that the reduction events of the complex are C₆₀ centered and oxidation of the complex has metal centered. 1st, 2nd and 3rd reduction potential (table 5.1) of the complex suggested that C₆₀ moiety of the complex is reduced easily compared to pure C₆₀. In case of monosubstituted complexes (Ph₃P)₂Pt(η^2 -C₆₀) and (Et₃P)₂M(η^2 -C₆₀) three to four sequential one electron reduction waves are observed and these are shifted to more negative potentials relative to C₆₀ [218]. Addition of more metals continues to lower the electron affinity of the C₆₀ core, with the reversible potential for [(Et₃P)₂Pt]_nC₆₀ shifting 0.36 V more in the negative direction with each metal added to n=0-4 [218]. This suggested that compound is a mononuclear metal center and the peak potential of this compound is shifted in opposite direction than the literature reported [125] C₆₀ metal derivative. Thus in this case C₆₀ donates its π electron to the metal. Hence tungsten atom are not bonded in the η^2 fashion with C₆₀ in this compound and formation of the W(CO)₅(C₆₀) in this case is quite unlikely.

The ratio i_{pc}/i_{pa} of the first, second, and third reduction wave of the pure C₆₀ is 1. However i_{pc}/i_{pa} of the complex for the first reduction wave is 0.8 and for the second wave it is 1.15. This deviation of the current from pure C₆₀ indicates that some rearrangement takes place in the C₆₀ center of the compound in electrochemical response.

5.3.3 X-ray Photoelectron Spectroscopy

X-ray photoelectron spectroscopy (XPS) measurements of the compounds give C 1s and O 1s peaks at 285... and 535.. eV respectively. Peak analysis of the C 1s is shown in figure 5.10(a) and data are presented in table 5.2. It shows three peaks at 285.2 (40%), 286.0 (35%) and 287.3 (25%) eV. The total area of the C 1s arises from both C₆₀ and carbon monooxide. The peak 1 is shifted 0.2 eV in the higher binding energy side compared to reported free C₆₀ [199]. Thus 40% area of the total C 1s may come from the bare carbons of C₆₀ center. The peak 2 shifted (FWHM= \sim 2 eV) 0.8 eV compared to peak 1 in the higher energy side. Possibly this may arise from the -W-C₆₀ moiety. The large chemical shift 2.0 eV in the higher energy side of the C 1s of peak 3 compared to peak 1 possibly come from the carbon atom which are directly bonded with electronegative oxygen.

O 1s peak analysis of the compound are shown in figure 5.10 (b) and data are presented in table 5.2. It has three peaks at \sim 529.6 (8.5%), \sim 530.3 (5.5%) and \sim 532 (85%). We are unable to predict the nature of shifting of oxygen in the compound.

XPS of the W 4f_{7/2} and W 4f_{5/2} is shown in figure 5.11 It shows broad peaks and center was found at 40.6, 38.35, 36.85 and 34.6 eV. Peak center at 34.6 eV and 36.85 eV for W 4f_{7/2}, 4f_{5/2} are shifted \sim 0.7 eV in higher energy compared to the metallic tungsten (W 4f_{7/2}, 4f_{5/2} = 36, 34 eV and these two peaks are separated by 2.15 eV) [204]. Electrochemical studies of the complex suggest that C₆₀ donates its electron to the metal center. The peak centered at 38.35 and 40.6 eV which is considerably higher for any metal carbon bond. The chemical shift \sim 4 eV against 4f_{7/2} is only possible if it directly attached with highly electronegative molecule like fluorine or oxygen.

The prepared compound was kept in a dessicator in argon (99.8%) atmosphere for 4 days and IR spectrum of this compound is shown in figure 5.10. It shows new absorption bands compared to figure 5.6 appeared at 1021, 872, 787, 735 cm⁻¹. These type of IR absorption bands are observed, when photolysis of M(CO)₆ molecules (M= Cr, Mo, W) are carried out in O₂ doped Ar or CH₄ matrices at 10-20 K, which produce

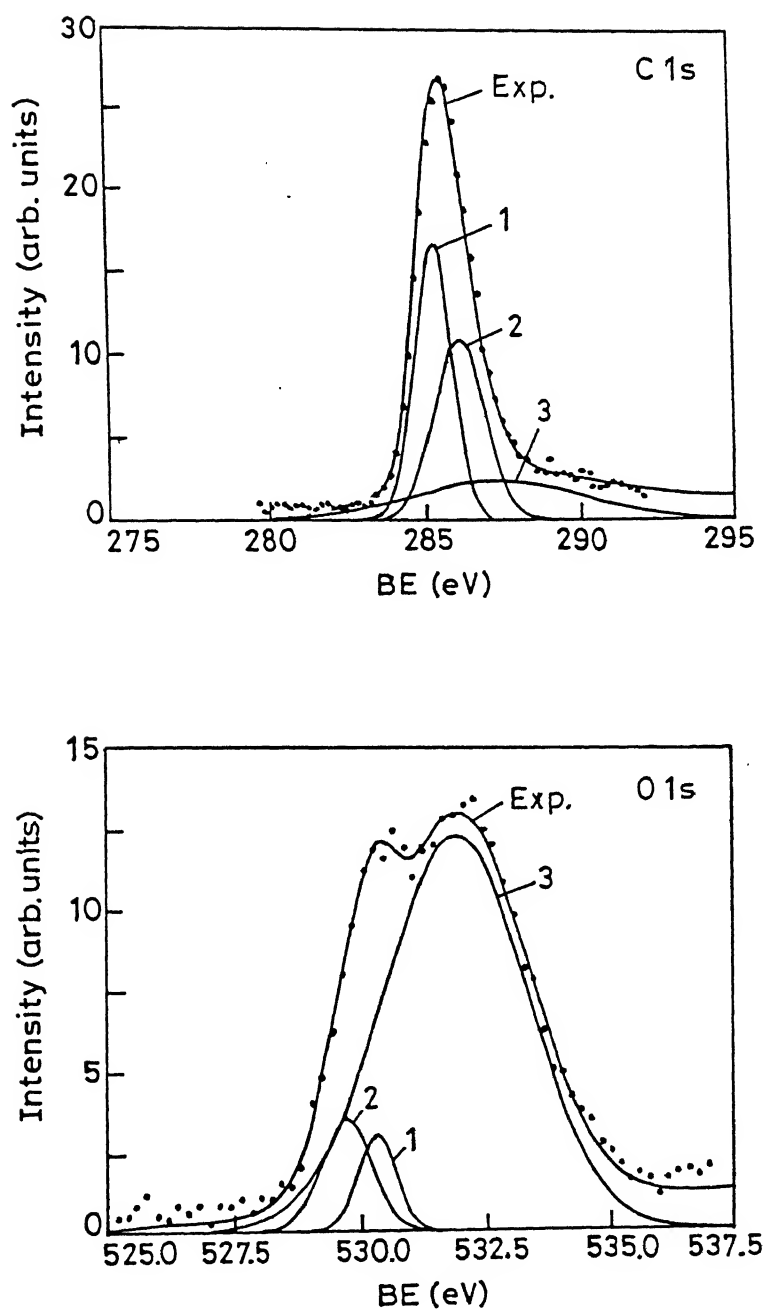


Figure 5.10: XPS Peak analyses of the compound, (a) C 1s (b) O 1s.

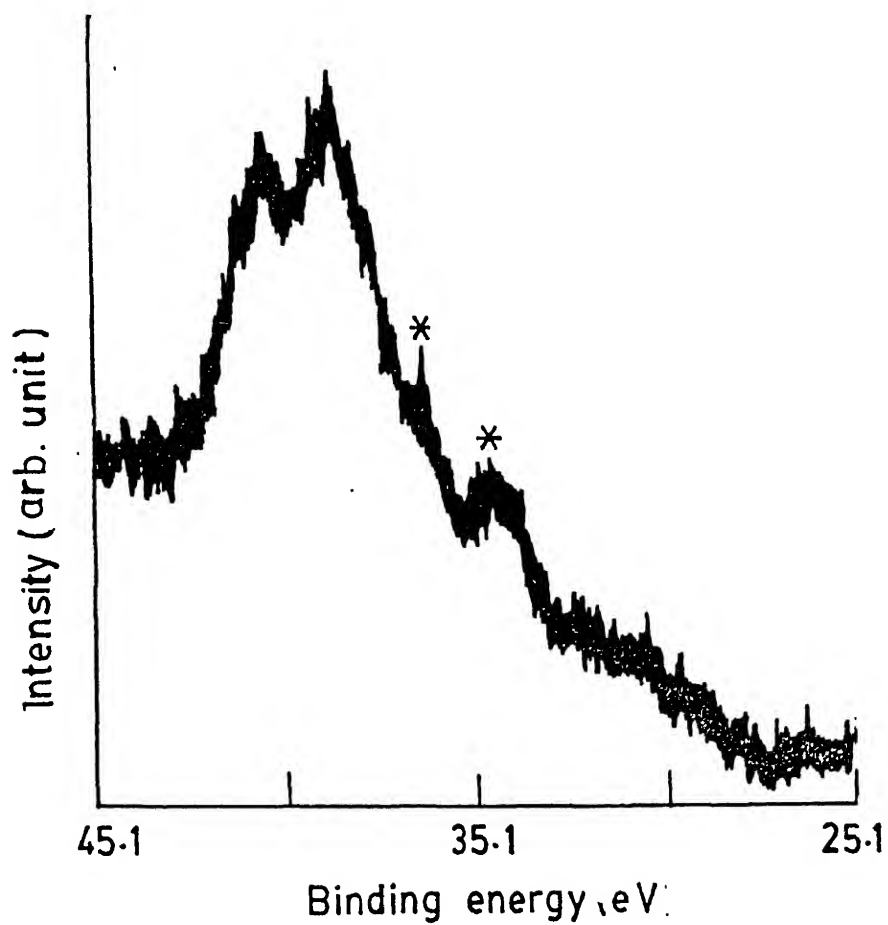


Figure 5.11: XPS binding energy, W $4f_{7/2}$, W $4f_{5/2}$ of the complex.

Table 5.2: C 1s peak summary of the compound.

Peak	Type	Amplitude	center (eV)	FWHM (eV)	% Area
1	Gaussian	16.966202	285.23203	1.4359635	39.816622
2	Gaussian	11.045867	286.05816	1.9393552	35.010253
3	Gaussian	2.4286735	287.27237	6.6857117	25.173125

binary oxide molecules like MO_2 ($\text{M} = \text{Cr}, \text{Mo}$) and MO_3 ($\text{M} = \text{Mo}, \text{W}$) via an oxo-carbonyl intermediates [219, 220]. Photosensitizer C_{60} or C_{60} derivatives convert oxygen to reactive oxygen like O^- , O_2^- , O_2^{2-} in presence of light [149, 156] These highly reactive species, possibly formed during XPS sample preparation time or traces of oxygen in the sample, may be react in this complex. This oxygen attached tungsten species most likely responsible for the large chemical shift of W $4f_{7/2}$, $4f_{5/2}$ at higher energy.

5.3.4 XPS Numerical Summary

Curve-fit analysis has been done with the following polynomial:

$$y = a + bx + cx^2 + dx^3$$

(a) Other details of the table 5.2

Total Points: 63 Active points: 63

Curve-Fit Std. Error= 0.354946798

Background Coefficients: $a = -10.93651$, $b = 0.0158458$, $c = 0$, $d = 3.041 \times 10^{-7}$

Confidence Limit= 99%

(b) Other details of the table 5.3

Total Points: 66 Active points: 60

Curve-Fit Std. Error= 0.440157988

Background Coefficients: $a = -16.2237$, $b = 0.0015106$, $c = 0$, $d = 1.074 \times 10^{-7}$

Confidence Limit= 99%

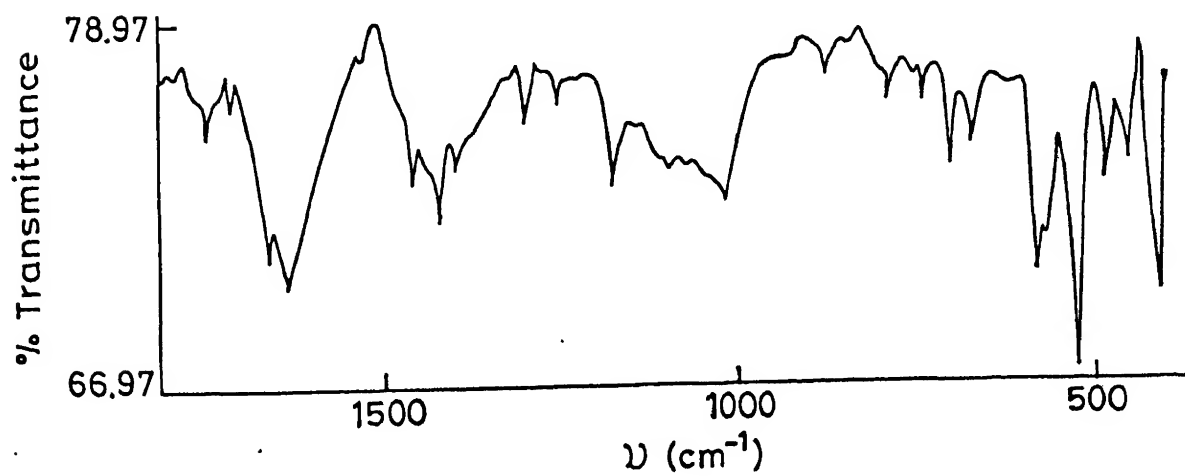
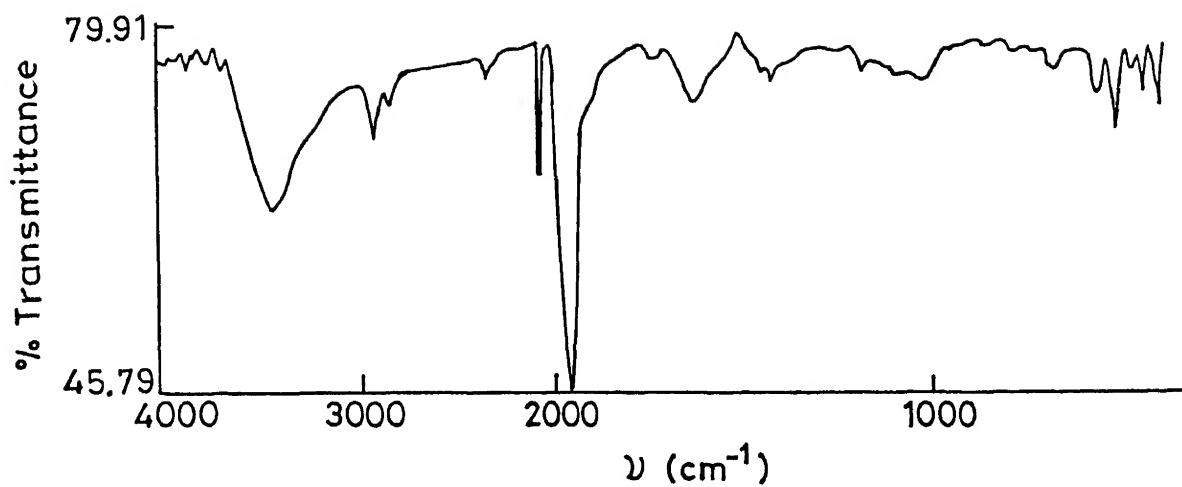


Figure 5.12: FTIR spectrum of the aging compound

Table 5.3: O 1s peak summary of the compound.

Peak	Gaussian	Amplitude	center (eV)	FWHM (eV)	% Area
1	Gaussian	3.490671	529.69973	1.1810285	8.5620426
2	Gaussian	3.0134019	530.30843	0.8922732	5.5785167
3	Gaussian	12.28667	531.86219	3.368688	85.859441

5.3.5 IR Spectroscopy

IR spectroscopy is the indispensable physical methods for characterizing metal carbonyls because $\nu(\text{CO})$ stretching is generally free from coupling with other molecule and is not obscured by the presence of other vibrations. Studies of $\nu(\text{CO})$ alone often provide valuable information about the structure and bonding of carbonyl complexes [197]. From CV experiments followed by XPS it is appeared that the composition of the complex which we previously described as $\text{C}_{60}:\text{W}(\text{CO})_x=1:1$ may be $\text{C}_{60}:\text{W}:\text{CO} = 1:1:3$. The presence of $\text{W}(\text{CO})_5$ or $\text{W}(\text{CO})_4$ moiety in this complex can be ruled out with the experimental observation as well as the physico chemical studies done on the complex.

If $\text{W}(\text{CO})_5$ moiety to be present to accommodate C_{60} , as per 18-electron rule, the local structure of the carbonyl fragments must be square pyramidal or tetragonal pyramidal with C_{4v} symmetry and in this case IR active modes are $2\text{A}_1+\text{E}$. Moreover to retain this symmetry C_{60} should have attached to the fragments by η^2 -coordination. Accommodation of C_{60} in apical position of the $\text{W}(\text{CO})_5$ moiety will impose steric crowding to the CO attached to tungsten in equatorial positions and coplanarity of the equatorial carbonyl groups with tungsten atom is lost as well as trans CO ligands are not co-linear with other axial positions. Thus most likely it will give three IR active vibration if $\text{W}(\text{CO})_5(\text{C}_{60})$ is the composition of the products. The electrochemical behaviour of the present complex also suggest that the bonding of C_{60} with tungsten is not in η^2 fashion.

For the composition of $\text{W}(\text{CO})_4(\text{C}_{60})$, the bonding of C_{60} should be in η^4 fashion to satisfy the 18 electron rule. For $\text{W}(\text{CO})_4(\text{C}_{60})$ the local symmetry either tetrahedral or tetragonal pyramidal would lead to one IR active mode of vibration for the irreducible representations F_2 or E_u respectively. In both these structures accomodation of one

C_{60} is not possible on retaining the local symmetry as discussed just above. Thus the composition of the complex best described when it is $W(CO)_3(C_{60})$. Support of these structures comes from electrochemical study as well as the appearance of the molecular ion peak at $m/z=988$ in the FAB mass spectrum as discussed above.

The general reactivity of this complex where in it has been observed that C_{60} can be displaced readily (judged from the development of the purple colour in solution) with σ and π molecules like acetonitrile, 2,2' bi-pyridyl, THF, PPh_3 in solvents like benzene, methylene chloride, chloroform and carbon tetra chloride, carbon di sulfide. When this complex is dissolved in neat solvents like benzene, methylene chloride or carbon di sulfide it slowly decomposes to release C_{60} . In the solid state it is relatively stable under inert atmosphere and at lower temperature (≤ 5) for days but on ageing it slowly decomposes to yield C_{60} . The trend of these reactions are similar to the general reactivities of $[W(CO)_3\eta^6(Arene)]$ [210].

Thus the IR bands appeared at 2083 cm^{-1} assigned to A_1 mode of vibration and the band at 1957 cm^{-1} is due to E mode of vibrations. The IR spectrum of the complex recorded in the expanded form in the ranges $2200\text{--}1800\text{ cm}^{-1}$ and $800\text{--}400\text{ cm}^{-1}$ are shown in figure 5.12 In the lower region the bands at 446.6 and 442 cm^{-1} are may be due to A_1 and E modes of $\nu(W-C)$ respectively. The vibration appeared in $550\text{--}600\text{ cm}^{-1}$ region with the vibration of C_{60} . The appearance of other bands strongly suggest reduced symmetry of the bonded C_{60} .

5.3.6 Discussion: Photochemical Reactivity of Metalhexacarbonyls with C_{60} and Importance of the $W(CO)_5$ Fragment.

The shape of $W(CO)_5$ fragment produced from the dissociation of $W(CO)_6$ either thermally or photochemically is governed the overall geometry and stoichiometry of the $W(CO)_{6-x}(C_{60})_x$ compounds. Majority reports suggested that photochemically generated $W(CO)_5$ has C_{4v} structure [197, 219]. The orbital correlation diagram, as shown in

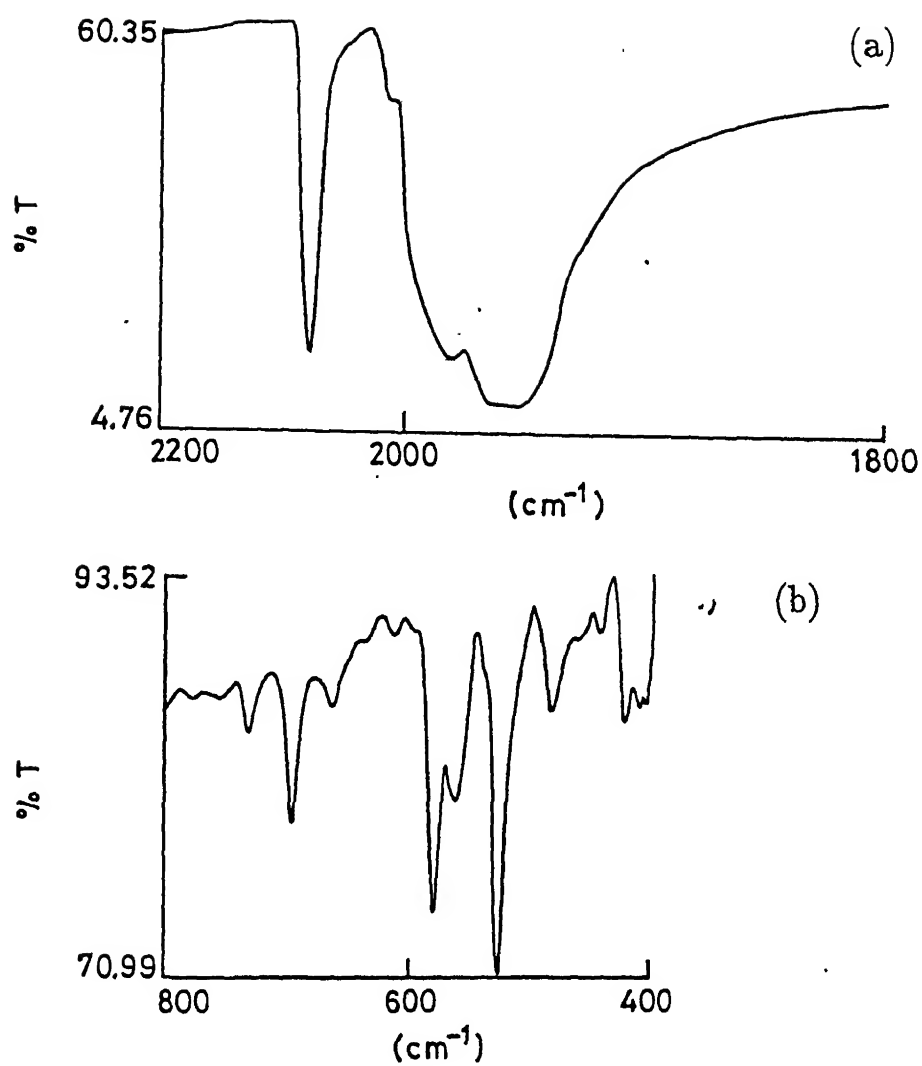


Figure 5.13: FTIR spectra of the compound. (a) Expanded spectrum in the carbonyl region. (b) Spectrum in the 800-400 cm^{-1} region.

figure 5.13(a), also suggests that low spin d^6 metal pentacarbonyl complexes have square-pyramidal geometry since its e -orbital lie below those of the e' orbitals of the trigonal bipyramidal complexes [205]. It also further indicates that $W(CO)_5$ moiety generated thermally from $W(CO)_6$ produce square-pyramidal geometry (C_{4v}). The true square planer geometry from VSEPR prediction of the $W(CO)_5$ moiety is not fulfilled due to it has an incomplete d-shell as a result it has slightly distorted from the idealized octahedrally based fragment geometry and carbonyl groups bend some what towards the vacant octahedral site [210], as shown in figure 5.13(b). Figure 5.13 (b) shows that any bonding in the axial positions by C_{60} operates four-strong axial-equatorial interaction between the π cloud of C_{60} and π electron cloud of carbonyl groups. This kind of structures are energetically unfavourable according to VSEPR theory. This may be one of the reason for non-responding the thermal reactions of $M(CO)_6$, where $M=Cr, Mo$ and W with C_{60} , as in thermal reactions square pyramidal geometry of $W(CO)_5$ is favoured [205]. This also suggests that the formation of η^2 -bonding between tungsten hexacarbonyl and C_{60} is energetically unfavourable as indicated by CV and IR studies.

Photosubstitution reactions are often 'antithermal' this means stereochemistry of the reaction is different from the thermal reaction [221]. Promotion of an electron in photochemical reaction from e to a_1 in square-pyramidal structure, as shown in figure 5.14(a), leads to geometrical unstability. The geometry of five-coordination is a delicate balance between trigonal bipyramidal and square pyramidal, one being converted into the other by Berry pseudorotation [207]. The Jablonski type diagram for photosubstitution/photoisomerization reaction's of d^6 hexacoordinate complex is schematically shown in figure 5.14 (b). The ground electronic state $^1A_{1g}$ has a t_{2g}^6 electronic configuration and on one-electron excitation to $t_{2g}^5e_g^1$ yields the $^1,^3T_{2g}$ excited states [208], as shown in the d-orbital one-electron energy level diagram for $[M(CO)_6]$ in figure 5.14 (a). The excited state initially formed is not necessary the one directly responsible for the observed photochemical reactions and the initial excitation is often followed by internal conversion to state of lower energy by inter system crossing (ISC) to state of different multiplicity like $^1,^3T_{2u}$ often give the desired reaction for d^6 metal- carbonyl complex in

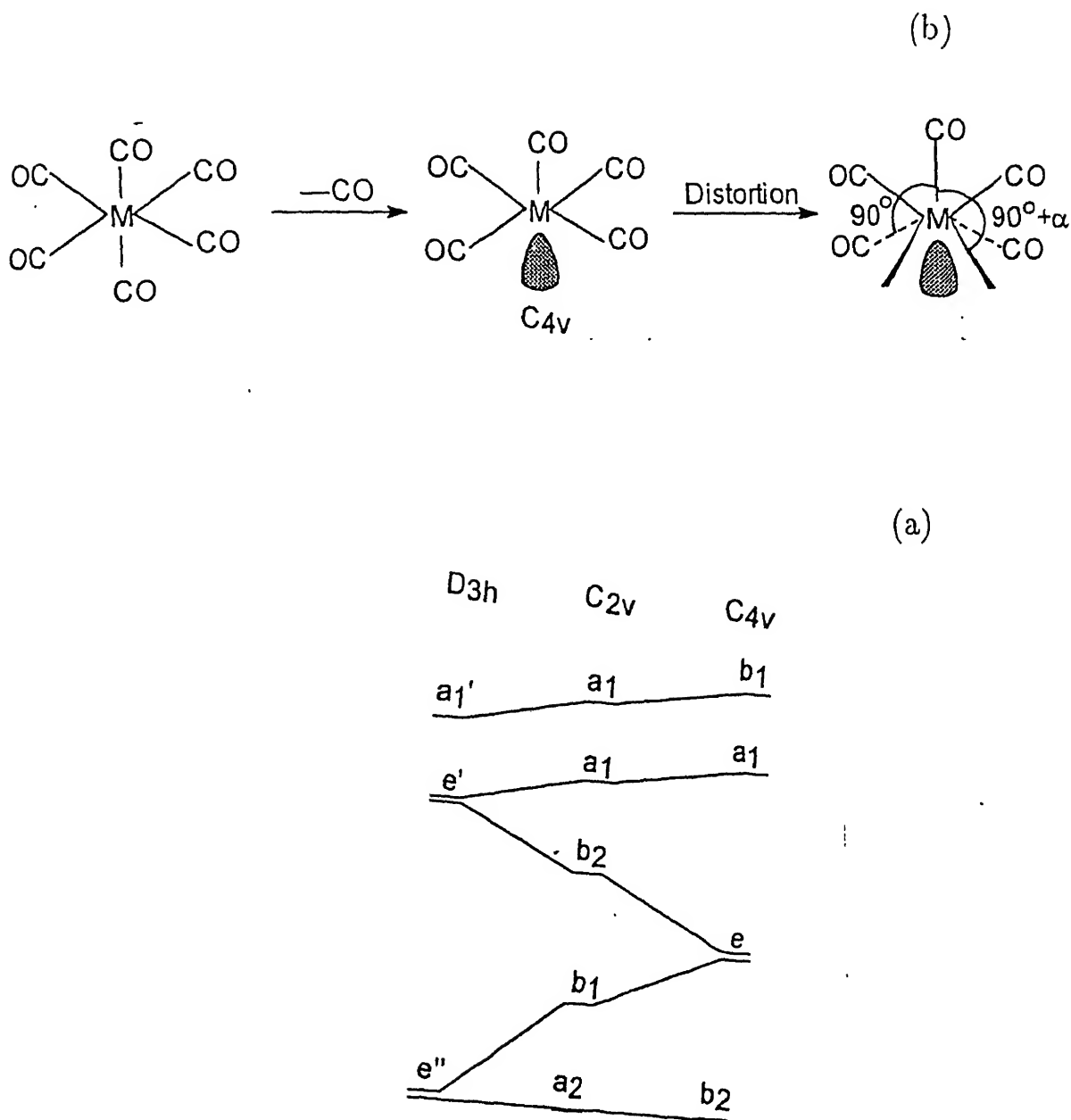


Figure 5.14: (a) Orbital correlation diagram of metal carbonyl (ref.[205]). (b) Movement of the d-orbital towards the vacant side (ref.[205])

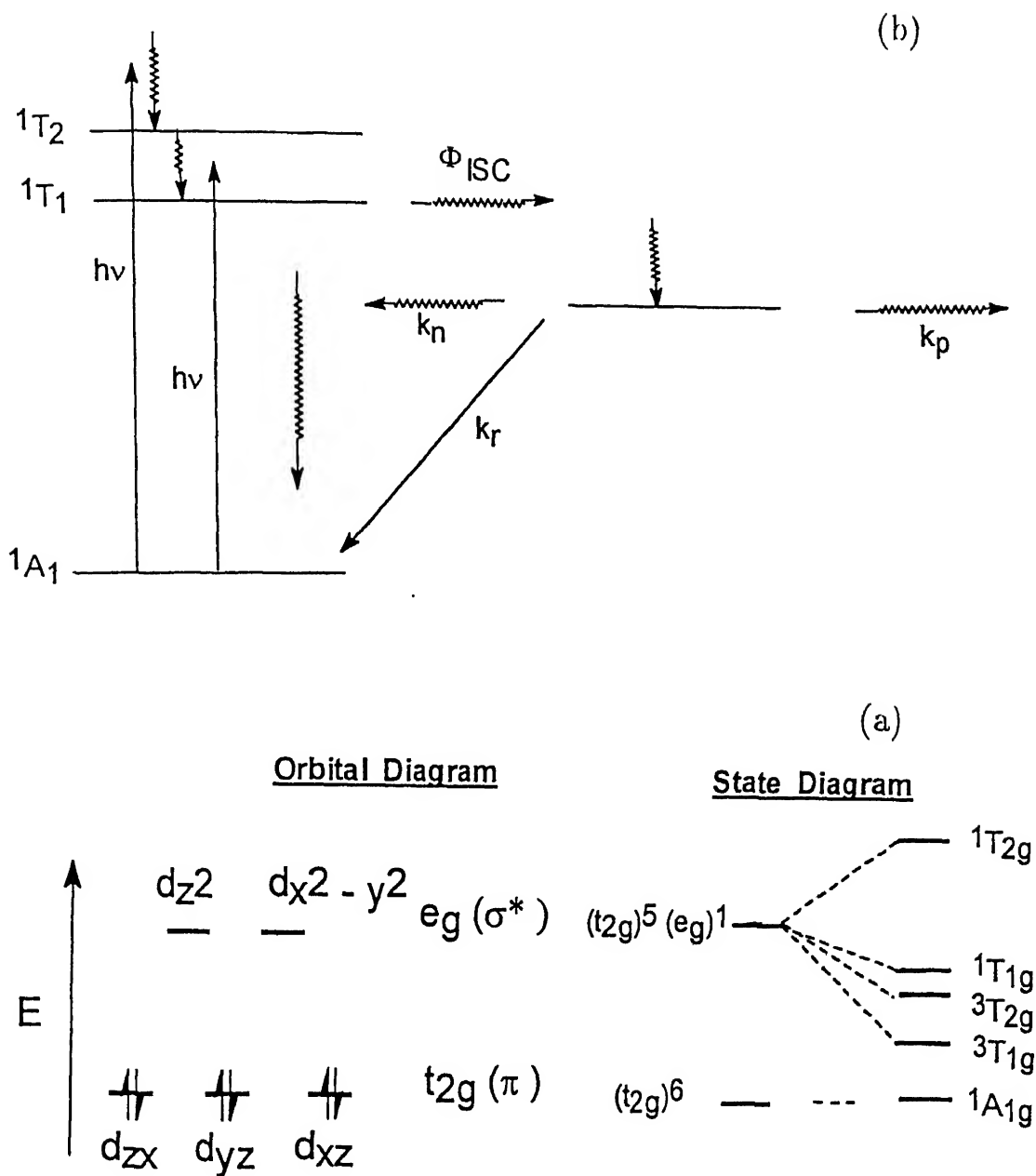


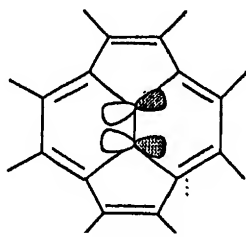
Figure 5.15: (a) Possible Excited state in the metal center (ref.[208]). (b) Reaction path for metal hexacarbonyl in photochemical reaction (ref. [222]).

the photochemical process [222].

In the identical photochemical conditions $\text{W}(\text{CO})_6$ reacts with C_{60} but $\text{Cr}(\text{CO})_6$ and $\text{Mo}(\text{CO})_6$ are reluctant to react (figure 5.3) suggest possibly excited state of different multiplicity is responsible in this reaction. Population of the different multiplicity state is increased through the efficient inter-system-crossing of the excited state electron. As tungsten has greater spin-orbit coupling compared to chromium and molybdenum then geometry in the different multiplicity state is likely playing the staller role. In the photochemically excited state metal-hexacarbonyl molecule distorts toward a trigonal bipyramidal geometry before relaxing to the square-pyramidal ground state [222]. Thus the population of the trigonal bipyramidal (D_{3h}) structure of $\text{W}(\text{CO})_5$ is much greater in number than $\text{Mo}(\text{CO})_5$ and $\text{Cr}(\text{CO})_5$. Three equatorial CO of $\text{W}(\text{CO})_5$ in D_{3h} symmetry make an angle 120° with each other and C_{60} can attached in the equatorial positions with the distortion of the CO groups from the same plane.

The 5d-orbital of W which may also have a critical role in this reaction. The spatial occupancy of the d-orbital follow the order $\text{W} < \text{Mo} < \text{Cr}$. Thus, when d-orbital of Cr and Mo carbonyls come close to the C_{60} molecule experience a strong repulsion compared to d-orbital of W due to the outer surface of large C_{60} (diameter of 10 \AA , [68]) covered by the π electron cloud. Possibly there may be several other factors also involved in this photochemical process, to our knowledge possibly this is another reason, other than inter-system crossing as discussed above, for $\text{Cr}(\text{CO})_6$ and $\text{Mo}(\text{CO})_6$'s non participation in the excited state.

As we are unable to grow single crystal of this compound, thus details of the bonding is not quite clear in this moment. The compound is not stable enough to record the ^{13}NMR in the solution. CV, IR and general reactivity of this compound suggested that η^6 bonding is most likely in this complex. The stable metallocene complex is formed when π orbitals of the arenes are perpendicular to the center of the benzenoid ring [223] however in the case of C_{60} the π -orbital has tilted away from the center of the benzenoid ring, as shown bellow,



Thus π -orbitals of C_{60} has poorly oriented for overlap with the metal d-orbital for η^6 bonding. The geometry optimization studies of η^6 bonding, in C_{60} metal derivatives, suggested that C_{60} can form this, η^6 , bonding only with the 5d and 5f orbital [174, 114]. Excited state of C_{60} may have some role in this complex formation as preliminary photochemical studies suggested that in the excited state it behave like an aromatic molecule, *viz.* benzene [88, 89, 92, 93], though the excited state of C_{60} is still unclear.

5.4 Conclusions

CV studies suggested that C_{60} in the compound does not form η^2 bond with the metal center. Mass peak at 988 has been indicated that composition of the compound is $[W(CO)_3C_{60}]$. CV, IR, chemical shift of C 1s and general reactivity of the compound suggested η^6 mode of bonding is likely in this case. Another important aspect of this reaction that mild irradiation is very useful for the synthesis C_{60} metal-hexacarbonyl derivatives.

Chapter 6

Reactivity with Oxygen and Solvent

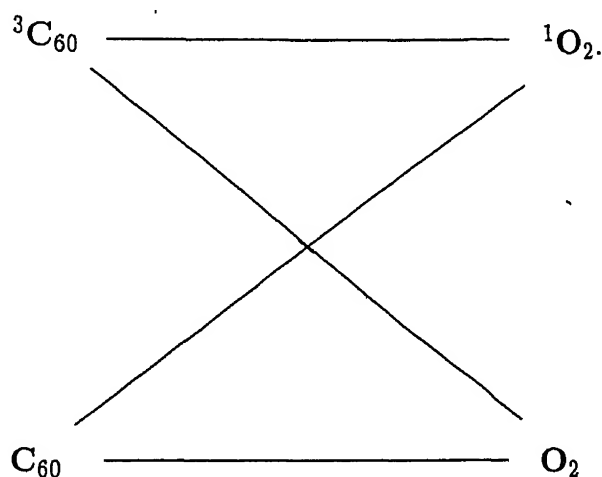
A major focus of fullerene research has been directed toward the synthesis of new C_{60} based materials that can exhibit unique physical, chemical and electronic properties. But the practical applications of these materials are hindered due to C_{60} is not stable at ambient conditions [175, 176]. C_{60} , a photochemically active molecule, has large number of structural isomers in the excited state which are less stable compared to icosahedron structure [183] and these photochemical transformation can easily achieved in presence of the day light. These may be one of the reasons of C_{60} 's unstability at ambient conditions.

We observed on keeping C_{60} in benzene for days the purple colour changes to a reddish blue. The time required to changed this colour is varied with the batch of preparation. In several cases, purple colour of C_{60} remained unchanged for a month however it also observed in some cases within a week purple colour changed to reddish blue. When benzene solution of C_{60} was irradiated with the laser pulses at 514, 488 and 454 nm wave-lengths, of power 1600, 18000, and 1400 mW/cm² respectively, for an hour, colour of the benzene solution remained unchanged (*vide section 5.9*). In another case C_{60} in benzene was irradiated with sunlight (constitute 18% UV of the total sunlight [212]) for 2 days but the colour of the benzene solution remained unchanged during this period (*vide section 4.2.5*). It has been reported, regarding the stability of that structure

of C_{60} is destroyed under the photochemical conditions [224, 225]. On contradictory, a large number reports suggested that C_{60} is a photochemically stable molecule [88, 89, 92, 226, 227]. All these experiments and observation indicates that C_{60} is normally a stable under sunlight and laboratory conditions.

Subsequently it has been also proposed, oxygen is the other main constituents for C_{60} cage destruction at ambient conditions. The nature of oxygen addition with C_{60} is little known. According to Taylor and Walton, 'the extraordinary facility for adding oxygen, which is not yet understood, may find many uses, and lead to a separate field of fullerene chemistry'. Based on the reported results [149, 177, 178, 181, 182], [228-232] the possible interaction of C_{60} with oxygen is schematically shown bellow.

Scheme:



C_{60} convert triplet to singlet oxygen [88] in presence of light. To established C_{60} or fullerenes as useful photosensitizer of oxygen for the practical application, like photodynamic therapy, catalysis in organic reaction and others, the first question need to be addressed is the inter action of C_{60} with oxygen. The singlet oxygen reacts with unsaturated $-C=C-$ bonds via three kinds of mechanisms [233]. These are dioxetane (1, 2 cycloaddition), ene (1, 3 cycloaddition) and endoperoxide (1, 4 cycloaddition). The dioxetane are usually explosive and they are converted into very stable di carbonyl compounds at ambient conditions [233]. But IR spectrum of C_{60} at ambient conditions do

not produce any strong carbonyl absorption band (*vide figure 3.10*) The ene reaction forms hydroperoxide and requires hydrogen atom to stabilize the final products, thus singlet oxygen reacts with C_{60} moiety and destroy the C_{60} molecule via ene reaction quite unlikely. The reported ene reactions [226] of olefins with oxygen using photosensitizer C_{60} and C_{70} shows olefins are oxygenated with high yield and photosensitizer C_{60} are stable in the reaction mixtures.

Tailiani et.al reported that $-C=C-$ of the C_{60} framework reacts with 1O_2 to produce endoperoxide like $C_{60}O_2$ and $C_{60}O_4$ [184]. However these products are not isolated and characterized. The only oxygenated derivative of C_{60} known is C_{60} epoxide which is prepared by the UV irradiation in benzene solution of C_{60} in oxygen atmosphere [146]. To our knowledge till no C_{60} endoperoxide derivative is known, however ascaridol, a peroxide, is synthesized from the reaction between α -terpene and singlet oxygen which is generated in situ in the reaction mixture by using photosensitizer C_{60} and C_{70} [227]. We are unable to prepare any oxygenated derivative of C_{60} with 1O_2 (*vide section 4.2.6*) and Juha et. al [185] also reported that the solid C_{60} is unreactive with singlet oxygen at ambient conditions. Thus it would be interesting to explore the reactivity of C_{60} with oxygen in photochemical process as whether it generates singlet oxygen only or it transforms to oxygenated products like $C_{60}O_2$ or $C_{60}O_4$ which finally involve to bring the transformation of the substrate.

X-ray photoelectron spectrum of air exposed C_{60} , for 4 days, shows the intensity of the O 1s peak is nearly same that of C 1s peak [234]. These authors further suggested that the oxygen is not lightly adsorbed with C_{60} , such as water or molecular oxygen. But in case of freshly prepared C_{60} (after separation it is immediately analyzed), XPS shows C_{60} is not contaminated with oxygen.

IR spectrum of pure C_{60} (*vide figure 3.10*) contains several weak vibrations including the four characteristic IR absorption bands for pure C_{60} . These weak vibrations appeared at 2923, 2851, 2346, 2372, 2191, 1747, 1654.2, 1538.3, 1456, 725 and 405.3 cm^{-1} . The features at ~ 2930 , ~ 2850 , ~ 2330 , ~ 1538 , ~ 1456 cm^{-1} are seen in almost every spectrum

published [35, 83, 235] so far. In some spectrum ~ 1747 , and $\sim 725\text{ cm}^{-1}$ bands are also seen [167]. The bands at ~ 1538 and $\sim 2330\text{ cm}^{-1}$ are attributed to the interaction of C_{60} with atmospheric oxygen and CO_2 and the bands at ~ 2930 , ~ 2850 ~ 2850 and 1456 cm^{-1} are due to the solvent impurity. Noticeably these bands appeared at the aliphatic $\nu(\text{C-H})$ region but solvent used for C_{60} separation needs mainly benzene and toluene. However strong aromatic out of plane vibrations $\pi(\text{C-H})$ in the region of $(700-800)\text{ cm}^{-1}$ and $\nu(\text{C-H})$ in region of $\geq 3000\text{ cm}^{-1}$ are missing in the all the spectrum [196]. Atake et.al [236] reported that the solvent like benzene and toluene used in the sample preparation are hardly removed from the sample of C_{60} under vacuum even at elevated temperatures. This indicates that solvents are strongly trapped in C_{60} .

We observed in most cases, solid C_{60} (kept for around 10 days after chromatography separation) was dissolved in benzene produce the characteristic purple colour of C_{60} . When the same C_{60} was kept in benzene solution for the same number of days at ambient conditions a reddish hue was developed and the solution became turbid. On flash chromatography the characteristic purple colour of the C_{60} was regenerate from the clear filtrate. It indicates that solid C_{60} is more stable compared to that it is keeping in solution, under ambient laboratory conditions. On longer time keeping C_{60} in solutions, it slowly transform to a buff coloured solid which settled down at the bottom of the flask. This observation is similar to that observation by Taylor and co-workers [175, 176].

X-ray structural analyses of C_{60} by different group of workers invariably demonstrated the presence of solvent molecules in C_{60} lattice [68, 237, 238, 239]. The benzene solvated C_{60} shows triclinic lattice (space group $\bar{P}1$) with hexagonal close packing structures [238]. However in n-hexane solvated C_{60} the structure is resported to be cubic (space group $\text{Fm}\bar{3}\text{m}$) with face centered cubic packing [68]. From the above discussions it is evident that the nature of the solvent molecule present in the lattice of C_{60} mainly tunes the intermolecular forces in dictating the packing pattern. Quantification of this interaction is yet materialized due to the non availability of the structural details of pure unsolvated C_{60} .

Origin of the paramagnetic center in the neutral C_{60} (1A_g) is a remote possibility. However Pacc et.al [186] reported, EPR signal of C_{60} is dependent on oxygen concentration. On contrast Cox et. al. [167] reported, ether washed C_{60} do not give any EPR signal at ambient conditions. C_{60} on irradiation with light give an EPR signal [240, 241] and in the low temperature this EPR signal are assigned for $^3C_{60}$ [242, 243], however at room temperature the EPR signal of C_{60} under light excitation is still ambiguous [244]. Dinse et. al [245] suggested that at room temperature intersystem crossing is complete in several nanoseconds and energy transfer make C_{60} to a anion radical.

Another possibility is the formation of a cation radical of C_{60} . But its existence at room temperature in the solid or in solvents are not reported, to best of our knowledge. In gas phase [246] as well as astronomical samples [32, 33] the existence of C_{60}^+ is established. On electrochemicl study on thin film of C_{60} showed the presence of an irreversible oxidation at about +1.6 vs Fc/Fc⁺ [105]. However in trichloro- ethylene (TCE) solvent, the CV of C_{60} at -10° showed an one reversible oxidation at 1.26 vs Fc/Fc⁺ [247]. In both the studies the change in potential of the oxidation process and its irreversible and reversible nature of C_{60} is strongly dependent on the nature of supporting electrolyte used as well as on the solvents.

In the light of the above discussions it is important to investigate the role of oxygen as well as that of solvent with C_{60} in greater details. The experiments to focus these aspects along with interaction of the results consistent with the existing knowledge are described below.

6.1 Experimental Sections: Part I

6.1.1 General Conditions

All the reactions and experiments were performed in oven dried apparatus. Reaction mixtures were stirred magnetically unless otherwise specified.

6.1.2 Materials

Analytical grade Benzene and Hexane were purified by washing with H_2SO_4 , followed by distillation from Na- wire and CaH_2 and stored over activated molecular seive. Pure C_{60} was prepared according to chapter 3.

Solvents CCl_4 , ethanol, iso-propanol, CS_2 were distilled prior to use.

6.1.3 Physical Measurements

Melting Points :

Melting points (m.p.) were determined with a uni-melt capillary melting point apparatus.

Elemental Analysis :

C, H, N, analysis was done as described as section 4.1.3

IR Spectra :

IR spectra were recorded on KBr pellets with the JASCO IR MODEL. Instrumental error is $\pm 2 \text{ cm}^{-1}$. For liquid samples neat sample was used in the Perkin Elmer 1800 series.

UV - Visible Spectra :

UV-visible spectra were recorded in the dry solvent as described as 3.1.2. Band position in the UV region was calibrated with the standard potassium di chromate solution.

FAB Mass :

Matrix and experimental conditions were same as as described as section same as 3.1.2

XPS :

Instruments and operating parameters were same as section 4.1.3. The peak position were calibrated with the reference to Au 4f binding energy at 84.00 eV. Peak were further resolved similar as described in section 4.1.3.

X-ray Powder Diffraction :

X-ray powder diffraction was performed with CuK_α radiation ($\lambda = 1.5418 \text{ \AA}$) in Rich Seifert Iso Debyelex-2002, Germany, X - ray powder diffractometer. The experiment were perform with $\sim 25 \text{ mg}$ sample which was taken in glass slide. X-ray was generated

by 20 mA/30 KV power. The chart paper speed was maintained 0.6 cm/min and 2θ was scanned with a speed $0.6^\circ/\text{min}$. Peak position was measured with reference to the instrumental standard silica (SiO_2) peak at $2\theta = 28.44^\circ$. Sample was vacuum dried at 10^{-3} torr at 150°C before X-ray measurements unless otherwise specified.

The crystallite size was calculated from the Scherrer equation.

$$t = \frac{0.9x\lambda}{B \cos \theta_B}$$

$$\lambda = 1.542 \text{ \AA}$$

$$B^2 = B_M^2 - B_S^2, \text{ radians.}$$

$$\theta = \text{peak position.}$$

(6.1)

^1H NMR :

Spectra were taken in a JEOL 60 MHz instruments. Chemical shifts (δ) are reported in parts per million (ppm) down field from internal reference tetramethyl silane (TMS). Multiplicity is indicated using the following abbreviations: s(singlet), d(doublet), t(triplet), q(quartet), m(multiplet), br(broad) etc.

EPR :

Instruments and experimental parameter were same as section 4.3. Spin concentration was measured from the standard copper sulphate. Minimum detectable paramagnetic species is 10^{13} spin/g. Concentration of the unknown paramagnetic species are calculated according to the formula [248]:

$$[x] = \frac{[std]A_x(scan_x)^2 G_{std}M_{std}(g)^2}{A_{std}(scan_{std})^2 G_x M_x(g)^2}$$

(6.2)

[std]= Concentration of the standard sample.

G = Gain of the signal.

M = Modulation amplitude

The sample and standard were recorded in the same (20 mW) microwave power.

A = Area under the curve.

Area under the absorption curve is proportional to the intensity of the signal and the approximate area is calculated from the following expressions:

$$[area] \propto Intensity$$

and,

$$Intensity \propto Y'(\Delta_{pp})$$

where,

$2Y'_{max}$ = Peak to Peak derivative amplitude.

ΔH_{pp} = Peak to peak width.

Computer simulation was done, in a IBM 486 PC, as follows : first draw the experimental spectrum using commercial software (Lotus 1-2-3). The theoretical spectrum were drawn from the first derivative of Lorentzian and Gaussian function.

By iteration method the theoretical spectrum was adjusted and . 200 points are taken for simulation.

The expressions used in this simulation were shown bellow: Lorentzian,

$$y = \frac{a_0}{1 + \left(\frac{x-a_1}{a_2}\right)^2} \quad (6.3)$$

Lorentzian Derivative,

$$y' = -\frac{2a_0(x-a_1)}{a_2^2} \left(1 + \left(\frac{x-a_1}{a_2}\right)^2\right)^{-2}$$

Gaussian,

$$y = a_0 \exp\left(-0.5\left(\frac{x-a_1}{a_2}\right)^2\right)$$

Gaussian derivative,

$$y' = -\frac{a_0(x - a_1)}{a_2^2} \exp\left(-0.5\left(\frac{x - a_1}{a_2}\right)^2\right)$$

Electrochemistry :

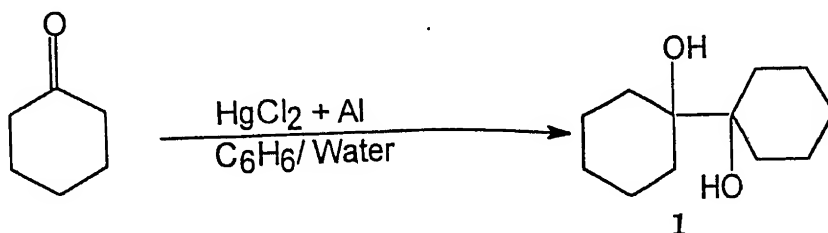
Electrochemistry was done similarly as described as 5.1.3

Chromatography :

Analytical thin layer chromatography (TLC) was performed on Merck precoated glass backed silica del 60F- 254, 0.25 mm plates. Visualization of the spots was effected by one or more of the following techniques: (a) Ultraviolet illumination (b) exposure to iodine vapour (c) immersion of the plate in a 10% solution of phosphomolybdic acid in ethanol followed by heating to *ca* 200°.

6.2 Experimental Part II : Synthetic Methodology

6.2.1 Preparation of 1:1'-dihydroxy-1:1' dycyclohexyl

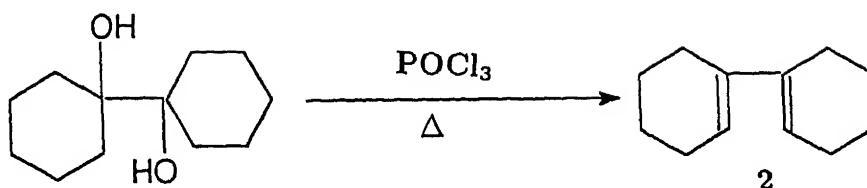


Pinacolic reduction of cyclohexanone (50 gm) in dry benzene (100 ml) with course Aluminium powder (7 gm) in presence of mercuric chloride (2.8 gm) was done according to the procedure [249]. A gel type of mass was obtained and it on further treatment with water (150 ml), dry benzene (250 ml) and reflux for 1/2 hour produce a thick oil in the benzene layer. After filtering the hot mixture and extracting the solid mass with 250 ml of boiling benzene the united filtrate were concentrated to 250 ml. On treatment with 300 ml petroleum ether (40-60 °C) the resulting white solid 1 was collected on a Buchner funnel and was washed with Petroleum ether (40-60 °C) giving 1:1'-dihydroxy-1:1'-dicyclohexyl and m.p and IR data of the 1 is well matched with the reported data [249].

m.p 130 ° C.

IR (neat in KBr disc.), $[\nu \text{ cm}^{-1}]$: 3410 and 2970

6.2.2 Synthesis of Bi-1-cyclohexene-1-yl

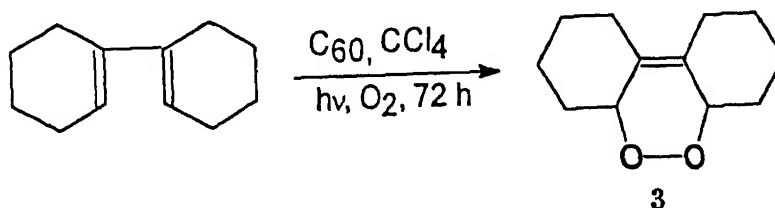


Dehydration of pinacol was done by according to the procedure [250] on a mixture of 8 gm 1, 10 ml Phosphorus oxychloride and 100 ml dry Pyridine was moderately heated ($\sim 100^\circ\text{C}$) for 8 hours. Then 150 ml ice cold water was added to the hot mixture with stirring and the solution then stirred for 30 minutes. Then the mixture was extracted with 250 ml n-pentane The extract was then washed with 10% HCl, aq NaCO_3 and finally dried with Na_2SO_4 . The pentane was removed and the remaining liquid was distilled at 0.05 mm of Hg. A light yellow mobile liquid 2 at $32^\circ\text{C}/0.05 \text{ mm}$ was collected.

IR (neat in KBr disc.), $[\nu, \text{cm}^{-1}]$: 3020, 2975.

^1H NMR (CCl_4), $\delta(\text{ppm})$: 0.9-1.0 (m, 6H); 1.3-1.4 (m, 6H); 1.6 (m, 8H); 2.2 (br, 6H); 5.7 (br, s)

6.2.3 Preparation of Peroxide, 1, 2, 3, 4, 4a, 6a, 7, 8, 9, 10-decahydrodibenzo-o-dioxin

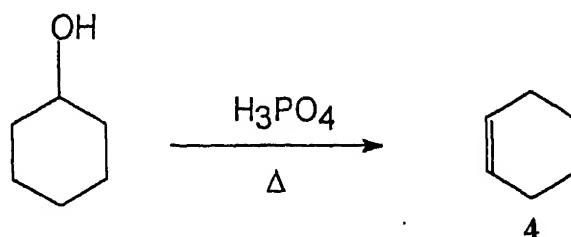


5 ml 2 and 1ml (10^{-4} M) C_{60} and 20 ml CCl_4 were taken in a 50 ml flask. These mixture were irradiated using a 500 W tungsten lamp at 0°C in presence of air for 24 hours.

CCl_4 was removed in vacuo and left a thick brown colour solution 3.

IR (cm^{-1}) = 3450 (br), 1650, 950. ^1H NMR (CCl_4), $\delta(\text{ppm})$: 0.9-1.0 (m, 6H); 1.3-1.5 (m, 6H), 2.2-2.4 (br, 6H), 4.6 (br) and 5.1 (br).

6.2.4 Preparation of Cyclohexene

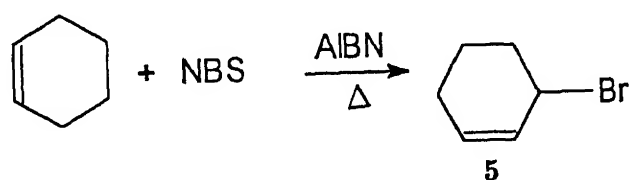


100 ml of orthophosphoric acid was added dropwise to 150 ml cyclohexanol according to the procedure^{ref} and prepare the cyclohexene. These crude cyclohexene was further purified by distilled at 81-82 ° C and this product 4 were taken for further synthesis.

IR (cm^{-1}) = 3040, 2975.

^1H NMR (CCl_4), $\delta(\text{ppm})$: 1.5 (m, 4H); 2.1 (m, 2H); 5.7 (d, $j=1$ Hz, 2H)

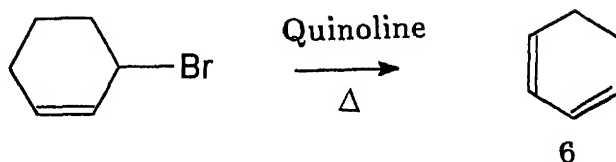
6.2.5 Preparation of 3, Bromo-Cyclohexene



~5 gm cyclohexene and 7.5 gm N-bromosuccinimide were taken in 200 ml CCl_4 solution and the mixture was refluxed at 80° C. Catalytic amount of (328 mg) AIBN was added into this reaction mixture and refluxed for another 3 hours. N-succinimide was removed from the reaction mixture by filtration. The CCl_4 and cyclohexene was removed from the filtrate by fractional distillation and left a thick yellow colour mobile liquid. This was further distilled at 72-77 ° C / 32-35 mm Hg and distillate were collected. liquid 5. ^1H NMR (CCl_4), $\delta(\text{ppm})$: 1.6 (m, 4H); 2.1 (m, 2H); 4.7 (br, 1H); 5.7 (d, $j=2$

Hz); 5.85 (d, $j=2$ Hz)

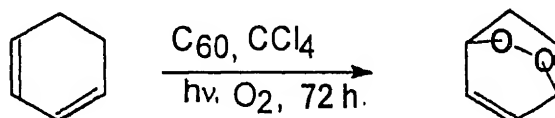
6.2.6 Preparation of Cyclohexa-1,3 diene



Cyclohexa-1,3 diene **6** was prepared by dehydrobromination of 3- bromocyclohexene **3** in presence of dry quinoline at 160-170 ° C. according to the procedure [251]

^1H NMR (CCl_4), $\delta(\text{ppm})$: 1.65 (m, 2H); 2.0 (m, 2H); 2.1(m, 2H); 5.65 (d, $j=2$ Hz); 5.85 (d, $j=2$ Hz).

6.2.7 Preparation of Norascaridol



5 ml **6**, 1 ml (10^{-4} M) C_{60} was taken in 25 ml CCl_4 solution and irradiation of these mixture was done for 72 hours. Other conditions were maintained identical to that described in section 6.2.3. But not observed any change of **6** in this period.

6.3 Results and Discussion

Gas chromatographs of C_{60} in CCl_4 , **2** and It shows photosensitizer C_{60} converts diene to a new compound , as indicated from the figure 6.1 (b) and 6.1 (c). 50% conversion of **3** is achieved in this method. Purification of the desired compounds were not achieved as **3**

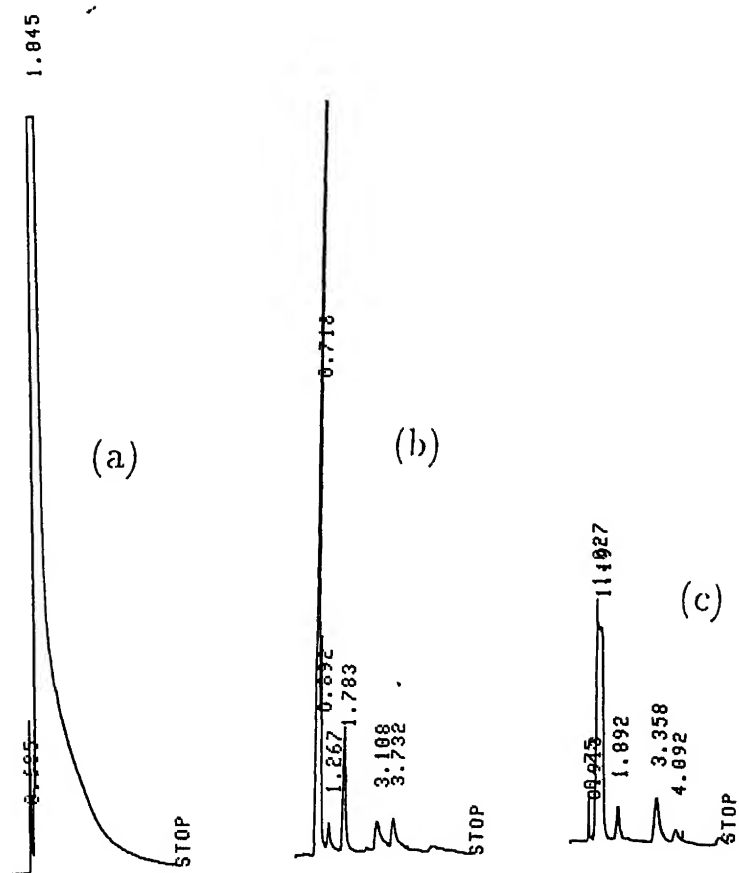


Figure 6.1: Gas chromatograph: (a) C_{60} in CCl_4 (b) diene and (c) reaction mixture.

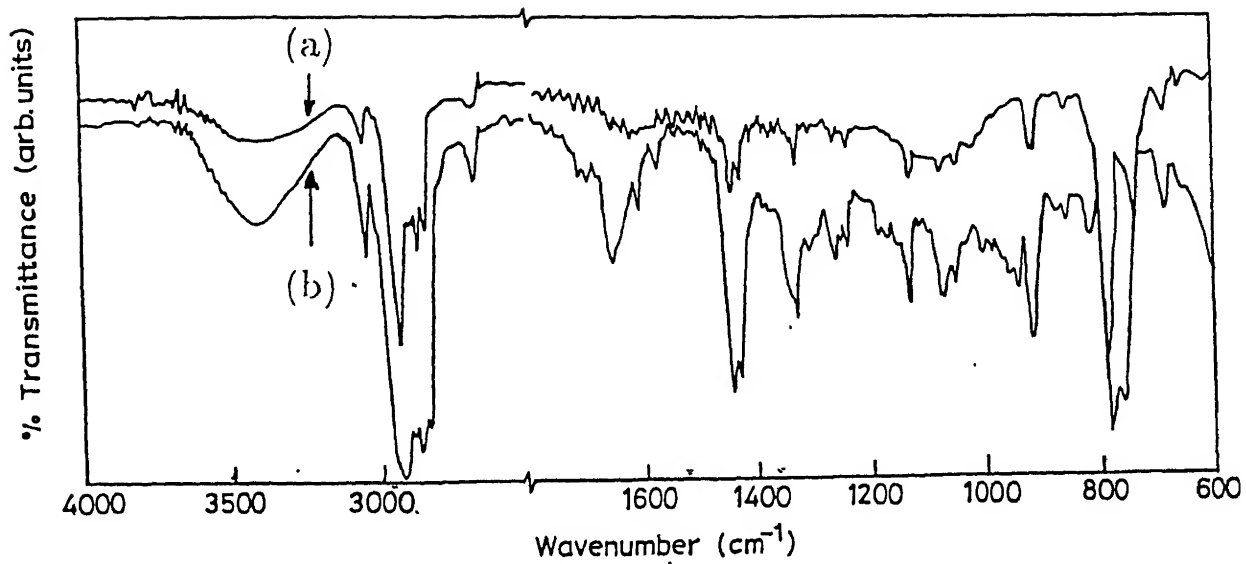


Figure 6.2: IR spectra: (a)diene 2 and (b)reaction mixture 3

(mixture) were not stable in the TLC silica-gel. However in hexane a pink colour spot was observed, at $R_f = 0.69$, which we were assigned as C_{60} spot because pure C_{60} also produced a pink spot in n-hexane at $R_f = 0.71$. This indicates C_{60} is not degraded in these photolytic conditions (quantitative transformation was not carried out). The IR spectra of **3** and **2** are shown in figure 6.2. The absorption band of **3** at 3450, 1650 and 950 cm^{-1} , as shown in figure 6.2 (a), is absent in pure diene which is shown in figure 6.2 (b). The 980 cm^{-1} band are observed typically for -O-O- linkage [197] and appearance of carbonyl (1650 cm^{-1}) and hydroxy (3450 cm^{-1}) functionality may be arises from broken peroxy linkage (-O-O-). Life-time of the singlet oxygen in solvent CCl_4 is higher compared to benzene, toluene solvent [221, 253, 254]. It has been well studied that singlet oxygen react with **2** and converted to **3** in presence of photosensitizer methylene blue or rose bengal [252]. Interestingly preparation of norascaridol from cyclohexadiene need more than 9 days in presence of methylene blue [252]. Here also we did not get any norascaridol within 4 days, however in this duration C_{60} was present in the solution. Thus singlet oxygen generated from C_{60} is reactive with diene not molecule itself.

6.3.1 X-ray Photo-electron Spectroscopy (XPS)

The benzene solution of C_{60} (10^{-3} M) was kept for 7 days at ambient conditions and it was added dropwise on one side of a Indium (In) metal substrate until a thick black layer of C_{60} was deposited on the metal surface. To remove the solvents, sample was kept at 10^{-5} torr for 5 hours in the XPS chamber before insert it into the main analyzing chamber. The XPS spectrum of it, C_{60} , shows two peaks at 285.6 for C 1s and 535 eV for O 1s. The appearance of similar kind of oxygen peak in the C_{60} sample also earlier reported [234], when this author kept the solid C_{60} for 4 days at ambient conditions.

The deconvolution analysis of the C 1s peak is shown in fig 6.3(a). Data of these analyses is presented in table 6.1. It give two absorption peaks centered at 285.57 and 285.75 eV and the ratio of the area between these two curves is 1:8. The binding energy at 285.57 eV (peak 1) is assigned to pure C_{60} due to its narrow full width half maxima

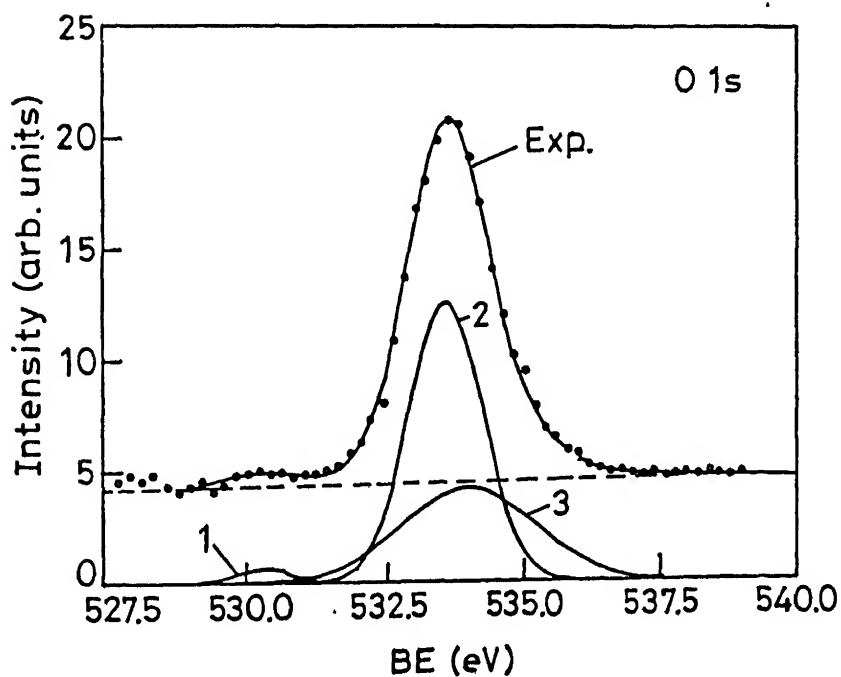
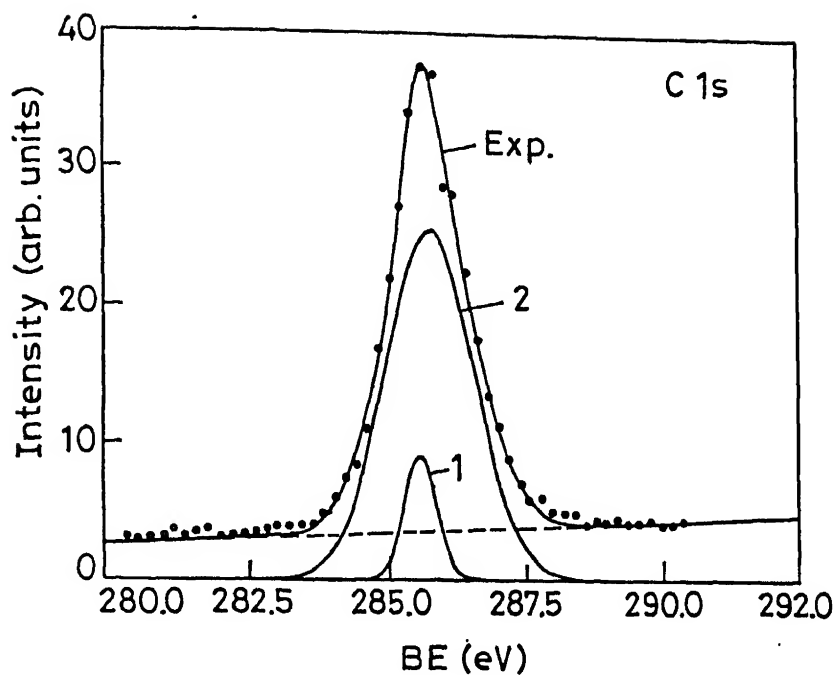


Figure 6.3: (a) Deconvolution analyses; (a) C 1s and (b) O 1s, of the XPS signal of C₆₀

(FWHM=0.679 eV). The narrow FWHM (0.65 eV), of C 1s, [255] is the characteristic feature of pure C₆₀. The major contribution (88%) of the experimental C 1s has come from the peak at 285.75 eV (peak 2). This peak is shifted to higher energy by 0.18 eV compared to other peak. The FWHM (1.87) eV of this single peak indicates that carbon atom are homogeneously charged. For carbon bonded to other carbon and/or to hydrogen, the C 1s core level energy remains near 285 eV, as it was observed in case of C₆₀ [203]. When oxygen is directly bonded to carbon the chemical shift of C 1s binding energy varies 1-4 eV [204] in the higher energy side according to the nature of the bonding as discussed earlier (*vide section 4.3*). The small chemical shift (0.18 eV) of peak 2 compared to peak 1 suggested that C₆₀ is not strongly oxidized.

The O 1s peak analysis is shown in figure 6.3(b) and other details are shown in table 6.2. It shows, the maximum absorptions are centered at 533.6 eV (61.1%) and 534 eV (37%). The chemical shift between these two peaks is 0.4 eV. A weak absorption at 530.3 eV is present which are assigned for O⁻, O₂²⁻ and O₂⁻ from literature [149, 256]. Benning et. al. [256] reported that with the increase of oxygen concentration on C₆₀ the O 1s peak at ~ 530.8 eV shifts to 533.8 eV. Two C 1s peaks (figure 6.3) indicates that some layer of the C₆₀ is affected by the oxygen molecule and negatively charged oxygen molecule cover the C₆₀ molecule.

6.3.2 Peak Fit Numerical Summary

Peak fit has been done by the following polynomial:

$$y = a + bx + cx^2 + dx^3$$

(a) Summary of table 6.1

Total Points: 51, Active Points: 51

Curve-fit Std. Error= 0.744871149

Table 6.1: C 1s peak analysis of the ageing C₆₀.

Peak	Type	Amplitude	Center	FWHM	Area
1	Gaussian	9.11011748	285.57389	0.679726	11.492795
2	Gaussian	25.456433	285.75147	1.8718834	88.507205

Table 6.2: O 1s peak analysis of the ageing C₆₀.

Peak	Type	Amplitude	Center	FWHM	Area
1	Gaussian	0.5871127	530.30985	1.0284732	1.8676494
2	Gaussian	12.508652	533.58231	1.5808191	61.160229
3	Gaussian	4.1753578	534.00374	2.8629633	36.972121

Background Coefficient: $a=-12.59524$, $b=0$, $c=0$, $d=6.932 \times 10^{-7}$

Confidence Limit= 99%.

(b) Summary of the table 6.2

Total Points: 71, Active Points: 57

Curve-fit Std. Error= 0.28824098

Background Coefficient: $a=-2.94494$, $b=0$, $c=0$, $d=4.858 \times 10^{-7}$

Confidence Limit= 99%.

6.3.3 IR-spectroscopy

Chromatographically separated C₆₀ was dried in vacuum (at 10^{-2} torr at 150° temperature) and it was kept in a dessicator over silica gel. IR spectra of this sample was recorded in a month duration and its spectrum at 7th and 25th days are shown in figure 6.4. It was clearly evident from the figure 6.4 that the intensity of the absorption band at 1530 cm⁻¹ do not change during one month. The infrared spectrum of C₆₀O ([60]fullerene epoxide) is known^{52b} and exclude it's presence based on the lack of lines between 770 and 800 cm⁻¹.

When solid C₆₀ was purged in CO₂ atmosphere for 3 hours and it IR spectrum shows the absorption band at 2300 cm⁻¹ do not change. This time dependent IR studies

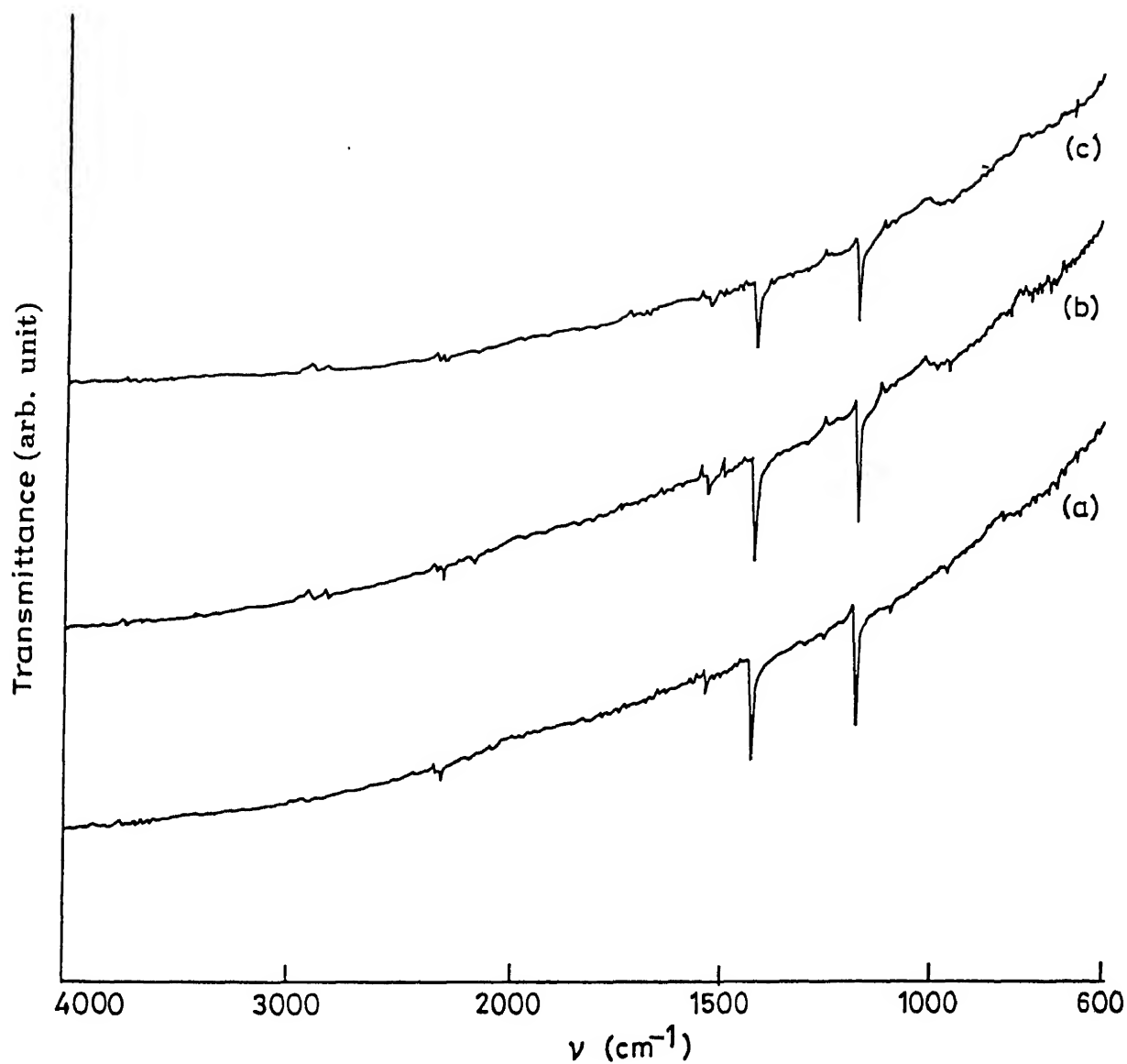


Figure 6.4: IR spectra: Record after (a) after separation (b) 7 days (c) 25 days. Intensity of the band at 1530 cm^{-1} remains constant.

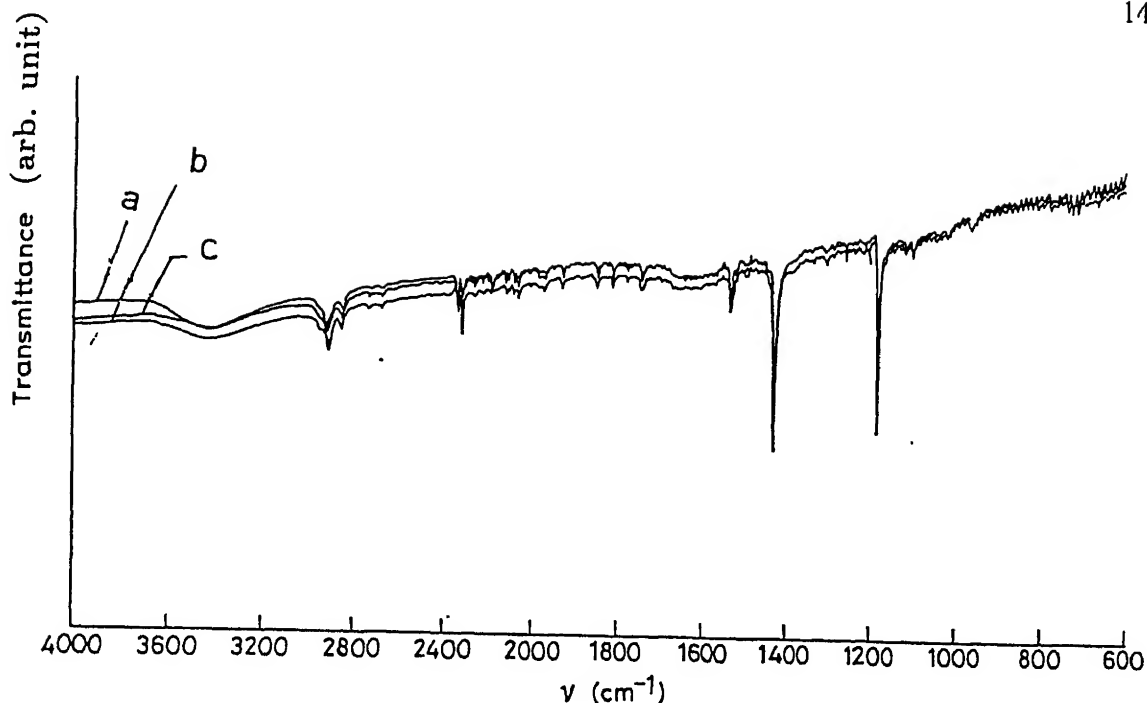


Figure 6.5: IR spectra record in presence of sunlight; (a) without exposed (b) exposed for 2 hours and (c) irradiation for 5 hours.

at ambient conditions suggested that carbon carbon double bonds of C_{60} are not form a strong bond with oxygen. CO_2 studies indicate that the band at $\sim 2320\text{ cm}^{-1}$ is not appeared due to the interaction of atmospheric CO_2 but probably it came intrinsically from the molecule itself, though reaction path of this formation is unknown to us.

Concentrated C_{60} solution ($\sim 10^{-3}\text{M}$) was added dropwise on one side of a freshly prepared KBr pellet ($\sim 0.5\text{ mm}$ thickness) until a dark colour was developed. Spectra recorded immediately after the deposition, is shown in figure 6.5(a). This pellet was exposed in sunlight for 2 and 5 hours and its IR spectra, as shown in figure 6.5(b) and (c), shows the bands at 1538 , 1428 and 1180 cm^{-1} are remained unchanged from the unexposed sample. This suggested that reactive oxygen which is produced in presence of light [149] not oxidize solid C_{60} at ambient conditions.

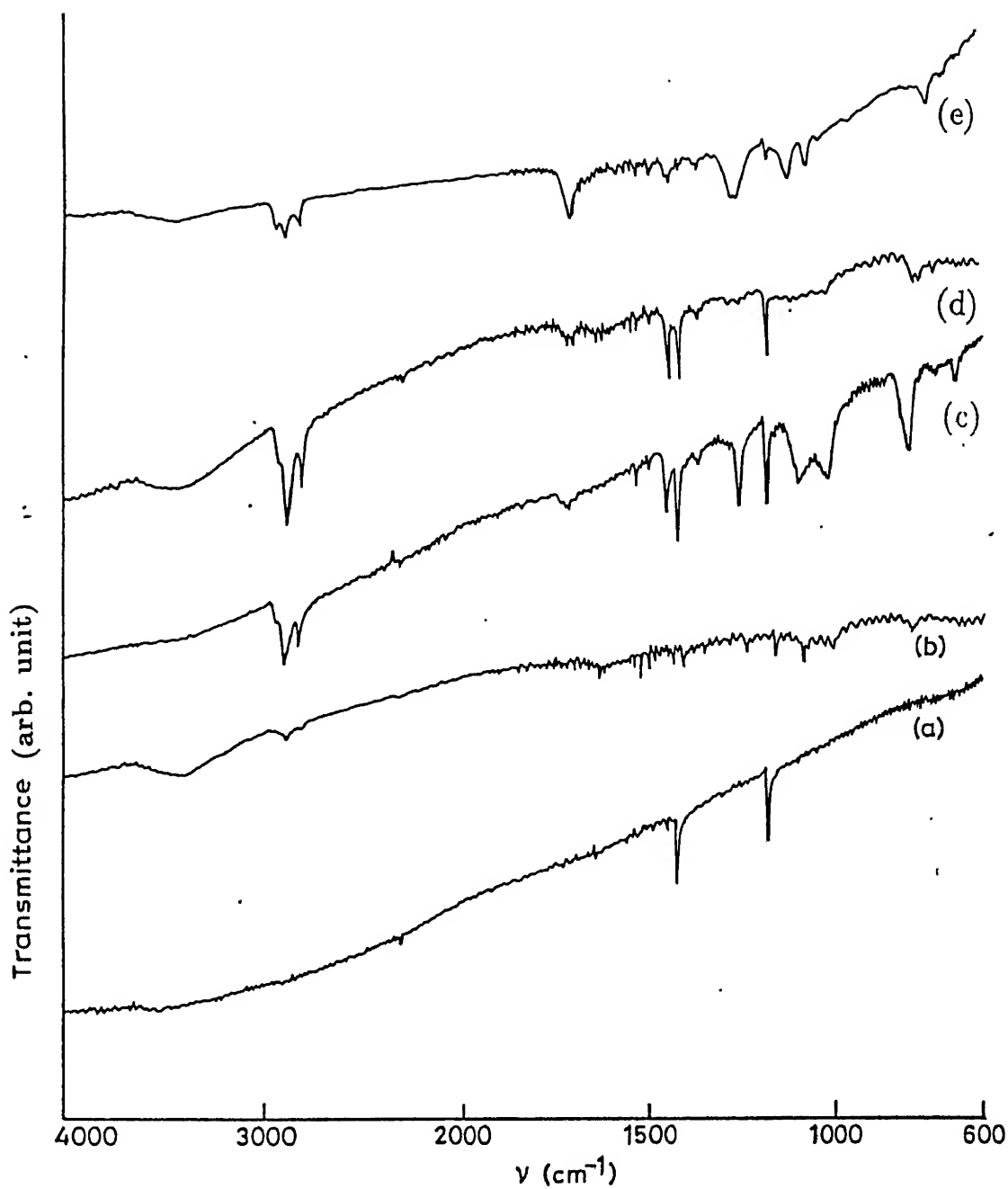


Figure 6.6: IR spectra; (a) C_{60} washed in benzene (b) washed in benzene (c) 5 times dissolved in benzene (d) 5 times in CCl_4 (e) twice with CS_2 .

30 mg of C_{60} , dissolve in dry benzene to remove the n-hexane impurity and evaporated the solvent in vacuum and its IR spectrum shows the absorption bands at 2950 and 2850 cm^{-1} are present in the same positions which is shown in figure 6.6 (a) and (b). Interestingly the intensity of this bands are increased slightly (intensity ratio of the bands are measured between the 1181 cm^{-1} band of C_{60} and 2850 cm^{-1} bands of the spectrum). When the C_{60} was dissolved and simultaneously vacuum dried for 5 times (total time taken 16 hrs) and IR spectrum shows the intensity of the bands at 2920 and 2850 cm^{-1} are increased 10 fold compared to the previous spectrum which is shown in figure 6.6 (a). This spectrum displayed a complicated feature around (1700-1400) cm^{-1} and assigned peaks of this spectrum are given in the table 6.3. We have used two kinds of aliphatic solvents, n-hexane for chromatography separation and di ethyl ether as washing solvent for soot and soxhlet extracted solid. Absence of $\nu(\text{C-O-C})$ band at 1100 cm^{-1} [196] in figure 6.6 (a) for di-ethyl ether ruled out the possibility of the bond formation of di-ethyl ether with C_{60} . Solubility measurements of C_{60} in various solvents (*vide section 1.8*) indicates that it is not soluble in di-ethyl ether. Thus it strongly suggested that $\nu(\text{C-H})$ absorption at 2950 and 2850 cm^{-1} do not come from the impurity of di-ethyl ether. With the increase in number of the solvation of C_{60} in benzene, the absorption bands in the finger print region are increased. Thus the absorption bands at 2950 and 2850 cm^{-1} are not appeared from the n-Hexane impurity.

Interestingly the intensity of the at 1530 cm^{-1} band is not changed from the initial C_{60} absorption spectrum (Figure 6.6(a)). Broad band at 1740 cm^{-1} (figure 6.6 (c)) indicates that carbonyl ($\nu(\text{C=O})$) type functionality are appeared in the C_{60} molecule. Moreover absence of aromatic and olefinic stretching vibrations, $\nu(\text{C-H})$ above 3000 cm^{-1} , suggested that solvent interacts with C_{60} in a very complex way.

In stead of dissolving the C_{60} in hydrocarbon solvents, it was dissolved and dried for 5 times in CCl_4 (experiments are performed similarly to that of benzene solvation) and IR spectrum (figure 6.6(d)) shows the absence of strong $\nu(\text{C-Cl})$ stretching vibration, in the region of 800-700 cm^{-1} . However the bands at 2930 and 2850 cm^{-1} are appeared with considerable intensity. Similarly when the solid C_{60} was dissolved twice in CS_2 and

Table 6.3: IR absorption band of C_{60} , after washing five times with C_6H_6 (figure 6.6 (c)).

Bandposition (cm^{-1})	Intensity	Assignment
2950	sh	$\nu(C-H)$ Stretching
2920	s	"
2850	m	"
1740-1720	w	$\nu(C=O)$ Stretching
1540	w	C-C Ring stretch
1460	s	$\nu(C-H)$ Bending
1428	s	C_{60}
1370	w	$\nu(C-H)$ Bending
1260	vs	$\nu(-C-O-C)$ Stretching
1180	s	C_{60}
1100	vs(br)	O-C-C assym. stretch
1020	"	C-O-C symmetric
820		not assigned
800		
680		

its IR spectrum (figure 6.6(e)) shows the absence of strong the $\nu(C-S)$ vibration, in the region $1400 - 1600\text{ cm}^{-1}$ though it consisting of strong bands at 2975, 2935, 2950 and 1650 cm^{-1} . The reported IR spectrum of C_{60} in CS_2 give a strong band in the $1400-1600\text{ cm}^{-1}$ region [140]. We interpreted these observation, the solvent which contact first with the C_{60} occupy the void space of the lattice are hardly removed. It further indicates that π bonded solvent like C_6H_6 , CS_2 has different role for displaying this kind of spectrum (figure 6.6. (c), (d) and (e)) Thus the $\nu(C-H)$ stretching vibrations observed not due to the aliphatic solvent impurity, instead solvents occupied in the lattice interact with the π bond of C_{60} in a very complex way.

6.3.4 X-ray Powder Diffraction

The diffraction pattern for $2\theta = 6 - 35^\circ$ is illustrated in figure 6.7. for freshly prepared C_{60} (in this preparation n-hexane and benzene were used and soot were not washed with di ethyl ether). The first three reflections (111, 220 and 311) are observed with comparable intensity. This X-ray powder diffraction are well matched with the reported

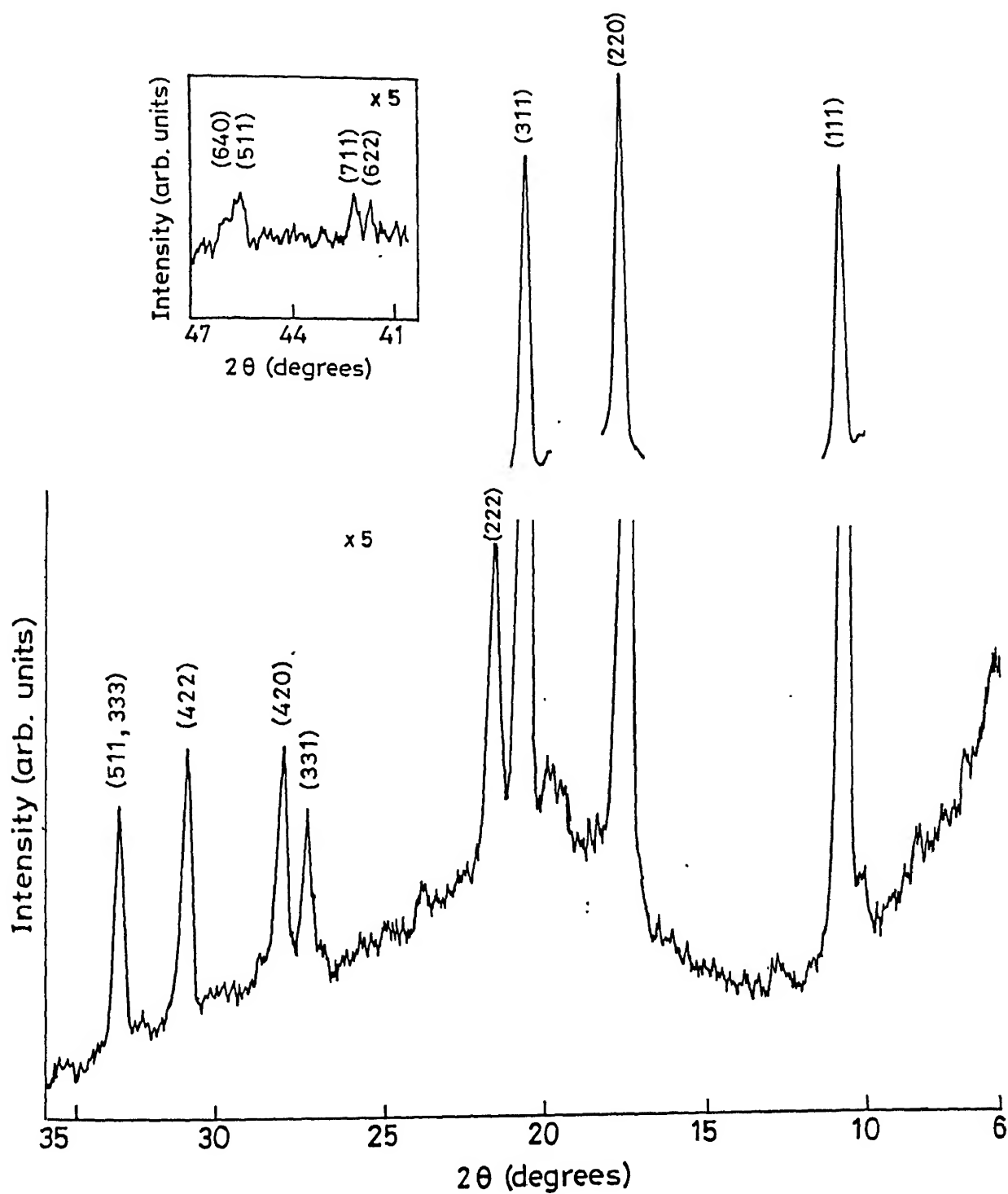


Figure 6.7: X-ray powder pattern of freshly prepared C₆₀

Table 6.4: X-ray diffraction results of pure C₆₀ (figure 6.7).

$2\theta_{obs}$ (deg)	Measured d-spacing (Å°)	Assignment (hkl)	Lattice parameter (nm)	Crystallite size (nm)
10.1	8.758			40.5
10.75	8.230	111	a=14.25	
17.5	5.068	220	a=14.3	
20.7	4.291	331		
21.6	4.114	222		
27.35	3.261	331*	14.21	
28.00	3.187	420 *		
30.8	2.903	422		
32.75	2.739	511,333		
41.75	2.163	533 *	14.18	
42.25	2.139	622		
45.625	1.989	711*	14.2	
45.665		511*		
46.25	640			

X-ray diffraction which recorded in synchrotron radiation [257, 258]. The indexing (hkl) are assigned for the resolved peaks which is shown in figure 6.7 and d-spacing, lattice parameter and crystal size are presented in table 6.4. The indexing of this well resolved peaks are done herein which are shown by asterisk in table 6.4 Lattice constants 1.418 and 1.42 Å° were measured from this new assigned peaks at (533) and (711) respectively and are well matched with the reported value of 14.17 Å° [258]. The size calculated from the line widths of the (111), (220) and (311) peaks is 40 ± 5 nm which is higher than reported 29 ± 5 nm [259] which indicates that C₆₀ used in this study are better crystalline. The lattice constant 14.18 Å° implies, the mean atom to atom diameter of the C₆₀ molecule is 7.1 Å° and it known with this mean to mean diameter, lattice has very good close packed [258].

This C₆₀ was kept in a vacuum dessicator for 7 days and before measuring the X-ray diffraction, the sample holder was for 45 minutes in presence of sunlight. The diffraction pattern of it is given in figure 6.8. Its contain extra peak compared to freshly prepared C₆₀ (figure 6.7) at $\theta_{obs} = 8.45, 10.15, 19.65, 19.95, 21.95$ with considerable intensity.

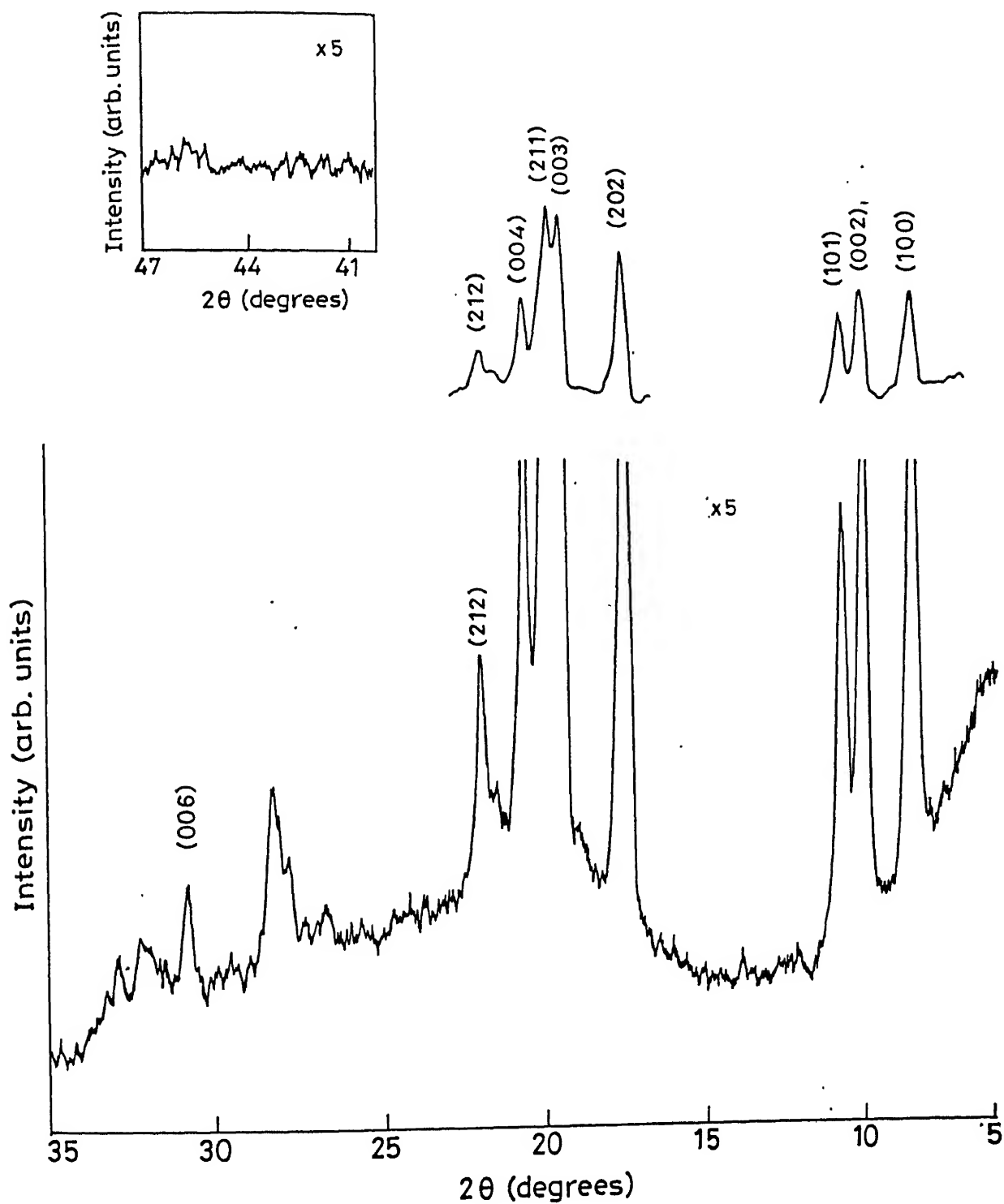


Figure 6.8: X-ray powder pattern of the C_{60} in presence of sunlight

Table 6.5: X-ray diffraction results of sunlight irradiated C₆₀ (figure 6.8).

$2\theta_{obs}$ (deg)	Measured d-spacing (\AA)	Assignment (hkl)	Lattice parameter (nm)	Crystallite size (nm)
8.45	10.465	100	a=13.95, c=17.43	30.9
10.15	8.715	002		
10.85	8.153	101		
17.625	5.032	202		
19.65	4.518	033		
19.95	4.450	211		
20.75	4.428	004		
21.65	4.105	104		
21.95	4.049	212		
22.05	4.040			
27.85	3.198			35
28.1	3.175			
28.35	3.153			
30.825	2.903	006		
31.85	2.903			
32.1				
32.75				

other peaks are also shifted from the original position.

The increased of diffraction line in figure 6.8 suggested that the lattice is distorted from the cubic form. It is known [260] that (111) and (222) peaks of the cubic form are not splitted in tetragonal or orthorhombic form and θ_{obs} remains almost constant. Similar kind of observation also seen in cubic and tetragonal BaTiO₃ where 2θ position of the (111) lines are appeared in the same position in these two crystal systems [261]. For monoclinic and triclinic system a greater number of reflections in $6^\circ \leq 2\theta \leq 35^\circ$ region are occurred due to the multiplicity of the cubic form greatly reduced [260]. Though prediction of the disordered system is not always matched with this general observation of the X-ray pattern. Thus X-ray powder pattern of figure 6.8 most likely belongs to a hexagonal system where (111) peaks splits into (100), (102), (101) peaks though (102) lines are not quite distinct in this spectrum and the intensity of (101) reflection is strongest in the present case. Hexagonal system thus produced is disorder system where

$c/a = 1.3$ which is 18% small compared to ideal hexagonal system. Measured d value, indexing of the hkl plane, lattice parameter and crystal lattice size are given in Table 6.8. (220) line remains in the the same position to that of unexposed C_{60} (figure 6.7) and 420, 422, 538, 711, 511 and 640 lines are shifted very little from figure 6.7 Peak asymmetry and complex nature of these lines may be arises due to the incomplete transformation of cubic lattice to hexagonal lattice. Quantitative estimation of this transformation is not taken care.

When the C_{60} (separated as described in section 3.1.6 and the sample was vacuum dried at 10^{-3} torr at 150° C for 3 hours) was kept in a drawer cover with a black paper for 25 days in aerobic conditions, and its X-ray diffraction is shown in the figure 6.9. The observed d -spacing are same as figure 6.7.

The chromatographically separated (soot was not washed with di-ethyl ether) C_{60} was dissolved in CS_2 and vacuum dried and its X-ray diffraction is shown in figure 6.10. It comprised of peaks at $2\theta = 8.5, 9.8, 10.1, 10.75, 11.5, 17.75, 19.00, 19.75, 20.75, 22.05, 22.4, 22.8$ and 29.5 degree. In comparesion to the pure (after separation, it was not treated with further any solvent) C_{60} , table 6.4, it consists of several new peaks at $2\theta = 8.5, 9.8, 11.5, 19.00, 19.75, 22.05, 22.4$ and 22.8 . Intersistently diffraction pattern, $8 < 2\theta < 11$ and $19 < 2\theta < 23$, is similar to the sunlight exposed C_{60} sample (figure 6.8).

The diffraction pattern of C_{60} , was washed for 15 minutes with di ethyl ether and vacuum dried immediately, shows (figure 6.11) peak position reamine unchanged from the solvent untreated C_{60} (figure 6.7). In figure 6.(b) X-ray diffraction of C_{60} was recorded after solvated with 5 times in benzene which shows most of the peaks are very week in intensity compared to pure C_{60} suggesting its crystallinity is lost considerably.

When the C_{60} was immersed in 100 ml di ethyl ether and kept over night, X-ray diffraction of the dried powder shows (figure 6.11(c)) peak at $2\theta = 17.9, 19.0, 20.1, 20.9$ and 21.8 . which is absent in the simply washed powder (figure 6.11(a)). Keeping it for 45 minutes in the atmospheric conditions the peak at 19.0 degree is vanished and new

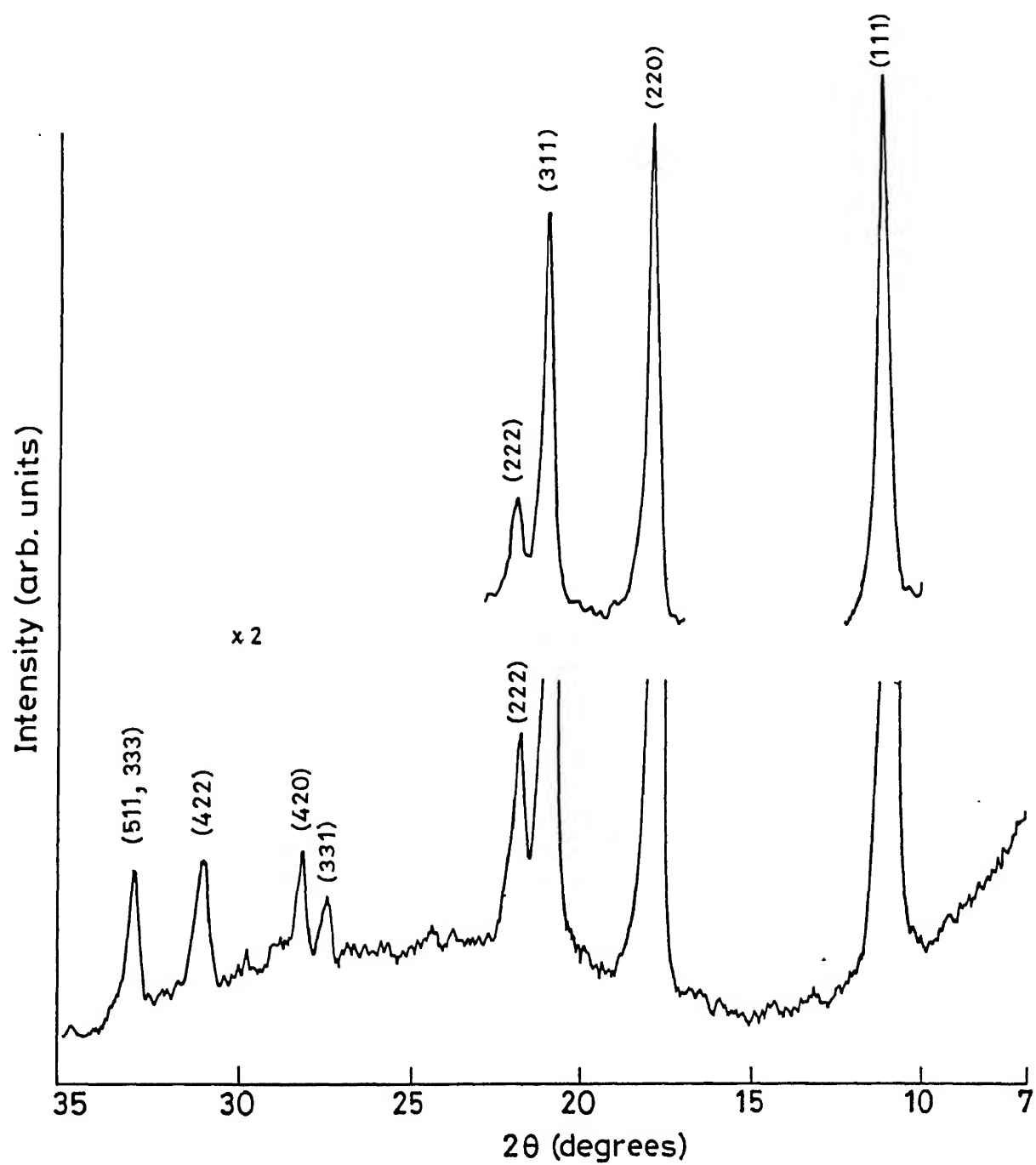


Figure 6.9: X-ray powder pattern of C_{60} taken after 25 days

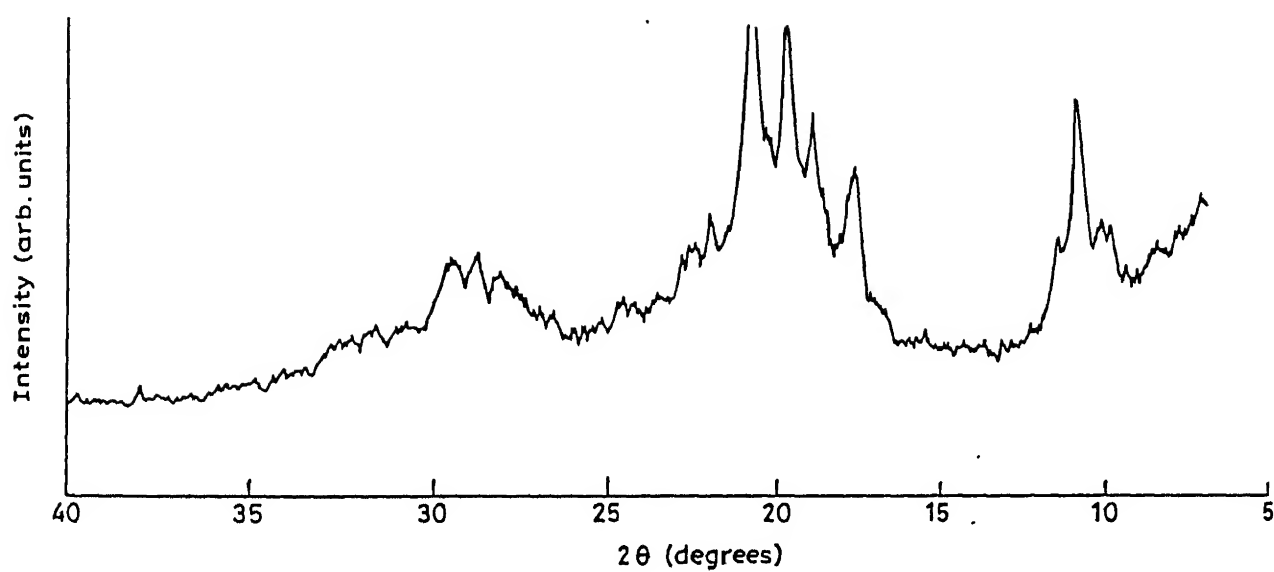


Figure 6.10: X-ray Powder pattern of C₆₀ after dissolved in CS₂.

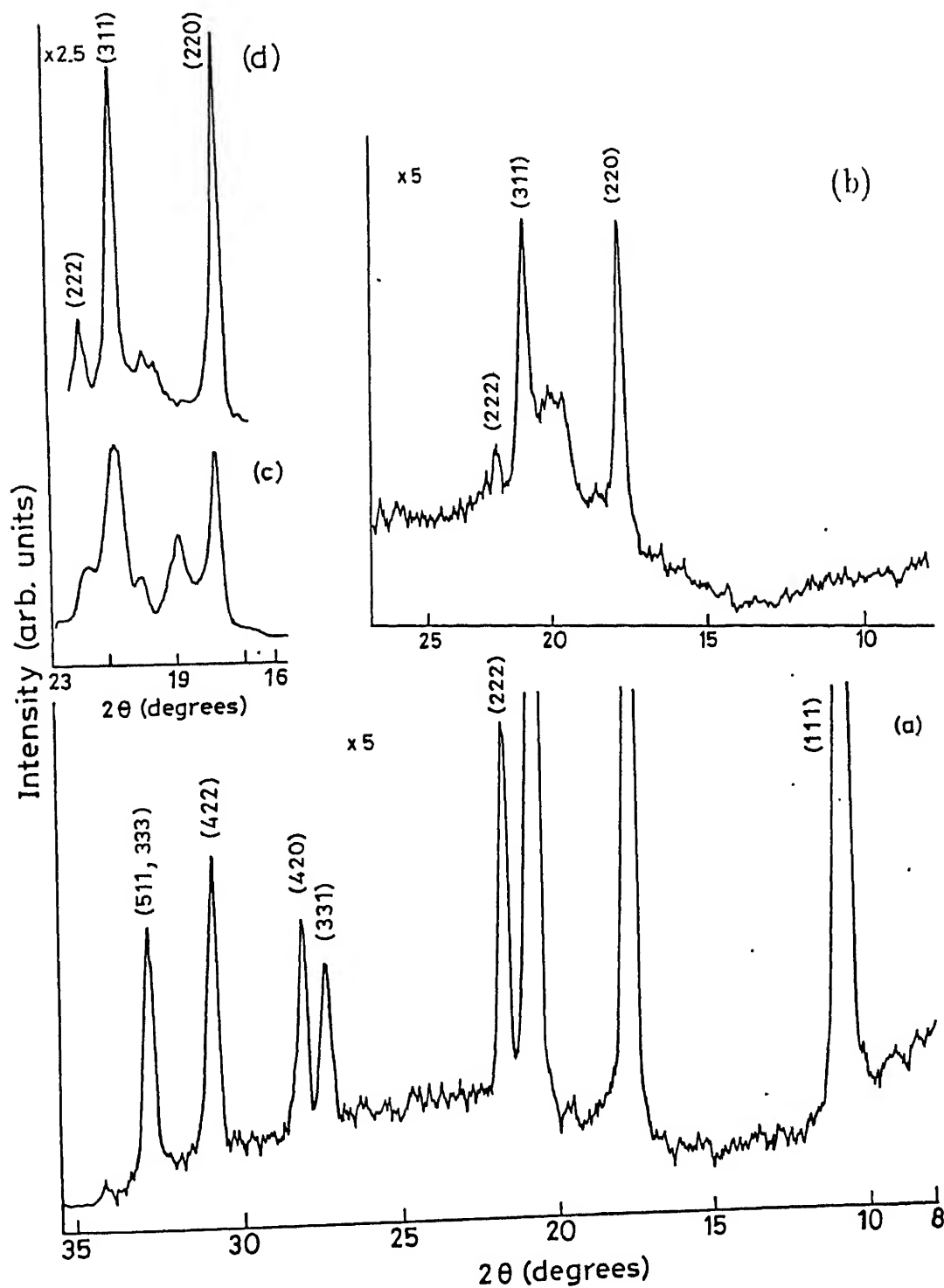


Figure 6.11: X-ray powder diffraction of the (a) washed in ether (b) 5 times washed in benzene (c) immersed in ether for 24 hours (d) record (c) after 45 minutes.

peak positions are found at 17.5, 19.75, 20.2 and 21.8 which is shown in figure. 6.11(d) and crystallinity of it, is decreased compared to the earlier material. This suggested the solvent treated C_{60} is less stable in X-ray conditions or laboratory conditions.

6.3.5 Electron Paramagnetic Resonance

Ether washed C_{60} give an EPR signal in the X-band Bruker Varian ESR-300 spectrometer at ambient conditions which is shown in figure 6.12(a). Its g value calculated is ~ 2.003 with line width (ΔH) ~ 1.8 G. When the same sample was kept for 7 days at ambient conditions in a closed vessel, EPR signal of it appeared, as shown in figure 6.12 (b), with the $g=\sim 2.003$, $\Delta H=1.4$ G and concentration of the spin is lower by a factor 6. After 30 days from the freshly prepared sample the intensity of this EPR signal was found to be very poor (figure 6.12 (c)) and and concentration of the spin is lower by 80 times than the freshly prepared sample (figure 6.12 (a)). The line shape analyses of the EPR signal of C_{60} shows, it is best fitted in Lorentzian than Gaussian function. The line shape of the EPR signal in Lorentzian function is shown in figure 6.13(a). and line width (ΔH_{pp}) of it is 1.8 G which is large from the reported value (0.14 G) [244].

The ether-washed soxhlet mixture that consists of C_{60} (70%), C_{70} (20%) and rest are higher fullerenes give an EPR signal, as shown in figure 6.13(b), has the g -value= ~ 2.0033 and line width (ΔH_{pp})= 1.74 . Line shape analyses of this signal shows it also best fit in Lorentzian functions. The line shape analyses of C_{60} and fullerene mixture indicate, likely most of the fullerenes produce similar kind of paramagnetic species at ambient conditions. As higher fullerenes have also closed shell electronic configurations [60] like C_{60} . But the appearance of paramagnetic center in fullerene due to the oxygen interaction or from the triplet state of C_{60} is not very clear from this EPR signal. Though ΔH of this signal indicates that the EPR signal is not arises due to triplet C_{60} as δH of the triplet C_{60} is max. 0.7 G.

Separation of macroscopic quantities of C_{60} (from chromatographically) in absence

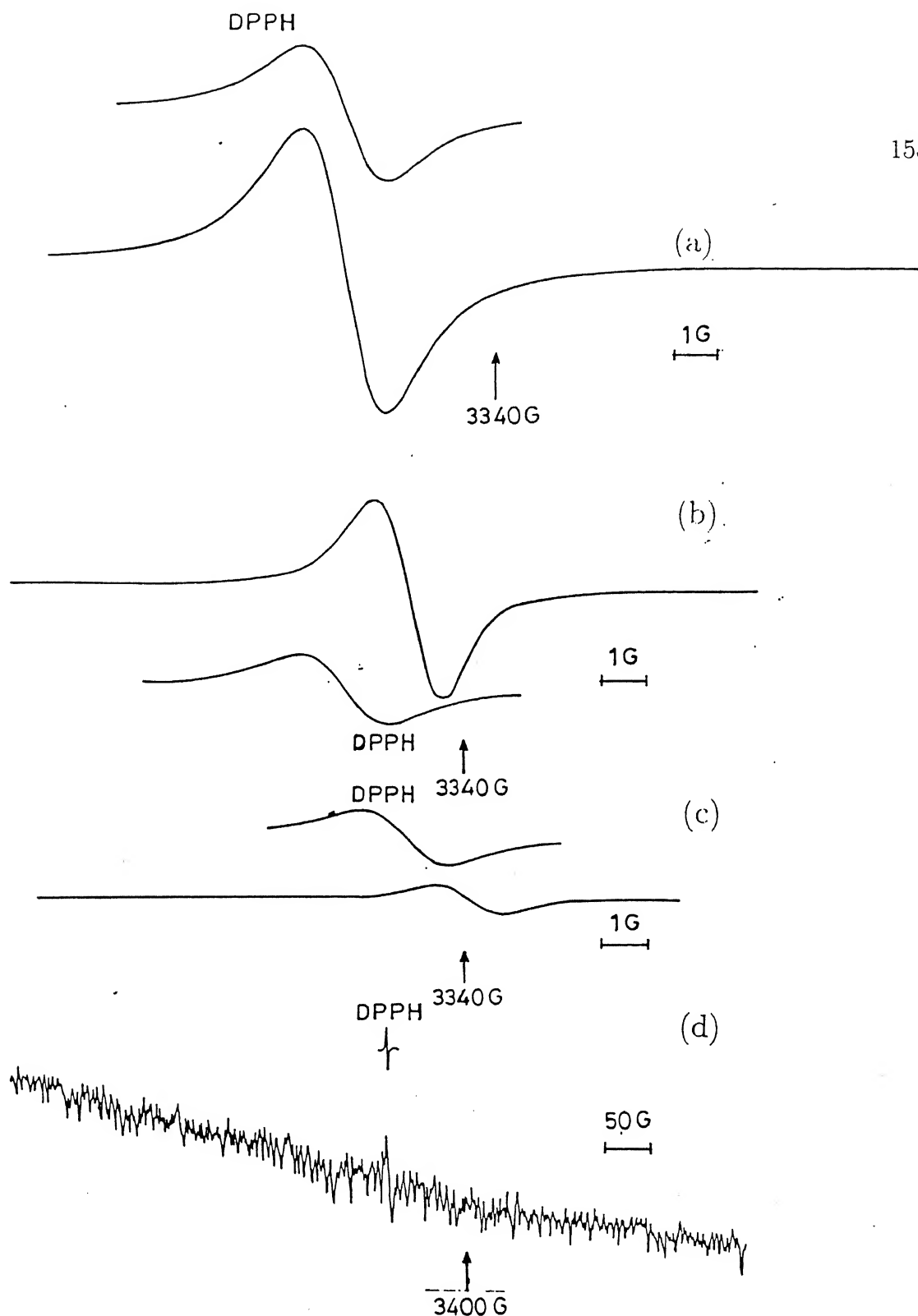


Figure 6.12: EPR spectra of the solid C₆₀. $\nu = \sim 9.4$ GHz, mod; 1.6×1 G; Power = 20 mW. (a) Freshly prepared $g = 2.003$, $\delta = 1.8$ G and gain 5×10^3 (b) after 7 days $g = 2.0029$, $\delta = 1.5$ G and gain 8×10^3 and Spin concentration decreases by a factor 6 from (a). (c) Spectra recorded after 30 days where spin concentration decreases by 78% from (a), other parameters are same of the above. (d) At liquid Nitrogen temperature.

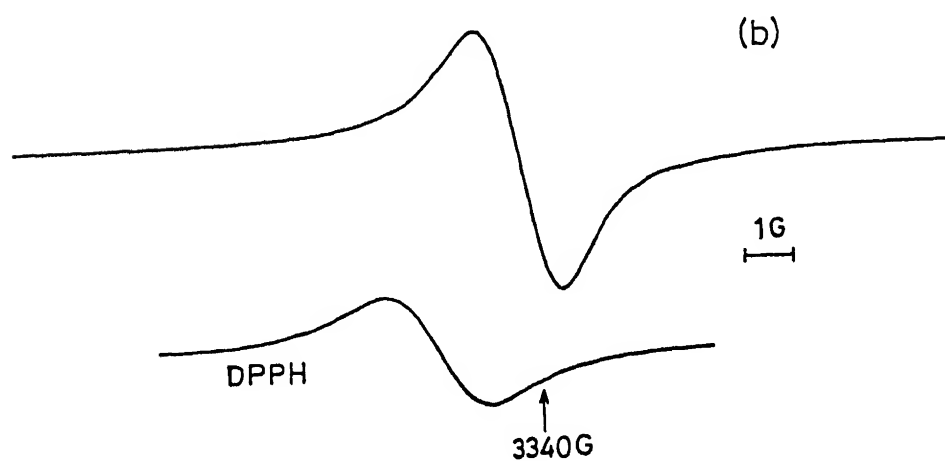
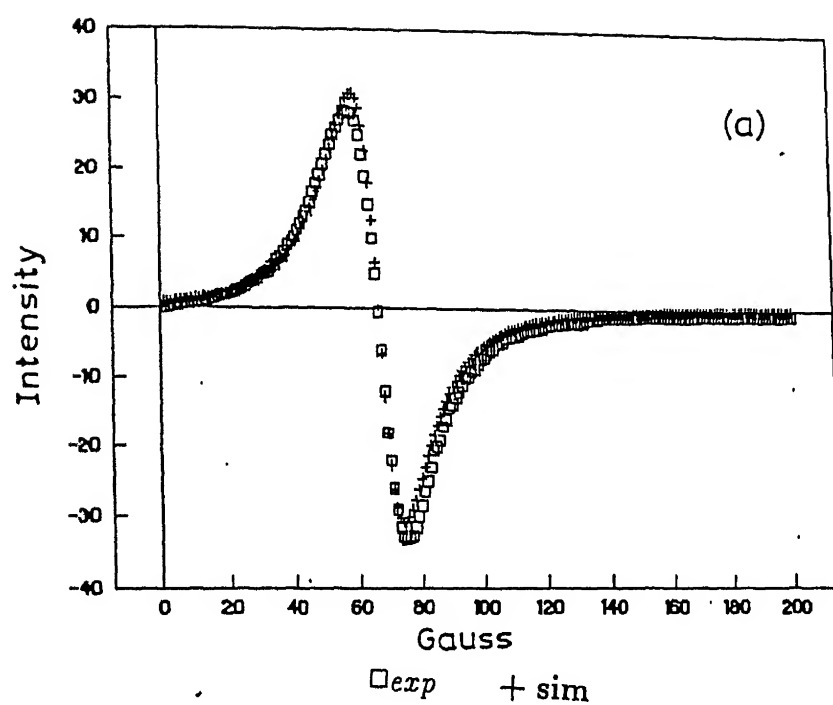


Figure 6.13: (a) Simulation of the figure 6.12 (a) in Lorentzian function. (b) EPR spectrum of the soxhlet mixture at $\nu \sim 9.4$ GHz, mod.=1.6 G, power=20mW. ca $g=2.0033$ and $\delta H=1.7$ G.

of light has experimental limitation in our laboratory. EPR spectrum of the fullerene soot (which was collected in presence of air but in absence of light) shows the signal was not observed at modulation 1.6 G and 20 mw of power, as shown in figure 6.14(a), However when the modulation was increased by 10 times and at gain 5×10^4 , the signal (figure 6.14(b)) was observed with $g \sim 2.003$ and having peak to peak line width $(\Delta H) = 4.4$ G. This broad signal compared to C_{60} appeared possibly due to the other types of carbons are also present in the soot. The sample was taken out from the microw-wave cavity and quartz tube hold for less than a minute in presence of laboratory light and record the EPR spectrum which is shown in figure 6.14(c). It shows the signal in the same modulation and same microwave power is increased from the previous signal. This quartz tube containing the sample was kept for overnight cover with a black paper and end of tube was kept opened for air circulation. In another quartz tube soot was collected in the similar fashion and as expected signal (figure 6.15) was not observed at modulation 1.66 G, power 20 mw and gain 8×10^3 . This experiment give the reproducible results. The sample tube was kept in the presence of a 500 W lamp and EPR spectrum of these samples shows (figure 6.15(c)) the signal is increased by 190% from the initial recording, however in case of black covered sample signal increase to 40%. Black paper was removed and this sample was kept in presence of tungsten lamp for another 24 hours and the EPR signal of it (figure 6.14(d)) has comparable intensity that of figure 6.15(c). These results suggested that the light acts as catalysis in getting the EPR signal. The initial broad line width to finally a narrow line width suggest that more than one kind of radical produced in the initial stage and finally with some unknown process produced a narrow signal.

The soot collected in the dark and covered it (in a sample tube) with a black cover and record the spectrum at different time interval. The EPR spectra of it is shown in figure 6.16. Figure 6.16(a), (b) and (c) represents the similar kind of observation as discussed earlier in figure 6.14 and figure 6.15. After 72 hours the EPR signal shows (figure 6.16(d)), smooth line is not passed through the center position. This indicates also that the formation of more than one kind of radicals take place. After keeping it for another 48 signal is increased by 10.5% from the previous signal. On the other hand

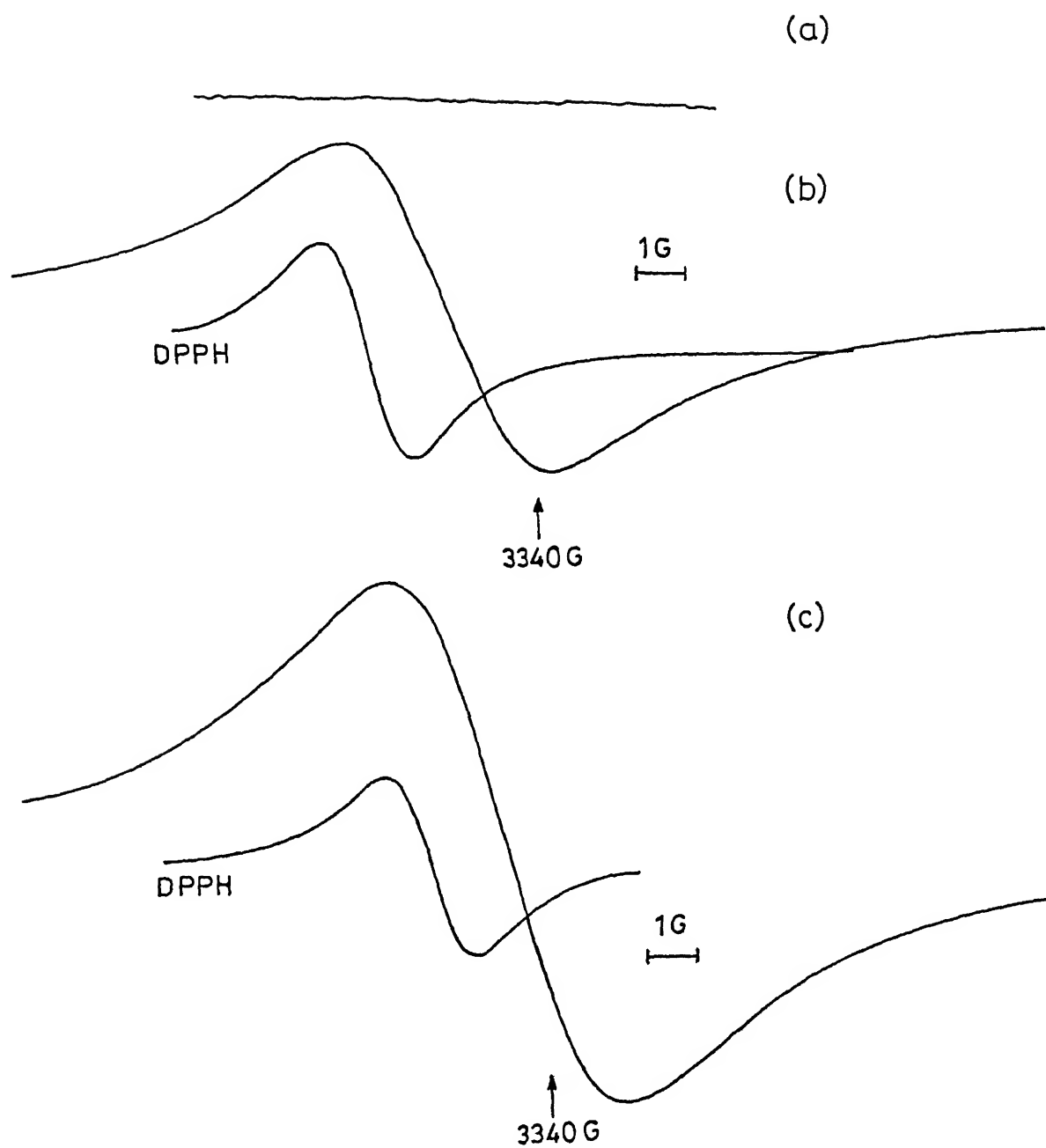


Figure 6.15: EPR spectra of the soot (a) collected same as previous figure (b) record in the same scale of the previous figure (c) kept 24 hours in presence of light.

after 24 hrs from the collection of the soot, signal is increased by 64% and after keeping it for another 48 hrs this signal (figure 6.16(e)) is increased by 132%. This time dependent studies on the fullerene soot shows after a critical time formation of the paramagnetic species in the fullerene carbon center reached its limit position. The highest intensity signal achieved, in the black cover sample (figure 6.16 (d)) after 96 hrs where as same intense signal is achieved within 24 hours on light irradiation on it. However the at liquid nitrogen temperature this highest intensity signal is vanished. which is shown in figure 6.16 (f). The line shape analyses of the signal of figure 6.16 (b) and figure 6.16 (d) are performed in both Lorentzian and Gaussian functions, which is shown in figure 6.17. It is clearly shown that EPR spectrum of the fullerene soot has also approximately Lorentzian line shape similar to C_{60} . Thus the paramagnetic species are formed in the C_{60} center, figure 6.12(a), due to the interaction of oxygen in presence of light. The g value=2.0028 indicated, paramagnetic species are fullerene carbon center.

Electrochemically [262], photochemically [150] in presence of donor molecules and chemically generated C_{60} radical anion [129] is quite extensively studied. The line width of C_{60}^- is 6 G at low temperature (120 K) and increase dramatically with increase in temperature (60-80 G) at 300 K, depending on the environment). The g value is near 1.995 and also exhibits both host and temperature dependent. Thus assignment of the narrow spectrum for C_{60}^- , produced photochemically, as shown in figure 6.12(a), is unlikely.

Kukolich and Huffman [263] reported the EPR spectrum of the C_{60} cation radical which has narrow resonance line of $g=2.0030$. They produced the C_{60} cation radical by partially dissolving the small quantities of C_{60} in concentrated sulfuric acid. The measured line widths in their spectrum is 2 G however this line widths varied with concentration of sulfuric acid and also in presence of fuming sulfuric acid. They get the minimum obtainable line widths 0.24 G in presence of fuming sulfuric acid. This result indicates that EPR line widths of C_{60}^+ is environmental dependent like C_{60}^- .

Dynamics of the triplet C_{60} is depended on the phase diagram of the solvent and above the melting point of toluene it forms a loose ion pair within an aggregate which

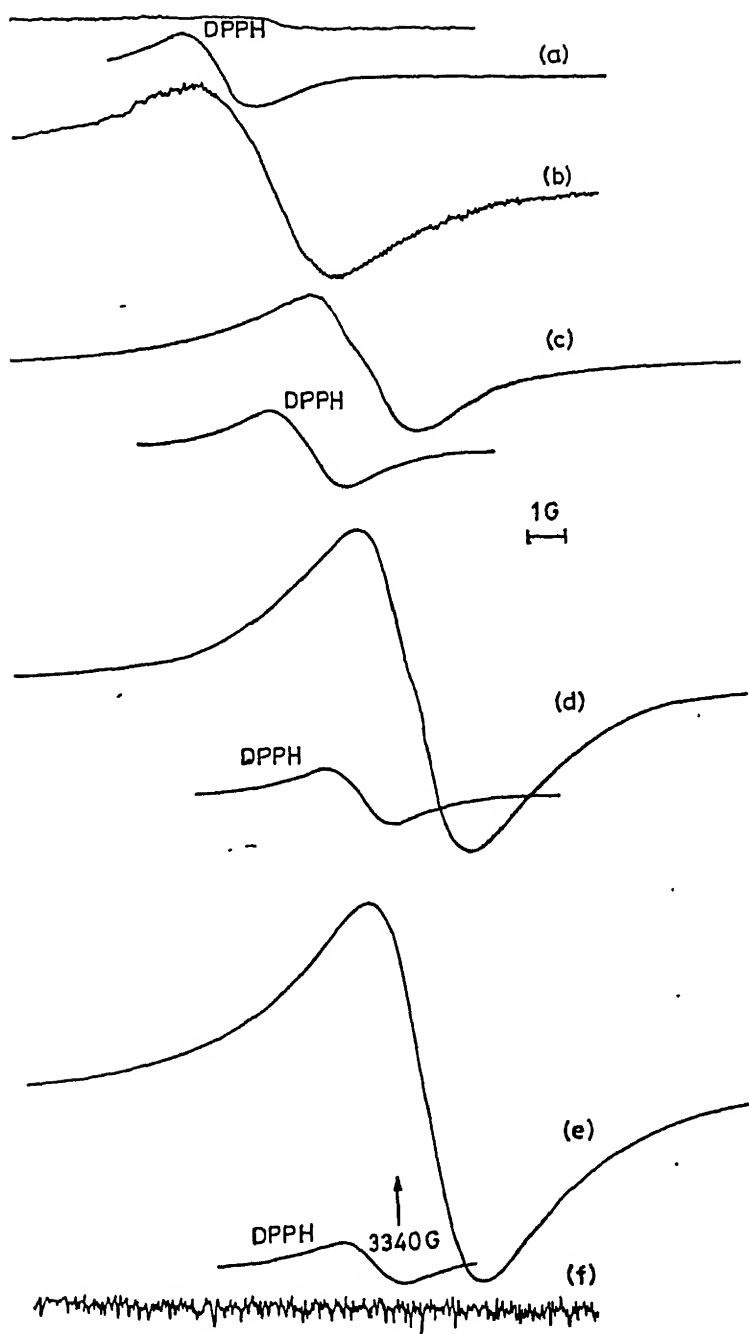


Figure 6.16: EPR spectra, soot collected in dark cover with a black paper. (a), (b) measured in the identical condition of figure 6.14 (a),(b) and figure 6.15 (a),(b). (c) Record after 24 hours. (d) Record after 72 hours from (a). (e) Record after 96 hours from (a). (f) Signal, (d), in liquid nitrogen temperature.

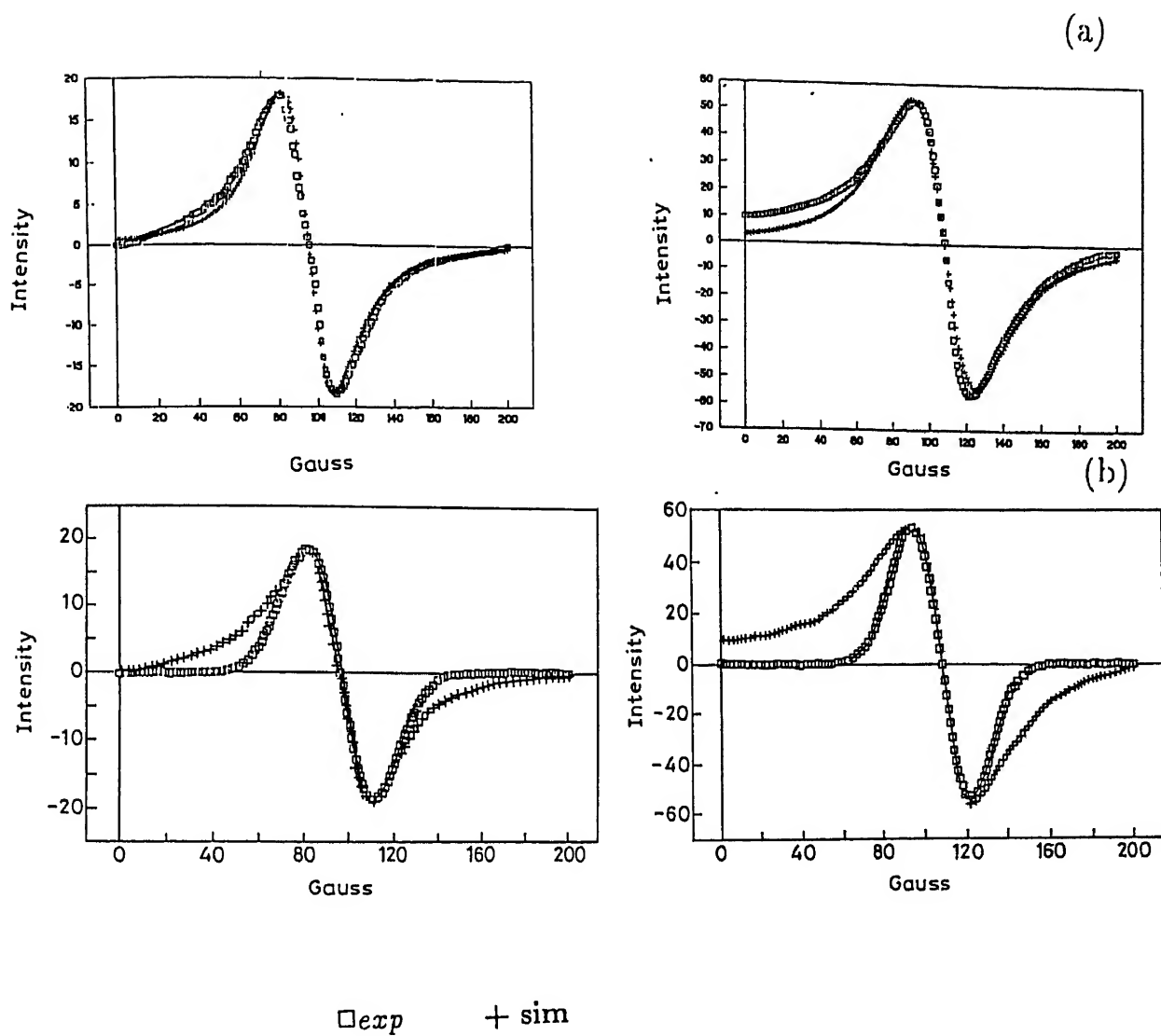


Figure 6.17: (a) Lorentzian line shape analysis of figure 6. 16 (b) and 6. 16 (d). (b) Gaussian line shape analysis of figure 6. 16 (b) and 6. 16 (d)

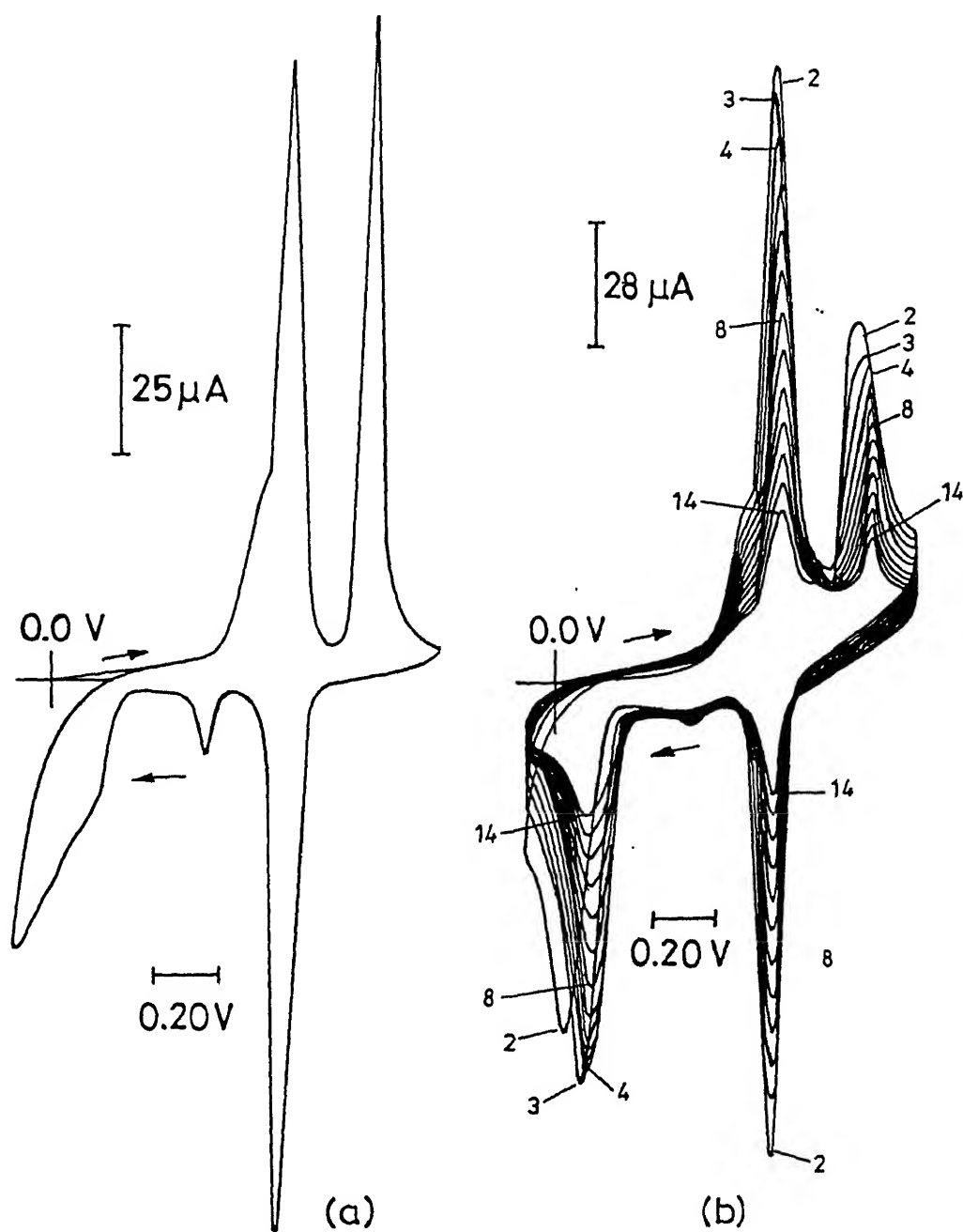


Figure 6.18: Cyclic voltammogram of the C_{60} film. (a) Film prepared at ambient conditions (b) Voltammogram recorded in the continuous cycling. Pt working electrode, scan rate 200 mV/s and TBAP, supporting electrolyte.

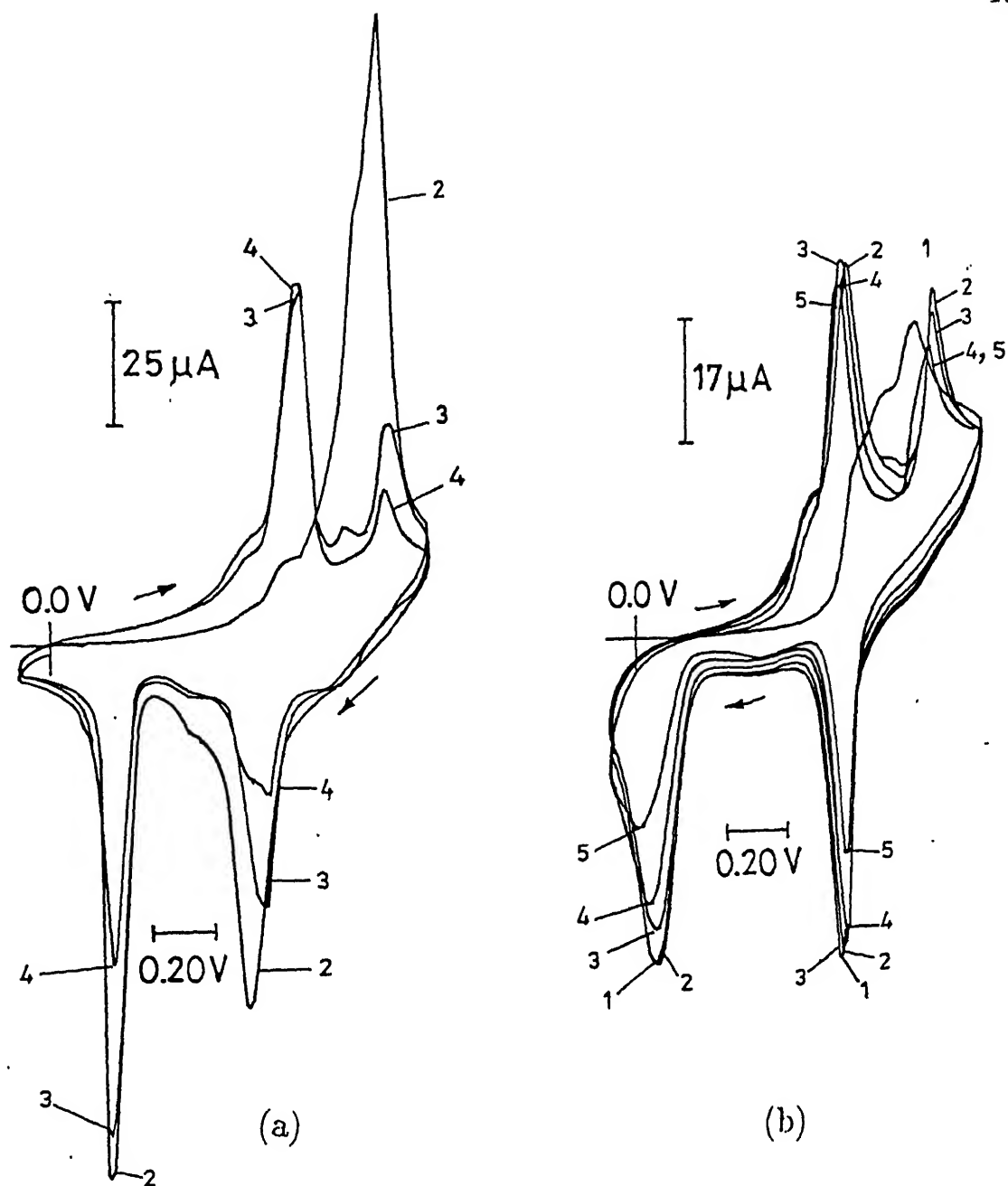


Figure 6.19: Cyclic voltammogram of the sunlight irradiated (a) Pt-electrode (1 mm dia.) (b) Pt-wire. Supporting electrolyte 0.1 M TBAClO₄ and scan rate 200 mV/s.

Table 6.6: Peak potential and peak separation for the first and second reduction wave in figure. 6.a.

	First reduction wave					Second reduction wave		
	E _{pa1} V	E _{pa2} V	E _{pc} V	ΔE _{p1} mV	ΔE _{p2} mV	E _{pa} V	E _{pc} V	ΔE _p mV
1st Scan	0.08	-0.46	-0.64	7.20	180	-0.75	-0.96	210

4th, 8th and 13th scan. The peak positions are given in the Table 6.3

In the 3rd scan onwards, peak current decreases gradually. After 14th cycle the peak current of the 1st reduction wave decrease, i_{pa} 60% and i_{pc} 70% from the peak current of observed in the 2nd cycle. Similarly peak current of the 2nd reduction wave is decreases by 77% and 68% from the second cycle. It is reported^{ref} that C_{60}^- and C_{60}^{2-} are formed during eletrochemical reduction and cation TBA^+ form a complex $C_{60}^-TBA^+$ which deposited in the electrode surface and acts as a blocking layer on the eletroactive surface.

In the 2nd scan onwards this C_{60} film behave similarly to the reported C_{60} film⁴² however its peak current decrease much faster rate. In the 14th cycles (total time taken to recorded the 14th cycle is 8 minutes) cathodic peak current of the 1st reduction wave decrease to 70% whereas Jehoult et. al [106] reported the same peak current has decreased only 27% after 25 minutes. This suggest that the C_{60} film prepared at ambient conditions has different electrochemical behaviour. XPS, IR and EPR studies on solid as discussed earlier suggested oxygen from a very weak bond in the C_{60} surface and EPR studies indicates species like $-C_{60}^+...O^{-1-}$ is formed at ambient conditions which is responsible this type of electrochemical behaviour, as shown in figure 6.18(a). The oxidation potential at +0.8 V indicates the presence of C_{60}^+ in this species.

The voltammogram of this oxygen adsorbed C_{60} film is different from the reported [106] intercalated compound of C_{60} because its intercalated compound with Li^+ , K^+ , Cs^+ , TEA^+ have a characteristic feature that it contains a large reduction peak and two small anodic peaks in the 1st reduction wave. Oxygen with small diameter can easily fit into void space of the C_{60} lattice. May be solvent plays a crucial role (from IR studies it is observed that solvent form a strong bond compared to oxygen) to prevent the oxygen

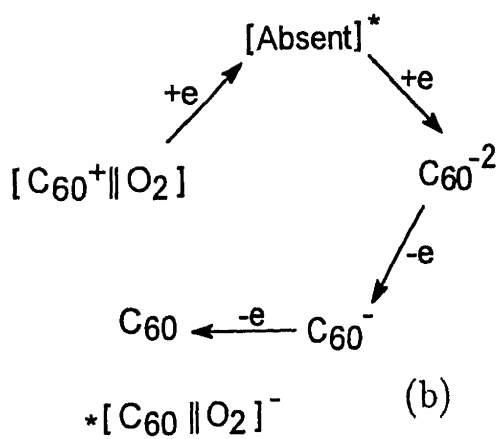
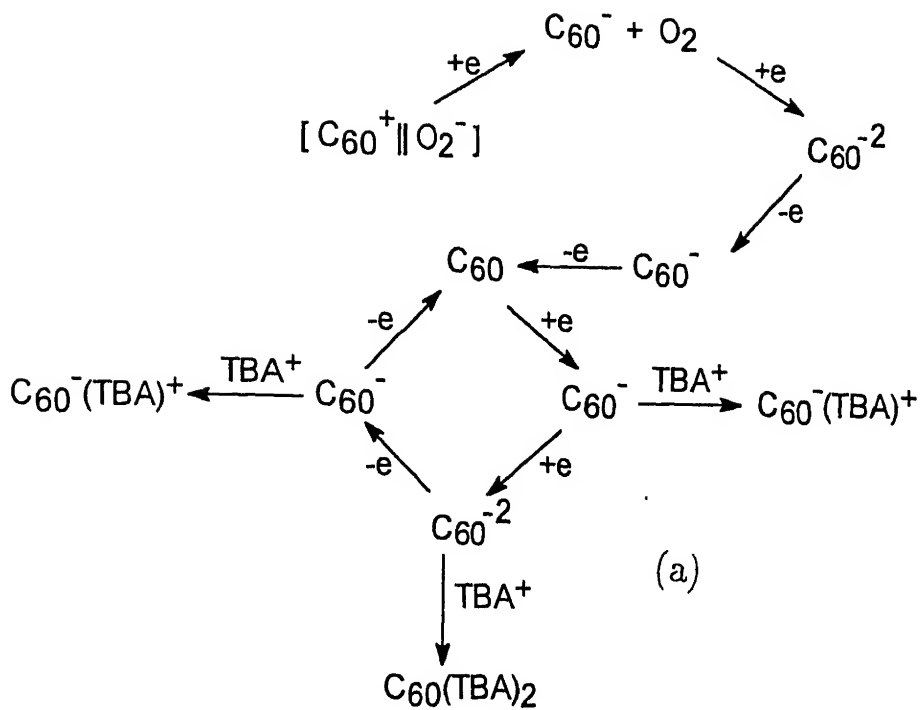


Figure 6.20: Mechanism of the C_{60} film in electrochemical process. (a) At ambient conditions and (b) on sunlight exposure.

Table 6.7: Peak potential and peak separation of figure 6.18 (b)

	First reduction Wave			Second reduction wave		
	Epa ₁ V	Epc V	ΔE mV	Epa V	Epc V	ΔE mV
2nd Scan	-0.02	-0.66	640	-0.73	-1.0	270
3rd Scan	-0.12	-0.65	530	-0.73	-1.04	320
4th Scan	-0.16	-0.70	540	-0.73	-1.05	320
8th Scan	-0.14	-0.74	600	-0.73	-1.06	330
14th Scan	-0.10	-0.74	640	-0.74	1.06	320

Table 6.8: Peak potential and peak shifts in figure 6.19(a)

Scan	First Reduction Wave			Second Reduction Wave		
	Epa V	Epc V	ΔE mV	Epa V	Epc V	ΔE mV
1	-0.26	-0.74	480	-0.62	-1.02	400
2	-0.26	-0.66	400	-0.72	-1.06	340
3	-0.22	-0.64	420	-0.74	-1.06	320

Table 6.9: Peak potential and peak shifts in figure 6.19 (b)

Scan	First Reduction Wave			Second Reduction Wave		
	Epa V	Epc V	ΔE mV	Epa V	Epc V	ΔE mV
1	-0.1	-0.66	560	-0.72	-1.04	320
2	-0.1	-0.66	560	-0.72	-1.02	300
3	-0.1	-0.69	580	-0.74	-1.03	290
4	-0.06	-0.74	680	-0.74	-1.02	280
5	-0.02	-0.94	920	-0.74	-0.98	240

occupancy in the the interstitial hole. Scanning tunneling microscopy studies, by Bard and coworkers [106] suggested that upon reduction, TBA^+ ion diffuse into the film to balance the negative charge of C_{60} and after reoxidation TBA^+ leaves the film and by structural rearrangement C_{60} regenerate to its initial structure. In the 2nd scan onwards our oxygenated C_{60} film behave similarly that of the reported C_{60} film but peak current decrease much faster rate, as discussed earlier, suggesting that oxygen adsorbed C_{60} films are more porous than the known C_{60} film. Peak shapes, peak potential and peak splitting of figure 6.18 (b) suggest that oxygen 'corrodes' the C_{60} surface, itself does not diffuse in the film layer much and does not form an intercalated compound like small cations. Based on the above electrochemical response a mechanism is proposed which is shown in figure 6.20(a) and (b). In the continuous cycling, the $\text{C}_{60}\text{-O}_2$ films (figure 6.19 (b)) are retained the C_{60}^- and C_{60}^{2-} reduced form which helps to knocked out the negatively charged oxygen in the reoxidation process by the known process [105].

Figure 6.19 is the electrochemical behaviour of the sunlight irradiated $\text{C}_{60}\text{-O}_2$ film. Figure 6.19 (a) is the electrochemical behaviour in 1mm diameter electrode and figure 6.19 (b) is the same behaviour observed in a Pt-wire. These electrochemical behaviour were measured in continuous cycle. In both the cases, cathodic peak of the 1st reduction wave in the 1st cycle significantly changes from the 2nd and 3rd cycle. Table 6.8 and table 6.9 shows the peak splitting of the 2nd reduction wave which continuously decrease for 2nd and 3rd peak.

The above observation indicates that structural rearrangement is maximum in the 1st reduction wave because C_{60} is leave out from the oxygen ion atmosphere. From Table 6.4& 6.5 it is noted that reduction and reoxidation of the 2nd reduction wave occurred at less negative potential. This indicates that formation of C_{60}^{2-} needs less energy. We think that this less energy arises due to C_{60} has some residual' positive charge. The EPR studies as discussed earlier (*vide section 6.2.6*) that triplet C_{60} transfer it energy to the surrounding oxygen from an oxygen adsorbed species. On irradiation with sunlight the voltammogram (figure 6.19 (a) and 6.16 (b) in the 1st cycle) suggested a negatively charge species, $[\text{C}_{60}\text{.....O}_2]^-$, is responsible for the absence of the 1st cathodic peak. The

small peak comes in the same position probably due to the oxygenated species is soluble in MeCN. This negative species dissociate in the 2nd reduction wave as C_{60}^{-2} is more stable than C_{60} due to the formation of $(4n+2)\pi$ electron system (*vide section 1.10*) Based on the above electrochemical studies the following reaction sequence is shown in figure 6.20.

6.3.7 Electronic Spectra

Solid C_{60} after its separation was kept in ambient conditions for 7 days and the electronic spectrum of this ageing C_{60} in MeCN, is shown in figure 6.21 (a), shows absorption band at $\lambda_{max} = 209, 318$ nm. Pure C_{60} is not soluble in MeCN (*vide table 1.3*) and the stability of this new species in this solvent indicates that the ageing C_{60} is more polar compared to the freshly prepared C_{60} . The electronic spectra of the same ageing C_{60} was recorded in di-ethyl ether and iso propanol which are given in figure 6.21(b) and (c). In case of isopropanol bands at 214, 260, and 357 nm appeared in the same absorption position of C_{60} in n-hexane and one absorption peak appeared at ~ 980 nm. Palit et. al.[94] observed a broad band at 800-1100 nm in ethanol during radiolysis, which they assigned for C_{60}^+ . In acetone this ageing C_{60} produce a very broad absorption at > 600 nm. The spectrum in di-ethyl ether is complex in nature. Solubility of the ageing C_{60} in alcohol, acetonitrile and di-ethyl ether strongly suggested that ageing C_{60} is polar which occurred due to the changed polarizability of C_{60} in presence of oxygen.

A concentrated benzene solution of $C_{60}(10^{-3} \text{ M})$ was kept at ambient condition for 25 days in a closed round bottom flask. The electronic spectrum of this solution, is shown in figure 6.22 (a), has absorption band at $\lambda_{max} = 980$ and 875 nm. The 980 nm band is very broad compared to 875 nm band. The reason for this very broad peak at 980 nm is not clear to us. However on flash chromatography of this solution these two peaks are not observed as shown in figure 6.22(c) The spectral feature changed at (400-750) nm in benzene in the figure 6.22(b) compared to figure 3.11, is transparency of this solution is decreased. C_{60} radical ions are prepared in low- temperature 77 K by γ -irradiation of the photoinduced C_{60} in different glassy matrices where C_{60}^+ and C_{60}^- are absorbed at 980

and 1076 nm respectively [264]. Gaysyna et. al [265] reported the electronic absorption spectra of the C_{60} radical anion and cation in solid argon and argon CCl_4 matrix. They assigned 973 nm band for C_{60}^+ and 1068 nm band for C_{60}^- , both of which are produced by photoionization. Chemically [129], electrochemically [266] and photoinduced electronic absorption spectra of C_{60}^- at room temperature in the common organic solvents are well studied and its value is consistent with the result published from these two groups. To our knowledge the electronic absorption spectra of the cationic radical of C_{60} is not known at room temperature in solvents like benzene, toluene etc. The absorption band of C_{60} cation is shifted ± 7 nm that produced in the above two different environments.

The aged C_{60} were kept in isopropanol and acetone for 24 hours and electronic absorption spectrum is shown in figure 6.21(d) and figure 6. 22 (d) The band at 980 nm in isopropanol and broad band in acetone suggested that the band arises at 980 nm band is invariant of the solvent properties. Thus we assigned 980 nm band of C_{60} in benzene due to the formation of C_{60}^+ . Since the first three highest occupied molecular orbitals of the parent C_{60} are of the symmetries of h_u , h_g and g_g , there should be many lowlying electronic transitions for the radical cation of C_{60} . This transitions are symmetry allowed or forbidden. It has been proposed, by Bendale et. al. [267], geometry of the neutral C_{60}^+ has an h_u electronic configuration and must distort from ideal icosahedral systems. Possibly 875 nm absorption is takes place from the symmetry allowed Jahn-Teller distortion.

We are unable to detect any EPR signal from C_{60} benzene solution at room temperature and the reason behind this is not clear to us. Table 1 presents the C_{60} spectrum in n-Hexane at different concentration. We observed that after the critical concentration $\sim 1.370 \times 10^{-5}$ M, a red shift of the band at 212 nm and 257 nm is observed. However we have not seen the red shift of 327 nm peak. In absence of charge transfer complex probably this shift, of the symmetry allowed transition of 212 nm and 257 nm bands, occurred by a contact type interaction with $[C_{60} \cdots O_2]^-$ species and n-hexane. This type of contact absorption of C_{60} with n-hexane is also observed by Leach et.al [87]. Thus in presence of solvent C_{60} it produced a species like $[C_{60} \cdots O_2]^- \cdots (\text{solvent})$ or $[\text{solvent} \cdots C_{60} \cdots O_2^-]$

Table 6.10: Wave-length of C_{60} in n-hexane at different conc.

Conc.(M)	Wave-length (nm)		
0.058×10^{-5}	213.5	257	328.5
0.1215×10^{-5}	212	257	328.5
0.196×10^{-5}	212	257	328.5
0.652×10^{-5}	212	257	328.5
0.8137×10^{-5}	212	257	328.5
0.947×10^{-5}	212.5	256.5	328.5
1.370×10^{-5}	213.5	256	328.5
1.482×10^{-5}	214	261	329
1.896×10^{-5}	215.5	261	328.5
1.903×10^{-5}	216.5	263	328.5
1.9980×10^{-5}	218	263.5	329
2.215×10^{-5}	222	264.5	329

when ageing or C_{60} is solvated.

6.3.8 Mass Spectra

The mass spectrum of the ether washed C_{60} (after x-diffraction, figure 6.11 (c), is kept for another 10 days) shows mass peak at $m/z=720$ has negligible intensity. The spectrum is shown in figure 6.23. This strongly suggested that solvent has substantial role in the C_{60} cage destruction. From the above results we discussed the probable mechanism for C_{60} cage destruction in the following section.

6.3.9 Discussion: The Probable Path of C_{60} degradation

In 1986 Stone and Wales (S-T) [183] suggested a process by which number of spheroidal isomer of C_{60} is possible and it needs a simple local transformation which connects the ground-state structure with other isomeric forms and according to them that the motion of only two atoms are required to go from one isomer to another which is shown in figure 6.24. These transformations are thermally forbidden in the Woodward-Hoffmann sense but photochemically allowed. The photofragmentation spectrum of C_{60} was reported by

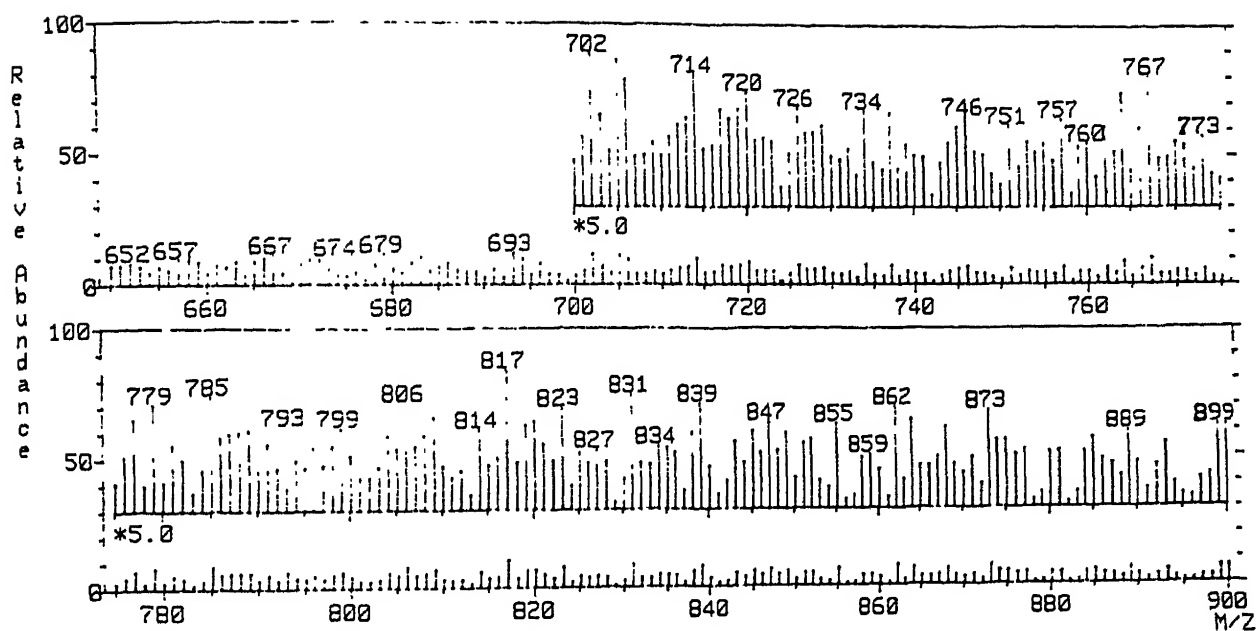


Figure 6.23: Part of the FAB mass spectrum of the ether washed C₆₀

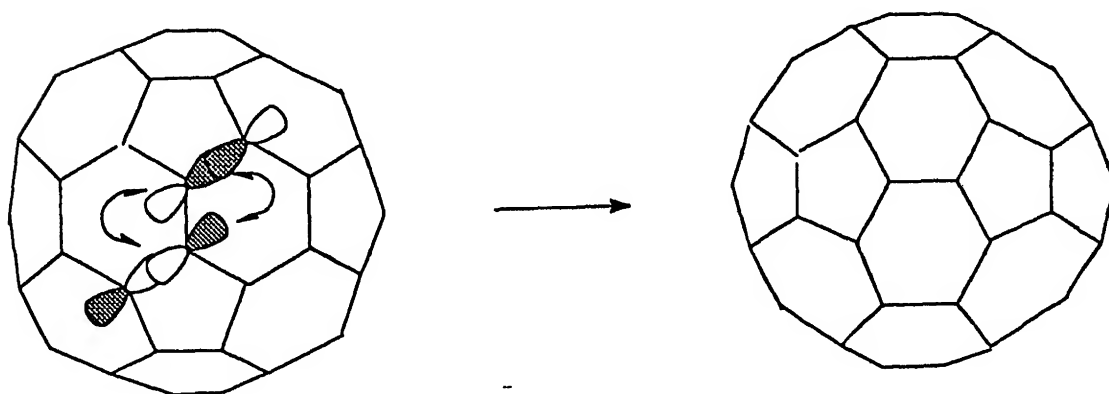


Figure 6.24: Isomeric structure from S-T transformation.

O'Brien et. al. [224] shortly after the original 'discovery' of the species and have proposed a mechanism by which defect C_{60} could 'unzip', sequentially removing 2, 4, or 6 atoms, but this defect form has never been experimentally observed. On the other hand, Stanton [268] has done an extensive study of the energetics of the mechanism proposed O'Brien et. al. [224], and illustrate that it is consistent with experiment.

Raghavachari et. al. [269] have computed the quantitative evaluation of the energies of low-energy alternative of spheroidal structures from semi-empirical (MNDO) and ab initio Hartree-Fock molecular orbital technique. These isomers one characteristic feature that presence of two or more pairs of adjacent pentagonal (figure 6.24(b)) rings unlike ideal icosahedron (figure 6.24(b)). Pentalene is generally regarded as antiaromatic and its derivatives are all reactive [270]. The energy contribution of these adjacent pentagonal defects making the icosahedron structure less stable by ~ 1 eV and the lowest energy alternative isomers of C_{60} has C_{2v} symmetry and lies ~ 2 eV higher in energy than the icosahedral ground state [269]. Thus only ~ 620 nm radiation can only alternate the stability. In contrast to the above proposition the XRD (figure 6.9) and IR (figure 6.4) are suggested that solid C_{60} is stable over 1 month at ambient conditions.

EPR (figure 6.12) indicates that the paramagnetic center of solid C_{60} is decreases with time. X-ray diffraction study (figure 6.8) suggested that the crystal structure is not distorted during this period however it is neutral compared to freshly prepared C_{60} . XPS spectrum (figure 6. 3(b)) and cyclic voltammogram of the C_{60} thin film suggested (as discussed earlier) that oxygen is negatively charged. Based on these observation we proposed a mechanism of oxygen interaction with C_{60} at ambient conditions which is shown in figure 6.25. It shows in the first stage, C_{60} produced triplet state in the presence of light (the quantum yield of the triplet state is nearly one [88]). This proposition based on the EPR spectrum of the fullerene soot, which shows very weak signal in presence of oxygen in the absence of light (vide figure 6.14, 6.15 and 6.16) however the intensity of this signal considerably increased in presence of light.

In the second step triplet C_{60} transfer its energy to the surrounding oxygen molecule

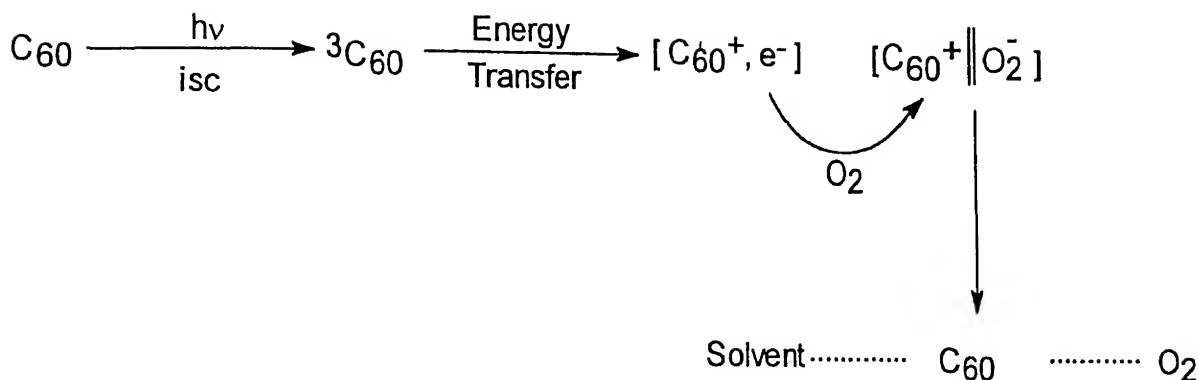


Figure 6.25: Oxygen and solvent interaction with C_{60}

and form an adsorbed species like $[\dots\text{C}_{60}^+\dots\text{O}_2^-\dots\text{C}_{60}^+\dots\text{O}_2^-\dots]$ as discussed earlier via the formation of an intermediate like $[\text{C}_{60}^+, e^-]$. Absence of strong charge transfer complex with the solvent suggested that C_{60}^+ may not form a strong bond with oxygen which is reflected from the binding energy of XPS (*vide section 6.2.1*). It is known [271] that macromolecule like γ cyclodextrine [271] and [8]calixerene [272] encapsulated the C_{60} molecule and protects its photochemical activity. Here negatively charged oxygen may be playing the same role as macromolecule, by forming a clathrate layer over C_{60} which is hinted earlier [177].

In presence of solvent the adsorbed oxygen pseudo-sphere which covered the C_{60} has been lost. The cyclic voltammogram shows (figure 6.18(b)) in the 2nd cycle the anodic peak of the 1st reduction wave is appeared in more positive potential than the reported thin film of C_{60} which is prepared in the inert atmosphere [105]. This indicates that C_{60} contains some residual positive charge. Therefore in the sea of solvent, ion atmosphere of oxygen has lost but the polarizability of C_{60} molecule has changed from the pure C_{60} . This change polarizability of C_{60} influence the solvent molecules to interact which is shown in figure 6.25.

Fcc lattice of C_{60} is transformed to hcp lattice in the presence of sunlight. Molecular dynamics calculation by Guo et. al. [273] suggested face centered cubic (fcc) packing is more stable than hexagonal close packing (hcp), by $0.90 \text{ kcal mol}^{-1}$. But reports

[274, 275, 276] also published regarding the coexistence of the fcc and hcp lattice for C_{60} molecule. C_{60} X-ray diffraction pattern of C_{60} in benzene, carbon di sulfide and diethyl ether clearly indicates according to the nature of solvent crystal structure changes and this would possible if a strong intermolecular force of attraction operates between solvent and C_{60} molecule. In the absence of clear evidence for strong charge-transfer complex formation and still now no adequate morphology of the C_{60} molecule is reported from X-ray diffraction therefore arrangement of the C_{60} molecule in the solid state itself may highlights some inside behind this transformation.

The interaction between the occupied solvent and C_{60} in the lattice is shown in figure 6.26. The existence of $2(C_{60}^{+}...O_2^{-})$ confirmed by EPR, XPS, CV and electronic spectra. Due to the electron deficiency of C_{60} molecule in **2**, cyclohexatriene unit (π electron is very much localized in the 6 MR of C_{60} so it is not behave like an benzene molecule) of it behave more like a cyclohexadiene unit. It is well known cyclohexadiene can go to cycloadditions reactions (via 1, 4 addition) with arenes, alkenes and alkynes in favourable conditions [270]. The single crystal X-ray structure of benzene solvated C_{60} shows rotational disorder of C_{60} is vanish [238]. This lattice is approximately a hexagonal close-packed arrangement separated by benzene molecules and the benzene rings lie parallel to the C_{60} molecular surface. The distance from the center of the benzene rings to the C_{60} surface is $\sim 3.30 \text{ \AA}$. According to this structure solution, one benzene molecule lie almost directly over the five membered ring of the C_{60} molecule.

This structure solution of benzene solvated C_{60} indicates that benzene are properly oriented for cycloaddition. Thus it can go cycloaddition reaction by two ways either with the cyclohexadiene **3** or cyclopentadiene **4** unit of the C_{60} molecule, as shown in figure 6.26. The cyclopentadiene **4** can form by an allylic rearrangements. and cyclopentadiene is very reactive towards cycloaddition both thermally and photochemically. Possibly this may be one of the reason that C_{60} molecule get ordered as free rotation of the C_{60} molecule is restricted due to a strong intermolecular force of attraction is operating between the benzene molecule and C_{60} .

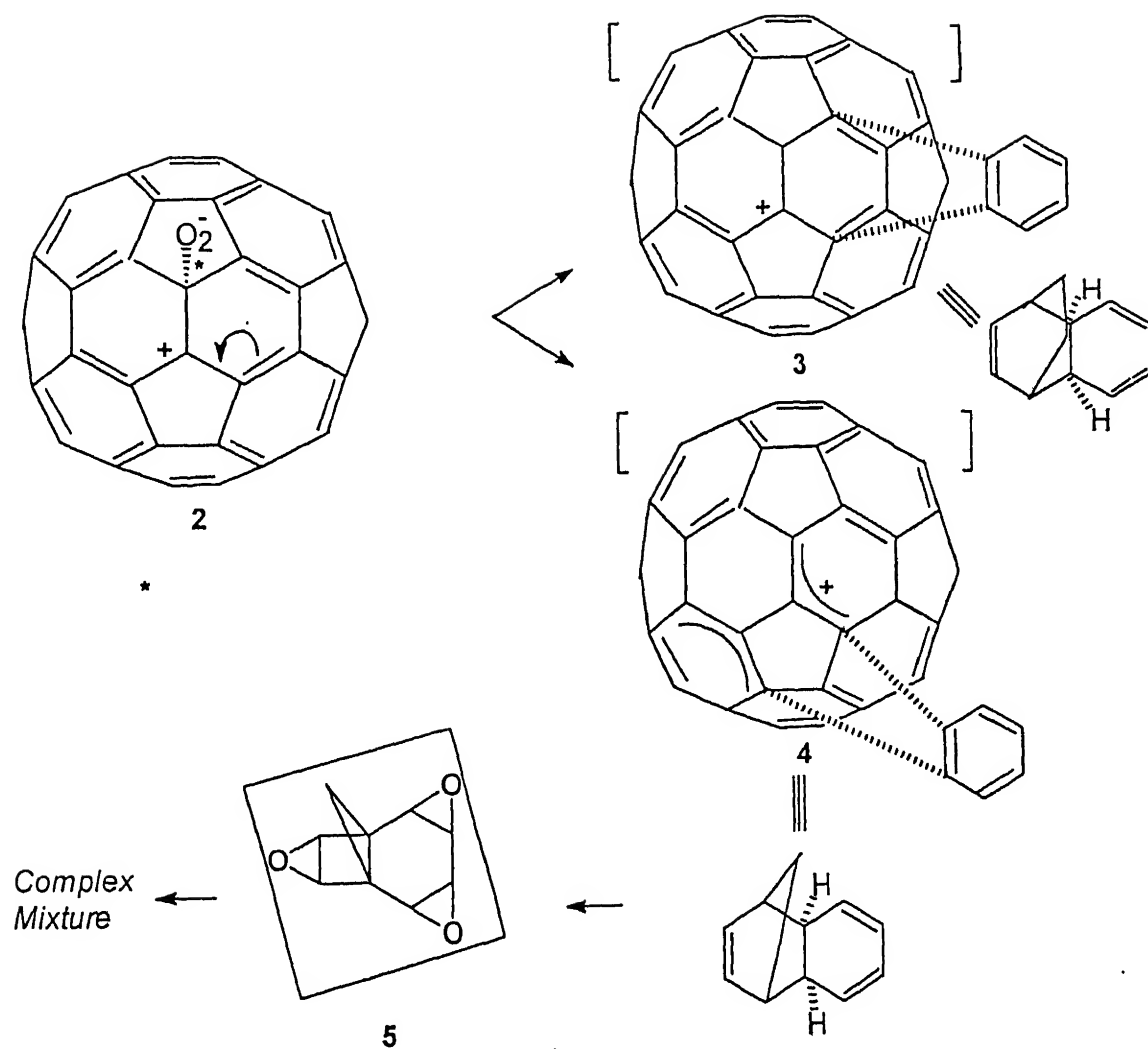


Figure 6.26: Mechanism of cycloaddition with benzene and C₆₀. 2 oxygenated C₆₀, 3 benzene interaction with cyclohexadiene unit of C₆₀, 4 benzene interaction with cyclopentadiene and 5 Oxygenated products (shown in the inset). Hydrogen positions are shown in the inset.

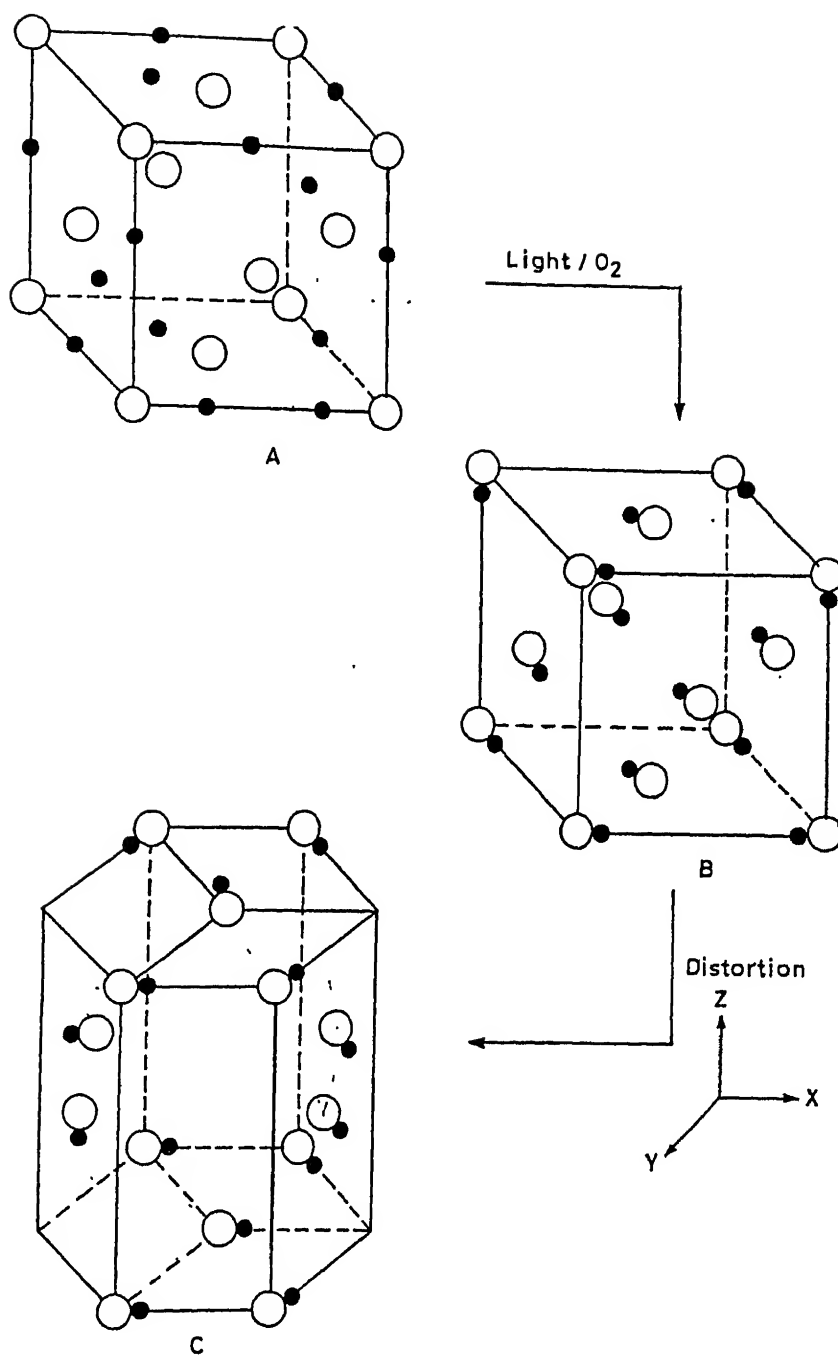


Figure 6.27: Transformation of fcc to hcp. A is fcc, B is fcc where solvent interacted with the C₆₀ atom and produce strain in the lattice. C is hexagonal system with solvated molecules.

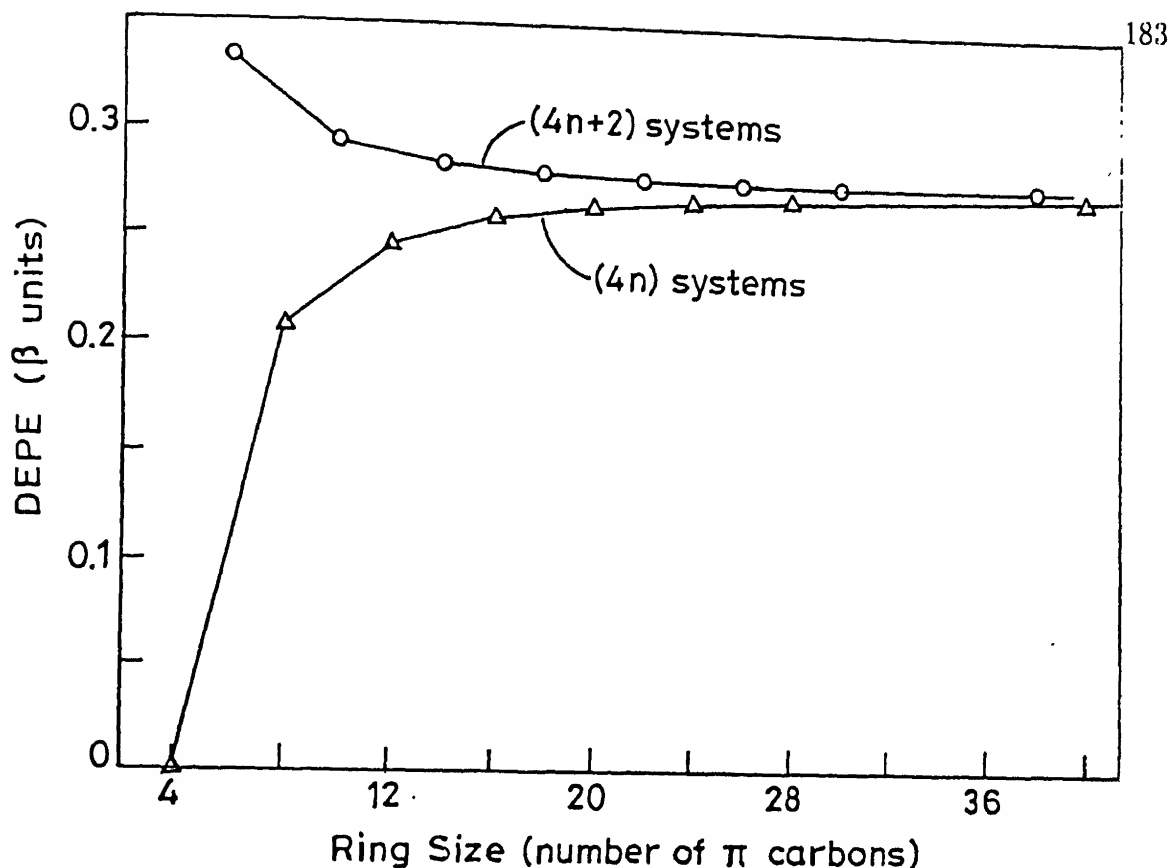


Figure 7.1: Delocalization energy vs ring size

strate that the planar conjugated molecules which shown in figure 1.10 are not a very good model for the comparison of C_{60} reactivity.

The works present in chapter 6 highlights that oxygen protect the fullerene molecule but the nature of oxygen interaction with C_{60} has still some doubt. Particularly what kind of radicals (how many variety?) are produced in the C_{60} center. However due to the oxygen interaction polarizability is developed in the neutral C_{60} molecule and influence the lattice occupied solvent (benzene) for cycloaddition reaction with C_{60} .

The poly aromatic hydrocarbons (PAH) are generated singlet oxygen^{ref} but mechanism of the generation of singlet oxygen is very poorly known and chemistry of the PAH is not well studied. Thus our assumption is C_{60} 's chemical behaviour will be resemble some of the higher annulenes (likely 20 annulene onwards). The energy levels of [26]- to [30]- annulenes is closely spaced (it happened in case of C_{60} also) and small ring distortion

could easily removed the degeneracy of the highest level in the $4n$ systems and thus lift one of the difference between the $4n\pi$ and $(4n+2)\pi$ series. Reported [278] delocalization energy per electron for the annulene type system is plotted as a function of the ring size which is shown in figure 7.1 suggested that the two curves converge rapidly as the ring size exceeds 20. Thus it will very helpful to understand the C_{60} chemistry by the comparative reactivity of greater than 20 annulenes with [60]annulene having without hydrogen. In near future this will help to understand the annulene as well fullerene chemistry.

Soot produced in the combustion of fuel at ambient conditions do not give appreciable quantity of fullerene, though Calcot, Honmann et. al., [279, 280, 281, 282, 283, 284] from the soot inception kinetics suggested that all carbon atom species (fullerene) is present in the flame. The chapter 6 indicates that fullerene is degraded very rapidly in presence of light, oxygen and solvent. In the flame a large number of reactive alkenes, alkynes, arenes, and PAH are formed which can attached to the fullerene moiety. This derivatives are easily oxidized by the reactive oxygen which are produced from the tar and PAH. Now it is times to think how fullerene yield will suppressed in presence of arenes, alkenes, PAH, oxygen and others.

Bibliography

- [1] Krätschmer, W.; Lamb, L.D.; Fostiropoulos, K.; Huffman, D.R.; *Nature*, **1990**, *347*, 354.
- [2] Braun, T. *Angew. Chem. Int. Ed. Engl.*, **1992**, *31*, 588.
- [3] Cullotta, E., Koshland, D. E., Jr., *Science*, **1991**, *254*, 1706.
- [4] Kroto, H.W.; Heath, J.R.; O' Brien, S.C.; Curl, R.F.; Smalley, R.E.; *Nature*, **1985**, *318*, 162.
- [5] Kroto, H. W., *Angew. Chem. Int. Ed. Engl.*, **1992**, *31*, 111.
- [6] Kroto, H. W., Allaf, A. W., Balm, S. P., *Chem. Rev.*, **1991**, *91*, 1213.
- [7] Curl, R. F.; Smalley, R. E. *Vigan, Sci. Am.*, **1991**, *32*.
- [8] Yang, S. H., Pettiette, C. L., Conceicao, J., Cheshnorsky, O., Smalley, R. E., *Chem. Phys. Lett.*, **1987**, *139*, 233.
- [9] Heath, J. R., Curl, R. F., Smalley, R. E., *J. Chem. Phys.*, **1987**, *87*, 4236.
- [10] Zhang, Q. L.; O'Brien, S. C.; Heath, J. R.; Liu, Y.; Curl, R. F.; Kroto, H. W.; Smalley, R. E. *J. Phys. Chem.*, **1986**, *90*, 525.
- [11] Heath, J. R.; O'Brien, S. C.; Zhang, Q.; Liu, Y.; Curl, R. F.; Kroto, H. W.; Tittel, F. K.; Smalley, R. E.; *J. Am. Chem. Soc.*, **1985**, *107*, 7779.
- [12] Newton, M.D.; Stanton, R. E. *J. Am. Chem. Soc.*, **1986**, *108*, 2469.

- [13] Stanton, R. E.; Newton, M. D. *J. Chem. Phys.*, **1989**, *90*, 4744.
- [14] Wu, Z. C.; Jelski, D. A.; George, T. F.; *Chem. Phys. Lett.*, **1987**, *137*, 291.
- [15] Weeks, D. E.; Harter, W. G.; *Chem. Phys. Lett.*, **1988**, *144*, 366.
- [16] Huffman, D. R.; *Physics Today*, Nov. 1991, 22.
- [17] Huffman, D. R.; *Adv. Phys.*, **1977**, *26*, 129.
- [18] Krätschmer, W.; Fostiropoulos, K.; Huffman, D. R. in *Dusty Objects in the Universe eds. Bussoletti, E. R.; Cittone, A. A.*
- [19] Krätschmer, W.; Fostiropoulos, K.; Huffman, D. R. *Chem. Phys. Lett.*, **1990**, *170*, 167.
- [20] Chai, Y.; Gno, T.; Jim, C.; Haufier, R. E.; Chibante, L. P. F.; Fure, J.; Wang, L.; Alford, M. J.; Smalley, R. E. *J. Phys. Chem.*, **1991**, *95*, 7564.
- [21] Chibante, L. P. F.; Thess, A.; Alford, J. M.; Diener, M. D.; Smalley, R. E. *J. Phys. Chem.*, **1993**, *97*, 8696.
- [22] Pitts, R. P.; Hale, M. J.; Bingham, C.; Lewandowski, King, D. E.; Fields, C. L. *J. Phy. Chem.*, **1993**, *97*, 8701.
- [23] Peters, G.; Jansen, M.; *Angew. Chem. Int. Ed. Engl.*, **1992**, *31*, 223.
- [24] Howard, J. B.; Mckinnon, J.; Makarovsky, Y.; Laffleun, L.; Johnson, E. L.; *Nature*, **1991**, *352*, 139.
- [25] Rao, C. N. R.; Pradeep, T.; Seshadri, R.; Nagarajan, R.; Murthy, V. N.; Subbanna, G. N.; Souza, F. D.; Krishnan, V.; Nagannagowada, G. A.; Suryaprakash, N. R.; Khetrpal, C. L.; Bhatt, S. V. *Ind. J. Chem.* **1992**, *31*, F5.
- [26] Taylor, R.; Langly, G. J.; Kroto, H. W.; Walton, D. R. M.; *Nature*, **1993**, *366*, 728.
- [27] Mukhopadhyay, K.; Krishna, K. M.; Sharan, M.; *Phys. Rev. Lett*, **1994**, *72*, 3182.

- [28] Daley, T.K.; Buseck, P.R.; Williams, P.; Lewis, C.F.; *Science*, **1993**, *259*, 1599.
- [29] Buseck P.R.; Tsipursky, S.J.; Hettich, R.; *Science*, **1992**, *257*, 215.
- [30] Becker, L.; Bada, J. L.; Winans, R. E. ; Hunt, J. E. ; Bunch, T. E. ; French, B. M. *Science*, **1994**, *265*, 645.
- [31] Heymann, D.; Chibante, L. P. F.; Brooks, R. P.; Wolbach, W. S.; Smalley, R. E.; *Science*, **1994**, *265*, 645.
- [32] Foing, B. H.; Ehrenfreund, P; *Nature*, **1994**, *369*, 296.
- [33] Kroto, H. W.; *Nature*, **1994**, *369*, 274.
- [34] Becker, L.; Bada, J. L.; Winans, R. E.; Bunch, T. E.; *Nature*, **1994**, *372*, 507.
- [35] Ajie, H.; Alvarex, M. M.; Anz, S. J.; Beck, R. D. ; Diederich, F. ; Fostiropoulos, K. ; Huffman, D. R. ; Krätschmer, W. ; Rubin. ; Schriver, K. E. ; Sensharma, D. ; Whetten, R. L. *J. Phys. Chem.*, **1990**, *94*, 8630.
- [36] Taylor, R. ; Hare, J. P. ; Abdul-Sada, A. ; Kroto, H. W. *J. Chem. Soc. Chem. Commun.*, **1990**, 1423.
- [37] Bhyrappa, P. ; Penicand, A. ; Kawamoto, M. ; Reed, C. A. *J. Chem. Soc. , Chem. Commun.*, **1992**, 936.
- [38] Chatterjee, K. H. ; Parker, D. H. ; Wurz. P. ; Lykke, K. R. ; Gruen, D. M. ; Stock. L. M. *J. Org. Chem.*, **1992**, *57*, 3253.
- [39] Khemani, K. C. ; Prato, M. ; Wudl, F. ; *J. Org. Chem.*, **1992**, *57*, 3254.
- [40] Constable, E. C. *Angnew. Chem. Int. Ed. Eng.*, **1994**, *33*, 2269.
- [41] Scrivens, W. A. ; Bedworth, P. V. ; Tour, J. M. ; *J. Am. Chem. Soc.*, **1992**, *114*, 7917.
- [42] Atwood, J. L. ; Koutsantonis, G. A. ; Raston, C. L. *Nature.*, **1994**, *368*, 229.

- [43] Suzuki, T. ; Nadashima, K. ; Shinkai, S. *Chem. lett.*, **1994**, 699.
- [44] Yoshida, Z. ; Takekkuma, H. ; Takekuma, S. ; Matsubarn. Y. *Angnew. Chem. Int. Ed. Eng.*, **1994**, *33*, 1597.
- [45] W.A. Scrivens; Cassel, A. M. ; North, B. L. ; Tour, J. M. ; *J. Am. Chem. Soc.*, **1994**, *116*, 6939.
- [46] Heath, J. R.; *Fullerenes*, Hammond, G. S.; Kuck, V. J.; Eds., ACS 481, Washington DC, 1992, chapter 1.
- [47] Hawkins, J. M. ; Meyer, A. ; Loren, S. ; Nunlist, R. *J. Am. Chem. Soc.*, **1991**, *113*, 9394.
- [48] Smalley, R. E. *Acc. Chem. Res.*, **1992**, *25*.
- [49] Gröscer, T. ; Hirsch, A. *Angnew. Chem. Int. Ed. Eng.*, **1993**, *32*, 1340.
- [50] Helden, G. V. ; Göttts, N. G. ; Bowers, M. T. *Nature*, **1993**, *363*, 60.
- [51] Bowers M. T.; Kemper. P. R.; Helden, G. V.; Von Koppen. P. A. M. *Science*, **1993**, *260*, 1446.
- [52] Helden, V. V. ; Göttts. N. G. ; Bowers, M. T. *J. Am. Chem. Soc.*, **1993**, *115*, 4363.
- [53] Schwarz, H.; *Angew. Chem. Int. Ed. Engl.*, **1993**, *32*, 1412.
- [54] Pallasser, R.; Pang, L. S. K.; Prochazka, L.; Rigby, D.; Wilson, M. A. *J. Am. Chem. Soc.*, **1993**, *115*, 11634.
- [55] Haddon, R. C. ; Brus, L. E. ; Raghavachari, K. *Chem. Phys. lett.*, **1986**, *125*, 459.
- [56] Haddon , R. C. ; Brus , L. e. ; Raghara. Chari. *Chem. Phys. lett. , 1986 , 131 , 165.*
- [57] Schmaltz, T. G.; Seitz, W. A.; Kleien, D. J.; Hite, G. E.; *J. Am. Chem. Soc. , 1988 , 110 , 113.*
- [58] Haddon. R. C. *Acc. Chem. Res. , 1992 , 25 , 127.*

- [59] Haymet A. D. J. *Chem. Phys. Lett.* , 1985 , 122 , 421.
- [60] Fowler , P. W. ; Woolrich , J. *Chem. Phys. Lett.* , 1986 , 127 , 78.
- [61] Newton, M. D.; Stanton, R. E.; *J. Am. Chem. Soc.*, 1986, 108, 2469.
- [62] Schulman, J. M.; Disch, R. L.; Miller, M. A.; Peck, R. C.; *Chem. Phys. Lett.*, 1987, 141 45.
- [63] Marynick, D. S.; Estreicher, S.; *Chem. Phys. Lett.*, 1986, 132, 383.
- [64] Disch, R. L.; Schulman, J. M.; *Chem. Phys. Lett.*, 1986, 125, 465.
- [65] Scuseria, G. E.; *Chem. Phys. Lett.*, 1991, 176, 423
- [66] Haser, M.; Almlöf, J; Scuseria, G. E.; *Chem. Phys. Lett.*, 1991, 181, 487.
- [67] Yannoni, C. S.; Bernier, P. P.; Bethune, D. S.; Meijer, G.; Salem, J. R. *J. Am. Chem. Soc.*, 1991, 113, 3190.
- [68] Liu, S. ; Lu, Y. J. ; Kappec, M. M. ; Ibers, J. A. *Science*, 1991, 254, 408.
- [69] Hedberg, K.; Hedberg, L.; Bethune, D. S.; Brown, C. A.; Dorn, H. C.; Johnson, R. D.; Vries, M. D.; *Science*, 1991, 254, 410.
- [70] David, W. I. F.; Ibbeerson, R. M.; Mathewman, J. C.; Passides, K.; Dennis, T. J. S.; Hare, J. P.; Kroto, H. W.; Taylor, R.; Walton, D. R. M.; *Nature*, 1991, 353, 147.
- [71] Pan. C.; Sampson, M. P.; Chai, Y.; Hauge, R. H.; Margrave , J. L. ; *J. Phys. Chem.* , 1991 , 95 , 2944.
- [72] Beckhans, H. D.; Ruchardt, C.; Kao, M.; Diedrich, F.; Foote, C. S.; *Angew. Chem Int. Ed. Engl.* , 1992 , 31 , 63.
- [73] Rudzinski, J. M.; Slanina, Z.; Togasi, M.; Osawa, E.; Lizuka, T.; *Thermochem. Acta.* , 1988 , 125 , 155.
- [74] Schulman , J. M. ; Disch. R. L. ; *J. Chem. Soc. Chem. Commun.*, 1991, , 411.

- [75] Beck, R. D.; John, P. S.; Alvarez, M. M.; Diedrich, F.; Whetten, R. L. *J. Phys. Chem.*, **1991**, *95*, 8402.
- [76] Duclos, S. J. ; Brister, K. ; Haddon, R. C. ; Kortan. A. R. ; Thiel, F. A. *Nature*, **1991**, *351*, 380.
- [77] Randic, M., *J. Am. Chem. Soc.*, **1977**, *99*, 444.
- [78] Schmalz, T. G.; Seitz, W. A.; Klein, D. J.; Hite, G. E. *Chem. Phys. Lett.*, **1986**, *130*, 203.
- [79] Kroto, H. W. ; *Nature*, **1987**, *329*, 529.
- [80] Taylor, R. C. *Tetrahedron lett.*, **1991**, *32*, 3731.
- [81] Taylor, R. C. *J. Chem. Soc. Perkin Trans.2.*, **1992**, *4*, 1992.
- [82] Negri, F. ; Orlandi, G. ; Zerbetto, F. *Chem. Phys. lett.*, **1988**, *144*, 31.
- [83] Bethune, D. S.; Meijer, G.; Tang, W. C.; Rosen, H. J.; Golden, W. G.; Seki, H. S.; Brown, C. A.; Vries, M. S. D.; *Chem. Phys. Lett.* **1991**, *179*, 181.
- [84] Sivaraman , N. ; Phemodaran , R. ; Kaliappan , I. ; Srinivasan , T. G. ; Vasudeva Rao , P. K. , Mathews , C. K. *J. Org. Chem.* , **1992** , *57* , 6077.
- [85] Ruoff. R. S. ; Tsc , D. S. , Malhotra. , Lorents , D. C. *J. Phys. Chem.* , **1993** , *97* , 3379.
- [86] Hare, J.P.; Kroto, H.W.; Taylor, R.; *Chem. Phys. lett.*, **1991**, *177*, 394.
- [87] Leach , S. ; Vervoet , M. ; Despres , A. ; Breheret . E. ; Hare , J. P. ; Sennis , T. G. ; Kroto , H. W. ; Taylor , R. ; Walton , D. R. M.; *Chem. Phys.* , **1992** , *160* , 451.
- [88] Arbogast , J. W. ; Darmanyany , A. P. ; Foote , C. S. ; Rubin , Y. ; Diedrich , F. N. ; Alvarez , M. M. ; Whetten , R. B. ; *J. Phys. Chem.* , **1991** , *95* , 11.
- [89] Arbogast , J. W. ; Foote , C. S. ; *J. Am. Chem. Soc.* , **1991** , *113* , 8886.

- [120] Huang , Y. ; Freiser , B. S. *J. Am. Chem. Soc.* , 1991 , 113 , 9418.
- [121] Huang , Y. ; Freiser , B. S. *J. Am. Chem. Soc.* , 1991 , 113 , 8186.
- [122] Strnu , J. J. ; Garrey , J. F. *J. Am. Chem. Soc.* , 1992 , 114 , 7914.
- [123] Sunderlin , L. S. ; Paulino , J. A. ; Chow , J. ; Kahr , B. ; Ben-Amotz , D. ; Squires , R. R. *J. Am. Chem. Soc.* , 1991 , 113 , 5489.
- [124] Hawkins , J. M. *Acc. Chem. Res.* , 1992 , 25 , 150.
- [125] Fagan , P. J. ; Calabrese , J. C. ; Malone , B. *Acc. Chem. Res.* , 1992 , 25 , 134.
- [126] Balach , A. L. ; Catalano , V. J. ; Lee , J. W. *Inorg. Chem.* , 1991 , 30 , 3980.
- [127] Haddon , R. C. ; Hebard , A. F. ; Rosseinsky , M. J. ; Murphy , D. W. ; Duclos , S. J. ; Lyons , K. B. ; Miller , B. ; Rosamilia , J. M. ; Fleming , R. M. ; Kortan , A. R. ; Glarum , S. H. ; Makhija , A. V. ; Elick , R. H. ; Zahurak , S. M. ; Tycko , R. ; Dablagh , G. ; Thiel , F. A. *Nature* , 1991 , 351 , 320.
- [128] Allemand , P. M. ; Khemani , K. C. ; Koch , A. ; Wudl , F. ; Holczer , K. ; Donoran , S. ; Gr"uner , G. ; Thompson , J. D. *Science* , 1991 , 253 , 301.
- [129] Bhyrappa , P. ; Paul. P. ; Stinchcombe , J. ; Boyd , P. D. W. ; Reed , C. A. *J. Am. Chem. Soc.* , 1993 , 115 , 11004.
- [130] Stinchcombe , J. ; Penicaud , A. ; Bhyrappa , P. ; Boyd , P. W. D. ; Reed , C. A. *J. Am. Chem. Soc.* , 1993 , 115 , 5212.
- [131] Paul. P. ; Zie, Z. ; Bau, P. D. W. ; C. A. Reed. *J. Am. Chem. Soc.* , 1994 , 116 , 4145.
- [132] Haufler, R. E. ; Conceicao, J. ; Chibante, L.P.F. ; Chai, Y. ; Byrne, N.E. ; Flanagan, S. ; Haley, M.M. ; O' Brien, S.C. ; Pan, C. ; Xiao, Z. ; Billups, W.E. ; Ciufolini, M.A. ; Hauge, R.H. ; Margrave, J.L. ; Wilson, L.J. ; Curl, R.F. ; Smalley, R.E. ; *J.Phys.Chem.*, 1990, 94, 8634.
- [133] Henderson , C. C. ; Cahill , P. A. *Science* , 1993 , 260 , 1885.

- [134] Hirsch , A. ; Soi , A , Karfunkel , H. R. ; Haufler. et. al. *Angew. Chem. Int. Edn. Engl.* , **1992** , *31* , 766.
- [135] Fagan , P. J. ; Krusic , P. J. ; Evans , D. H. ; Lerke. S. A. ; Johnston , E. J. *J. Am. Chem. Soc.* , **1992** , *114* , 9697.
- [136] Dixon, D. A. ; Matsuzwa, N.; Fukunaga, T.; Tebbe, F. N. *J. Phys. Chem.* , **1992** , *96* , 6107.
- [137] Olah , G. A. ; Bucsi , I. ; Lambert , C. ; Aniszfeld , R. ; Trivedi , N. J. ; Sensharma , D. K. ; Surya-Prakash , G. K. *J. Am. Chem. Soc.* , **1991** , *113* , 9385.
- [138] Selig, H. ; Lifshitz, C. ; Perce, T. ; Fischer, J. E. ; Meghie, A. R. ; Romanow, W. J. ; Mecauley, J. P. ; Jr; Smith, A. B. III; *J. Am. Chem. Soc.*, **1991**, *113*, 5475.
- [139] Hollway, J. H. ; Hope, E. G. ; Taylor, R. ; Langley. G. J. ; Avent, A. G. ; Dennis, T. J. ; Hare, J. P. ; Kroto, H. W. ; Walton, D. R. M. *J. Chem. Soc., Chem. Commun.*, **1991**, *966* .
- [140] Birkett, P. R. ; Hitchcock, P. B. ; Kroto, H. W. ; Taylor, R. ; Walton, D. R. M. *Nature*, **1992**, *357*, 479.
- [141] Tebbe , F. N. ; Harlow, R. L. ; Chase , D. B. ; Thorn , D. L. ; Campbell , G. C. Jr, ; Calabrese , J. C. ; Herron , N. ; Young , R. ; J. Jr. ; Wasserman , E. *Science* , **1992** , *256* , 822.
- [142] Matsuzawa, N. ; Fukunaga, T. ; Dixon, D. A. *J. Phys. Chem.*, **1992**, *96*, 10747.
- [143] T. Suzuki, Li. Q.; Khemani, K. C.; Wudl. F. ; Almarsson, Ö. *Science*, **1991**, *254*, 1186.
- [144] Hirsch, A. *Anfew. Chem. Int. Ed. Engl.*, **1993**, *32*, 1138.
- [145] Rao, A. M. ; Zhou, P. ; Wang, K. A. ; Hager. G. T. ; Holden, J. M. ; Wang, Y. ; Lee, W. T. ; Bi, X. X. ; Eklund. D. C. ; Cornett, D. S. ; Duncan, M. A. ; Amster, I. J. *Science*, **1993**, *259*, 955.

- [106] Jehoulet, C.; Obeng, Y. S.; Kim, Y. T.; Zhou, F.; Bard, A. J. *J. Am. Chem. Soc.*, **1992**, *114*, 4237.
- [107] Elser, V.; Hadden, R. C. *Nature*, **1987**, *325*, 792.
- [108] Mallion, R. B. *Nature*, **1987**, *325*, 760.
- [109] Haddon, R. C.; Schneemeyer, L. F.; Waszczak, J. V.; Glaurum, S. H.; Tycko, R.; Dabbagh, G.; Kortan, A. R.; Muller, A. J.; Muijsce, A. M.; Rosseninsky, M. J.; Zahurak, S. M.; Makhija, A. V.; Thiel, F. A.; Raghsvachari, K.; Cockayne, E.; Elser, V. *Nature*, **1991**, *350*, 46.
- [110] Ruoff, R. S.; Beach, D.; Cuomo, J.; Meguire, T.; Whetten, R. L.; Diederich, F. *J. Phys. Chem.*, **1991**, *95*, 3457.
- [111] Johnson, R. D.; Bethune, D. S.; Yannoni, C. S. *Acc. Chem. Res.*, **1992**, *25*, 169.
- [112] Johnson, R. D.; Meijer, G.; Bethune, D. S. *J. Am. Chem. Soc.*, **1990**, *112*, 8983.
- [113] Pasquarello, A.; Schluter, M.; Haddon, R. C. *Science*, **1992**, *257*, 1660.
- [114] Haddon, R. C. *Science*, **1993**, *242*, 1017.
- [115] Taylor, R.; Walton, D. R. M. *Nature*, **1993**, *363*, 685.
- [116] Fagan, P. J.; Calabrese, J. C.; Malone, B. *Fullerenes*, Hammond, G. S.; Kuck, V. J. Eds., ACS series 481, **1992**, chapter 12.
- [117] Diederich, F.; Issacs, L.; Philip, D.; *Chem. Soc. Rev.*, **1994**, 243
- [118] Wood, J. M.; Kahr, B.; Hoke(ii), S. H.; Dejaram, L.; Cooks, R. G.; Ben-Amotz, D. *J. Am. Chem. Soc.*, **1991**, *113*, 5907.
- [119] Roth, L. M.; Huang, Y.; Schwedler, J. T.; Cassady, C. J.; Ben-Amotz, D.; Kahr, B.; Freiser, B. S. *J. Am. Chem. Soc.*, **1991**, *113*, 6298.

- [158] Prato, M.; Bianco, A.; Maggini, M.; Scorrano, G.; Tonido, C.; Wudl, F.J. *Org. Chem.*, **1993**, *58*, 5578.
- [159] Parker, D.H.; Wurtz, P.; Chatterjee, K.; Lykke, K.R.; Hunt, J.E.; Pellin, M.J.; Hemminger, J.C.; Gruen, D.M.; Stock, L.M.; *J. Am. Chem. Soc.*, **1991**, *113*, 7499.
- [160] Baum, R. *Chem. Eng. News.*, **1993**, *71* (35), 21.
- [161] Koch, A.S.; Khemani, K.C.; Wudl, F.; *J. Org. Chem.*, **1991**, *56*, 4563.
- [162] Pradeep, T.; Rao, C.N.R.; *Mat. Res. Bull.*, **1991**, *26*, 1101.
- [163] Surya Prakash, G. K.; Bucsi, I.; Aniszef, R.; Olah, G. A. *Buckminsterfullerene*, Billups, W. E.; Ciufolini, M. A.; Eds., VCH, Newyork, 1993, chapter 12.
- [164] Scrivens, W. A.; Tour, J. M. *J. Org. Chem.*, **1992**, *57*, 6932.
- [165] Iacoe, D. W.; Potter, W. T.; Teeters, D.; *J. Chem. Edu.*, **69**, 663.
- [166] Craig, N. C.; Gee, G. C.; Johnson, A. R. *J. Chem. Edu.*, **69**, 664.
- [167] Cox, D. M.; Behal, S.; Disko, M.; Gorun, S. M.; Greaney, M.; Hsu, C. S.; Kollin, E. B.; Millar, J.; Robbins, J.; Sherwood, R. R. D.; Tindall, P.; *J. Am. Chem. Soc.*, **113**, 2940.
- [168] Levine, I. N. *Quantum Chemistry*, 4th ed., Prentice-Hall of India Private Limited, New-Delhi, **1994**, chapter 15-16.
- [169] Scuseria, G. E. *Buckminsterfullerene*, Billups, W. E.; Ciufolini, M. A.; Eds., VCH, Newyork, 1993, chapter 5.
- [170] Curl, R. F.; Smalley, R. E. *Science*, **1988**, *242*, 1017.
- [171] March, J. *Advanced Organic Chemistry: Reaction, Mechanisms, and structure*, 3rd eds., Wiley Eastern Limited, New-Delhi.
- [172] Zhang, S.; Brown, T. L.; Du, Y.; Shapley, J. R. *J. Am. Chem. Soc.* **1993**, *115*, 6705.

- [173] Douthwaite, R. E.; Green, M. L. H.; Stephens, A. H. H.; Turner, J. F. C.; *J. Chem. Soc. Chem. Commun* **1993** 1522.
- [174] Rogers, J. R.; Marynick, D. S. *Chem. Phys. Lett.*, **1993**, *205*, 197
- [175] Taylor, R.; Parsons, J. P.; Avent, A. G.; Rannard, S. P.; Dennis, T. J.; Hare, J. P.; Kroto, H. W.; Walton, D. R. M. *Nature*, **1991**, *351*, 277.
- [176] Kroto, H. W.; Prassides, K.; Stace, A. J.; Taylor, R.; Walton, D. R. M. *Buckminsterfullerene*, Billups, W. E.; Ciufolini, M. A.; Eds., VCH, Newyork, 1993, chapter 2.
- [177] Werner, H. ; Herein, D. ; Blöcker, J. ; Henschka, B. ; Bradshaw, A. M. ; Schlögl, R. *Chem. Phys. Lett.*, **1992**, *194*, 62.
- [178] Werner, H. ; Bublak, D. ; Göbel, U. ; Henschke, B. ; Bensch, W. ; Schlögl, R. *Angew Chem. Intern. Ed. Engl.*, **1992**, *104*, 868.
- [179] Silverstein, R. M. ; Bassler, G. C. ; Morrill, T. C. *"Spectroscopic Identification of Organic Compounds."* 4th edition, John Wiley & Sons; New York., 1981.
- [180] Chen, H. S.; Kortan, A. R.; Haddon, R. C.; Kaplan, M. L.; Chen, C. H.; Mujsce, A. M.; Chou, H.; Fleming, D. A. *Appl. Phys. Lett.*, **1991**, *59*, 2956.
- [181] Chen, H. S.; Kortan, A. R.; Haddon, R. C.; Flemming, D. A. *J. Phys. Chem.*, **1992**, *96*, 1016.
- [182] Malhotra, R.; Lorents, D. C.; Bae, Y. K.; Becker, C. H.; Tse, D. S.; Jusinski, L. E.; Wachsman, E. D.; *Fullerenes*, Hammond, G. S.; Kuck, V. J.; Eds., ACS series 481, Washinton DC, **1992**, chapter 9.
- [183] Stone, A. J. ; Wales, D. J. *Chem. Phys. Letter.*, **1986**, *128*, 501.
- [184] Taliani, C.; Ruani, G.; Zambóni, R.; Danieli, R.; Rossini, S.; Denisov, V. N.; Buralakov, V. M.; Negri, F.; Orlandi.; Zerbetto, F. *J. Chem. Soc. Chem. Commun.*, **1993**, 220.

- [185] Juha, L.; Hamplora, V.; Kodymora, J; Spalek, O *J. Chem. Soc. Chem. Commun.*, **1994**, 2437
- [186] Pace, M. D.; Christidis, T. C.; Yin, J. J.; Milliken, J. *J. Phys. Chem.*, **1992**, *96*, 6855.
- [187] Heiney, P. A.; Fischer, J. E.; McGhie, A. R.; Romanow, W. J.; Denenstein, A. M. ; McCauley, J. P. ; Jr. ; Smith, A. B. ; III ; Cox, D. E. *Phys. Rev. lett.*, **1991**, *66*, 2911.
- [188] Yannoni, C. S.; Johnson, G.; Meijer, G.; Bethuene, D. S.; Salem. J. R. *J. Phys. Chem.*, **1991**, *95*, 9.
- [189] Hamed, A., Sun, Y. Y.; Tao, Y. K.; Meng, R. L.; Hor, P. H. *Phys. Rev. B*, **1993**, *47*, 10873.
- [190] Roth, A. *Vacuum Sealing Techniques*, Pergamon Press, Oxford, **1966**.
- [191] Diederich, F.; Whetten, R. L. *Acc. Chem. Res.*, **1992**, *25*, 119.
- [192] Hoyanx, M. F. *Arc Physics*, Springer-Verlag, newyork, **1968**.
- [193] Shelva, E. H. *Vogel's Text Book of Macro and Semimicro Inorganic Analysis*, Orient Longman, New Delhi, **1979**, p.312.
- [194] Cotton, F. A. and Wilkinson, G. *Advanced Inorganic Chemistry*, *5th ed.* John Wiley & sons, New York; **1988**.
- [195] Khan, A. U.; Kasha, M.; *J. Chem. Phys.*, **1963**, *39*, 2105.
- [196] Silverstein, R. M.; Bassler, G. C.; Morrill T. C. *Spectroscopic Identification of Organic Compounds*, *4 th edition*, John Willey & Sons, New york, **1981**.
- [197] Nakamoto, K.; *Infrared and Raman Spectra of Inorganic and Co-ordination compounds 4th ed.*, , John wiley & Sons, **1986**, New york.
- [198] Rohlfing, E. A. ; Cox, D. M. ; Kaldor, A. *J. Chem. Phys.*, **1984**, *81*, 3322.

- [199] Lichtenberger, D. L., Nebesny, K. W., Ray, C. D., Huffman, D. R., Lamb, L. D. *Chem. Phys. Lett*, 1991, 176, 203.
- [200] Ghosh, P. K. *A Whiff of Photoelectron Spectroscopy*, John-Wiely, New Delhi, 1978.
- [201] Hollander, J. M.; Jolly, W. L. *Acc. Chem. Res.*, 1970, 3, 193.
- [202] Pradeep, T.; Vijayakrishnan, V; Santra, A. K.; Rao, C. N. R. *J. Phys. Chem.* 1991, 95, 10564.
- [203] Cox. D. M.; Cameron, S. D.; Tuinman, A.; Gakh, A.; Adcock, J. L. ; Compton, R. N. ; Hagaman, E. W. ; Kniaz. K. ; Fischer, J. E. ; Strongin, R. M. ; Cichy, M. A. ; Smith, A. B. III. *J. Am. Chem. Soc.*, 1994, 116, 1115.
- [204] Moulder, J. F.; Stickle, W. F.; Sobol, P. E.; Bomben, K. D. ; *Hand Book of X-ray Photoelectron Spectroscopy*, Perkin Elmer Corp. Norwakk. CT., 1992.
- [205] Shivers D. F.; Atkins P. W.; Longford, C. H.; *Inorganic Chemistry*, 2nd Ed., ELBS, Oxford University Press, 1994.
- [206] Cary, F. A.; Sundberg, R. J. *Advanced Organic Chemistry, 3rd ed., Part A, Structure and Mechanisms*, Plenum Press, Newyork, 1993, chapter 12.
- [207] Huheey, J. E., *Inorganic Chemistry, Principles of structure and Reactivity, SI Ed. 3rd ed.*; Cambridge, 1983.
- [208] Geoffroy, G. L., Wrighton, M. S. *Organometallic Photochemistry*, Academic Press, 1979, New York.
- [209] Davis, R.; Kane-Maguire, L. A. P. *Comprehensive Organometallic Chemistry, The Synthesis, Reactions and structures of Organometallic Compounds. Vol. 3*, editors, Wilkinson, G.; Stone, F. G. A.; Abel, E. W. Pergamon Press, 1982, Oxford.
- [210] Mingos, D. M. P *Comprehensive Organometallic Chemistry, The Synthesis, Reactions and structures of Organometallic Compounds. Vol. 3*, editors, Wilkinson, G.; Stone, F. G. A.; Abel, E. W. Pergamon Press, 1982, Oxford.

- [211] Basolo, F *Inorg. Chim. Acta.*, **1981**, *50*, 65.
- [212] Duffie, J. A.; Beckman, W. A. *Solar Energy Thermal Process*, **1974**, Willey-Interscience, New York.
- [213] Miller, J. M.; Chen, L. Z. *Rapid Commun. Mass Spectrum*, **1993**, *6*, 184.
- [214] Ball, C. P.; Derrick, P. J. *Annual Reports*, v. 90, 1993, sec. B, Organic Chemistry, The Royal Society of Chemistry, Camdridge, Page-21.
- [215] Fastow, M., Kozirovski, Y., Folman, M., Heidberg, J., *J. Phys. Chem.* **1992**, *96* 6126.
- [216] Koeford, R. S.; Xu, C.; Lu, W.; Shapley, J. R.; Hill, M. G.; Mann, K. R. *J. Phys. Chem.*, **1992**, *96*, 2928.
- [217] Koh, W. ; Dubois, D. ; Kutner, W. ; Jones, M. T. ; Kadish, K. M. *J. Phys. Chem.*, **1992**, *96*, 4163.
- [218] Lerke, S. A., Parkinson, B. A., Evans, D. H., Fagan, P. J. *J. Am. Chem. Soc.* **1992** *114* 7807.
- [219] Almond, M. J., Crayston, J. A., Downs, A. J., Poliakoff, M., Turner, J. J. *Inorg. Chem.* **1986**, *25*, 19
- [220] Almond, M. J. *Chem. Soc. Rev.*, **1994**, 203.
- [221] Turro, N. J.; *Modern Molecular Photochemistry*, The Benjamin/ Cummings Pub. Co., Inc.; Mento Park, 1978.
- [222] Ford, P. C.; Wink, D.; Dibenedetto. *Progress in Inorganic Chemistry, An Appreciation of Henry Taube*, Lippard, S. J. editor, v.30, John Willey & Sons, New York, 1983.
- [223] Cotton, F. A. *Chemical Application of Group Theory*, 2nd edition, Wiley Eastern Limited, New Delhi, 1971.

- [251] Furniss, B. S.; Hannaford, A. J.; Rogers, V.; Smith, P. W. G. ; Tatchell, A. R. ; *Vogel's Textbook of Practical Organic Chemistry*, 4th edition, English Language Book Society/Longman, England, 1978.
- [252] Schönberg, A.; Schenck, G. O.; Newmüller, O. A. *Preparative Organic Photochemistry*, Springer-Verlag, Berlin, 1968.
- [253] Foot, C. S. *Acc. Chem. Res.*, **1968**, *2*, 104.
- [254] Wasserman, H. H.; Murray, R. W. *Singlet Oxygen*, Academic Press, New York, 1979.
- [255] Weaver, J. H.; Martins, J. L.; Komeda, T.; Chen, Y.; Chno, T. R.; Kroll, G. H. Troullier, N. ; Hanfler, R. E. ; Smalley, R. E.; *Phys. Rev. Lett.*, **1991**, *66*, 1741.
- [256] Benning, P. J.; Poirier, D. M.; Obno, T. R.; Chen, Y. ; Jost, M. B. ; Stepniak, F. ; Kroll, G. H. ; Weaver, J. H. ; Fure, J. ; Smalley, R. E. *Phys. Rev. B.*, **1992**, *45*, 6899.
- [257] Flemming, R. M.; Kortan, A. R.; Hessen, B.; Siegrist, T. ; Thiel, F. A. ; Marsh, P. M. ; Haddon, R. C. ; Tycko, R. ; Dabbagh, G. ; Kaplan, H. L. ; Mujsce, A. M. *Phys. Rev. B.*, **1991**, *44* 888.
- [258] Fisher, J. E.; Heiney, P. A.; Smith, A. B. III, *Acc. Chem. Res.*, **1992**, *25*, 112.
- [259] Scanlon, J. C.; Ebert, L. B. *J. Phys. Chem.*, **1993**, *97*, 7138.
- [260] Cullity, B. D. *Elements of X-ray Diffraction*, 2nd edition, Addison Wesley Pub. Comp. Massachusetts, 1978, chapter 10.
- [261] West, A. R. *Solid state Chemistry and its application*, John Wiley & Sons., 1986, p. 183.
- [262] Allmand, P.-M.; Srdanov, G.; Koch, A.; Khemani, F.; Wudl, F.; Rubin, Y.; Diederich, F.; Alvarez, M. M.; Anz, S. J.; Whetten, R. L. *J. Am. Chem. Soc.*, **1991**, *113*, 2780.

- [263] Kukolich, S. G.; Huffman, D. R. *Chem. Phys. lett.*, 1991, 182, 263.
- [264] Kato, T.; Kodama, T.; Shida, T.; Nakagowa, T.; Matsui, Y. ; Suzuki, S. ; Shiromaru, H. ; Yamauchi, K. ; Achiba, Y. *Chem. Phys. lett.*, 1991, 180, 446.
- [265] Gaysyna, Z.; Andrews, L.; Schatz, P. N. *J. Phys. Chem.*, 1992, 96, 1525.
- [266] Greaney, M.; Gorun, S. J. *J. Phy. Chem.*, 1991, 95, 7142.
- [267] Bendale, R. D.; Stanton, J. F.; Zerner, M. C.; *Chem. Phys. Lett.*, 1992, 194, 467.
- [268] Stanton, R. E. *J. Phys. Chem.*, 1992, 96, 111.
- [269] Ragahachari, K.; Rohlfing, C. M. *J. Phys. Chem.*, 1992, 96, 2463.
- [270] Garret P. G. *Aromaticity*, John Wiley & Sons, New York, 1986.
- [271] Priyadarsini, K. I.; Mohan, H; Mittal, J. P. *J. Phy. Chem.*, 1994, 98, 9565.
- [272] William, R. M.; Zwier, J. M., Verhovan, J. W.; Nachtegaal, G. H.; Kentgens, A. P. M. *J. Am. Chem. Soc.*, 1994, 116, 6995.
- [273] Guo, Y.; Karasawa, N.; Goddard, W. A.; III. *Nature*, 1991, 351, 464.
- [274] Zhennan, G.; Jiuxin, Q.; Xihuang, Z.; Sunqi, F.; Zizhao, G. *J. Phys. Chem.*, 1991, 95, 9615.
- [275] Li, Z. G.; Fagan, P. J.; *Chem. Phys. Lett.*, 1992, 194, 461.
- [276] Li, J. Q.; Zhao, Z. X.; Zhu, D. B.; Gan, Z. Z.; Yin, D. L.; *Appl. Phys. Lett.*, 1991, 59, 3108.
- [277] Raghavachari, K. *Chem. Phys. letter.*, 1992, 195, 221.
- [278] Yates, Y. *Hückel Molecular Orbital Theory*, Academic Press, 1978, NewYork, chapter 4.
- [279] Gerhardt, P.; Löffler, S.; Homann, K. H. *Chem. Phys. lett.*, 1987, 137, 306.

- [280] Calcote, H. F. *Combust. & Flame*, **1988**, *71*, 105.
- [281] Calcote, H. F. *Combust. & Flame*, **1981**, *42*, 215.
- [282] Harris, S. J. *Combust. & Flame*, **1986**, *66*, 211.
- [283] Haynes, B. S.; Wagner, H. G. *Prog. Energy. Combust. Sci.*, **1981**, *7*, 229.
- [284] Grittenden, B. D. and Long, R. *Combust. Flame*, **1973**, *20*, 359.

LIST OF PUBLISHED PAPERS

.. NO₂ Adducts of C₆₀ : Synthesis of Polynitro-polyhydroxy Fullerenes.
Subrata Roy, S. Sarkar. *J. Chem. Soc. Chem. Commun.*, 1994, 275.

Five other manuscripts under preparation.

Errata

1. Page 2 line 3, the word invented should be read as modelled.
2. Page 3 line 4, x hexagones should be read as hexagons.
3. Page 5 line 4, ..quite expensive for which this... should be read as quite ...expensive thus this...
4. Insteadhemispherical radar in page 5 line 6 read as hemispherical radar-reflector.
5. Page 5 line 21 , before the sentences C_{60} and C_{70} were detected... a new sentence 'Mass spectroscopic evidence was not quite convincing for fullerene present in Shungite' is added.
6. Page 17 line 12, Table 1.3(ref. 33b) should be read as Table 1.3.
7. Page 18 line 26, Napthalene should be read as Naphthalene. Page 18 line 27, 1-Methyl napthalene should be read as 1-Methylnaphthalene.
8. Page 18 line 28, Dimethyl napthalene should be read as Dimethylnaphthalene.
9. Page 18 line 29, 1-Phenyl napthalene should be read as 1-Phenylnaphthalene.
10. Page 18 line 30, 1-Chloro napthalene should be read as 1-Chloronaphthalene.
11. Page 22 line 1, structureallam should be read as structure [99].
12. Page 22 line 8, orbitalswudl:acc should be read as orbitals [100].
13. Page 27, figure captions $[C_{60}(OSO_4)(4\text{-tert-butyl pyridine})_2]$ should be read as $[C_{60}(OsO_4)(4\text{-tert-butyl pyridine})_2]$.
14. Page 29 line 10, $[Na(\text{crown})(THF)^3]^3[C_{60}]$ should be read as $[Na(\text{crown})(THF)_3]_3[C_{60}]$.
15. Page 62 line 13, sim12 should be read as $\sim 12\%$
16. Page 94 line 21, bellow should be read as below.
17. Page 95 line 5, coloumn should be read as column.
18. Page 95 line 26 varry should be read as vary.
19. Page 81 Figure 4.7, δH should be read as ΔH
20. Page 99 line 17, responsiable should be read as responsible.
21. Page 102 line 11, responsiable should be read as responsible.
22. Page 99 line 25, separetly should be read as separately.
23. Page 102 line 5, Kodack should be read as Kodak.
24. Page 103 line 5, tungesten should be read as tungsten.
25. Page 106 line 3, $(\eta^5\text{-indeyl})(CO)Ir(\eta^2\text{-}C_{60})$ should be read as $(\eta^5\text{-indeyl})(CO)Ir(\eta^2\text{-}C_{60})$.

27. Page 134 line 2, cyclohexa-1,3 diene. should be read as cyclohexa-1,3-diene.
28. Page 140 line 14, known^{52b} should be read as known.
29. Page 155 Figure 6.12 line 2, $\delta=1.8\text{G}$ should be read as $\Delta\text{H}=1.8\text{G}$.
30. Page 155 Figure 6.12 line 3, $\delta=1.5\text{G}$ should be read as $\Delta\text{H}=1.5\text{G}$.
31. Page 156 Figure 6.13 line 3, $\delta\text{H}=1.7\text{G}$ should be read as $\Delta\text{H}=1.7\text{G}$.
32. Ref. 18, 19 Fostiropolous should be read as Fostiropoulos.
33. Ref. 35 Alvarex should be read as Alvarez.
34. Ref. 37 Penicand should be read as Penicaud
35. Ref. 40 Angnew should be read as Angew.
36. Ref. 49 Gröscer and Angnew should be read as Grösser and Angew.
37. Ref. 57 Seizt should be read as Seitz..
38. Ref. 68 Kappec, M. M should be read as Kappes, M. M.
39. Ref. 70 Passides, K. should be read as Prassides.
40. Ref. 80/81 Taylor, R. C should be read as R. Taylor.
41. Ref. 87 Despres, A. should be read as Dennis A..
42. Ref. 102 Dubosis should be read as Dubois.
43. Ref. 109 Raghsvachari should be read as Raghavachari.
44. Ref. 117 Issacs, L. should be read as Isaacs, L..
45. Ref. 139 Hollway, J. H. should be read as Holloway.
46. Ref. 144 Anfew should be read as Angew.
- Ref. 238 Hirtchcock, P. B. should be read as Hitchcock.
- f. 262 Allmand, P.-M. should be read as Allemand.
- . 265 Gaysyna, Z. should be read as Gasyna, Z.
50. Ref. 270 Garret P. G. should be read as Garret, P. J.

- [238] Meidine, M. F.; Hirtchcock, P. B.; Kroto, H. W.; Taylor, R. ; Walton, D. R. M. *J. Chem. Soc. ; Chem. Commun.*, 1992, 1535.
- [239] Balch, A. L.; Lee. W. J.; Noll, B. C.; Olmstead.; *J. Chem. Soc. Chem. Commun.*, 1993, 56.
- [240] Closs, G. L.; Gautam, P.; Zhang, D.; Krusic, P. J.; Hill, S. A.; Kasserman, E. J. *Phys. Chem.*, 1992, 96, 5228.
- [241] Levanon, H.; Meiklyar, V.; Michaeli, A.; Mechaeli, S.; Rager, A. ; *J. Phys. Chem.*, 1992, 96, 6128.
- [242] Regev, A.; Gambiel, D.; Meiklyar, V.; Michoeli, S. ; Levanon, H. *J. Phys. Chem.*, 1993, 97, 3671.
- [243] Levanon, H.; Meiklyar, V.; Michaeli, S.; Gamliel, D. *J. Am. Chem. Soc.*, 1993, 115, 8722.
- [244] Zhang, D.; Norris, J. R.; Krusic, P. J.; Wasserman, E. ; Chem. C. C. ; Lieber, C. M. *J. Phys. Chem.*, 1993, 97, 5886.
- [245] Rübsam, M.; Dinse, K. P.; Plüschau, M.; Fink, J.; Krätschmer, W.; Fostiropoulos;; Taliani, C. J. *J. Am. Chem. Soc.*, 1992, 114, 10059.
- [246] Wang, G.; Javahery, G.; Petrie, S.; Hopkinson, A. C.; Bohme, D. K. *Angew. Chem. Int. Ed. Eng.*, 1995, 33, 206
- [247] Xie, Q.; Arias, F.; Echegoyen, L. *J. Am. Chem. Soc.*, 1993, 115, 9818.
- [248] Wertz, J. E.; Bolton, J. R. *Electron Spin Resonance, Elementary Theory and Practical Applications*, Mcgrrow-Hill Book Company, Newyork, 1972.
- [249] Barneet, E. B.; Lawrence, C. A. *J. Chem. Soc.*, 1935. 1104.
- [250] Greidinger, D. S.; and Ginsburg, D.; *J. Org. Chem.*, 1957, 22, 146.

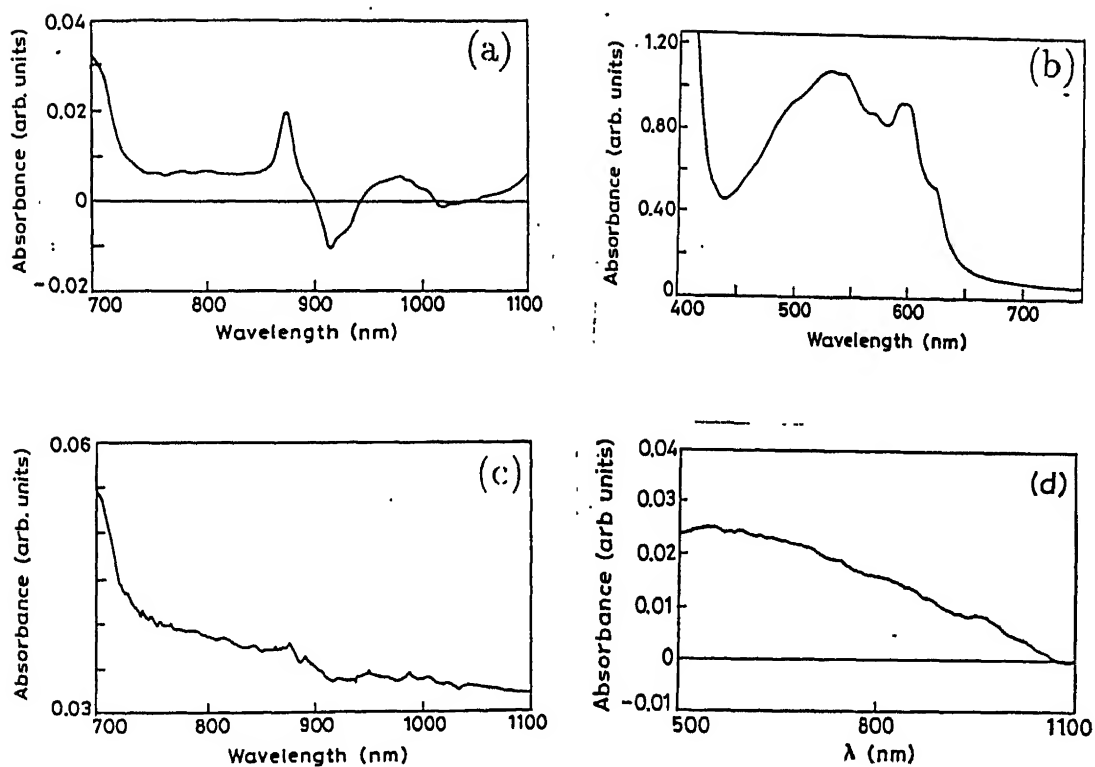


Figure 6.22: C_{60} cationic spectra (a) benzene (750-1100 nm) (b) Benzene (400-750 nm) (a) after flash chromatography of the (a). (d) In acetone

Chapter 7

Highlights and Future Scope of the Present Work.

The discovery, by Krätschmer et. al. [1], of a technique to produce and separate macroscopic quantities of the all carbon C_{60} molecule was a required first step in opening the door for exploring the molecular and bulk properties of this novel species. The excitement and challenge felt in exploring the emerging chemical reactivity of the C_{60} and fullerene resembles that which occurred during the development of aromatic chemistry last century as benzene had, for example, in the dye industry, and this phenomenological growth has been realized because benzene undergoes electrophilic substitution of its hydrogen atom but C_{60} has no easily replaceable hydrogen atom. It has been great hope that substitution of the substituted C_{60} or fullerene in near future may produce billions of commercial applicable compounds and so far chemical modification on the C_{60} moiety has been achieved by the nucleophilic addition reaction. However the reactivity studies in the chapter 4 suggested that mere a reactive nucleophile do not form bond with the C_{60} molecule.

Major obstacle in the fullerene research at present is the poor yield of the starting material, hence researcher has been handicapped from much trial for the preparation of imaginative derivatives. Reaction scheme presented in figure 4.1 and figure 5.1 demon-